A vibrational spectroscopic study of some surfactant systems

Witold F Pacynko

A VIBRATIONAL SPECTROSCOPIC STUDY OF SOME SURFACTANT SYSTEMS

A Thesis submitted to
The University of Durhan

by

Witold F. Pacynko, B.Sc.(Hons.)
(Graduate Society)

for the Degree of Doctor of Philosophy

April 1985

DECLARATION

The work described in this thesis was carried out by me in the Chemistry Department of the University of Durham and the Laboratories of Unilever Research at Port Sunlight, between September 1981 and October 1984. I declare that this work has not been accepted in substance for any degree, and is not being concurrently submitted in candidature for any other degree. The work is original except where indicated by reference.

Signed:

Date:

ACKNOWLEDGEMENTS

The work described in this thesis could not have been presented without the help and advice of many people. Two people, my supervisors, Dr. Jack Yarwood and Dr. Gordon Tiddy, have made indescribable contributions and their interest, patience and enthusiasm will be remembered for many years. I must also thank them and their families and friends for their hospitality and generosity which have also made the past few years very enjoyable.

I would further like to acknowledge the help of Rob Green, Bob Brown and all the technical staff here in the department.

Many thanks also to the S.E.R.C. and Unilever Research for financial support during the period of study.

Finally, many thanks to Mrs. Marion Wilson who converted the original manuscript into a typed form.

Wszystko co tu napisane

jest dla moje rodzice

A VIBRATIONAL SPECTROSCOPIC STUDY OF SOME SURFACTANT SYSTEMS

by

WITOLD F. PACYNKO

ABSTRACT

Infra red and Raman spectroscopy has been used to study:

(i) the aggregation process of some polyoxyethylene surfactants in apolar media,

(ii) the microenvironment of water at and near the micellar surface in some cationic surfactants, and

(iii) the nature of the hydrocarbon core within cationic surfactant micelles.

We have used the ν_s(O-H) stretching vibration of some polyoxyethylene surfactants of the type $C_{12}H_{25}(OCH_2CH_2)_n$-OH [where n = 0 to 8] to quantify the aggregation process in a variety of solvents. These have included heptane, decane, benzene, carbon tetrachloride, deutero-chloroform and decalin. In doing this we have gone some way in understanding the nature and mechanism for aggregation in such systems.

Mid and far ir spectroscopy has enabled us to study the nature of water at and near the micellar surface in dodecyl and hexadecyl trimethyl ammonium chloride mesophase systems. We have studied the decoupled ν_s(O-D) band of HDO and the $\nu_A(H_2O)$, the combination mode of water in the mid ir. In addition ν_T, the intermolecular translational mode of water, in the far ir of these systems, has also been investigated. The results have been treated collectively, and a generalized model for the state of water has been proposed. Spectra for dodecyltrimethyl ammonium bromide were also obtained and compared with the corresponding chloride data.

Raman spectroscopy of the hydrocarbon core in cationic surfactant micelles has shown that no abrupt changes occur in the gauche/trans equilibrium on crossing a phase boundary, with the exception of the gel/lamellar phase (where this is expected). However, examination of the C-H stretching region has shown that the anisotropic phases (*i.e.* H_1, L_α) display an increased lateral interaction. The isotropic phases (*i.e.* L_1, I_1, V_1), show less interaction while the first intermediate phase in C_{16}TACl shows behaviour between the two.

CONTENTS

CHAPTER ONE

INTRODUCTION

1.1 Introduction

The commercial importance of surface active materials extends to more than simply washing powders and detergents. Their uses range from emulsifiers in paint, fabric conditioners and cosmetic preparations to foaming agents in beers. It is not therefore surprising to find that industry spends millions of pounds every year researching into their development and application.

The more fundamental properties of surfactants such as micelle formation have, in the past, been studied with relatively conventional instrumentation, *i.e.* tensiometers, conductivity bridges, *etc.* Though these methods still have their uses, more modern techniques are now available giving more detailed results. In micellar systems light scattering and vapour pressure osmometry (VPO) have proved to be valuable tools in the detection of aggregates at low concentrations. In the former not only critical micelle concentrations (the concentration at which micelles are first formed, the "CMC") are obtained but, also their sizes and shape, *i.e.* whether sphere, rod or disc. At higher concentrations of surfactant it is known that liquid crystals form. These are micelles packed together in a regular array thus possessing long range order but also having fast molecular motion (rotational, translational). When such liquid crystals, or "mesophases" as they are often called, occur by the influence of a solvent, they are termed lyotropic (as opposed to thermotropic liquid crystals which occur under the influence of heat), and several structures are possible. Hexagonal and lamellar mesophases are the most common with several cubic structures also postulated (refer to

Chapter Five for detailed description). The best methods to study these systems have been by optical microscopy,[134] X-ray diffraction[99] and nuclear magnetic resonance techniques.[100] These techniques, especially the latter, have been able to provide information on both surfactant mobility and order. In particular, the advent of multinuclear NMR has enabled the counter ion, head group, hydrocarbon tail and solvent to be investigated. From the data collected it is possible to calculate diffusion coefficients, relaxation times and order parameters which may then be correlated with surfactant order, mobility, *etc.*[100] Calorimetric methods have also proved useful since they are able to detect phase transitions and heats of micelle formation.[51]

Vibrational spectroscopy is now also finding its place in this field of research. The work of Snyder, Larsson, Faiman and others[118,122-128] has given some insight into alkyl chain conformations in micellar and mesophase systems. Infra red spectroscopy has also made a significant contribution with particular reference to the aggregation of, *i.e.* alcohols and amines in apolar media.[30,46] In the past water has posed a difficult problem to the i.r. spectroscopist because of its high absorbing properties. However, the addition of small amounts of deuterium oxide (D_2O) has allowed the study of the ν_S(O-D) band of HDO occurring at 2520 cm^{-1}.[5] The advantages of this procedure are to allow the study of a symmetric low intensity water band in a relatively "clean" part of the i.r. spectrum.

In the work described here we have studied various binary systems using vibrational spectroscopy. Initially we have

observed the aggregation phenomenon of some polyoxyethylene surfactants of the type $C_{12}H_{25}(OCH_2CH_2)_n\text{-}OH$ (abbreviated to $C_{12}E_n$) in a series of solvents using infra red spectroscopy. The area of most interest has been the 3200-3800 cm^{-1} region where one observes the ν_s(O-H) alcohol stretching vibrations of these molecules. The spectra in general show several bands. These are the non hydrogen bonded species and the various hydrogen bonded species at lower frequencies. Our aim was to measure the monomer concentrations as a function of total surfactant concentration. From these we have been able to obtain average aggregation numbers from a thermodynamic model and hence determine free energies of aggregation. Heptane was the first solvent studied and the aggregation properties of polyoxyethylene surfactants ranging from $C_{12}E_0$ to $C_{12}E_8$ have been investigated. Further data was then obtained using $C_{12}E_4$ in various nonpolar solvents, *e.g.* Benzene, Decane, Carbon tetrachloride, *etc.* The work has not been entirely without difficulties, the major problem being quantification of <u>intra</u> molecularly hydrogen bonded species greater than 8 in ring size (*i.e.* occurring in $C_{12}E_2$-$C_{12}E_8$) and their contribution to the <u>inter</u>molecular hydrogen bonding absorbances.

The remainder of the time has been devoted to studying the vibrational spectroscopy of two cationic surfactant/water systems. The first of these, dodecyl trimethyl ammonium chloride (C_{12}TACl) has a fairly well documented phase diagram.[32] Three spectroscopic techniques have been used in this case; Raman, far i.r. spectroscopy and mid i.r. spectroscopy. The work has allowed us to study the microstructure of the water in various mesophases as well as hydrocarbon chain conformations.

The C_{12}TACl-water system shows four liquid crystalline regions; two cubic phases, a hexagonal (middle) phase, and a lamellar (neat) phase.[32] In this work we have attempted to identify any spectroscopic changes which might occur when crossing a phase boundary. In so doing we may be able to apply the knowledge to a less well known system (i.e. C_{16}TACl/water, see Chapter Seven). In the mid i.r. we chose two bands, these being ν_s(O-D), the decoupled O-D stretch of HDO and $\nu_A(H_2O)$, the combination mode of H_2O.[5] For these two bands we measured both the full width at half maximum intensity (band width) and also the frequency maximum. Phase boundaries were crossed isoplethally and isothermally and any changes in the above parameters were investigated.

Far i.r. spectroscopy allowed a study of ν_T, the intermolecular translational mode of water,[5] and the spectra obtained used to complement the mid i.r. observations. Several C_{12}TABr mesophase samples were also prepared and again the results were compared in both regions of interest. Raman spectroscopy was employed to investigate any changes in the head group geometry and alkyl chain geometry.

Finally the third system examined, the hexadecyl trimethyl ammonium chloride, $C_{16}H_{33}\overset{\oplus}{N}(CH_3)_3Cl^{\ominus}$ (C_{16}TACl)/water system, displayed some very interesting features in its phase behaviour.[86] The phase diagram though not fully elucidated[86] showed evidence for an "intermediate phase"[82,85] (or possibly two) with rectangular shaped micelles.[80] In addition, several phases present in the C_{12}TACl system also appeared here, *i.e.* hexagonal, cubic and lamellar phases. A further point of interest was the gel phase which existed at high concentrations

melting to the lamellar phase at elevated temperatures. This gel phase is thought to be composed of interdigited layers of surfactant molecules with "solid like" hydrocarbon chains.[80] Again water, surfactant chain and head group spectra were obtained in the hope of observing any anomalous features, particularly in the intermediate phase(s). Supplementary work using a polarizing microscope was also performed as a check on concentration and surfactant purity. This included use of the penetration techniques which allowed the lower temperature boundaries of the various phases to be determined.[80,134] Briefly, a small amount of water is allowed to permeate through a thin layer of powdered surfactant mounted on a microscope slide. After a time all the mesophases, which occur at that particular temperature, form as a series of bands. They form in order of concentration with phases appearing and disappearing as the temperature is increased.

The work mentioned above has not just been of academic interest. The process of "reverse" aggregation is now an active field of research because of its application in catalysis and oil recovery. Phase behaviour of surfactants is of considerable interest in the detergent and soap industry, where viscous mesophases are to be avoided during initial stages of manufacture (lamellar phases are preferred because of their favourable rheological characteristics). In addition, the lamellar phases found in many surfactant/water systems can be used as models for the study of biological membranes.

CHAPTER TWO

VIBRATIONAL SPECTROSCOPY, THEORY AND INSTRUMENTATION

2.1 Introduction

The majority of the work presented in this thesis has been performed using the infra red (I.R.) region of the electromagnetic spectrum. Although no fixed limits are set on this region, it is generally accepted that it extends between 1 (12 $Jmol^{-1}$) and 10,000 cm^{-1} (120 kJ mol^{-1}). Electromagnetic radiation of such energy is of the same magnitude as that of molecular or intermolecular vibrations. The region is often divided into the far I.R. ($\simeq$1-400 cm^{-1}), mid I.R.($\simeq$400-4000 cm^{-1}) and near I.R. ($\simeq$4000-10000 cm^{-1}) according to the type of vibrational transition studied.

(i) Far Infra Red

The most common types of vibration studied in this region are the molecular and lattice modes of molecules.[1] The former is of particular interest here, where one is able to observe hydrogen bonded interactions and also interionic modes of the type $RN(CH_3)_3^+ \ldots Cl^\ominus$ (see Chapters Six and Seven).

(ii) The Mid I.R.

Often referred to as the "fingerprint" region, vibrations at these frequencies correspond to the normal internal modes of molecules. As well as its use for qualitative analysis, the mid I.R. is often used for molecular structure and bonding studies,[1] molecular dynamics[2] and also quantitative analysis.[1]

(iii) The Near I.R.

Though not as extensively studied as the previous regions, the near I.R. displays mainly the overtone and

combination bands of molecules. It is most commonly used in quantitative analysis. One particular application of this region has been demonstrated using the ν_S(O-H) overtones of some n-alkanols.[3] Because the hydrogen bonded and non-hydrogen bonded vibrations are so well separated in this region, it is a relatively simple matter to spectroscopically distinguish between the various species (in the mid I.R. there is often partial overlap of these bands and study of one in particular is difficult).

2.2 Fundamental Principles of I.R. Spectroscopy

2.2.1 The Harmonic Oscillator

For a simple harmonic oscillator[4] one can relate the vibrational frequency ($\bar{\nu}$) with a mass (μ_M) and a force constant (K) such that:

$$\bar{\nu}(cm^{-1}) = \frac{1}{2\pi C}\sqrt{\left(\frac{K}{\mu_M}\right)} \quad \ldots\ldots \quad \text{(eqn. 2.1)}$$

However, since vibrational energies are quantized, the allowed energies may be calculated from solutions of the Schrödinger equation.

$$E_{vib}\ (cm^{-1}) = (v + \tfrac{1}{2})\bar{\nu} \quad \ldots\ldots \quad \text{(eqn. 2.2)}$$

Equation 2.2 shows that the vibrational energies, which are equally spaced for a harmonic oscillator, depend on v the vibrational quantum number.

2.2.2 The Anharmonic Oscillator

Figure 2.1 below shows the energies involved in extensions and compressions of bonds from their equilibrium distance. For a simple harmonic oscillator these

FIGURE 2.1 Extension and Compression Energies for a Diatomic Molecule

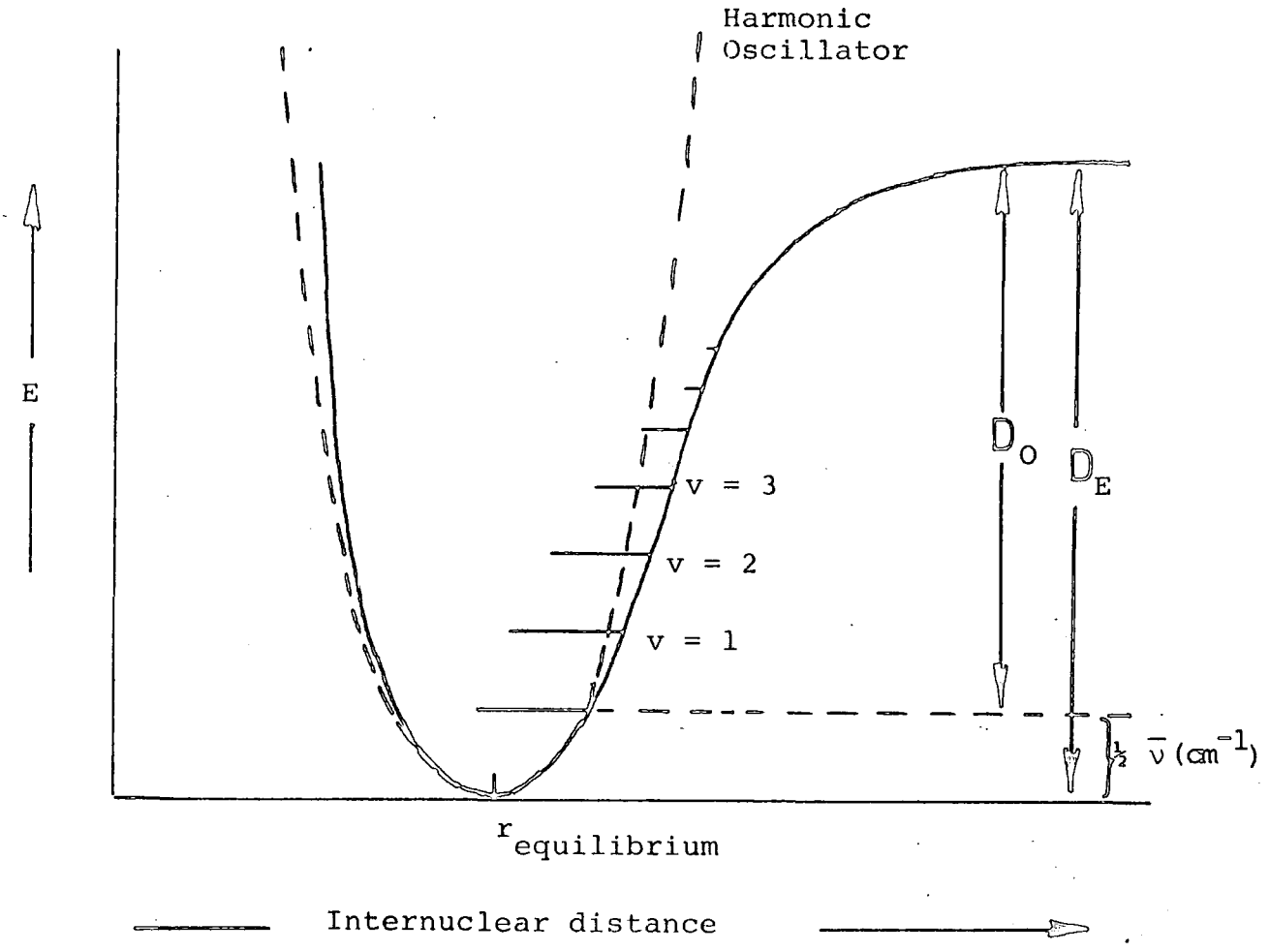

extensions and compressions are el-astic and hence the energy distribution is parabolic about the equilibrium bond distance. For an anharmonic oscillator the curve is more complex and does not obey Hookes' Law (equation 2.1). Extension of the bond beyond a certain internuclear distance leads to dis-

sociation. The full curve of Figure 2.1 may be described by the so-called morse function:

$$E = D_E[1 - \exp.(a_m(r_{eq}-r))]^2 \quad \ldots\ldots \quad \text{(eqn. 2.3)}$$

where a_m is a constant dependent on the molecule and D_E is the dissociation energy which includes a contribution from the zero point energy ($\frac{1}{2}\bar{\nu}$). When the above expression is used in the Schrödinger equation the allowed vibrational energies may be expressed as:

$$E_{vib} = (v+\tfrac{1}{2})\nu_e - (v+\tfrac{1}{2})^2 x_e \nu_e$$

$$\Delta v = \pm 1, \pm 2, \pm 3, \pm 4 \quad \ldots\ldots \quad \text{(eqn. 2.4)}$$

where x_e and y_e are anharmonicity constants and ν_e is the (hypothetical) vibration frequency of negligible amplitude about the equilibrium position. The third and higher terms of equation 2.4 are usually ignored because of their diminishing magnitude allowing the fundamental vibrational frequancy (the v=0 to v=1 transition) to be expressed as

$$\Delta E_{(0,1)} = \nu_e (1 - 2x_e) \quad \ldots\ldots \quad \text{(eqn. 2.5)}$$

Transitions from v=0 to v>1 decrease in probability and occur at approximately twice or three times the fundamental frequency. They are often referred to as overtones[4].

$$\Delta E_{(0,2)} = 2\nu_e (1 - 3x_e) \quad \ldots\ldots \quad \text{(eqn. 2.6)}$$

$$\Delta E_{(0,3)} = 3\nu_e (1 - 4x_e) \quad \ldots\ldots \quad \text{(eqn. 2.7)}$$

Transition from v≠1 are also of low intensity since at normal temperatures few molecules exist in this vibrational state.

However if the temperature is increased, transitions do occur and these "hot bands" increase in intensity.

As well as the selection rule mentioned in equation 2.4, *e.g.* $\Delta v = \pm 1, \pm 2 \ldots$ one other primary selection rule exists. This is the precept that there must be a change in dipole moment along the normal coordinate of the vibration, that $(\frac{\partial \mu_D}{\partial q}) \neq 0$. Thus for a homonuclear diatomic gas such as N_2, no change in dipole moment occurs and so no vibrational transitions are observed in this approximation. However, for heteronuclear diatomics which possess a permanent dipole, there is a change, and a single fundamental is observed.

2.2.3 Vibrations of Polyatomic molecules

It is well known that the number of fundamentals of a nonlinear polyatomic molecule may be calculated as 3N-6 modes (3N-5 for a linear molecule), where N is the number of atoms.[4] The water molecule, having C_{2V} symmetry, will thus exhibit three I.R. active fundamentals: there being the symmetric and antisymmetric stretches, and the bending mode, occurring at 3652 cm^{-1}, 3756 cm^{-1} and 1595 cm^{-1}, respectively.[4] Figure 2.2 shows the behaviour of the molecule during these vibrations.

Both ν_1 and ν_2 are symmetric vibrations, the term "symmetric" referring to whether or not the vibration is symmetrical about the main symmetry axis (in the case of H_2O, the C_2 axis). As well as being antisymmetric, the dipole moment of ν_3 changes in a direction perpendicular to the symmetry axis. It is hence called a "perpendicular mode".

Figure 2.2 Vibrational Modes of the Water Molecule [reproduced from Banwell][4]

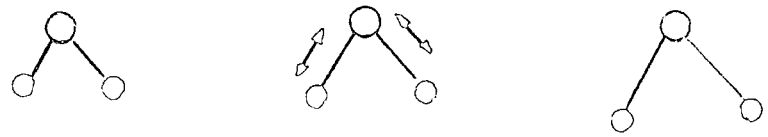

ν_1, symmetric stretch, parallel

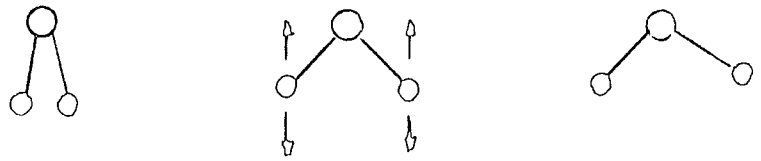

ν_2, symmetric bending, parallel

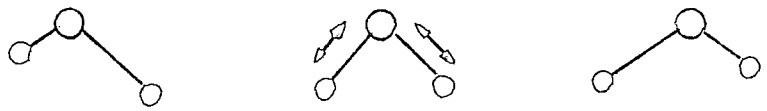

ν_3, antisymmetric stretch, perpendicular.

Quite often coupling between vibrational modes of the same symmetry and approximately the same energy is observed. One particular example of this type of interaction is when two vibrations couple, exchange energy and resonance occurs. The resulting interaction, being referred to as Fermi resonance,[4] causes large intensity increases for normally weak bands, *e.g.* overtones. Further complications to the I.R. spectra of polyatomic molecules arise when fundamentals and overtones add and subtract from one another,

termed combination and difference bands, respectively. Water exhibits a combination band at ≈2150 cm^{-1} and this is thought to arise from the bending mode occurring at 1645 cm^{-1} (ν_2), the librational mode extending between 300 and 900 cm^{-1} (ν_L) and the translational mode (ν_T), such that ν_{max} corresponds to $\nu_2 + \nu_L - \nu_T$.[5]

2.2.4 Vibrations in the Far I.R.

The absorption of radiation at low frequencies correspond to small vibrational energies, with bonds having small force constants or high masses, *c.f.* equation 2.1. This latter property is used in coordination chemistry to observe ligand replacement and other reactions.[1] Donor-acceptor interactions are another phenomenon much studied in this region, in particular those acceptors of hydrogen bonded species[6]. Such interactions may be more adequately described with the aid of an example. We shall use water since it has relevance to the work undertaken here.

When two non linear molecules of N_1 and N_2 atoms form hydrogen bonds, then $[3(N_1+N_2)-6]$ modes become possible. In the case of two water molecules, we observe six extra intermolecular modes.

(a) The Intermolecular stretching mode (ν_T) is characterized by the variation of centres of mass of partners of the complex, or of the atoms most closely associated with the hydrogen bond.

The band is usually situated in the 100-300 cm^{-1} region typical of "weakly" bonded species.

Figure 2.3(a) The Intermolecular stretching mode of water

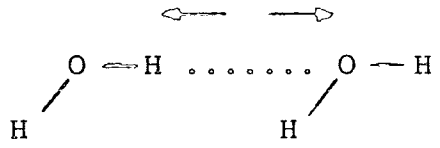

(b) The Intermolecular bending modes (Intermolecular librations) occur as two pairs, the degenerate rocking modes (ν_β and ν_δ) and the bending modes (ν_γ and ν_ε). These motions correspond to librations about the x- and z-axis, respectively[6] and occur as a broad band at approximately 600 cm^{-1} in water.

Figure 2.3(b) The Librational Mode of Water

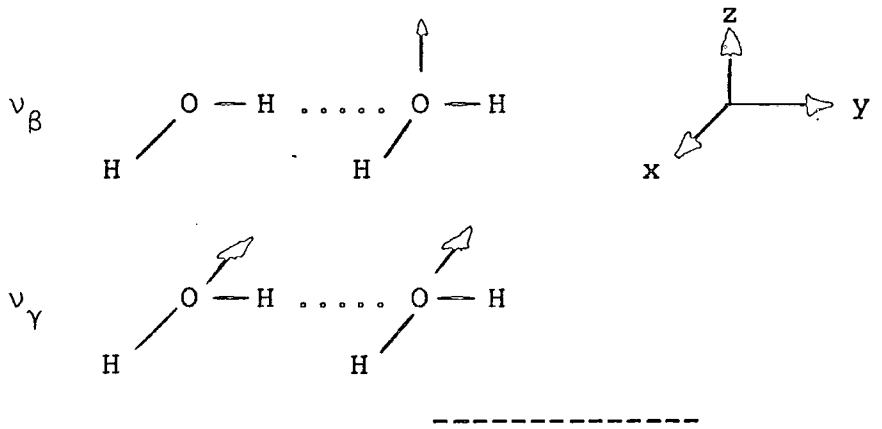

(c) The Torsional mode (ν_α) is a low energy mode corresponding to the torsional oscillation about the y-axis of one molecule relative to another.

Figure 2.3(c) The Torsional Mode of Water

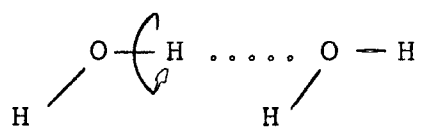

In water this vibration occurs at about 50 cm^{-1} (it is infra red inactive but is observed in the Raman).[7]

2.2.5 Spectroscopy of Hydrogen Bonded Systems

As mentioned in the previous section hydrogen bonding leads to the formation of new bands in the far i.r. region. As well as observing these intermolecular modes, certain changes are also evident in the fundamental region. In particular, the ν_S(X-H) stretching mode which has been the subject of much research in these systems. In water this band is complicated by Fermi resonance between ν_S, the symmetric stretch and the first overtone of the bending mode ν_2.[5] This coupling is usually removed by the addition of small amounts of deuterium oxide. At equilibrium the actual concentration of D_2O is small and the majority of deuterons are associated with the HDO species. There are several advantages of this isotopic dilution:

(i) The Fermi resonance is removed since the symmetric ν_S(O-D) stretch and the first bending mode overtone become well separated in frequency.

(ii) Since only a small amount of D_2O is involved, the intensity of the ν_S(O-D) is small relative to the ν_S(O-H). This is often an advantage because of the high absorbing properties of water.

(iii) The position of the ν_S(O-D) band is such that it is relatively free from most other overlapping fundamentals.[5]

It is generally accepted that the majority, if not all the water molecules, are hydrogen bonded to each other.[8] Subsequently the ν_S(O-D) band mentioned above corresponds to molecules having a reduced O-D force constant

and therefore a lower frequency maximum. Similarily, any molecule forming a complex of the type {-X-H...Y} will also exhibit a broad ν_S(X-H) band (the spectrum of the acceptor, Y, usually only show small changes). Examination of the bending modes of the above species show only small increases in frequency and intensity. Comparatively, the ν_S(X-H) integrated intensity is greatly enhanced by this complexation which suggests that electron redistribution occurs along the X-H axis. In addition to these changes, the band shows a considerable increase in width which may be influenced by several processes. By far the most important of these broadening mechanisms are those attributed to anharmonicity and anharmonic coupling. For example, one particular model which has been used for ν_S(X-H) broadening mechanisms is that of Stepanov[6,17]. The theory postulates the interaction of two "adiabatically separable" vibrational states, *i.e.* ν_S and ν_T such that sub levels of ν_T become superimposed upon the ν_S energy levels. Sum and difference bands of the type $\nu_S \pm n\nu_T$ may occur by vertical Franck-Condon type transitions between the various ν_T levels. Since the lower energy states tend to be more populated, the result is a broad band sometimes showing structure. The model relies on the fact that the two vibrational states are well separated in energy. Such a model may also be used to explain the $\nu_A(H_2O)$ combination band mentioned in Section 2.2.3. Williams[18] has postulated a combination of $\nu_S+\nu_L-\nu_T$ which may couple in a similar mechanism to that described above.

2.3 The Mid I.R., Instrumentation

2.3.1 The Double Beam Ratio Recording Spectrophotometer

Double beam spectrophotometers have been in existence for many years and are among the most reliable and economic of instruments. Their operation relies on beam division with one beam traversing the sample, the other acting as a reference signal. The reference signal may be attenuated to compensate for sample absorption (the attenuator then being linked directly to the chart recorder) or as in ratio recording instruments the sample signal being ratioed with the reference signal by a ratiometer.

Figure 2.4 is a schematic diagram of a simple double beam ratio recording i.r. spectrophotometer such as the one used in this work. Broad band i.r. radiation emitted from a source S (usually a glowbar) is split into two beams by a chopper, C_1. The sample beam is reflected by the chopper while the reference is allowed to pass through the sector. Having traversed the sample the transmitted radiation passes through a second chopper, C_2 in synchronization with C_1 and on to the monochromator, (the reference is reflected off the chopper). In such a way alternate and independent pulses of sample and reference beams impinge on the entrance slit of the monochromator. The diffraction grating, which is usually synchronized with the scan motor, disperses the beam through an exit slit, the width of which determining the signal to noise and resolution of the spectrophotometer. Before emerging at the detector, the dispersed beam passes through a filter which subtracts unwanted stray frequencies.

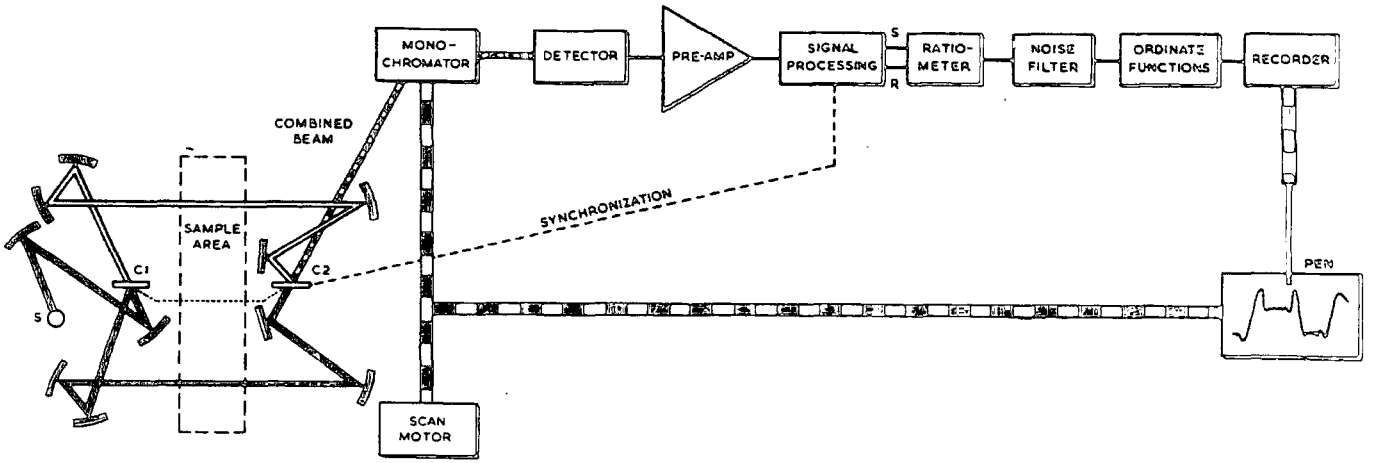

Figure 2.4 Schematic Diagram of a Ratio Recording Double Beam Spectrophotometer.

(reproduced from reference[9])

The alternating signals from the detector are amplified and separated into sample and reference signals. These are ratioed and filtered by the signal processing electronics giving a voltage signal which drives the recorder.

2.3.2 The Perkin Elmer 580B

Among the more conventional features, the PE580B has a number of salient points worthy of further mention.[9] Among these is the dual chopper assembly which operates at 12.5Hz and compensates for re-radiation originating from the sample area. The combination of the two choppers gives rise to a total of four regions in a single chopper cycle. Figure 2.5 shows these regions which fall on the monochromator successively from left to right.

FIGURE 2.5

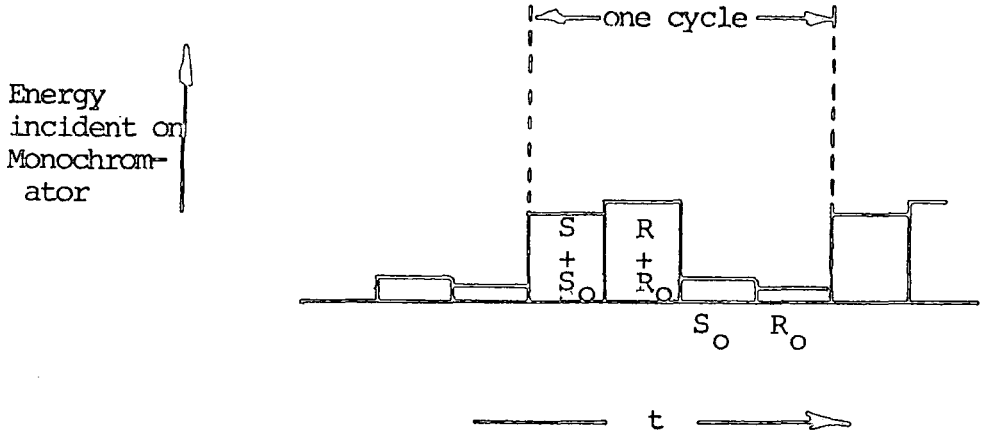

where $S + S_O$ = total sample beam energy

$R + R_O$ = total reference beam energy

R_O = re-radiation from reference area

S_O = re-radiation from sample area.

The signal processing electronics is able to distinguish between these signals and thus compensates for re-radiation.

The PE580 incorporates a mini computer which is able to control the spectrometer and also perform additional manipulations and data analysis. Such functions include repeated scans of low intensity spectra, solvent subtraction, data smoothing, *etc.* some of which have been used in the work described here (see Chapters Four, Six and Seven). For a more detailed discussion of software capabilities the reader is referred to the operators manual.[9]

2.4 Interferometric Spectroscopy

2.4.1 The Michelson Interferometer

Spectroscopy in the far I.R. may be performed using both dispersive and non dispersive techniques. However due to low source intensities and low detector sensitivity, the part played by conventional dispersive spectrometers is small. Under normal circumstances interferometers are used, the most common design being that of the Michelson, illustrated in Figure 2.6.

Chopper modulated radiation originating from a source S (usually a mercury discharge lamp) is divided by a beamsplitter. In the far I.R. the beamsplitter material is mylar of a given thickness; the thickness conferring unique reflection-transmission properties and different background energies. Figure 2.7 shows the transmission characteristics of some idealised dielectric beamsplitters of varying thickness.

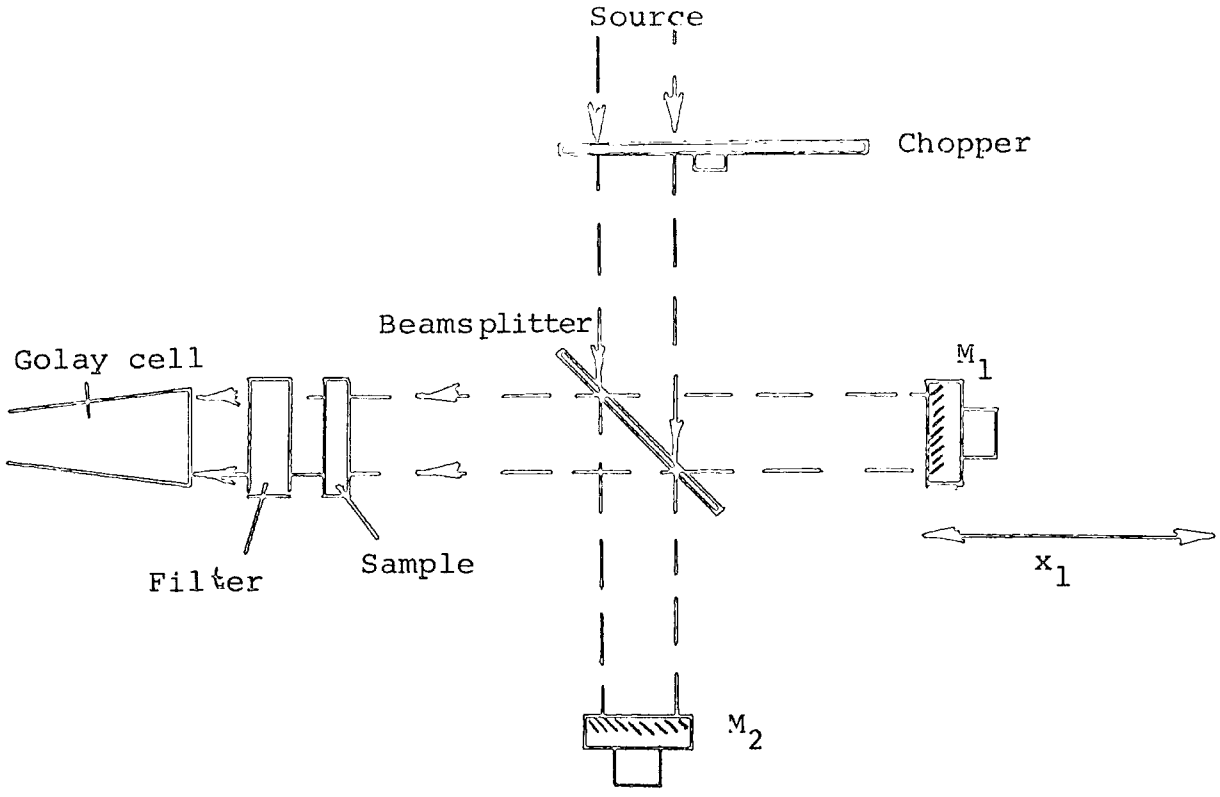

Figure 2.6 The Michelson Interferometer

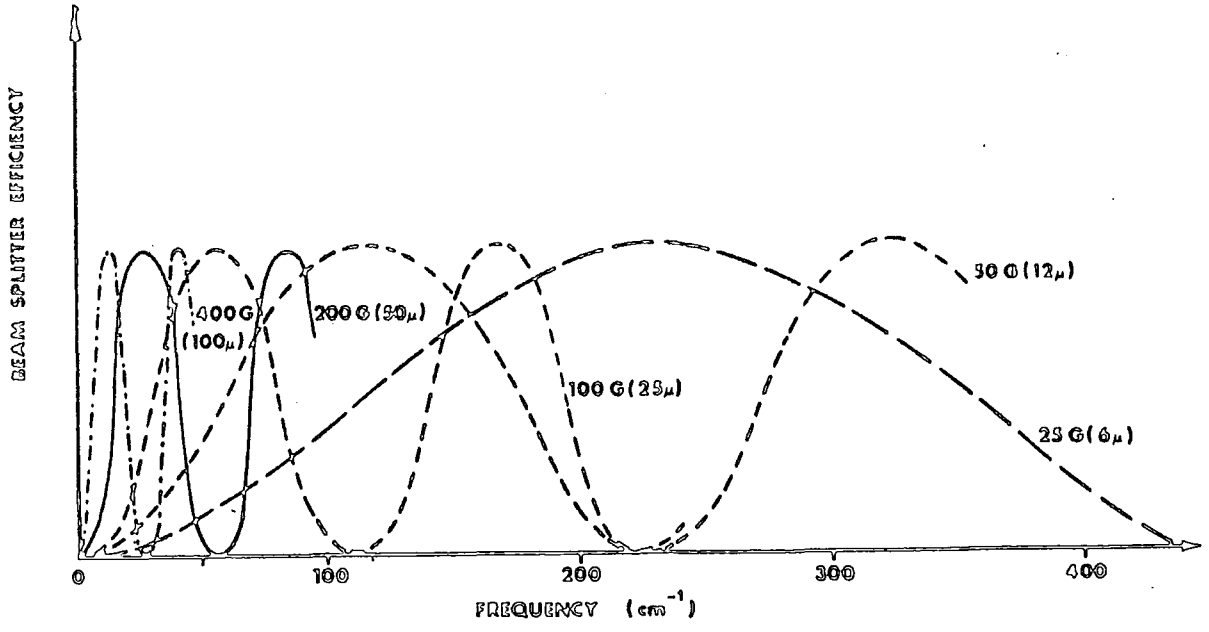

Figure 2.7 Transmission characteristics of some Mylar beamsplitters.[24]

The thickness is usually chosen so that its first maximum coincides with the frequency of interest. One arm of the beam is incident on a minor (m_2), set at a fixed distance, x, from the beamsplitter. The reflected beam is directed at a second mirror (m_1), which is able to move along the beam axis. The two beams subsequently recombine at the beamsplitter, with an interference pattern emerging at the detector. If one plots the intensity of radiation against the path difference of the two mirrors one obtains an interferogram as shown in Figure 2.8.

Figure 2.8 An Amplitude Modulated Interferogram

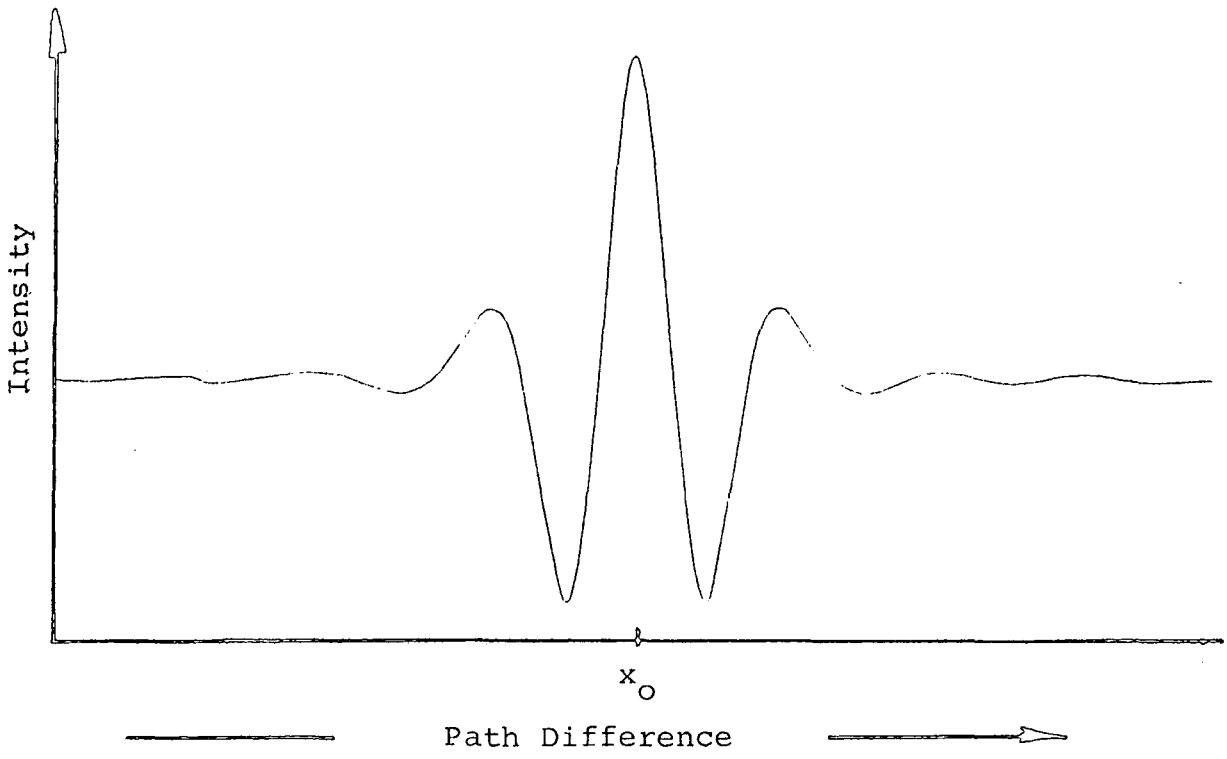

At a distance x_o there is total constructive interference of all the frequency components of the radiation and we see a central maximum corresponding to zero path difference (ZPD).

The above interferogram may be described mathematically as:[13]

$$I(x) = \int_{\bar{\nu}_1}^{\bar{\nu}_2} I(\bar{\nu})[1 + \cos 2\pi\bar{\nu}x]\,d\bar{\nu} \qquad \text{(eqn. 2.9)}$$

where $I(x)$ = intensity at x path difference

$I(\bar{\nu})$ = spectral intensity at frequency $\bar{\nu}$

The modulated part of equation 2.9 will be superimposed on a constant value shown as the left term of equation 2.10

$$I(x) = \int_{\bar{\nu}_1}^{\bar{\nu}_2} I(\bar{\nu})\,d\bar{\nu} + \int_{\bar{\nu}_1}^{\bar{\nu}_2} I(\bar{\nu})\cos(2\pi\bar{\nu}x)\,d\bar{\nu} \qquad \text{(eqn. 2.10)}$$

The right term of equation 2.10 above can be recognised as a Fourier term and will allow us to determine the intensity at the desired frequencies $I(\bar{\nu})$. This mathematical "sorting" is performed by Fourier analysis given by

$$I(\bar{\nu}) = \int_{0}^{x_{max}} I(x)\cos(2\pi\bar{\nu}x).dx \qquad \text{(eqn. 2.11)}$$

If a non symmetric interferogram is used then it has both real and imaginary parts as shown in equation 2.12.

$$I(\bar{\nu}) = \int_{o}^{x_{max}} I(x)\exp(-2\pi i\nu x)\,dx \qquad \text{(eqn. 2.12)}$$

(The *sine* component becomes zero if the interferogram is symmetric, eqn.2.11).

The detector systems used in far I.R. spectroscopy have much advanced with the advent of far I.R. responsive semiconductor materials. Golay cells, however, still find their use, operating on the principle of heat detection from a radiation absorbing cavity. The detector response is slow and so the chopper (or modulation) frequency is therefore small, usually of the order of 12Hz. Signal to noise ratios, however, are improved by orders of magnitude with the use of semiconductor detectors such as the Germanium Bolometers. A thermosensitive crystal of Germanium detects incoming radiation and converts if directly to a small voltage which is subsequently amplified.[10] The detector noise becomes very small when the crystal is cooled to beyond its λ point at 1.7K using liquid Helium.

The first step in determining the frequency spectrum is to record the background interferogram which will contain the instrumental frequency response, *e.g.* beamsplitter, lamp, detector characteristics. Fourier analysis of this background interferogram gives the energy profile of the instrument as a function of frequency. A second interferogram is then recorded with the sample in position (generally in front of the detector). Fourier transformation and ratioing with the above background spectrum (as shown in equation 2.13) produces the absorption spectrum of the sample only.

$$A_b = \log_e\left(\frac{I_o}{I}\right) \qquad \ldots\ldots \qquad \text{(eqn. 2.13)}$$

A_b is the absorbance, I_o and I are the background and sample-background frequency spectra, respectively. To obtain the absorption coefficient in Neper. cm^{-1} the absorbance data is

divided by the pathlength of the sample (in cm) and its concentration ($mol.l^{-1}$).

2.4.2 The Modified Beckman RIIC FS720

The Beckman RIIC FS720 is a conventional Michelson interferometer of the type shown in Figure 2.9. Several modifications have been performed to increase both the resolution and the signal to noise ratio. In original form, the FS720 employed a Moire grating drive[10] to sample points at the correct interval. Though the system was more than adequate for most experiments, the stepping motor displayed the exact displacement from zero path difference. This feature was important when the interferometer was used in the dispersive mode (see reference 13, Page 192).

The second modification, that of installing "phase modulation" also required additional hardware. Unlike "amplitude modulation" where a chopper is used to modulate the beam, the former superimposes a sinusoidal "jitter" on to the detector signal. The jitter is generated by small oscillations from a mirror mounted on a small loudspeaker coil. The frequency and amplitude of the modulation may be controlled by a power oscillator which is able to optimise the above conditions for a particular spectral range and detector. The signal from the detector is by a lock-in amplifier which discriminates between the noise and the spectral information. There are several advantages of such a system, the most obvious being an increase in energy throughput and an absence of a dc level.

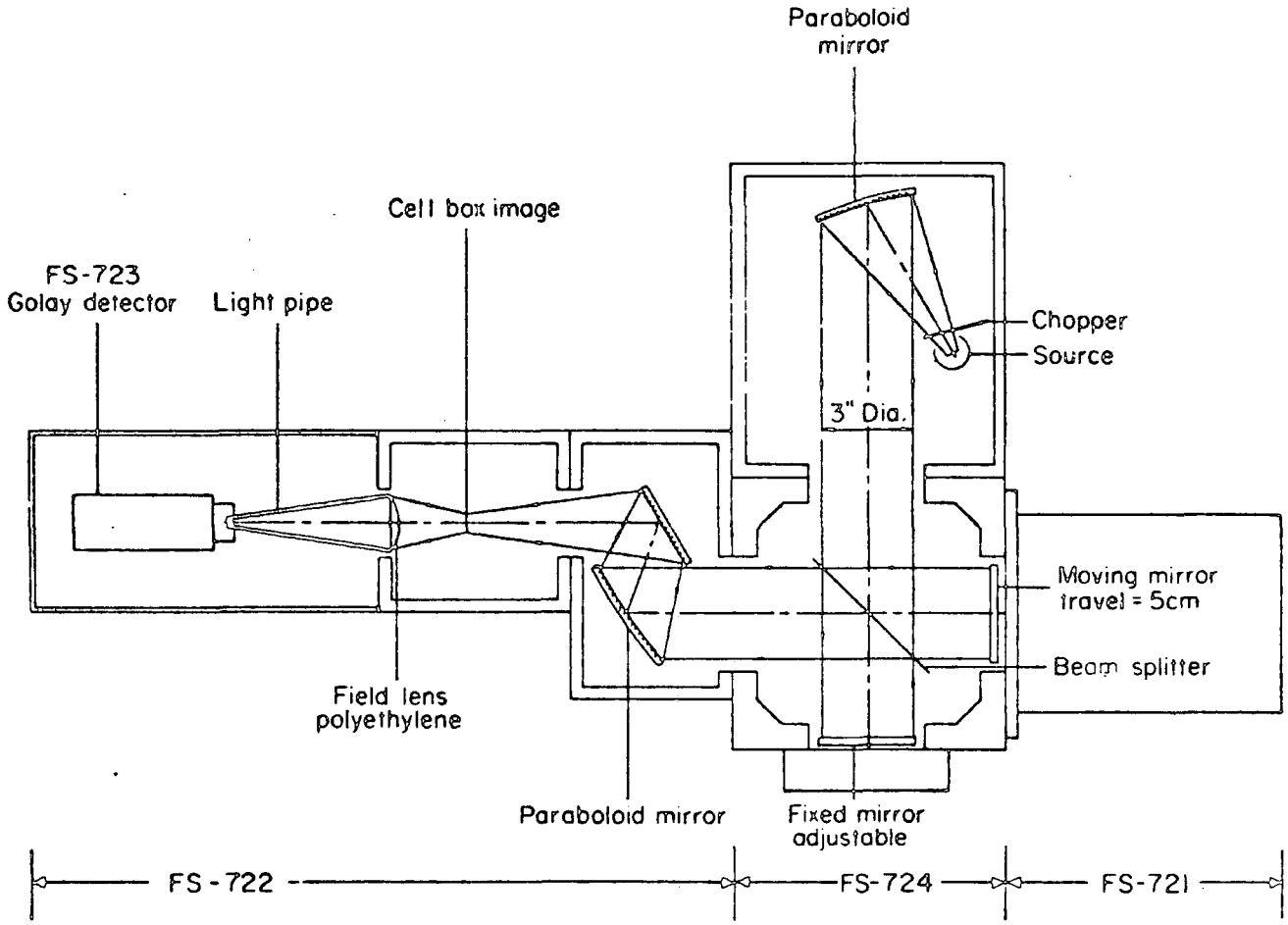

Firue 2.9 The Beckman RIIC FS720

(reproduced from reference[10])

The phase modulated interferogram is quite unlike that obtained using amplitude modulation (Fig.2.8). Inspection of Figure 2.10 shows that it becomes the first derivative of its amplitude modulated counterpart.

Figure 2.10 A Phase Modulated Interferogram

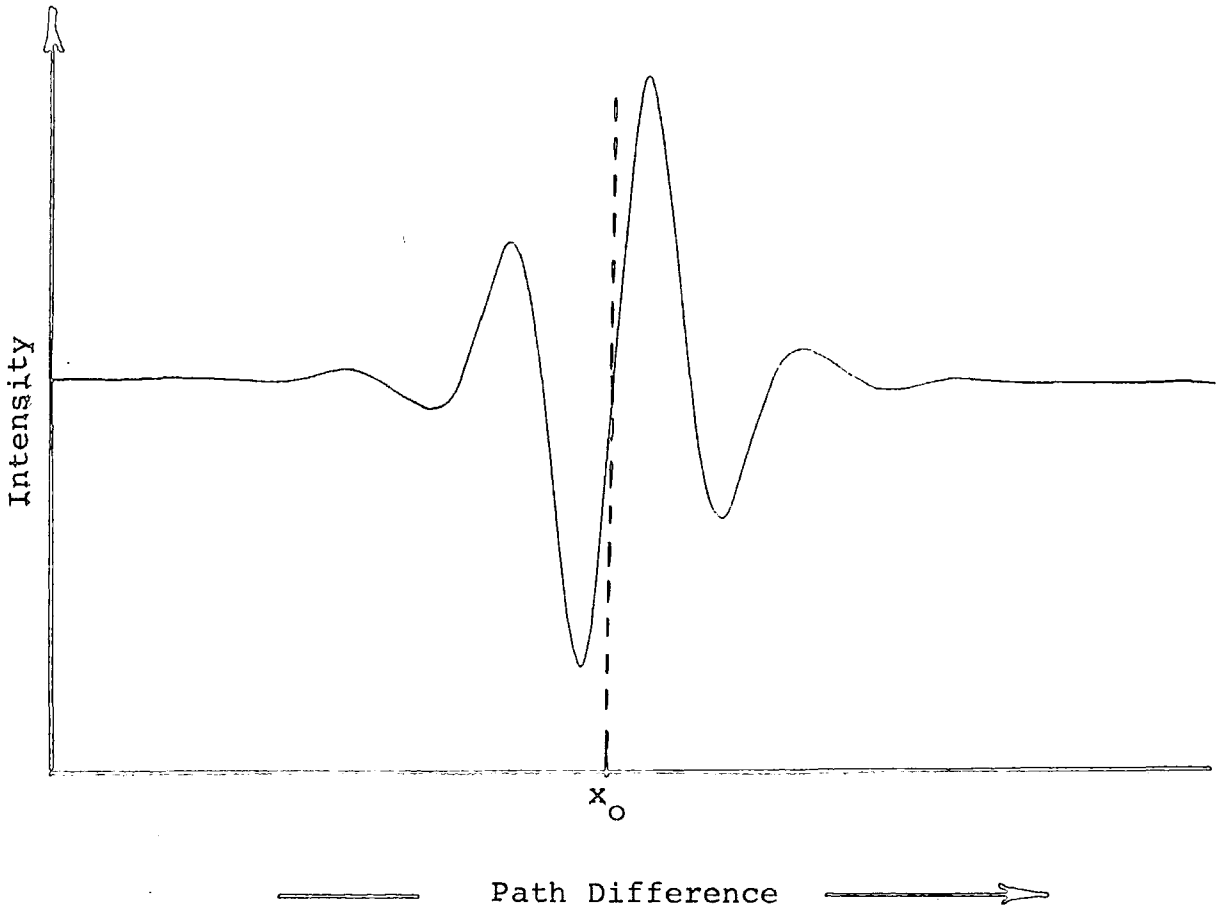

Such behaviour may be rationalized if one considers that the jitter causes a small phase delay. In the limit this phase delay causes the interferogram to appear as the first derivative, though even finite increments show this to be the case. The mathematical background has been well documented by Chamberlain[13] and Chantry[12] but in simple terms, Fourier transformation of the time dependent components describing the phase modulated flux turn out to be Bessel functions which

are both amplitude and frequency dependent. The amplitude of the oscillations thus, to some extent, control the energy profile of the spectrum (for a particular beamsplitter).

Finally, modifications have been made to signal electronics and data handling. A summary of the system as it stands is illustrated schematically in Figure 2.11. The stepping motor is triggered from a control box which also drives the analogue to digital (A to D) converter. The incoming analogue signal at that moment is then amplified and digitised in ASCII and collected by means of a Cifer microcomputer. Data is stored on disc and subsequent data analysis (*i.e.* Fourier transformation) becomes a relatively simple task.

2.4.3 Some Important Considerations

In our theoretical discussion of Section 2.3.1 we mentioned Fourier transformation of a fundamentally continuous function (equation 2.11). However, in reality two problems arise[11,12,13]:

(i) The first is realised if one considers that points must be sampled at finite sampling intervals. It is highly unlikely that a point will fall on the grand maximum, thus imposing a phase error on the data.

(ii) Artificial truncation of the interferogram at x_{max} has the unfortunate effect of generating a spike in the data and causes spurious features in the spectrum.

Generally two methods are used to overcome (i), the first employing a technique referred to as "autocorrelation".

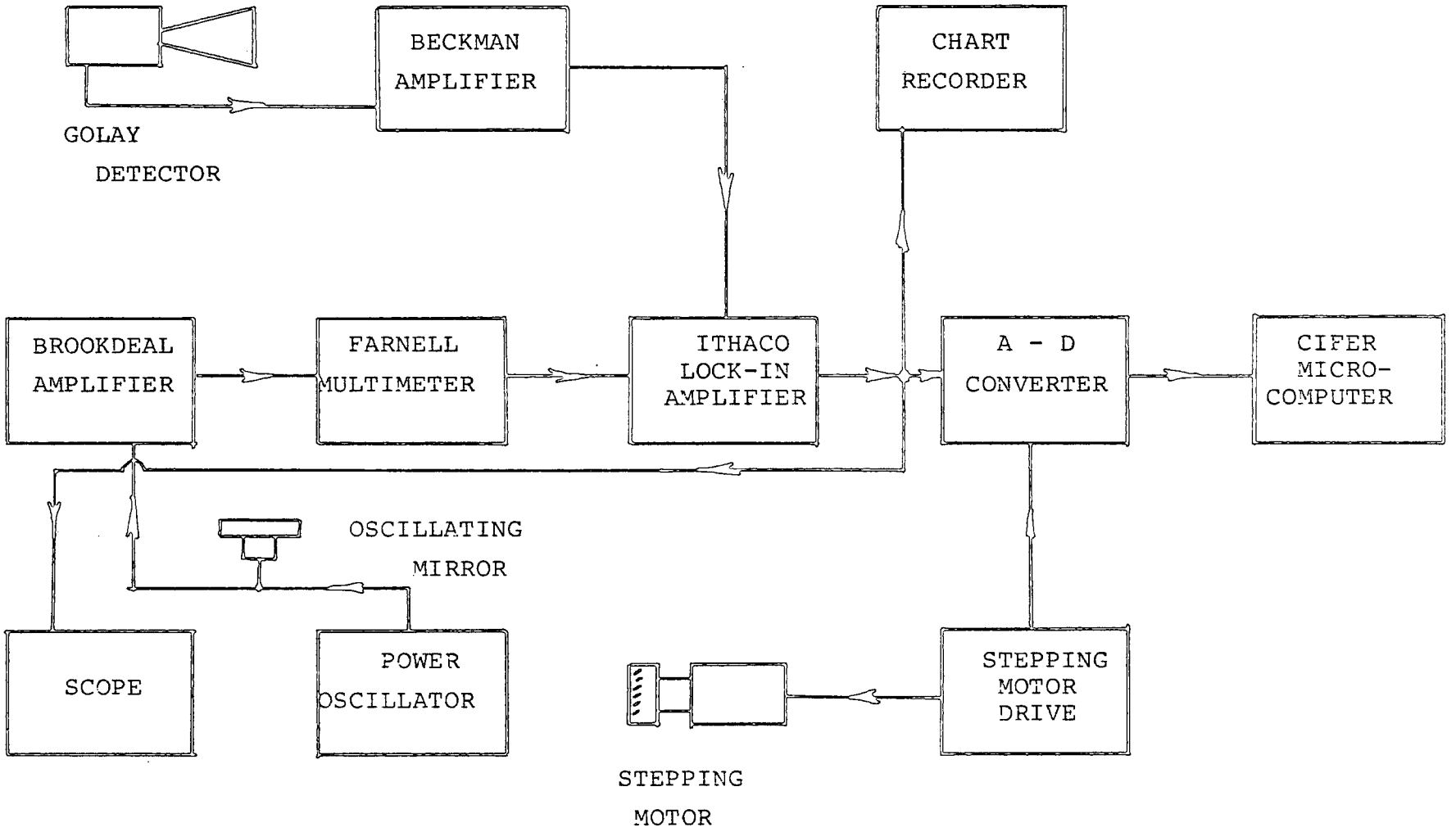

Figure 2.11 Schematic Diagram of Major System Electronics

Data points are collected equally on both sides of ZPD and then self-convoluted thus symmetrising the interferogram. The second method, "phase correction", only requires a few points past ZPD and assumes that the data has a finite but constant phase error. It is corrected using various computational methods which have been adequately described elsewhere.[13] The truncation of (ii) is overcome by a process termed "apodization". The method applies a "smoothing" function which gradually reduces the intensity such that it is zero at x_{max}.

The choice of sampling interval is an important consideration when spectral data at high frequencies is required. Sampling theory imposes an upper frequency limit which is dependent on the sampling interval by the expression[14]

$$\Delta x \leq \frac{1}{2\upsilon_{max}} \qquad \ldots\ldots \qquad \text{(eqn. 2.14)}$$

Thus a 10 μ sampling interval will have an upper frequency limit of 500 cm^{-1}. The problem is due to "folding" of the spectrum on itself and is known as "aliasing". It is usually overcome by either reducing the sampling interval or by the use of filters to block the high frequency components.

The resolution obtained by an interferometric method is a function of the time delay between the interfering beams and is thus dependent on the path difference. It can be shown that the theoretical resolution is given by:[13]

$$\text{Resolution} = \frac{1}{2x_{max}} \qquad \ldots\ldots\ldots \qquad \text{(eqn. 2.15)}$$

Apodization is known to reduce the resolution, usually by a factor of about 2 (approx).

2.4.4 Advantages of Interferometric Spectroscopy

Interferometry is usually linked with two well known advantages, the Fellgett (multiplex) advantage and the Jacquinot (throughput) advantage. Both lead to an increase in the signal to noise ratio. The Fellgett advantage arises from the fact that all spectral elements are analysed at the same time, whereas in dispersive spectrometers they are examined sequentially. The consequence of this is that the detector noise is relatively small compared to the size of the signal. Thus for a detector noise limited interferogram there is an improvement of signal to noise by a factor of $\sqrt{N_e}$, where N_e is the number of spectral elements equal to $\bar{\upsilon}_{max} - \bar{\upsilon}_{min}/\delta\bar{\upsilon}$.

Since no slits are used in the interferometer high energy throughputs are obtained and again the background energy from the detector is small compared to the signal. The improvement of signal to noise ratio in this way is referred to as the Jacquinot advantage.

2.5 Raman Spectroscopy

2.5.1 The Classical Theory of the Raman Effect[15]

Light incident upon a macroscopic system can be reflected, refracted, transmitted and scattered or absorbed. In this discussion we are more concerned with the scattering of light for which there are two theoretical approaches. The first, the classical theory while not wholly adequate leads to an understanding of a concept basic to this form of spectroscopy, the polarizability of a molecule.

When a molecule is placed in an electric field it suffers some distortion, its electron cloud is displaced relative to the nuclei. This generates an induced electric dipole moment (μ_D) within the molecule, the magnitude of which is a function of the applied field and the "ease of distortion" - the polarizability (α):

$$\mu_D = \alpha.F \qquad \text{..... (eqn. 2.16)}$$

When a sample of molecules is subjected to a beam of radiation of frequency ν the electric field experienced by each of the molecules oscillates according to equation 2.17

$$F = F_o \cos 2\pi\nu t \qquad \text{..... (eqn. 2.17)}$$

and the induced dipole also undergoes oscillation of frequency

$$\mu_D = \alpha.F = \alpha F_o \cos 2\pi\nu t \qquad \text{.... (eqn. 2.18)}$$

Such an oscillating dipole emits radiation of the same oscillation frequency. This interaction is termed Rayleigh Scattering. If, in addition, the molecule undergoes a vibration which changes the polarizability periodically, then the oscillating dipole will have superimposed upon it vibrational oscillation. If q_{vib} is a coordinate along the vibrational axis and is described by

$$q_{vib} = q_o \cos 2\pi\nu_{vib} t \qquad \text{..... (eqn. 2.19)}$$

at time t, then the polarizability will be

$$\alpha = \alpha_o + \left(\frac{\partial\alpha}{\partial q_{vib}}\right) q_{vib} \qquad \text{.... (eqn. 2.20)}$$

substituting for q_{vib} in equation 2.20 gives

$$\alpha = \alpha_o + \left(\frac{\partial \alpha}{\partial q_{vib}}\right) q_o \cos 2\pi\nu_{vib} \cdot t \qquad \text{(eqn.2.21)}$$

substituting in equation 2.18

$$\mu_D = \alpha_o F_o \cos 2\pi\nu t + \left(\frac{\partial \alpha}{\partial q_{vib}}\right) F_o q_o \cos 2\pi\nu_{vib} t \cdot \cos 2\pi\nu t$$

(eqn. 2.22)

If we then expand this expression and simplify trigonometrically we get

$$\mu_D = \alpha_o F_o \cos 2\pi\nu t + \tfrac{1}{2}\left(\frac{\partial \alpha}{\partial q_{vib}}\right) F_o q_o [\cos 2\pi(\nu - \nu_{vib})t + \cos 2\pi(\nu + \nu_{vib})t]$$

(eqn. 2.23)

Thus the oscillating dipole has frequency components $\nu \pm \nu_{vib}$ as well as the exciting frequency, these components are the Raman scattering frequencies. The above equation shows that if there is no change in polarizability during the vibration, *i.e.* $(\partial\alpha/\partial q_{vib}) = 0$, then the last two terms become zero and we observe only the Rayleigh scattering

$$\mu_D = \alpha_o F_o \cos 2\pi\nu t \qquad \ldots. \qquad \text{(eqn. 2.24)}$$

This is the primary selection rule for Raman scattering - "In order to be Raman active a molecular vibration must cause some change in the component of the molecular polarizability".

2.5.2 Quantum Theory and the Raman Effect

We consider the molecule in a stationary state as an unperturbed system, and investigate theoretically what happens when it is perturbed by an electric field that varies with time.

As in the classical treatment we use the polarizability of a particle, the distortion of the electron cloud. However, quantum mechanically this distortion is regarded as a perturbation of the electronic wave function. The ground state molecule is perturbed to a "virtual level" which corresponds to the original wave functions in addition to small contributions from all the other possible wave functions. This level does not really exist, it merely acts in perturbing the existing state.

If we consider the molecule in the vibrational ground state, the collision of a photon with energy $h\nu$, promotes the molecule to this virtual state. The molecule may then relax back down to the ground state or to a higher vibrational state, *i.e.* v, the vibrational quantum number = 1,2,3 *etc.*, with the release of a photon of appropriate energy. For example, relaxation to the first vibrational state results in the emission of a photon with frequency

$$\nu = \left(\frac{E_{v=1} - E_{v=0}}{h}\right) \qquad \ldots\ldots \qquad \text{(eqn. 2.25}$$

Relaxation back to the ground state results in Rayleigh scattering while the above process yields "Stokes" scattering. At temperatures where $kT(kJ\ mol^{-1})$ is greater than the energies of higher vibrational states, relaxation occurs to states lower in energy, so that the emitted photon has a frequency greater than the exciting frequency. This is "anti-Stokes" scatter, and its intensity at room temperature is very small since kT is smaller than the energy of the first vibrational level.

Figure 2.12 Diagram showing the Quantum Mechanical Formulation of Raman Scattering

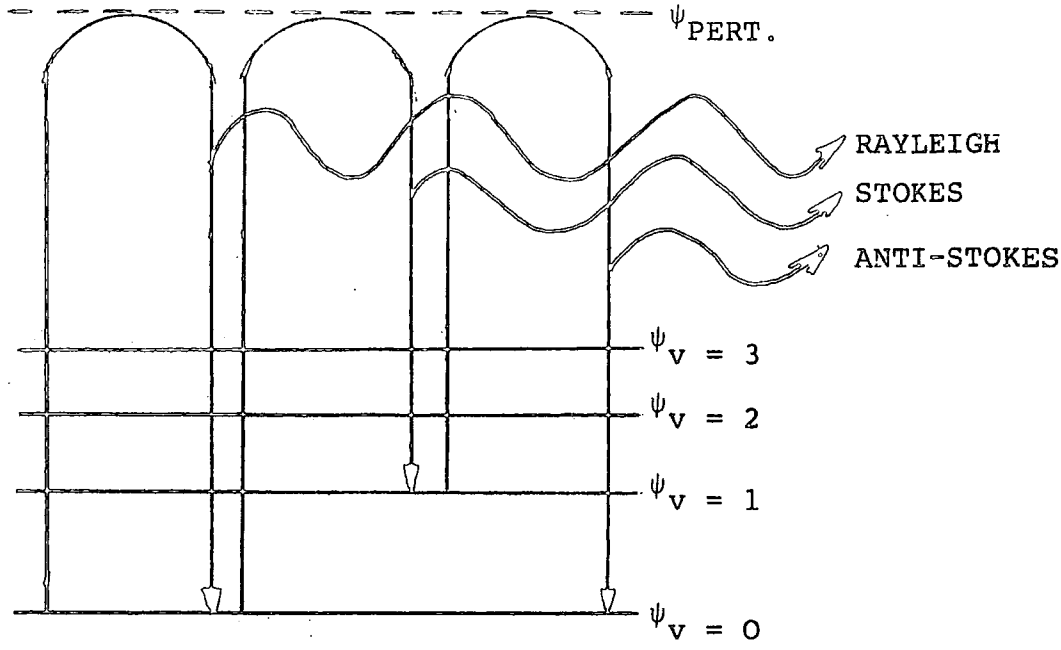

2.5.3 The Raman Tensor

We have seen that the quantum mechanical formulation of the Raman effect is analogous to the classical approach in that both lead to the idea of polarizability. Raman Theory eventually leads to the "Raman Tensor" and as a tensor property it must have the same symmetry properties as $\partial\alpha/\partial q_{vib}$ - it is this Raman tensor which controls the scattering of a molecule since it is governed by the selection rules.

$$\mu_D = \alpha F \qquad \ldots\ldots \quad \text{(eqn. 2.26)}$$

Since μ_D and F are vectors they must have directional properties, however, they are not necessarily in the same direction.

In order to define the induced dipole correctly, we must specify the direction in three dimensional space. This gives three simultaneous equations which specify the two vectors in cartesian coordinate space, *i.e.*

$$\mu_x = \alpha_{xx}F_x + \alpha_{xy}F_y + \alpha_{xz}F_z \quad \ldots \quad \text{(eqn. 2.27)}$$

$$\mu_y = \alpha_{yx}F_x + \alpha_{yy}F_y + \alpha_{yz}F_z \quad \ldots \quad \text{(eqn. 2.28)}$$

$$\mu_z = \alpha_{zx}F_x + \alpha_{zy}F_y + \alpha_{zz}F_z \quad \ldots \quad \text{(eqn. 2.29)}$$

These three simultaneous equations may be written as a matrix product:

$$\begin{pmatrix} \mu_x \\ \mu_y \\ \mu_z \end{pmatrix} = \begin{pmatrix} \alpha_{xx} & \alpha_{xy} & \alpha_{xz} \\ \alpha_{yx} & \alpha_{yy} & \alpha_{yz} \\ \alpha_{zx} & \alpha_{zy} & \alpha_{zz} \end{pmatrix} \begin{pmatrix} F_x \\ F_y \\ F_z \end{pmatrix} \quad \ldots \quad \text{(eqn. 2.30)}$$

The matrix involving the nine polarizability terms is the polarizability tensor. It is a second Rank tensor, that is, it has magnitude and nine components describing it in three directions. The above three matrices may be written as a matrix equation

$$\underline{\mu} = \underline{\alpha F} \quad \ldots \quad \text{(eqn. 2.31)}$$

Usually we find that $\alpha_{ij} = \alpha_{ji}$ so there are only six independent components and all may be assigned to irreducible representations in the character table of a molecular point group.

If a particular vibration is Raman active it will change one of the components of the polarizability tensor, one which has the same symmetry as the vibration. Irreducible

representations of the polarizability tensors (R_{ij}) are listed in character tables and may be obtained by performing each of the group operations on the α_{ij}'s as a basis set.

2.5.4 Polarization and the Raman Effect

In liquids we have an almost random orientation of molecules implying that the tensor description is constantly changing as well. However two properties of the tensor which remain constant are the "mean value" given the symbol $\bar{\alpha}$, and the "anisotropy" - $\gamma(\alpha)$. They may be defined as

$$\bar{\alpha} = \frac{1}{3}(\alpha_{xx} + \alpha_{yy} + \alpha_{zz}) \text{ and } \quad \ldots \quad \text{(eqn. 2.32)}$$

$$\gamma^2(\alpha) = \tfrac{1}{2}[(\alpha_{xx}-\alpha_{yy})^2 + (\alpha_{yy}-\alpha_{zz})^2 + (\alpha_{zz}-\alpha_{xx})^2 + 6(\alpha^2_{xy}+\alpha^2_{xz}+\alpha^2_{yz})] \quad \text{(eqn. 2.33)}$$

If we assume that molecules in the liquid state are randomly orientated, then because of the symmetric nature of the tensor the scattered light will have directional properties described by the "average scattering tensor", *i.e.*

$$\bar{\alpha}^2_{ii} = \bar{\alpha}^2_{zz} = \bar{\alpha}^2_{yy} = \bar{\alpha}^2_{zz} = \frac{1}{45}[45\bar{\alpha}^2 + 4\gamma^2(\alpha)] \quad \ldots \quad \text{(eqn. 2.34)}$$

and

$$\bar{\alpha}^2_{ij} = \bar{\alpha}^2_{xy} = \bar{\alpha}^2_{xz} = \bar{\alpha}^2_{yz} \equiv \frac{1}{15}\gamma^2(\alpha) \quad \ldots \quad \text{(eqn. 2.35)}$$

For convenience sake a set of orthogonal "laboratory axis" are chosen since the scattered light will have directional properties governed by the "average molecule". There will be two scattering geometries with respect to these laboratory axis:

(i) The Isotropic Scattering, originating from dipoles orientated in the same direction as the electric vector of the exciting light and given by the $\bar{\alpha}^2_{ii}$ components.

(ii) The Anisotropic Scattering, originating from dipoles orientated at 90^o to the electric vectors of the exciting light and given by the $\bar{\alpha}^2_{ij}$ components.

Generally vertically polarized light is used ($F_z \neq 0$) with both components (I_z and I_x) being collected at 90^o

Figure 2.13 Diagram illustrating the Scattering Geometry

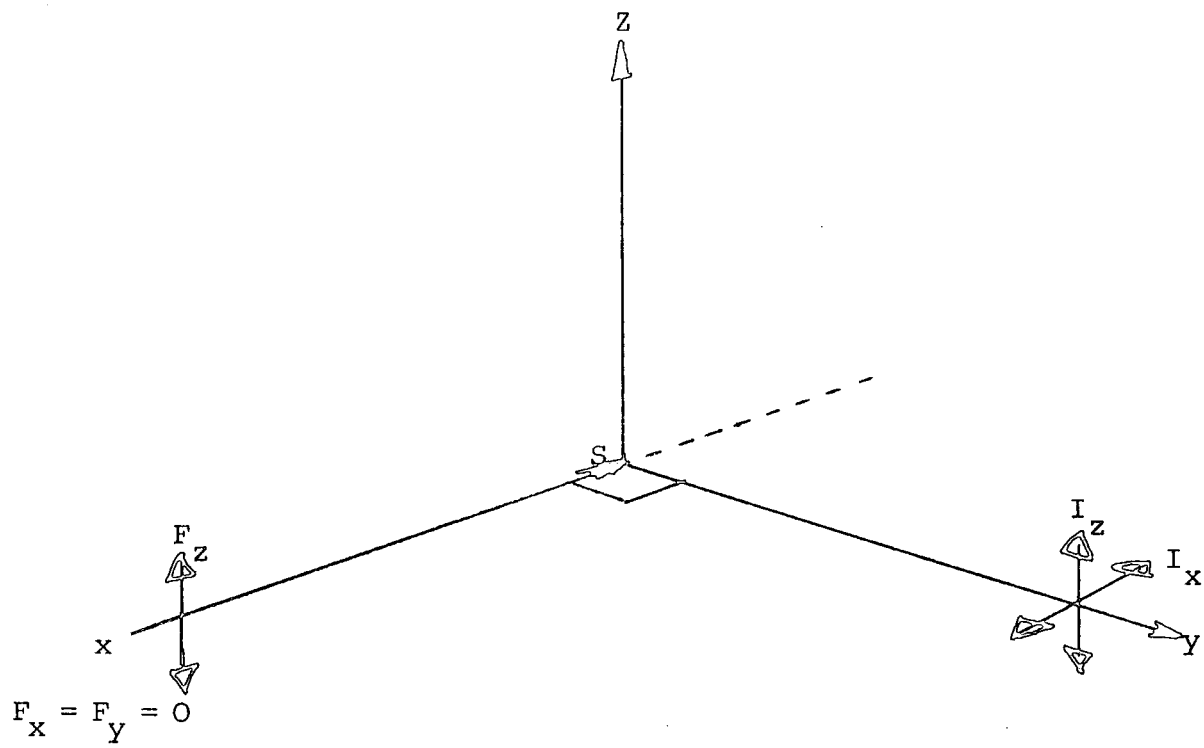

Since intensity is proportional to the square of amplitude, then

$$I_z = \bar{\alpha}^2_{zz} . F_z{}^2 k \qquad \ldots \qquad \text{(eqn. 2.36)}$$

and

$$I_x = \bar{\alpha}^2_{xz} \cdot F_z^2 \cdot k \qquad \ldots \quad \text{(eqn. 2.37)}$$

where k is the proportionality constant.

The extent of polarization of Rayleigh and Raman light is usually expressed in terms of the "depolarization ratio". For Raman light scattered at 90^o to the incident radiation this is given by:

$$\rho_1 = \frac{Ix}{Iz} = \frac{\alpha_{ij}^2}{\alpha_{ii}^2} \qquad \ldots \quad \text{(eqn. 2.38)}$$

$$= \frac{(1/15)\gamma^2(\alpha)}{(1/45)(45\bar{\alpha}^2 + {}^1{}^2(\alpha)} \qquad \ldots \quad \text{(eqn. 2.39)}$$

$$= \frac{3\gamma^2(\alpha)}{45\bar{\alpha}^2 + 4\gamma^2(\alpha)} \qquad \ldots \quad \text{(eqn. 2.40)}$$

For non totally symmetric vibrations, *i.e.* of E or T symmetry $\bar{\alpha}^2 = 0$, so that the depolarization ratio is equal to 3/4. However for totally symmetric vibrations of A_1 symmetry $\bar{\alpha}^2 \neq 0$ and the depolarization varies between two extremes, *i.e.*

$$0 \leqslant p \leqslant \tfrac{3}{4} \qquad \ldots \quad \text{(eqn. 2.41)}$$

Thus the depolarization ratio is a useful parameter in that it is able to distinguish between totally symmetric or other vibrations. The α and γ terms used in equations 2.38-2.40 refer to polarizability derivatives.

2.5.5 Instrumentation, the Cary 82

As with most Raman spectrometers, the Cary 82 may be divided into its radiation source, its optics and its signal processing. In this section we will describe briefly these aspects used in the above instrument.[16]

The radiation source in this case was a Spectra

Physics Argon ion laser operating on the "Green Line" (514.8nm). The laser was able to generate about 1.0 watt of power providing between 200 and 350 mW at the sample. The radiation is directed towards the sample by a series of mirrors, prisms and lenses. The first of these prisms (close to their Brewster angles) disperse the radiation thus separating the existing line from other unwanted plasma emissions (this feature was not necessary with the above laser). The beam is then collimated, and subsequently focussed on to the sample.

The scattered energy is collected at 90^{o} from the sample and enters a triple monochromator system. Figure 2.14 shows a schematic diagram of the optical arrangement within the spectrometer.[16] The monochromator system employs three diffraction gratings and four slits. The entrance and third slits actually define the operating conditions (*i.e.* the spectral slitwidth, *etc.*) with the second and fourth being set slightly broader and merely acting as stray light baffles. All four slits are coupled together by a common drive system as are the diffraction gratings. The analysed radiation, in the form of a 10mm image of the slit, is focussed on to the cathode of a photomultiplier tube.

The phototubes used in Raman are generally characterized by a wide spectral response, high gains, fast rise times and are often cooled to reduce their dark counts. The pulses are amplified by field effect transistors and are controlled from the front panel by the "sensitivity" switch. A discriminator sets a threshold voltage below which a signal is ignored, typically about 0.4V (with an average signal voltage of ≈1v). The pen period control (time constant) is

linked to the recorder, as is the scan speed thus synchronizing signal pulses with the monochromator assembly.

Figure 2.14 Schematic Diagram of the Optical arrangement of the Cary 82 Raman Spectrometer

(reproduced from ref.[16])

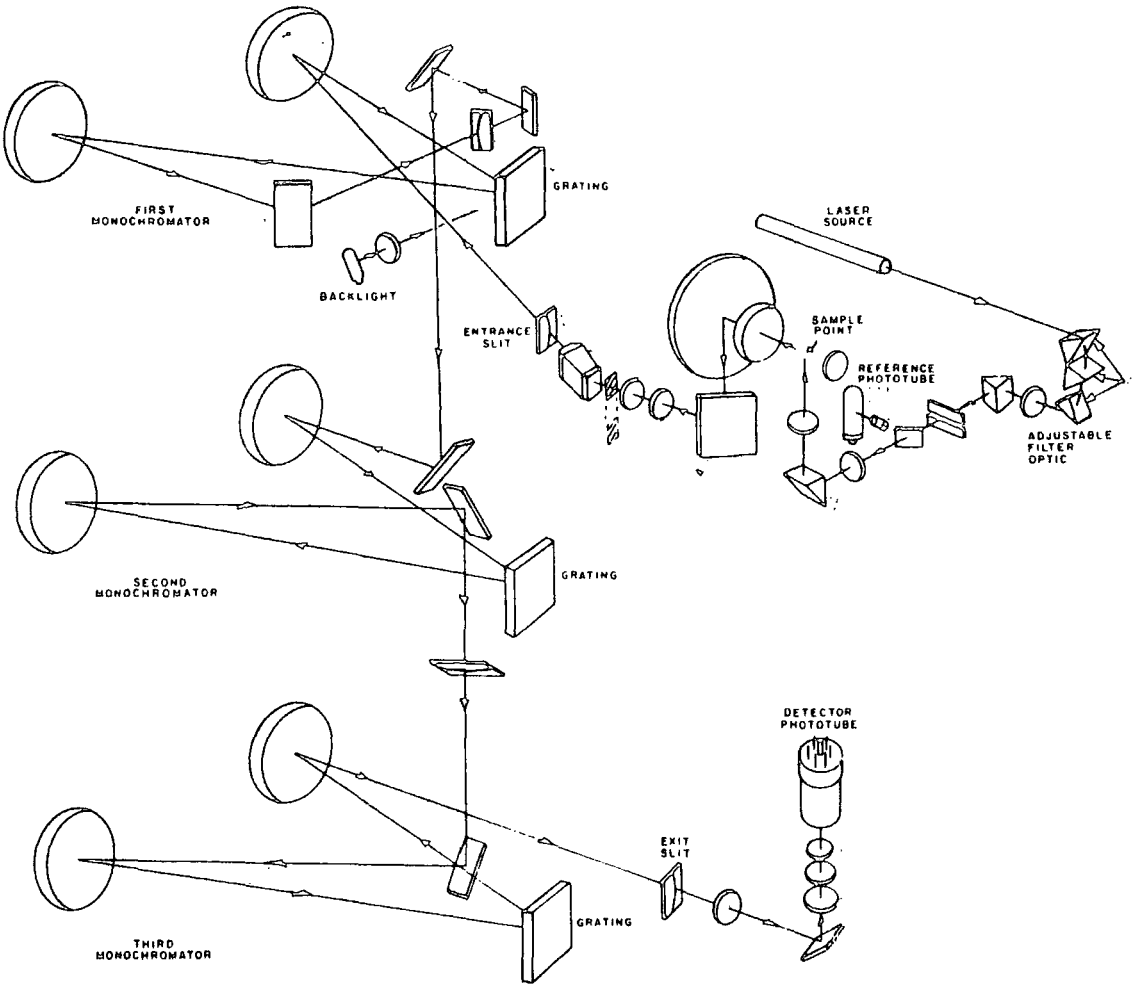

CHAPTER THREE

AGGREGATION BEHAVIOUR OF AMPHIPHILLIC MOLECULES IN POLAR AND APOLAR SOLVENTS. THE FORMATION OF NORMAL AND REVERSE MICELLES

3.1 Introduction

Molecules or ions which are said to be amphiphillic are usually made up of two parts, a hydrophillic or "water attracting" part, and a hydrophobic or "water repelling" part. This dual character confers unique properties on

Figure 3.1 Schematic Diagram of a Simple Amphiphile Molecule

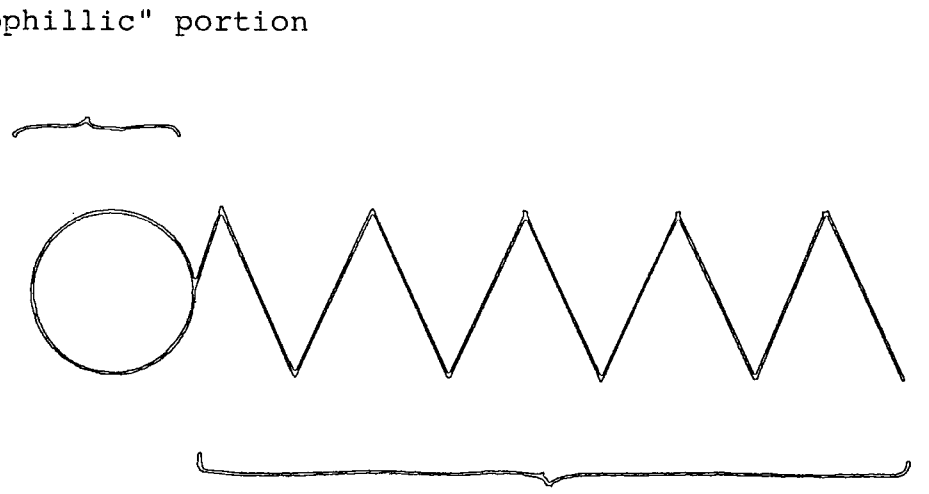

such molecules, particularly when they are dissolved in a solvent such as water. The hydrophobic portion of the molecules will seek an environment where water contact is at a minimum[19]. This environment may be an interface, or a self aggregated group of molecules known as a micelle. Figure 3.2 illustrates amphiphile behaviour at the air-water interface, the hydrophobic hydrocarbon chains being directed away from the solvent, while Figure 3.3 depicts one of the first notions of micellar structure as envisaged by Hartley almost fifty years ago.[20]

Figure 3.2 Behaviour of Amphiphiles at the Air-water Interface

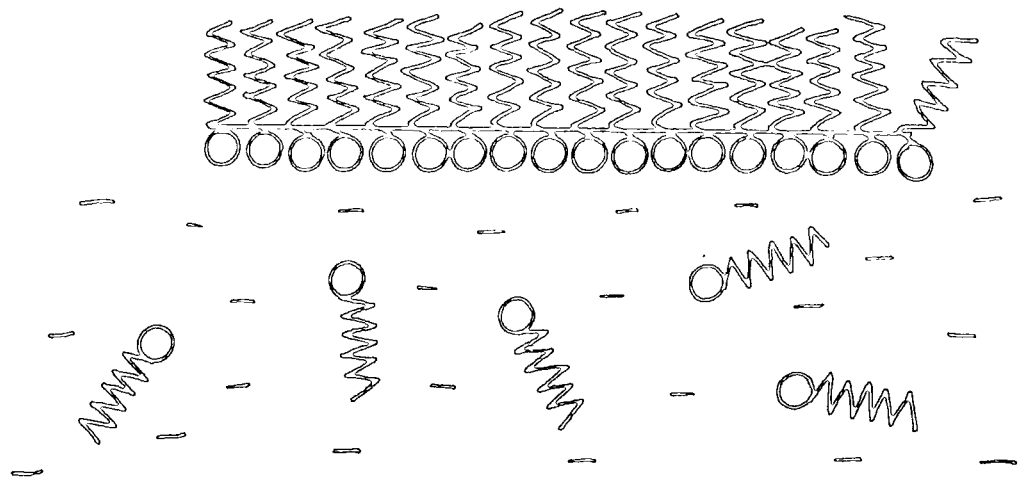

(Note: At low surfactant coverages the hydrophobic chains lie on the water surface).

Figure 3.3 The "Hartley" Micelle

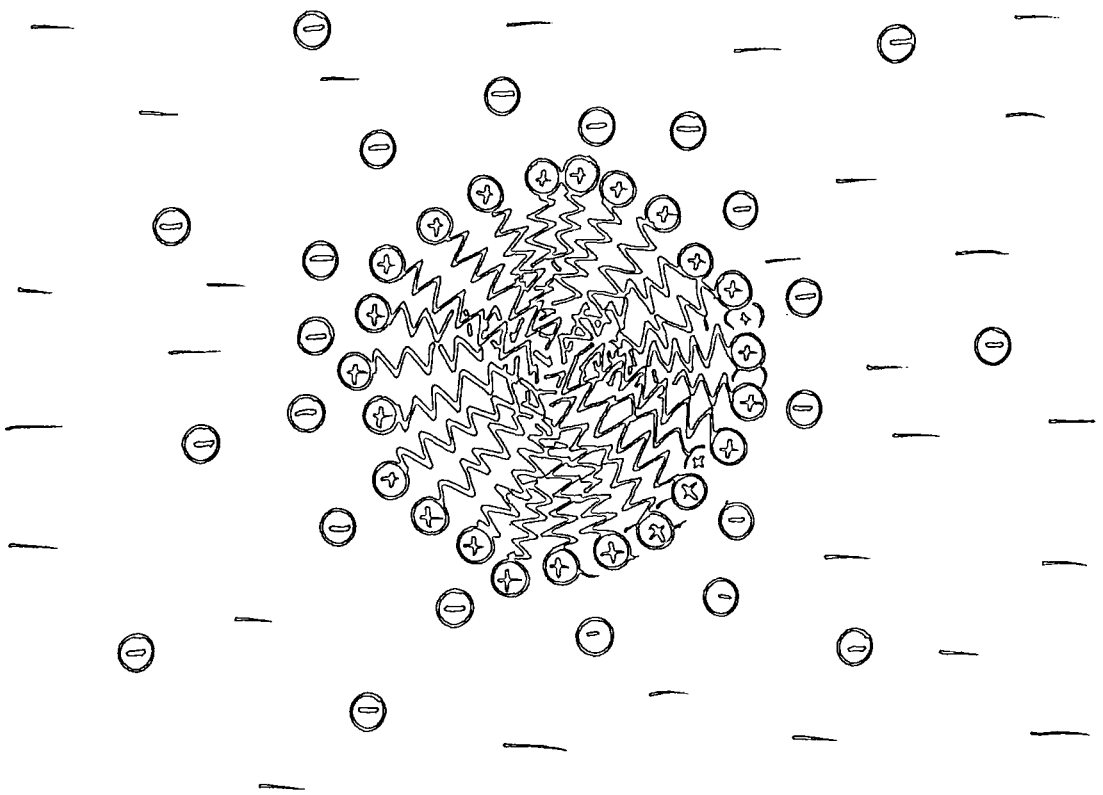

It is the micellar behaviour of these amphiphiles, or surfactants as they are often called, which concerns us in this chapter. The formation of micelles occurs over a narrow concentration range termed the critical micelle concentration (CMC). The value of the CMC is a function of many variables such as hydrocarbon chain length, headgroup dimensions, counter ion, *etc.*, and so one finds each surfactant has its own unique value. Amphiphiles are classified according to the charge (if one exists) of the head group. Cationic and anionic surfactants have positively and negatively charged head groups, respectively, while those having no charge are termed nonionic. For an amphiphile possessing a dodecyl chain the above ionic surfactants have CMCs of the order of 10^{-2} - 10^{-3} mol.ℓ^{-1} while nonionics have lower values, *i.e.* 10^{-5} mol.ℓ^{-1}. [21]

Determination of the CMC usually relies on some physical method which is able to detect the appearance of micelles, for example due to their size or to the change in the number of solute species (colligative properties). Figure 3.4 shows the behaviour of some physical properties at and around the CMC.[22] Surfactant aggregates tend also to show similar behaviour in their size distribution curves. The concentration of aggregates (of Size A) is plotted against aggregation number, N_A, as shown in Figure 3.5. Typically the maximum occurs between values of 50 and 200 for N_A, but in general, in aqueous media, the longer the hydrocarbon chain the greater the aggregation number.[21]

When studying micellar systems it is important to work above a temperature known as the Krafft point.[23] It is the

Figure 3.4 The Behaviour of Some Physical Properties near the CMC

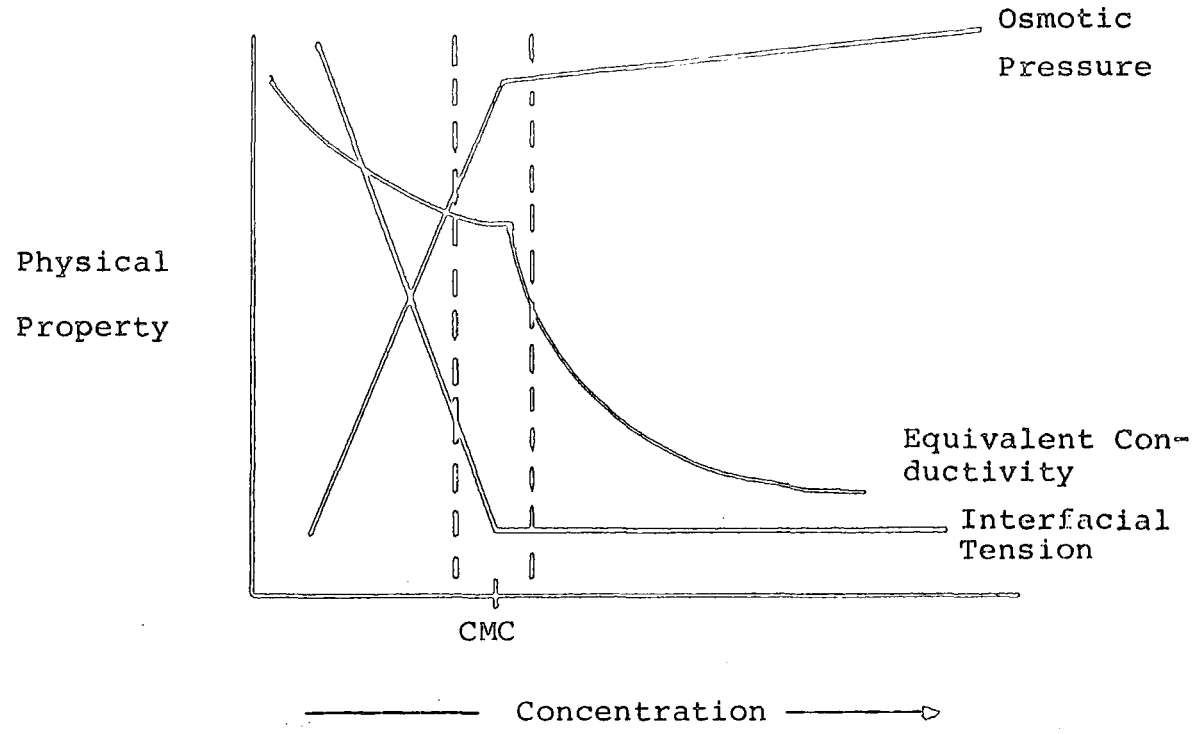

Figure 3.5 The Micelle size distribution Curve for a typical surfactant

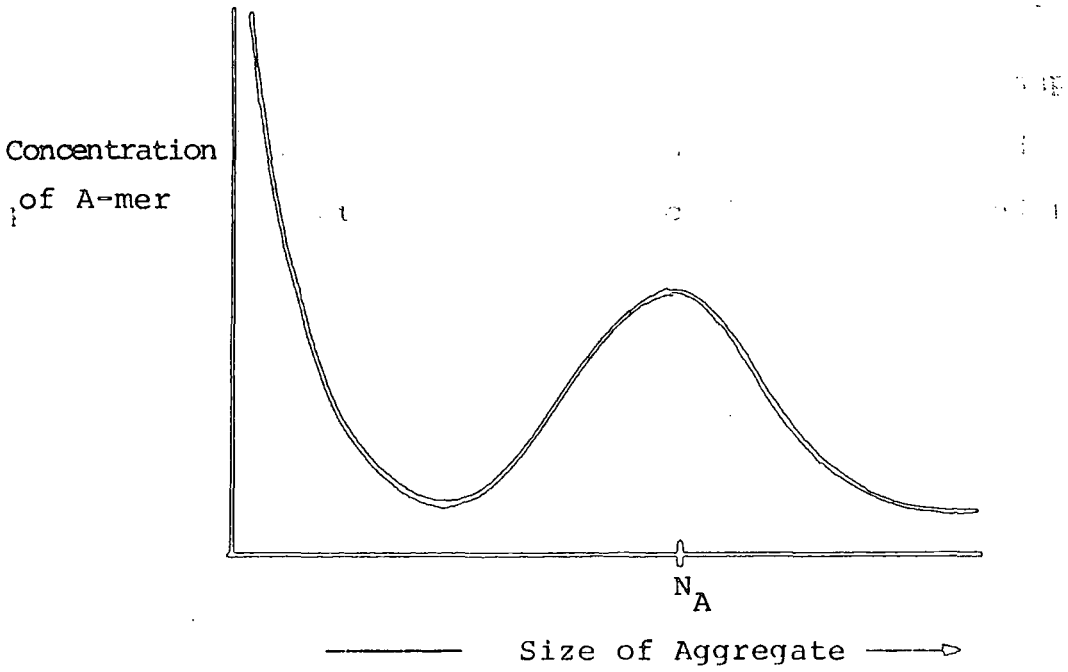

$\bar{N}_A$ is the average aggregation number of the A^{th} associated species (for a symmetrical distribution of A-mers)

temperature below which micelles cannot form due to limited surfactant solubility. The Krafft point may be extended across the whole concentration range to form a Krafft boundary. The more common nonionic surfactants, those of the polyoxyethylene type, usually show even more interesting behaviour at a temperature called the "cloud point". As the name suggests, surfactant solutions show an opalescence at this point which, like the Krafft point, may also be extended over the concentrations range to form a "consolute boundary". The boundary may be convex as shown by tetraoxyethylene octyl ether (C_8E_4) in water,[85] in which case it is called a lower consolute boundary.

Our understanding of micelles has much advanced since the days of Hartley.[20] It is now thought that as well as spherical micelles several other shapes are possible. These include rod and disc micelles. In addition some surfactants form reverse micelles particularly when the amphiphile possesses two alkyl chains and / or a small head group[87], (see Figure 3.7). Properties such as micelle size and shape may be considered in terms of head group interactions and chain packing considerations. The topic will be discussed further in Section 5.3.

3.2 Thermodynamics of Micelle Formation

In order to understand micellar behaviour one must consider all the forces and interactions between the surfactants themselves and their environment. When water is used as the solvent, it is the "antagonistic" balance between hydrophillic and hydrophobic effects which controls micelle formation.[19]

Figure 3.6 The Phase Diagram for C_8EO_4 (reproduced from Ref.24).

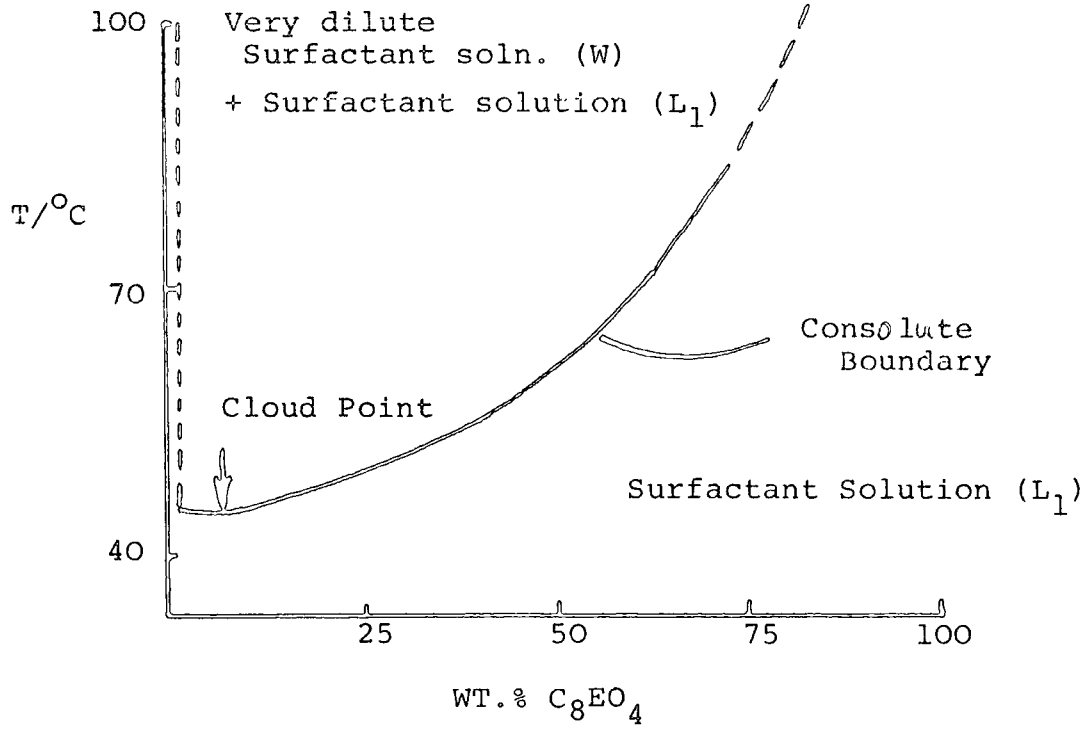

Figure 3.7 The Various Micellar Shapes

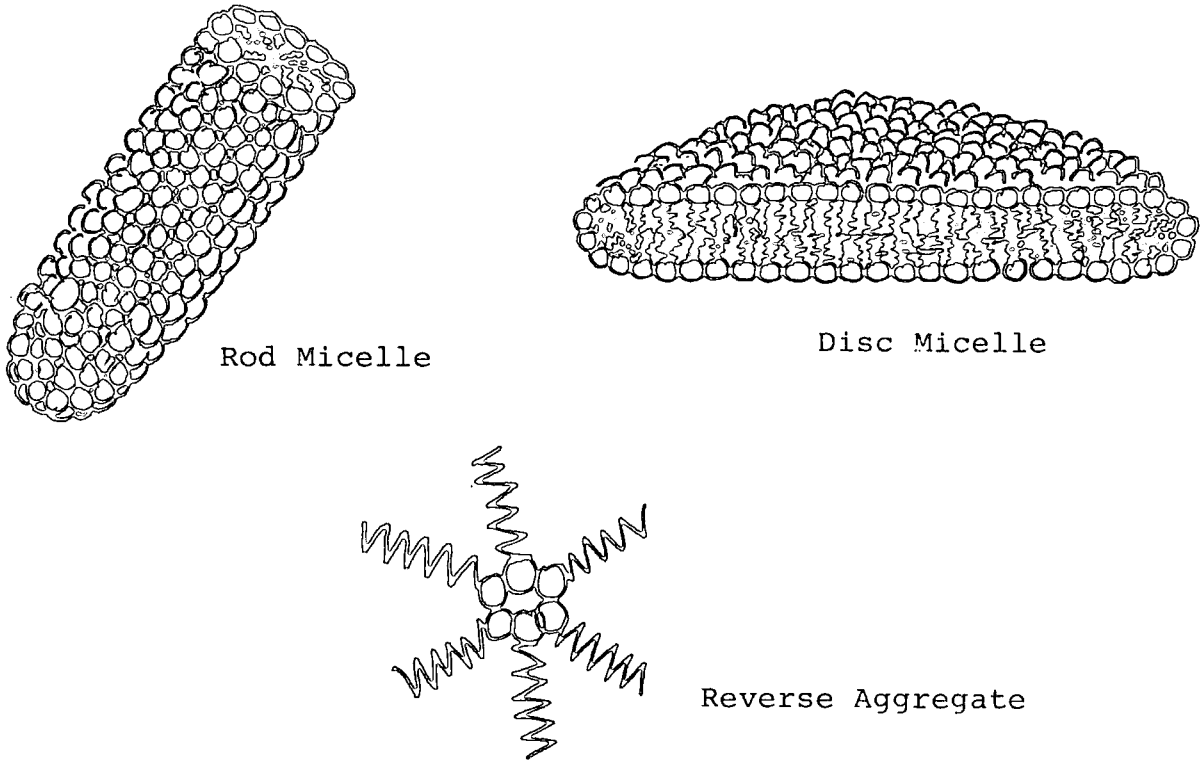

We may begin to understand, quantitatively, micellar behaviour if we consider the above effects in terms of a number of intensive variables, the most important of which being the surfactant chemical potential (μ). In particular, it is the change in chemical potential of the surfactant molecules, on going from a water environment to that of an aggregated one:

$$\Delta\mu = \mu_{agg} - \mu_{aq} \qquad \text{(Eqn. 3.1)}$$

There are four thermodynamical models to describe surfactant aggregation:[27] there being the phase separation model, the mass action model, the multiple equilibrium model and the small systems model. The first two approaches are approximations, the phase separation model assumes the micelle to be a separate phase while the mass action model assumes a single aggregation number.[27] The multiple equilibrium and small system models are entirely rigorous, though the former is most widely used for its simplicity.[28] The small system model has not been discussed here, the interested reader is directed to the review by Hall and Rethica.[29]

3.2.1 The Phase Separation Model

If one considers the micelle as a separate phase, then one may distinguish between the chemical potentials of surfactant in monomer and micellar form, μ_{AQ} and μ_{MIC} respectively. At low concentrations of surfactant, below the CMC, one may write the standard relation:

$$\mu_{AQ} = \mu^{\theta}_{AQ} + KT\ln(f.x) \qquad \text{(eqn. 3.2)}$$

where f and x are the activity coefficientand mole fraction of the monomer. However at the CMC the chemical potential of the two phases are equal such that

$$\mu_{AQ} = \mu_{MIC}^{\theta} \qquad \text{(eqn. 3.3)}$$

and one may write

$$\mu_{MIC} = \mu_{AQ}^{\theta} + KT\ln fx^{CMC} \qquad \text{(eqn. 3.4)}$$

Such a treatment does not however allow for micelle size and shape changes and assumes that the concentration of non-micellar molecules is constant above the CMC.[27]

3.2.2 The Mass Action Model

The model identifies the micelle as having a fixed aggregation number, N_A, such that one may write the equilibrium relationship:

$$AM_1 \rightleftharpoons (M_1)_A \qquad \text{(eqn. 3.5)}$$

and thus

$$K_A = \frac{(f_A x_A)}{(f_1 x_1)^A} \qquad \text{(eqn. 3.6)}$$

The treatment assumes a single aggregate size and that the activity coefficients are concentration independent.[27]

3.2.3 The Multiple Equilibrium Model

The model first proposed by Corkill *et al*[28] is probably the most used in surfactant chemistry. It is exact and allows one to obtain monomer concentrations from measurement of a single colligative property. Unlike the mass action

model this treatment assumes a distribution of aggregates from which an average may be calculated.[28]

If we define x_c as the colligative mole fraction *i.e.* a measure of the total number of particles, then

$$x_C = x_m + \sum_{A=2}^{A'} x_A \qquad \text{(eqn. 3.7)}$$

where x_m is the monomer mole fraction and x_A is the mole fraction of A^{th} aggregated species. Using the standard relation we may write

$$\mu_m = \mu_m^{\theta} + KT\ln x_m \qquad \text{(eqn. 3.8)}$$

$$\mu_A = \mu_A^{\theta} + KT\ln x_A \qquad \text{(eqn. 3.9)}$$

for the aggregated and unaggregated molecules. Now at equilibrium all molecules in either monomeric or aggregated states have equal chemical potential, such that:

$$N_A\mu_m = \mu_A \qquad \text{(eqn. 3.10)}$$

where N_A is the aggregation number of the A^{th} species. Substituting for μ_m and μ_A in equation 3.10

$$N_A(\mu_m^{\theta} + KT\ln x_m) = \mu_A^{\theta} + KT\ln x_A \qquad \text{(eqn. 3.11)}$$

If we make x_A the subject of the equation then 3.11 becomes

$$\ln x_A = (N_A.\mu_m^{\theta} - \mu_A^{\theta})/KT + N_A\ln x_m \qquad \text{(eqn. 3.12)}$$

Differentiation of the above expression with respect fo $\ln x_m$ deletes the first term on the right since it is a constant.

$$\Longrightarrow \frac{d\ln x_A}{d\ln x_m} = N_A \qquad \text{(eqn. 3.13)}$$

Equation 3.13 may be written as

$$\frac{dx_A}{d\ln x_m} \cdot \frac{1}{x_A} = N_A \qquad \text{(eqn. 3.14)}$$

$$\Longrightarrow \quad \frac{dx_A}{d\ln x_m} = N_A \cdot x_A \qquad \text{(eqn. 3.15)}$$

If we multiply equation 3.15 by N_A^k (where k is a positive integer) and sum with respect x_A then

$$\frac{d \sum_{A=2}^{A'} N_A^k \cdot x_A}{d\ln x_m} = \sum_{A=2}^{A'} N_A^{k+1} \cdot x_A \qquad \text{(eqn. 3.16)}$$

A' is the largest aggregate.

Differentiation of equation 3.7 with respect to $\ln x_m$ gives

$$\frac{dx_c}{d\ln x_m} = \frac{dx_m}{d\ln x_m} + \frac{d \sum_{A=2}^{A'} x_A}{d\ln x_m} \qquad \text{(eqn. 3.17)}$$

since

$$\frac{dx_m}{d\ln x_m} = \frac{dx_m}{dx_m} \cdot x_m \qquad \text{(eqn. 3.18)}$$

and substituting for $\frac{d \sum_{A=2}^{A} N_A^k \cdot x_A}{d\ln x_m}$ (with $k = 0$) of equation 3.16, equation 3.17 becomes,

$$\frac{dx_c}{d\ln x_m} = x_m + \sum_{A=2}^{A'} N_A \cdot x_A \qquad \text{(eqn. 3.19)}$$

The right hand side of equation 3.19 is equal to the total surfactant concentration which we shall call x_t:

$$\frac{dx_c}{d\ln x_m} = x_t \qquad \text{(eqn. 3.20)}$$

$$\Longrightarrow \ln x_m = \int x_t^{-1} . dx_c . \qquad \text{(eqn. 3.21)}$$

Thus the area under the curve of a plot of x_c against x_t^{-1} will give $\ln x_m$, the log of the monomer mole fraction.

Equation 3.21 is in the form often used when colligative properties of surfactant systems are measured to obtain monomer concentrations. Since the data obtained by i.r. spectroscopy already provides monomer levels as a function of total concentration, we require a relationship linking these parameters with the aggregation number (the Corkill model[28] uses the colligative and monomer mole fractions directly). Such a relationship has been derived by Aveyard *et al*:[30]

For the equilibrium below

$$AM_1 \rightleftharpoons (M_1)_A$$

we may write

$$x_t = \sum_{A=1}^{A'} N_A . x_A = x_m + \sum_{A=2}^{A'} N_A . K_{1,A} . (x_m)^A \qquad \text{(eqn. 3.22)}$$

where the notation is as before and $K_{1,A}$ is the equilibrium-constant describing the above equilibrium, *i.e.* $K_{1,A} = x_A/(x_m)^A$.

If we now simplify 3.22 by assuming a single average aggregation number, $\bar{N}_A$, (*c.f.* Mass action model) we may write

$$x_t = x_m + \bar{N}_A . K_{1,A} (x_m)^{\bar{N}_A} \qquad \text{(eqn. 3.23)}$$

$$\Longrightarrow x_t - x_m = \bar{N}_A . K_{1,A} . (x_m)^{\bar{N}_A} \qquad \text{(eqn. 3.24)}$$

Taking logs,

$$\ln(x_t - x_m) = \bar{N}_A \ln x_m + \ln \bar{N}_A . K_{1,A} \qquad \text{(eqn. 3.25)}$$

Thus the slope of a plot of $\ln(x_t - x_m)$ against $\ln x_m$ gives $\bar{N}_A$ the average aggregation number, *i.e.*

$$\frac{\partial \ln(x_t - x_m)}{\partial \ln x_m} = \bar{N}_A \qquad \text{(eqn. 3.26)}$$

The above equation has been used to determine the average aggregation numbers of polyoxyethylene surfactants in some apolar solvents (see Chapter Four).

3.3 Factors Influencing the CMC and Micelle Size

3.3.1 The Head Group

The CMC behaviour of nonionic surfactants is quite different to that found in ionic amphiphiles. The former lack the electrostatic repulsions of their ionic counterparts, consequently CMC values for nonionic surfactants (and zwitterionics) tend to be one to two orders of magnitude lower. An increase in the number of hydrophillic groups or moving one down the alkyl chain increases the CMC. With typical nonionic surfactants, such as those of the polyoxyethylene type, a decrease in the number of oxyethylene units results in a decrease of the CMC. The above effect is thought to arise from a decrease in the amphiphile hydrophillic character.[21]

The micellar size, most easily determined by light scattering,[19] tend to follow the same pattern as the CMCs. In general the greater the dissimilarity between the

amphiphile and the solvent, the larger the aggregation number. The actual distribution of micelles, *i.e.* the polydispersity, increases as the aggregation number increases. Thus very large micelles have very broad size distributions functions (see Figure 3.5).

3.3.2 The Hydrophobic Chain

Since the phenomenon of micelle formation is largely dependent on the hydrophobic effect, it is not surprising to find that the hydrocarbon tail of a surfactant strongly affects the CMC. Under normal circumstances of a straight chained saturated aliphatic hydrocarbon chain, an increase in length is associated with a decrease in the CMC. Figure 3.8 below shows the weight average micelle aggregation numbers ($\bar{M}_w$), as determined by light scattering.[19]

Unsaturation and substitution of polar groups, *e.g.* oxygen in the chain, increases the CMC while replacement of alkyl hydrogens with fluorine (perfluoro surfactants) decreases the CMC. Chain branching is thought to approximately double the CMC compared to a straight chained analogue with the same number of carbons.[21]

Figure 3.8 Aggregation Behaviour of Some Amphiphiles as a Function of Chain Length
(reproduced from reference 19).

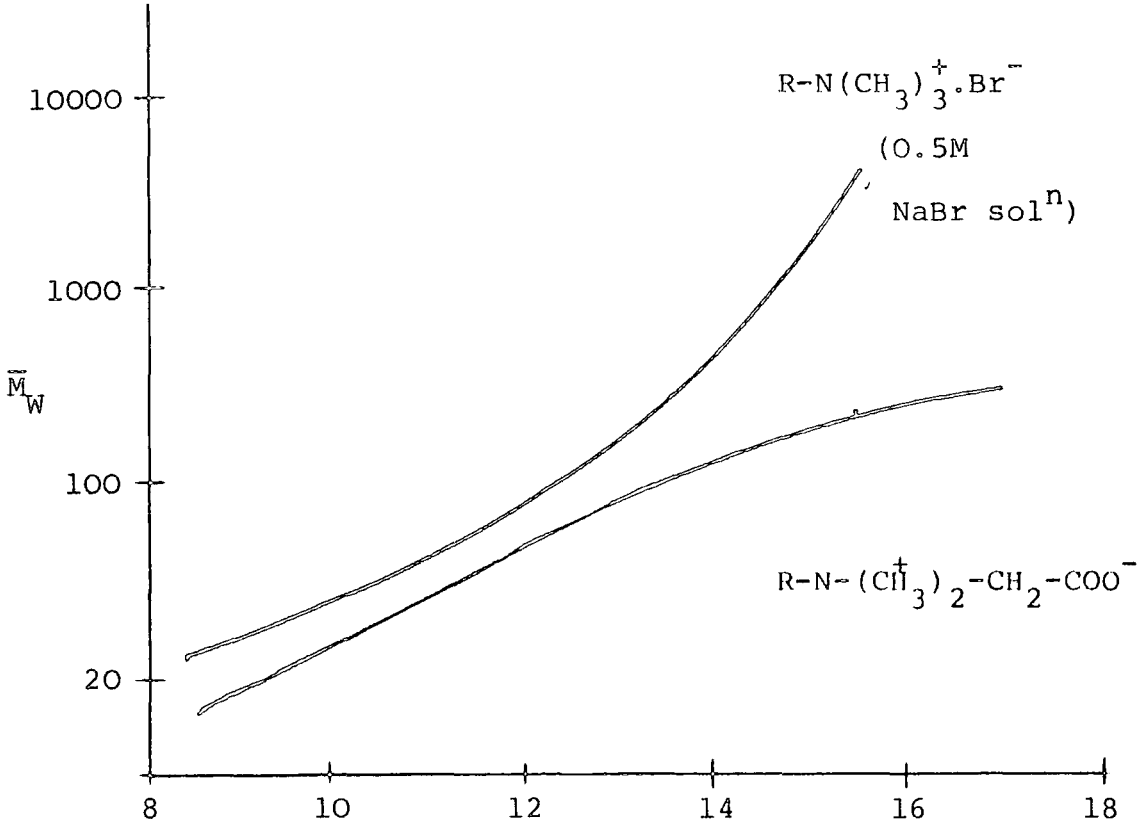

3.3.3 The Counter Ion

The behaviour of surfactant counter ions is a complex subject and only a brief resumé will be given here, (see Section 5.4 for a more detailed account of counter ion binding). However, if we make the generalization that increased counter ion binding is accompanied with a decrease in the CMC, then this latter property will be a function of the polarizability, hydration radius and valency.[21] Generally speaking it has been reported that the polarizability and valency increase the binding while an increased hydration radius has the opposite effect.[21] For aqueous solutions of

alkyl sulphates Rosen[21] has proposed the following series in order of decreasing CMC,

$Li^+ > Na^+ > K^+ > Cs^+ > N(CH_3)_4^+ > N(C_2H_5)_4^+ > Ca^{2+} > Mg^{2+}$ ⟶ Greater binding.

and for the cation dodecyl trimethylammonium,

$F^- > Cl^- > Br^- > I^-$.

3.3.4 Added Electrolyte and Temperature

It is reasonably well known that the effect of added electrolyte on nonionic surfactants is small.[27] However the behaviour of ionic amphiphiles is quite different with large decreases in the CMC being observed.[27] The effect is thought to arise from a reduction of electrostatic repulsion at the head group (which tend to be smaller in nonionic surfactants). Some care in interpretation is needed when the added electrolyte does not share the same ion as that of the surfactant. In these cases the results may be affected by changes in counter ion binding, as mentioned in the previous paragraph. Figure 3.9 shows the behaviour of two structurally similar ionic amphiphiles at 30°C with the addition of sodium chloride (surfactant concentration kept constant).

Both curves show an increase in micellar size (and a decrease in CMC), but the ammonium head group shows a greater dependence. One possible explanation for this behaviour may be due to the smaller size of the head group allowing easier shape changes, *e.g.* such as sphere to rod (see Chapter Five).

Figure 3.9 The Effect of Added Electrolyte on Micellar Aggregation at 30°C

(reproduced from reference 19)

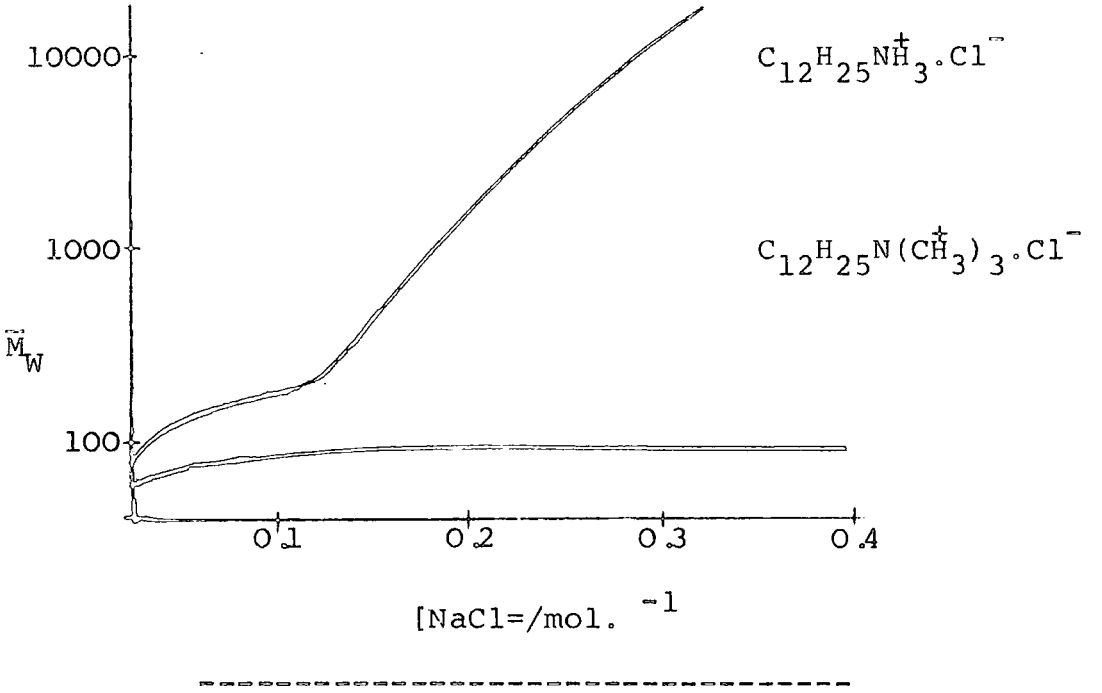

The effect of temperature on ionic amphiphiles is small. Nonionic surfactants however show a much larger temperature dependence. Of particular interest is the cloud point behaviour exhibited by many polyoxyethylene alkyl ethers.[24] These molecules often display a lower consulate boundary which is thought to be related to a dehydration of the head group as the temperature is increased. Zwitterionic surfactants have also been known to show cloud point behaviour. In the case of the ammonium decyl dimethyl ethyl sulphate-water system an upper consolute boundary is observed.[91]

3.4 The Kinetics of Micelle Formation

One may define a slow kinetic process as occurring with a relaxation time of $\tau > 1s$. The rate of attainment of equilibrium in micellar systems is often considered in terms of two independent kinetic processes. This treatment, that of Anianson and Wall, distinguishes a fast and slow process.[34,35] The fast process may be described as the association and dissociation of monomers from/to the micelle *i.e.*

$$M_{n-1} + M_1 \underset{K_{\mathbb{N}}^-}{\overset{K_{\mathbb{N}}^+}{\rightleftharpoons}} M_n \qquad \text{(eqn. 3.27)}$$

The second process is generally much slower and corresponds to the formation and dissociation of micelles leading to a change in the total number of aggregates, *i.e.*

$$mM_n \rightleftharpoons nM_m \qquad n,m \neq 1 \qquad \text{(eqn. 3.28)}$$

The theory makes two assumptions, firstly that the former process is much faster than the latter, and secondly that the concentration of oligomers (*i.e.* small aggregates, dimers, trimers, *etc.*) is low. The rate of the second process may be rationalized if one recollects the minimum in the size distribution curve of Figure 3.5. The diagram shows that the concentration of the oligomers is small and so attainment of true equilibrium will be slow.

Relaxation times for the fast process are generally obtained using a technique which has an observation window of around 10^{-2} - 10^{-8}s or less. Thus for larger

amphiphiles, $C_n > 14$, where the relaxation time is relatively large ($\simeq 10^{-4}$s), ultrasonic relaxation has proved to be a useful technique. As well as being used for the fast process, temperature and pressure jump techniques are generally used for measurement of slow process. In addition to the rates of reaction, further information may be obtained directly from the Aniansson and Wall treatment.[34,35] Particular emphasis is drawn to the calculation of the rate of monomer dissociation (K_N^-) and also the width of the micelle distribution (σ) which may be calculated from equation 3.29.[27]

$$1/\tau_1 = K_N^-/\sigma + K_N^- a_e/N_A^- \qquad \text{(eqn. 3.29)}$$

τ_1 is the relaxation time for the fast process, a_e is the deviation from equilibrium and $\bar{N}_A$ is the average aggregation number calculated using some other technique such as light scattering. For further details of the Aniansson and Wall treatment the interested reader should consult the respective references.[34,35]

3.5 Inverse Micelles and Reverse Aggregation

3.5.1 Introduction

Until fairly recently widespread interest in surfactant systems has been limited to aqueous environments. The study of surfactant behaviour in non aqueous systems has increased due to the potential application of such knowledge to catalysis, the mimicking of biological membranes, oil recovery and also for their use as solubilizing agents.

Although the majority of this chapter has been devoted to the understanding of basic principles of aggregation in aqueous systems, it is this section which is of direct relevance to the work carried out in Chapter Four. As mentioned in the introduction to this chapter it is important to establish the similarities and differences between the two systems. In this section we will thus elaborate on the physiochemical principles leading to aggregation in non aqueous systems.

3.5.2 Surfactant Association in Non Polar Media

Earlier in this chapter we found that micelle formation in aqueous systems is almost entirely due to the hydrophobic effect.[19] The formation of micelles (or not) in organic solvents, termed "inverse micelles", proceeds by a qualitatively different mechanism. For example, solvent-solute interactions tend to be smaller. In general, the driving force for aggregation of surfactants in apolar solvents is mutual attraction for the head groups. Though the solubility of ionic surfactants in apolar solvents is low,

dissolved amphiphiles will exist as ion pairs and exert strong dipolar attractions for each other. The addition of water to these systems causes gradual hydration and tends to draw the molecules together in an effort to minimise head group/water-solvent contact. For nonionic polyoxyethylene surfactants, such as those studied in Chapter Four, the mechanism of association is slightly different and the association process relies on other interactions. There may be dispersion interactions, dipole-induced dipole, *etc.* Further complications arise when one considers "coiling" of the head group (particularly with polyoxyethylene surfactants) thus generating an extra entropy term in the system thermodynamics.

When one particular physiochemical property of these systems is studied, *e.g.* light scattering, vapour pressure osmometry, a gradual change with concentration is often observed as opposed to an abrupt change which occurs at the CMC in aqueous systems. Figure 3.10 shows the behaviour of monomer concentration as a function of total amphiphile for some hypothetical surfactants. The diagram shows that it is difficult to define a CMC, and since workers have detected small aggregates as low as 10^{-6} moles per litre,[37] association must therefore follow some stepwise mechanism.

Aggregates in these systems tend to be small. Generally the size varies between 2 and 10-mers with a gradual increase in $\bar{N}_A$ (the average aggregation number) as the concentration is raised. With such small aggregates the determination of shape becomes difficult using techniques such as light scattering.

Figure 3.10 Monomer Levels expected with surfactants showing Gradual and Micellar Association

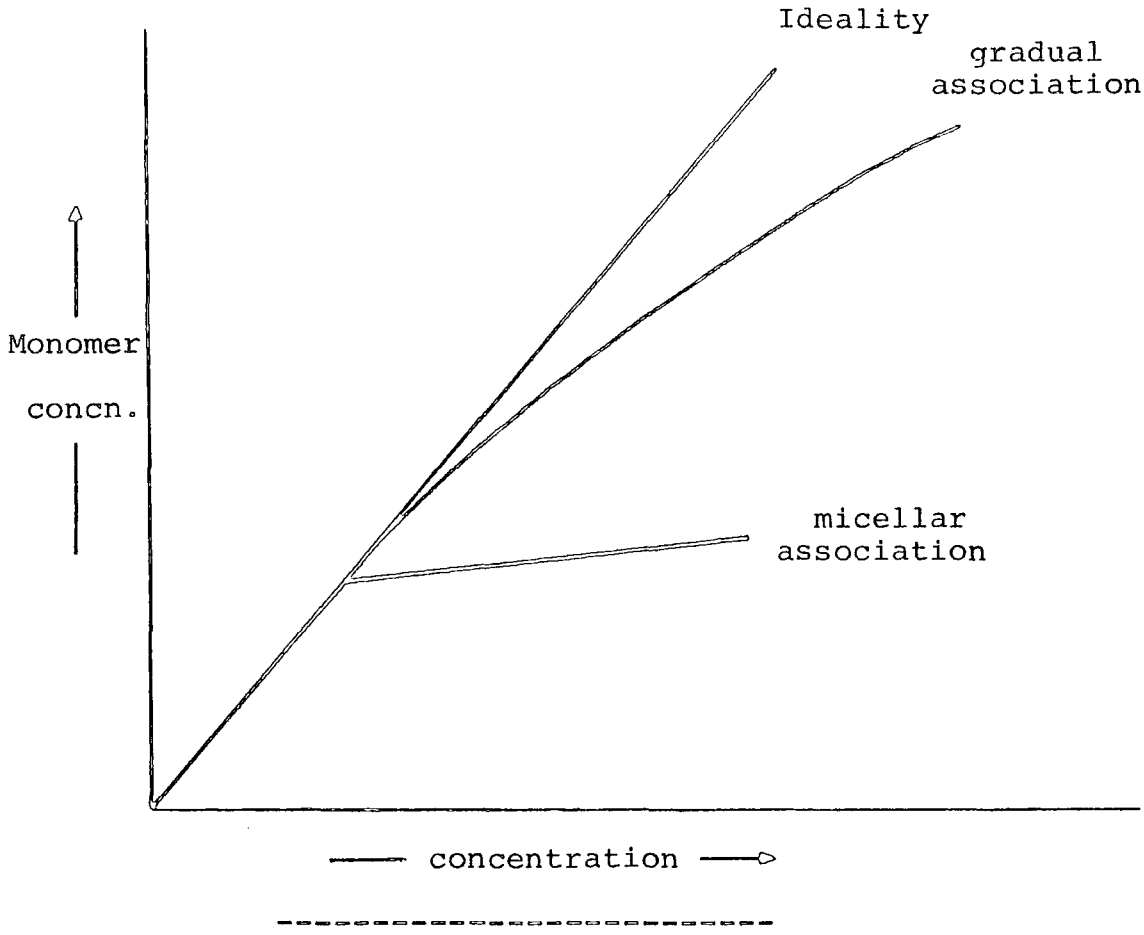

Water can often be incorporated into these systems, often without a phase change.[27] At low water concentrations, ionic surfactants experience partial hydration of the ion pairs, while nonionics show some head group interaction, *e.g.* hydrogen bonding.[71] As the concentration is increased the aggregation number increases accompanied with swelling and the formation of water pools. When large amounts of water are added to form a stable and clear phase the result is termed a microemulsion. Alcohols tend to encourage the formation of these reverse micelles and microemulsions which are of much use in catalysis. In addition, since oil and water mix spontaneously, they are of considerable importance in

in tertiary oil recovery.

3.5.3 Aggregate Size and Shape in Apolar Surfactant Solutions

As with aqueous surfactant systems, aggregate shape is to some extent dependent on steric considerations of the amphiphiles. But a much greater dependence is observed on solvent polarity. The simplified notion of "like with like" is correct to some extent and it is often observed that the mutual attraction of head groups decreases with the polarity of the solvent. The average aggregation number can be related with either the dipole moment or the dielectric constant, but most success has been obtained using the Hildebrand solubility parameter.[98] It is defined as "the square root of the cohesive energy density" and is most directly obtained from the Heat of evaporation as shown in equation 3.30 below.[132]

$$\delta = \left(\frac{\Delta E_V}{V}\right)^{\frac{1}{2}} = \left[\frac{D(\Delta H_V - RT)}{M}\right]^{\frac{1}{2}} \qquad \text{(eqn. 3.30)}$$

where δ = solubility parameter

D = density

M = molecular weight

ΔH_V = Heat of vaporization.

Some of the data reviewed by Eicke[98] show a remarkable linear dependence on this parameter using dinonyl naphthalene sulphonate surfactants. With non polar solvents such as heptane, cyclohexane, *etc.* hydrophillic portions of the surfactant aggregates are shielded from the environment. However in the case of liquids such as benzene and carbon tetrachloride, specific interactions may occur with the head group

dipoles. In the former an interaction with the π electrons of benzene may exist while in the easily polarizable CCl_4 molecules, strong dipole-induced dipole interactions may occur.

The critical balance between the enthalpic and entropic contributions in aggregate systems leads to a complex temperature dependence. Though the behaviour varies between surfactants, it is generally accepted that the effect of temperature on solubility is important. Some workers believe the existence of a Krafft boundary, as found in aqueous systems.[98]

CHAPTER FOUR

THE AGGREGATION OF POLYOXYETHYLENE SURFACTANTS IN APOLAR SOLVENTS

4.1 Introduction

The association process of amphiphillic molecules in apolar solvents is, at the moment, a subject of much research interest. In the simplest case one may chose an aliphatic alcohol (or amine) and study its aggregation phenomena in a relatively inert solvent such as carbon tetrachloride. With such systems, where hydrogen bonding provides the strongest attractive interaction, one may study the association equilibrium using infra red spectroscopy.[3,30,39-40,43-47] We have mentioned in Chapter Two that the 4000-3000 cm^{-1} region is particularly sensitive to hydrogen bonding and one may study the aggregation process by monitoring monomer concentrations as a function of total amphiphile concentration. Application of a particular equilibrium model[38] then allows the determination of an average aggregation number(s) and hence calculation of the free energy change for the process:

$$nRXH \rightleftharpoons (RXH)_n$$

The lack of understanding with "reverse aggregation" in general largely stems from the fact that aggregates tend to be small, and therefore difficult to measure at very low concentrations. The current literature on the subject suggests that association occurs at low concentrations in apolar solvents, $C<0.001$ mol.ℓ^{-1} for ionic surfactants[50] and generally higher for nonionic surfactants.[51,53-57,71] Plots of physical properties of these systems as a function of total amphiphile concentration reveal curves showing only a gradual change, quite unlike the sharp micellar transitions occurring in aqueous systems.[53]

As with simple aliphatic alcohols[30] the association process in apolar solvents may be quantified spectroscopically for polyoxyethylene surfactants of the type $C_{12}H_{25}(OCH_2CH_2)_N\text{-}OH$ (where N = 0, 1, 2, 3, 4, 5, 8) in apolar solvents. These oxyethylene glycol dodecyl ethers (abbreviated to $C_{12}E_N$) have a hydroxyl group which allows a study of hydrogen bonding equilibria using i.r. spectroscopy. However, their association behaviour is far more complex than that found in ordinary aliphatic alcohols.

Commercial polyoxyethylene surfactants tend to be distributions of varying oxyethylene chain length. However, those used here are pure and may be characterized by a "hydrophillic-lipophillic balance" value (the HLB).[92] This parameter, which is simply a measure of the relative amount of oxyethylene units per hydrocarbon chain, may be used as a qualitative measure of the surfactants properties.[49,48]

The study of aggregation as a function of additional oxyethylene units poses an interesting spectroscopic problem when one considers that the molecules may also form intra-molecular hydrogen bonds. Figure 4.1 shows a schematic diagram of some of the possible species. The interest arises with $C_{12}E_2$ and higher oxyethylene homologues where eight, eleven, *etc.* membered rings form. These hydrogen bonds have enthalpies of formation close to the values found for inter-molecular (aggregated) species and thus generally absorb i.r. radiation at approximately the same wavelength. Quantitatively, this means one cannot distinguish between some of the monomers and aggregated molecules. As well as overcoming the above problems we have been able to apply our methods to study the aggregation

FIGURE 4.1 THE INTRAMOLECULAR H-BONDED SPECIES OF SOME RE_N SURFACTANTS.

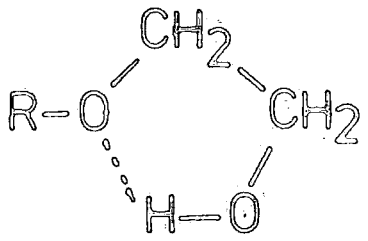

(a) 5-membered ring of RE_1

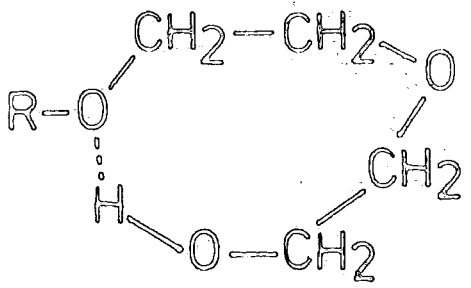

(b) 8-membered ring of RE_2

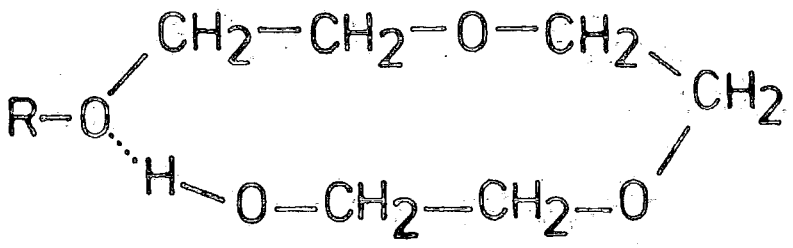

(c) 11-membered ring of RE_3

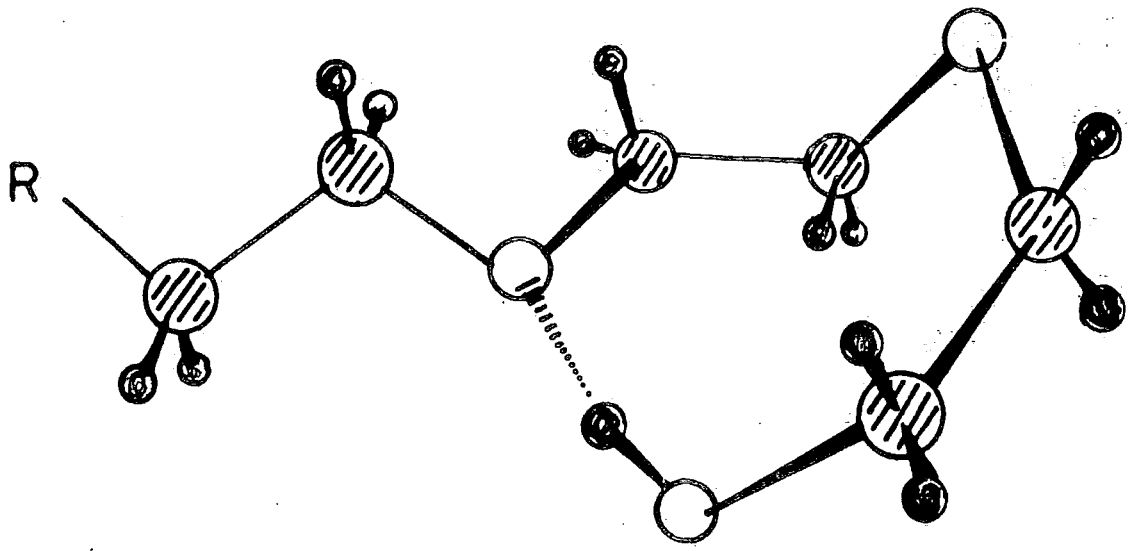

(d) A 3-D representation of an 8-membered ring in RE_2.

behaviour of $C_{12}E_4$ in a number of apolar solvents. In particular we chose decane, decalin, benzene, carbon tetrachloride, and deuterochloroform.

These data will thus provide interesting information concerning the effects of solvent on the nature and magnitude of aggregation by polyoxyethylene surfactants.

4.2 Experimental

4.2.1 Sample Preparation

Infra red spectroscopy, particularly of samples at low concentrations, necessitates the use of high grade materials and also careful sample handling. The solvents used, supplied by either BDH or Koch light laboratories, were generally of "AnalaR" grade and dried over zeolite before use. The surfactants themselves, consisting of a series of polyoxyethylene glycol dodecyl ethers, obtained from the Nikkol Company, Japan, were of at least 98% purity. They were stored in a refrigerator when not in use. Surfactant solutions were prepared by weight, with compositions varying between fractions of a per cent to greater than 16% w/w.

A Beckmann RIIC liquid cell was used for the measurements with either calcium fluoride or potassium bromide windows. Pathlengths of between 200 and 1500 microns were determined accurately using either interference fringes[58] or a micrometer (for pathlengths greater than 1 = 500μ).

The cells once filled were fitted into a variable temperature housing, water circulating through the housing thus

ensured thermal equilibrium. For higher temperatures (K≥323) a Beckman RIIC temperature controller was used. The temperature stability was thought to be no more than ±1K for both methods.

4.2.2 Spectroscopy and Data Handling

Before any use of the instrument, a phase correction was performed as well as an ordinate calibration over the wavenumber range investigated. Spectra were recorded for both solvent and solution at each pathlength, between 4000 and generally 3000 cm^{-1}. The slit width, scan speed, and time constant were set at 2 cm^{-1}, 380 cm^{-1}. min^{-1}, and 0.3s respectively, combined as an integrated scan mode of 4. The PE580 data station recorded data in a digital form which subsequently allowed solvent subtraction.

Initially a "solvent normalization" factor is calculated which allows for a reduction of solvent bands in solution spectra. One chooses a region of the solution spectrum where no solute contribution is observed. The spectra are then converted into absorbance units and an average value is calculated over the chosen region. The normalization factor is then merely a ratio of these values for solution and solvent spectra, respectively. The procedure is then to multiply the solvent spectrum by the normalization factor and thence to subtract one spectra from the other. Figure 4.2 shows the normalization region for $C_{12}E_8$ in n-heptane (taken as 3900-3700 cm^{-1}). The solvent subtracted absorbance spectra were then stored on disc for subsequent data analysis.

FIGURE 4.2 SUBTRACTED ABSORBANCE SPECTRUM OF $C_{12}E_8$ IN HEPTANE USING THE 3900-3700 cm^{-1} NORMALIZING REGION.

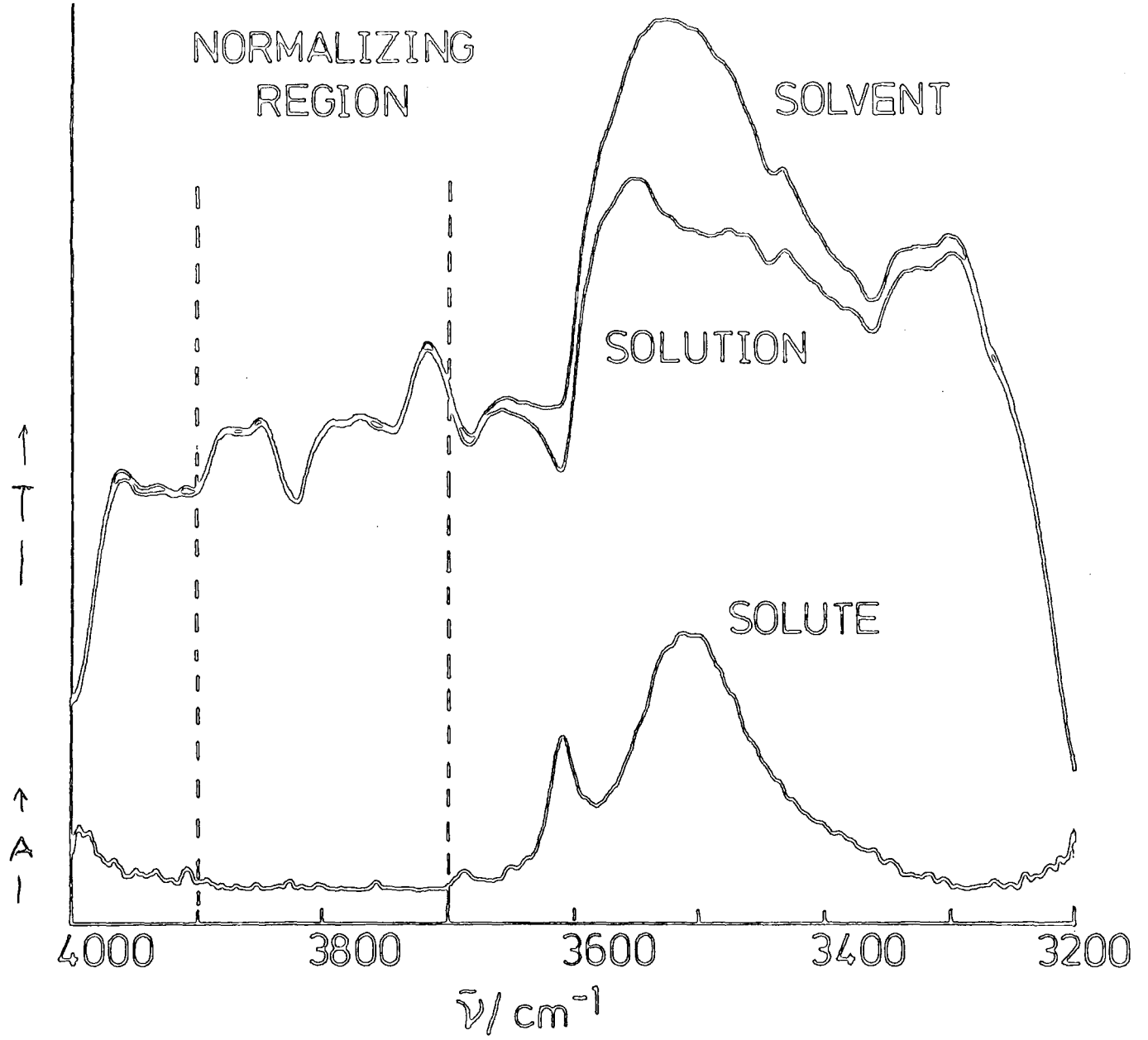

For reasons which shall be discussed in the next section the absorbance of the band centered at 3610 cm^{-1} (3635 cm^{-1} in dodecanol) was required, (see Figure 4.2). Three methods of calculating the integrated area of this band were initially researched. The first method involved transfer of data to a main frame computer where band fitting facilities were available. The deconvolution of the band envelope consisted of two sections, both written by Pitha and Jones.[59] Initially a series of input parameters describing each of the component band shapes making up the spectrum, are inserted into a "parameter" file. These parameters include frequency maxima, Lorentzian/Gaussian contribution, absorbance half width, *etc*. The first program then draws the spectral envelope and compares it to the actual data (in another file). An iterative procedure of changing the above parameters then commences which minimizes the difference (statistically) between the calculated, and actual spectrum. The second part of the procedure is then to generate the deconvoluted components (or their sums) using the newly calculated parameters. It is then a simple matter of determining the integrated absorbance of the band in question using a Simpsons rule type calculation on the computer. This program has been named "BAREA".

The statistical optimization above was performed with four spectral components, initially centred at 3610 cm^{-1}, 3500 cm^{-1}, 3405 cm^{-1} and 3348 cm^{-1}. The results obtained from one however showed various inconsistencies from one spectrum to another. In particular, contributions from the lower frequency bands to the absorbance of the 3610 cm^{-1} band were somewhat variable. The problem was more marked at high concentrations where interference with the C-H stretching modes were

observed. This had the effect of increasing the base line at the low frequency end of the spectrum such that the base line as a whole was no longer horizontal. Since the optimization program above could not properly treat sloping base line data, the effect resulted in artificial broadening of the low frequency band (originally at 3348 cm^{-1}) to such an extent that it caused overlap with the 3610 cm^{-1} band of interest as shown in Figure 4.3. In addition the band areas for monomer were determined at several concentrations. The results shown below highlighted the inconsistency of this particular method.

TABLE 4.1 Monomer Absorbances as calculated from Band Fitting

Wt. % $C_{12}E_4$ Surfactant	Monomer Absorbance cm^{-1}
5.17	6
7.00	6
8.45	17
10.11	22
12.11	21

For these reasons and the scattered values for the monomer absorbances when these were calculated, the idea of band fitting was abandoned.

The second method involved the use of a Dupont Curve Resolver and an Apple microcomputer with its graphics tablet. The curve resolver was able to give an immediate visual display of each component or their sums. The position, width and intensity of each band could be adjusted as could the band shape, *i.e.* whether Gaussian, Lorentzian or a convolution of both. The difference between these various convolutions occurs in the wings, with a greater Lorentzian character giving

FIGURE 4.3 THE RESULTS OF BAND FITTING AS APPLIED TO A 0.375 MF $C_{12}E_4$ SOLUTION IN HEPTANE.

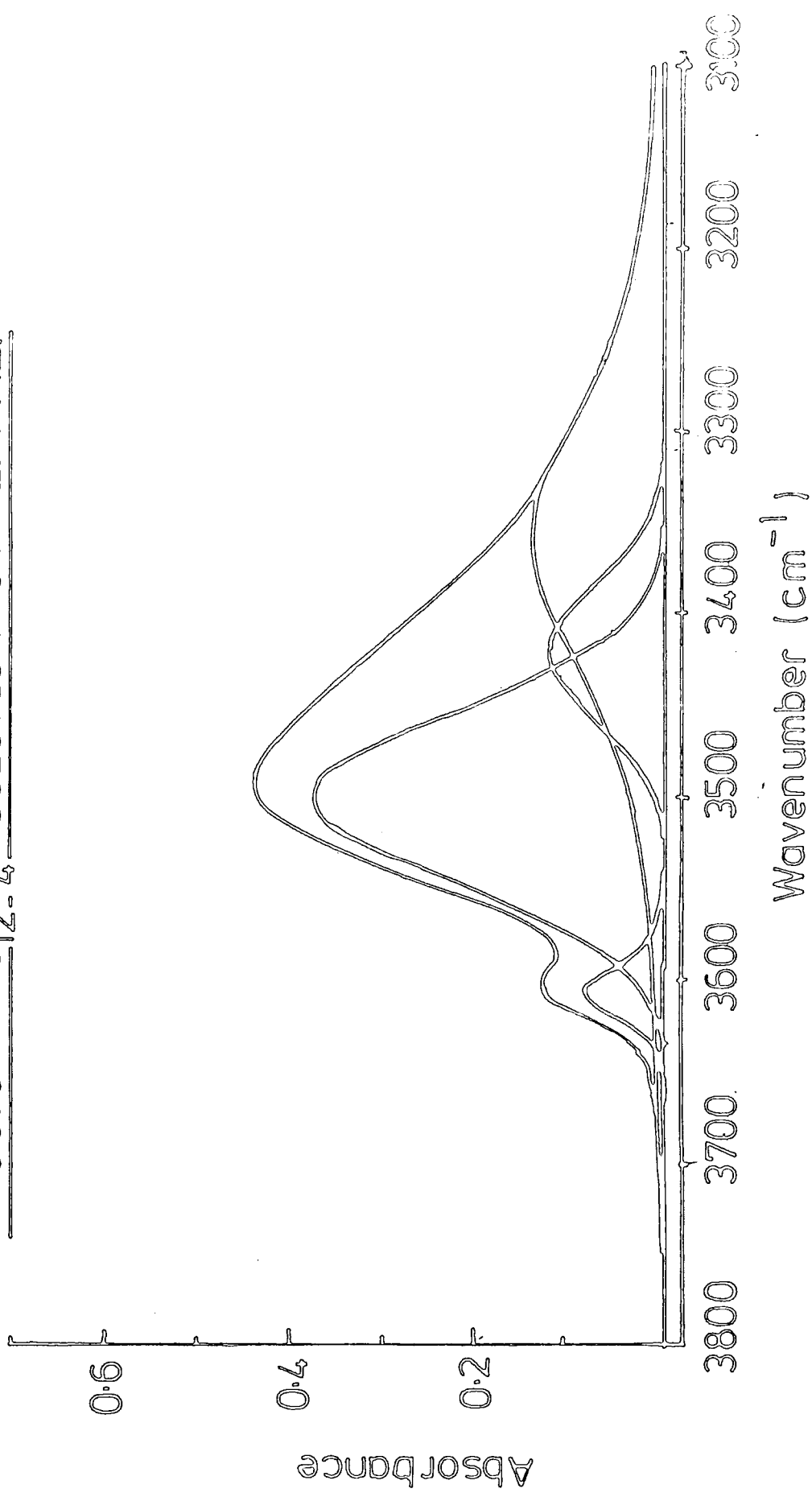

a greater area in the wings. A Gaussian band shape was chosen for the current investigations and was found to give satisfactory fits to the spectra. The 3610 cm^{-1} band was then drawn on to the chart paper for subsequent area determination using the Apple Graphics tablet software. This was done by simply placing the chart paper on the graphics tablet and tracing over the band using a pen interfaced to the computer. The software then merely calculated the area using Simpsons rule between the first and last points. This procedure was repeated five times and an average value calculated.

Finally a third method of area determination was investigated. This again involved the use of the curve resolver above, but calculation of the area was performed by measuring the width at half maximum height and multiplying by the height.

Of the three methods investigated the latter two provided the most consistent results, with the triangulation method proving to be the most successful of all. In some cases the 3610 cm^{-1} and 3500 cm^{-1} bands (see Figure 4.3) overlapped to such an extent that the half width could not be measured directly. When this occurred the half width was assumed to be invariant of concentration (demonstrated to be correct at lower concentrations) and the value of the previous sample was used.

4.3 The Spectroscopy of $C_{12}E_N$ Solutions in n-Heptane at 30°C

4.3.1 The Determination of Monomer Concentration

To be able to quantify the aggregation process in the various systems studied, we require a knowledge of monomer

behaviour as a function of total surfactant concentration. For dodecanol, which can be thought of as being the simplest of the $C_{12}E_N$ surfactants (N=0), this is a fairly straightforward process. The area of the band at 3635 cm^{-1} (see Figure 4.4) assigned as the non-hydrogen bonded stretching band,[30] is measured at low concentration where no association is observed. Simple use of the Beer-Lambert law (equation 4.1)

$$A = \varepsilon.C.L \qquad \text{(eqn. 4.1)}$$

allows the calculation of an absorption coefficient. Subsequent area determination at higher concentrations, where association is observed, and application of the previously calculated absorption coefficient yields the corresponding monomer concentration.

With $C_{12}E_1$ and higher oxyethylene homologues, the analysis becomes more difficult due to complications arising from intramolecular hydrogen bonding between ether oxygens and the terminal -OH group (see Figure 4.1). Examination of some low concentration spectra of $C_{12}E_1$ ($C \leqslant 0.0038$ mf) in Figure 4.5, indicate the presence of a band at 3607 cm^{-1} with a shoulder at 3635 cm^{-1}. Similarly, spectra of $C_{12}E_2$ at comparable concentrations (Figure 4.6) show three bands (the ratio of these band heights remain constant at these low concentrations). Comparison of Figures 4.4, 4.5 and 4.6 thus gives rise to the conclusion that the bands at 3635, 3607 and 3485 cm^{-1} correspond to the non-hydrogen bonded monomer (M_{NB}), the intramolecularly hydrogen bonded five and eight membered rings (M_{I5},M_{I8}), respectively. A series of papers by Prabhumirashi *et al*[61-64], and also Kuhn and Wires,[65] have spectroscopically examined similar compounds (*e.g.* $CH_3CH_2-(OCH_2CH_2)_{1,2}-OH$) in solutions of

FIGURE 4·4 DIAGRAM SHOWING THE ν_s(O-H) ABSORBANCE SPECTRUM OF DODECANOL IN NORMAL HEPTANE AT 30°C OVER A SERIES OF CONCENTRATIONS.

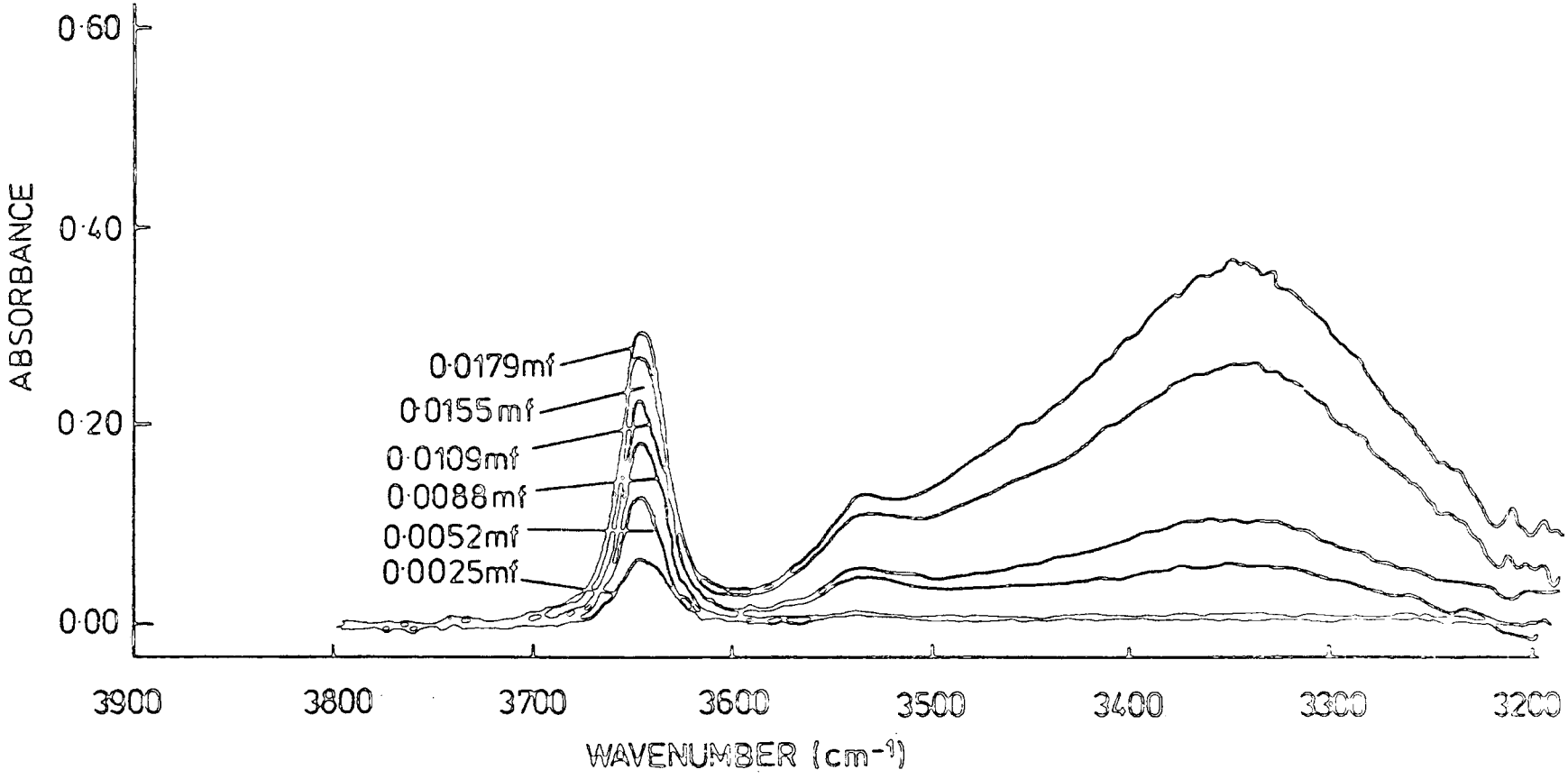

FIGURE 4.5. SPECTRA OF $C_{12}E_4$ IN HEPTANE.

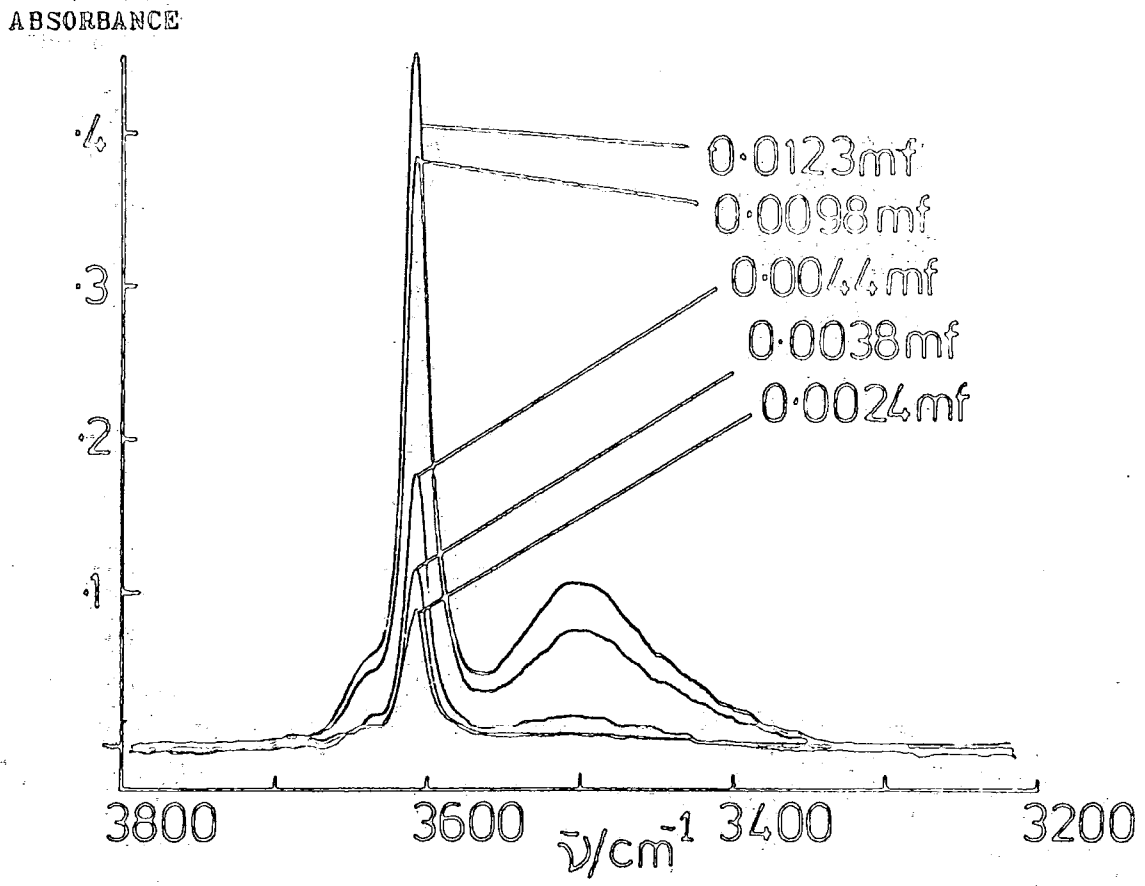

FIGURE 4.6. SPECTRA OF $C_{12}E_2$ IN HEPTANE.

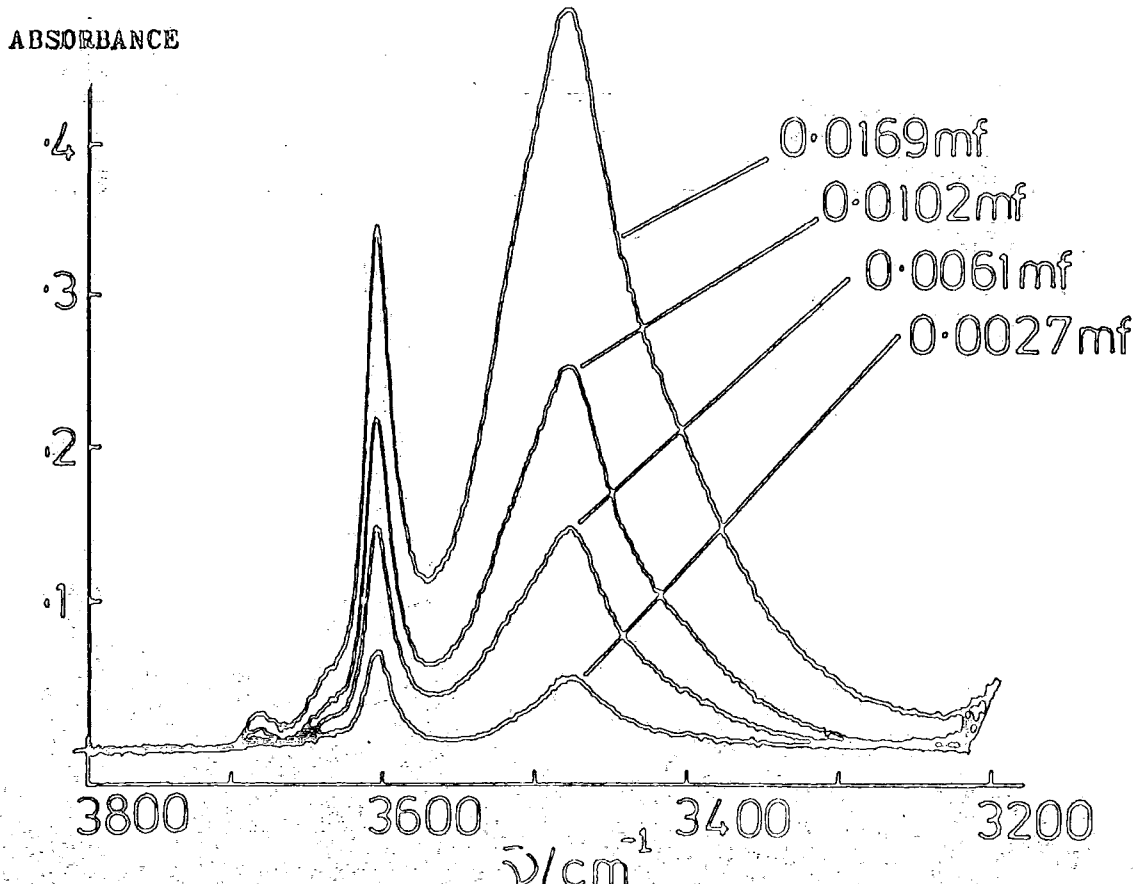

carbon tetrachloride. Their work, though in a different solvent, qualitatively support the existence of the above hydrogen bonded species.

In order to calculate monomer concentrations for $C_{12}E_1$, we must first determine the ratio of the two species present. This is not a simple procedure since the two bands are closer together making deconvolution an ambiguous exercise. However, an attempt to determine the M_{NB} area using the dodecanol absorption coefficient (thus assuming negligible inductive effects),[66] leads to a concentration of species which is no greater than 10% of the total. With this result in mind one may then simplify the calculation by assuming the total monomer concentration to be proportional to the M_{I5} absorbance. Since no noticeable change in M_{NB} relative absorbance at higher concentrations is observed, in agreement with the work of Prabhumirashi *et al*,[61] we feel that the above statement is justified. Calculation of the monomer concentration then simply follows the procedure of measuring the absorbance of the 3607 cm^{-1} band to obtain a pseudo absorption coefficient and hence subsequently, monomer concentrations.

The band at 3485 cm^{-1} in Figure 4.6 has been previously assigned as the ν_S(O-H) stretch of the M_{I8} hydrogen bonded species.[62] Similarly Figures 4.7, 4.8, 4.9 and 4.10 show spectra of $C_{12}E_3$, $C_{12}E_4$, $C_{12}E_5$ and $C_{12}E_8$, respectively and demonstrate that larger ring sizes (M_{I11}, M_{I14}, *etc.*) also absorb in this region. The difficulty in calculating monomer concentrations is realised when one finds that the intermolecular hydrogen bonded species also has its maximum in the 3500 cm^{-1} region. The determination of monomer levels thus requires a

FIGURE 4·7 SPECTRA OF $C_{12}E_3$ IN HEPTANE

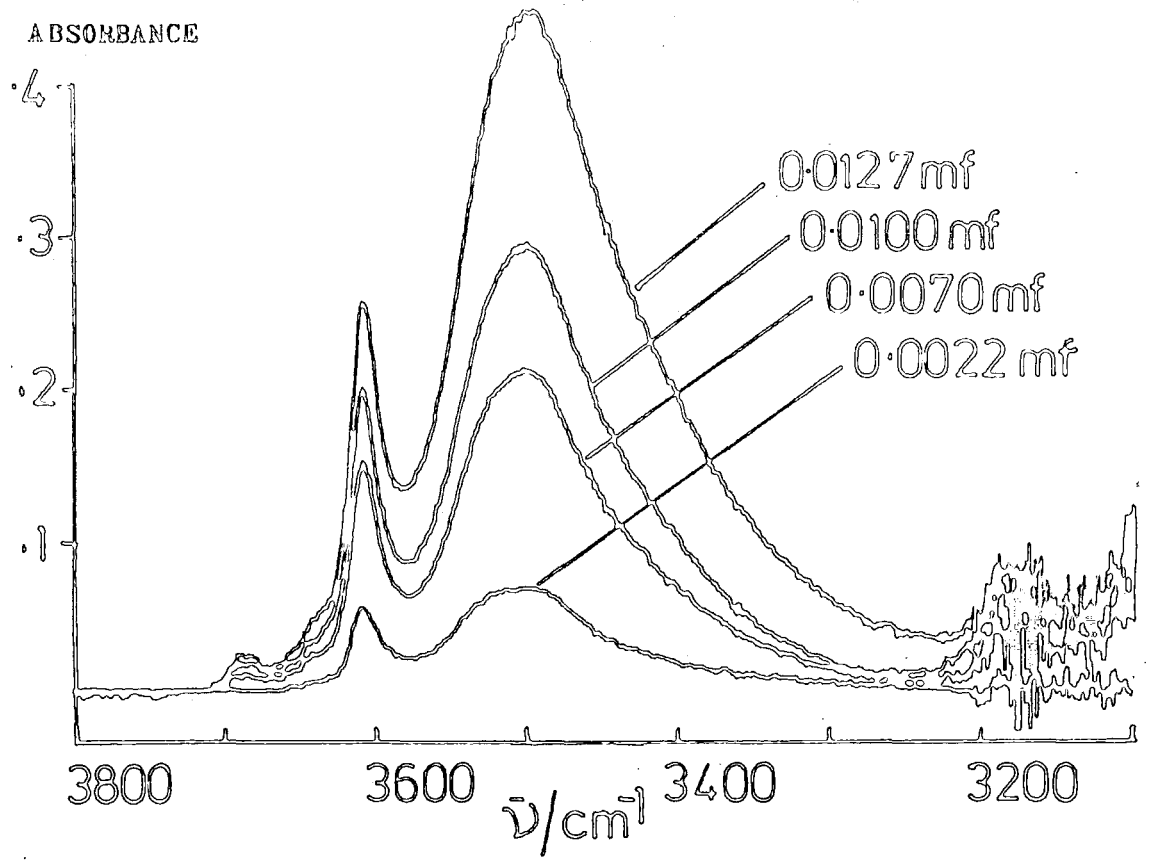

FIGURE 4·8 SPECTRA OF $C_{12}E_4$ IN HEPTANE.

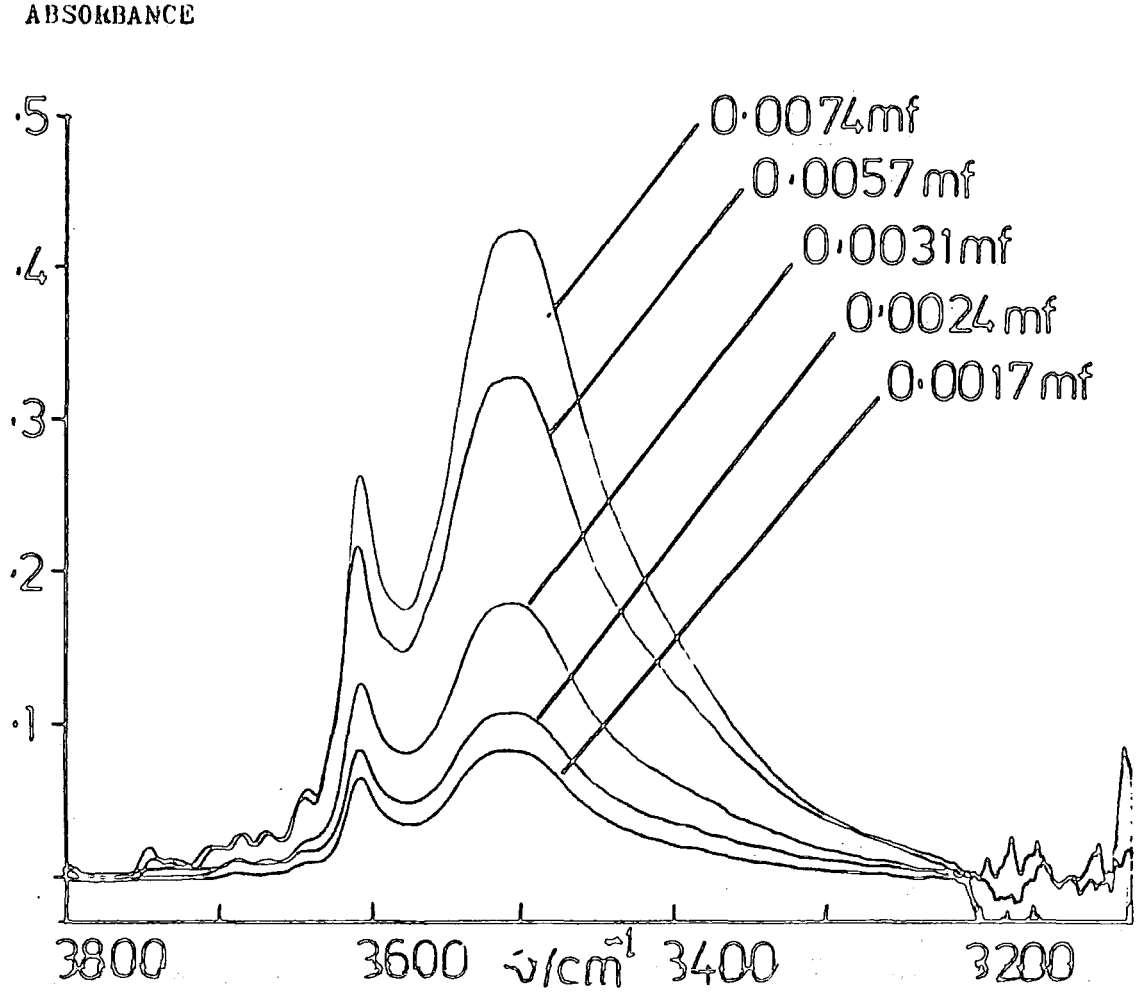

FIGURE 4·9 SPECTRA OF $C_{12}E_5$ IN HEPTANE.

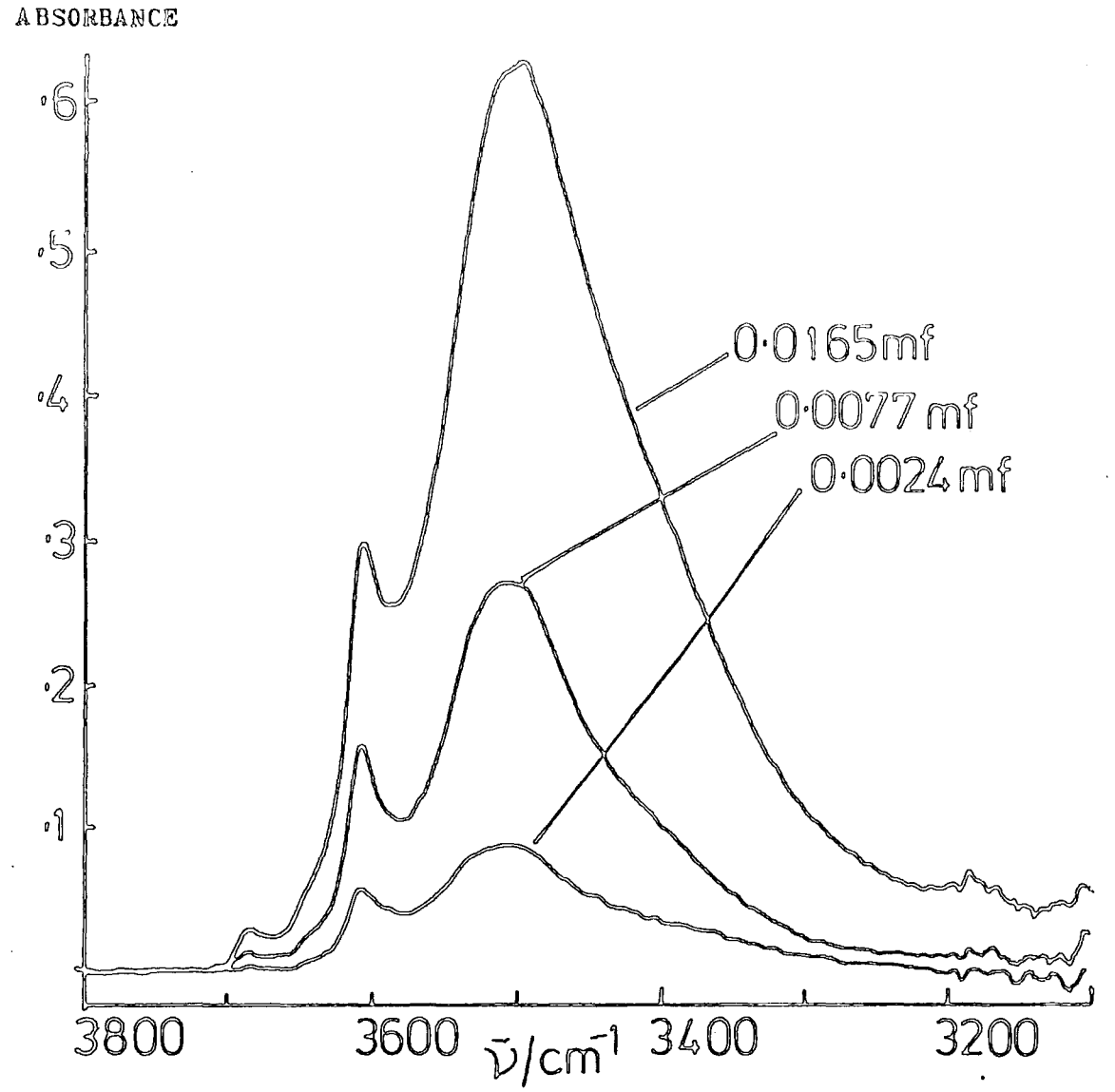

FIGURE 4·10 SPECTRA OF $C_{12}E_8$ IN HEPTANE.

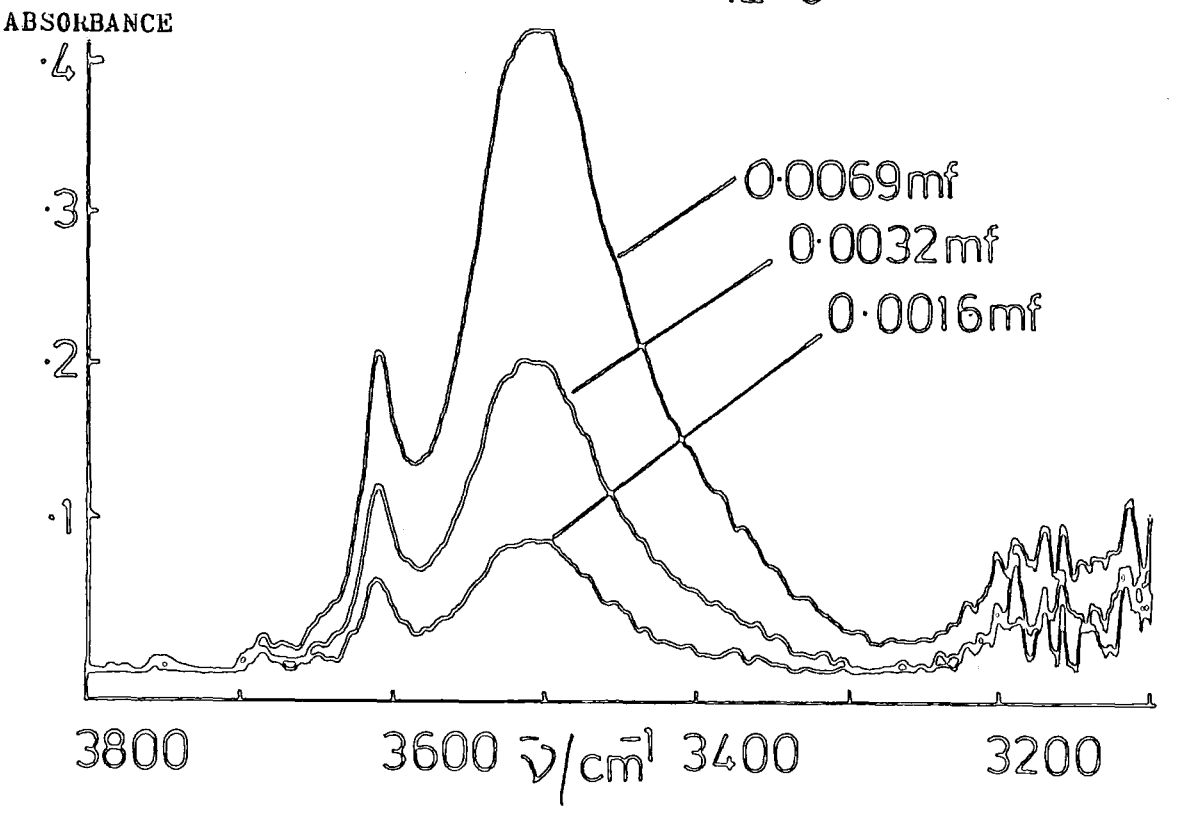

more sophisticated approach. At low concentrations, where the relative proportion of all species is constant, one may relate the molar concentrations of the spectroscopically distinguishable species as shown in equation 4.2.

$$M_{TOT} = M_{NB} + M_{I5} + \sum_{N=3}^{N=9} M_{(3N-1)I} \qquad \text{(eqn. 4.2)}$$

From an earlier assumption we may write

$$M_{TOT} = M_{NB+I5} + \sum_{N=3}^{N=9} M_{(3N-1)I} \qquad \text{(eqn. 4.3)}$$

i.e. $M_{NB} \simeq$ constant

M_{I5} may be determined from the spectra and from the absorption coefficient calculated from $C_{12}E_1$, leaving $\sum_{N=3}^{N=9} M_{3N-1}$ as the only unknown. Intramolecularly hydrogen bonded rings of eight and greater are thus treated collectively since they are spectroscopically indistinguishable. For this treatment, therefore, we must assume that either the concentration of higher ring size species is small or they have equal chemical potentials. A further discussion will be reserved for the next section. Now that we have the concentrations of all species we may express equation 4.3 as

$$\sum_{N=3}^{N=9} M_{(3N-1)I} = M_T - M_{NB+I5} \qquad \text{(eqn. 4.4)}$$

dividing by M_{NB+I5} gives the ratio of $M_{(3N-1)I}$ aggregated species

$$\frac{\sum_{N=3}^{N=9} M_{(3N-1)I}}{M_{NB+I5}} = \frac{(M_T - M_{NB+I5})}{M_{NB+I5}} \qquad \text{(eqn. 4.5)}$$

At high concentrations we may write

$$C_T = C_{NB+I5} + \sum_{N=3}^{N=9} C_{(3N-1)I} + C_A \qquad \text{(eqn. 4.6)}$$

where C_A and C_T are the associated and total surfactant concentrations above the point where association is seen to proceed, respectively.

If we divide equation 4.6 by C_{NB+I5} then we get

$$\frac{C_T}{C_{NB+I5}} = 1 + \frac{\sum_{N=3}^{N=9} C_{(3N-1)I}}{C_{NB+I5}} + \frac{C_A}{C_{NB+I5}} \qquad \text{(eqn. 4.7)}$$

At this point we must make the assumption that the ratio of the various intramolecularly hydrogen bonded species remains constant through the whole concentration range (valid under ideal solution theory).

This may be written as:

$$\frac{\sum_{N=3}^{N=9} C_{(3N-1)I}}{C_{NB+I5}} = \frac{\sum_{N=3}^{N=9} M_{(3N-1)I}}{M_{NB+I5}} \qquad \text{(eqn. 4.8)}$$

Substituting for the left hand term of equation 4.8 we get

$$\frac{C_T}{C_{NB+I5}} = 1 + \frac{\sum_{N=3}^{N=9} M_{(3N-1)I}}{M_{NB+I5}} + \frac{C_A}{C_{NB+I5}} \qquad \text{(eqn. 4.9)}$$

Further substitution and rearrangement gives:

$$C_T = C_{NB+I5} + C_{NB+I5}\left(\frac{M_T - M_{NB+I5}}{M_{NB+I5}}\right) + C_A \qquad \text{(eqn. 4.10)}$$

Of course $C_T - C_A$ is simply the monomer concentration so:

$$C_M = C_{NB+I5} + C_{NB+I5}\cdot\left(\frac{M_T - M_{NB+I5}}{M_{NB+I5}}\right) \qquad \text{(eqn. 4.11)}$$

Equation 4.11 allows us to calculate monomer concentrations from a knowledge of C_{NB+I5} and the constant, $(\frac{M_T - M_{NB+I5}}{M_{NB+I5}})$. In practice this constant is determined from the linear portion of the absorbance *versus* concentration plot, *i.e.* at low molar concentrations so that an average is calculated. The procedure is adopted individually for each $C_{12}E_N$ surfactant, since the equilibria vary slightly due to changes in the number of intramolecular species. For $C_{12}E_4$ in the various solvents the process can be simply repeated once the absorption coefficient of the five membered ring species has been determined. Again this is done by simply measuring for concentration absorbances of $C_{12}E_1$ in the chosen medium.

The analysis described above rests on the assumption that all intramolecular hydrogen bonding equilibria are effected in equal proportion. In chemical terms the equilibria which are of most interest to us shown below should have similar

$$A(C_{12}E_N)_{5I} \overset{K_1}{\rightleftharpoons} (C_{12}E_N)_A \qquad \text{(eqn. 4.12)}$$

$$A(C_{12}E_N)_{8I} \overset{K_2}{\rightleftharpoons} (C_{12}E_N)_A \qquad \text{(eqn. 4.13)}$$

equilibrium constants. Differences in these equilibrium constants will manifest themselves in errors to the monomer concentration at high surfactant concentrations. Quantitatively, the error will result in an underestimation of monomer concentration. Figures 4.18 and 4.20 show monomer curves as a function of total surfactant concentration determined for $C_{12}E_4$ and $C_{12}E_8$, respectively. The Figure shows data obtained using I.R. spectroscopy and also data obtained by vapour pressure osmometry.[67] The data in these figures demonstrate that our approximations are valid over the concentration range studied here.

4.3.2 The Hydrogen Bonded ν_S(O-H) Band

The amount of quantitative information obtainable from the ν_S(O-H) band envelope centred at ≈3500 cm^{-1} is limited. However, much information may be extracted if one considers that the species involved in these hydrogen bonds have very large absorption coefficients. The consequence of this is that subtle perturbations in the hydrogen bonded equilibria result in large spectroscopic changes.

In order to be able to interpret these spectra one must distinguish between high and low concentration spectra. The latter referring to concentrations where no visible association occurs and the intramolecularly hydrogen bonded equilibrium remains intact. The spectra at these low concentrations will therefore demonstrate the coexistence of several species. As well as the M_{NB} and M_{I5} species, the low concentration spectra of $C_{12}E_2$ contains a symmetrical band at 3485 cm^{-1} (Figure 4.6). It is noticeably sharper than its higher homologues which suggests a narrower distribution of hydrogen bonded species. As the concentration is increased, asymmetry is observed towards the lower frequency side of this band which must be attributed to the associated species. With further addition of surfactant the asymmetry is increased thus presenting a method of qualitatively studying the aggregation process. One suggestion has been to calculate an "asymmetry factor" (AF) from the ratio of half widths at a quarter height, as shown in Figure 4.11. The asymmetry is more pronounced at a quarter height and gives a more sensitive method of detecting aggregation. Figure 4.12 shows the results of such determination

Figure 4·11 The determination of the "asymmetry factor".

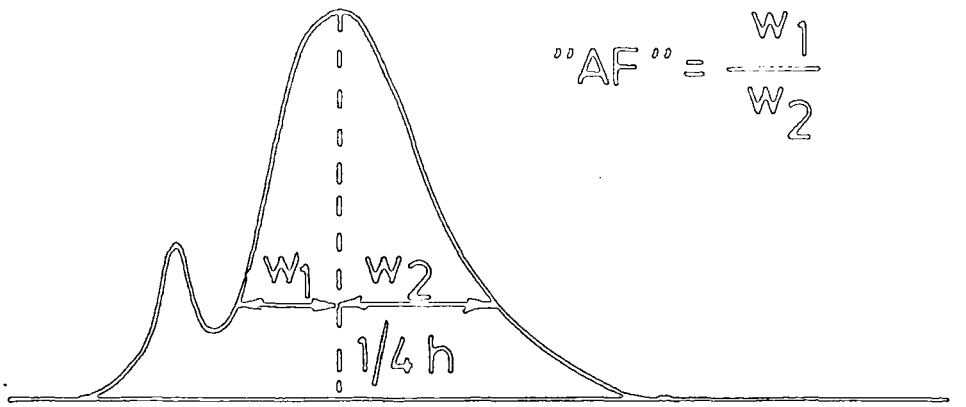

Figure 4·12 The behaviour of "AF" as a function concentration for $C_{12}E_2$ in heptane.

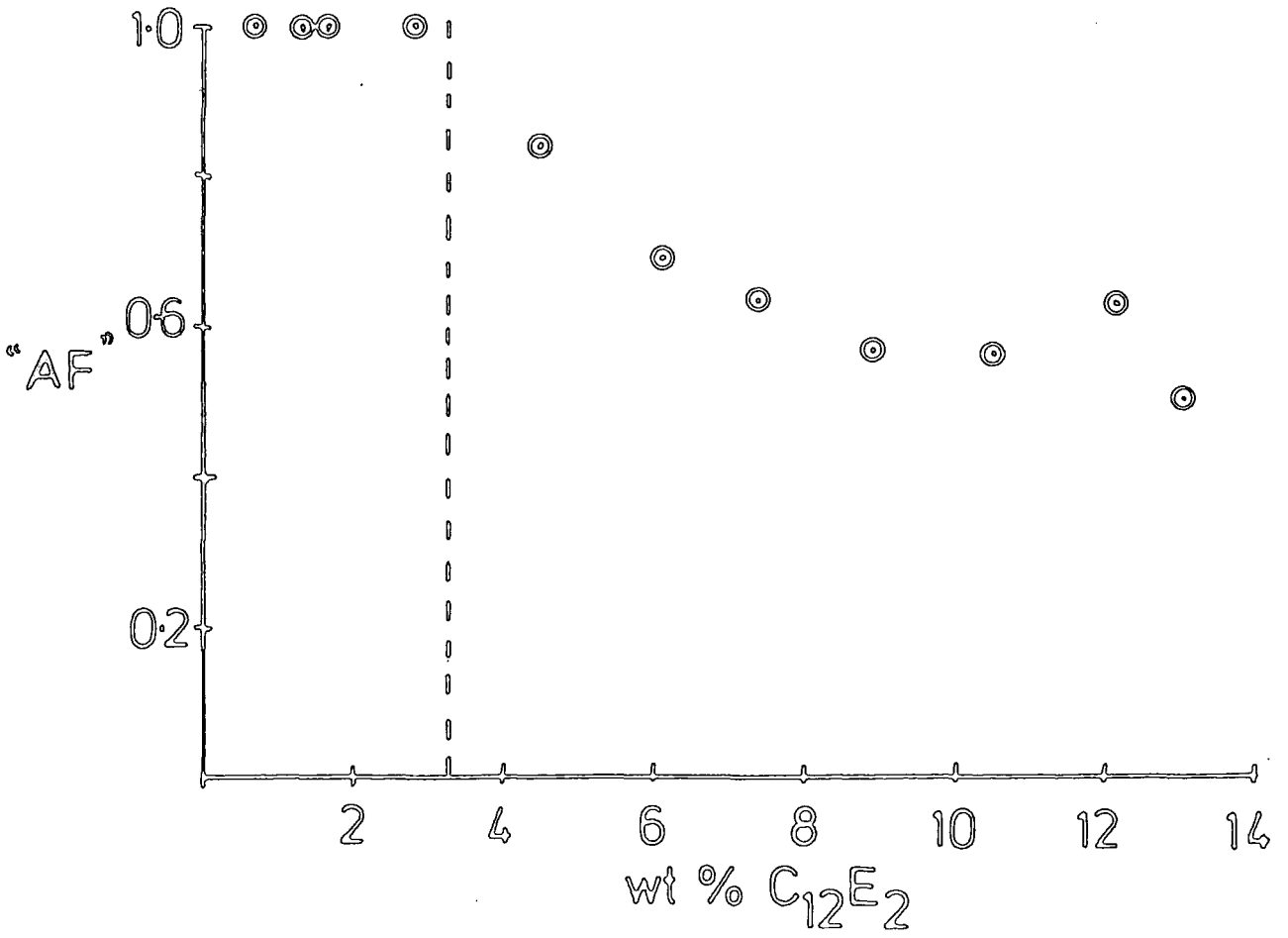

for $C_{12}E_2$ in heptane at 30°C. The diagram demonstrates that association, albeit small, is first observed at ≈3% W/W (0.0110 mf). Though AF=1.0 at low concentrations (*i.e.* the band is symmetrical about its maximum), one would not expect higher homologues to behave likewise. In these cases larger ring sizes cause asymmetry even at low concentrations and tends to obscure "structure" due to association. Under such circumstances a second method, of simply measuring the integrated absorbance relative to the M_{I5} band, is more sensitive. Figure 4.13 shows the behaviour of the (A_{3500}/A_{3605}) *versus* concentration curve for $C_{12}E_8$ in heptane. The graph exhibits an abrupt change which signifies the concentration at which aggregation begins. For $C_{12}E_8$, under the specified conditions, the aggregation concentration turns out to be 0.0075 mf. For the remaining oxyethylenes the changes are less well pronounced since aggregation proceeds in a more stepwise manner.

Further examination of some low concentration spectra of $C_{12}E_3$, $C_{12}E_4$, *etc.* (Figures 4.7-4.10) shows the 3485 cm^{-1} band move to 3505 cm^{-1} with an increased full width at half maximum intensity. The details are shown in Table 4.2 below.

TABLE 4.2 The Behaviour of ν_{max} and width at half height for some $C_{12}E_N$ surfactants.*

Surfactant	ν_{max} (cm^{-1})	$\Delta\nu_{1/2}$ (cm^{-1})
$C_{12}E_2$	3485±5	80±5
$C_{12}E_3$	3505±5	110±5
$C_{12}E_5$	3505±5	105±5
$C_{12}E_5$	3505±5	110±5
$C_{12}E_8$	3505±5	110±5

* All data obtained below 0.0050 mf.

FIGURE 4·13 THE BEHAVIOUR OF THE ν_s(O-H) ABSORBANCE RATIO AS A FUNCTION OF $C_{12}E_8$ CONCENTRATION.

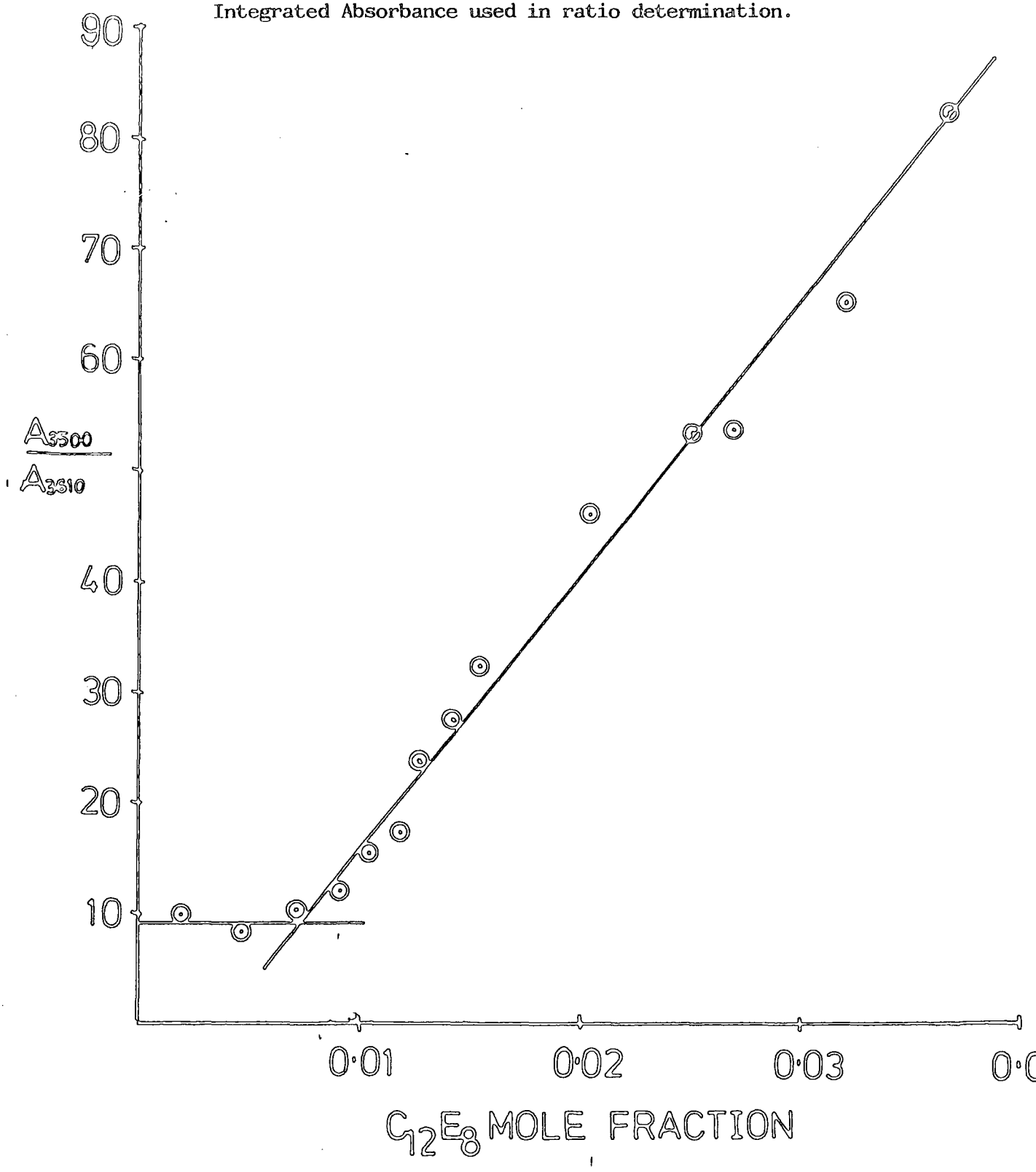

The M_{8I} species is shown to have a maximum at 3485 cm^{-1} while the presence of other intramolecularly H-bonded species, possibly the eleven membered ring peak at 3505 cm^{-1}. One would expect these species to absorb at frequencies below 3485 cm^{-1}, the fact that they do not suggests the enthalpy of formation of the eleven membered ring may possibly be higher than that of the M_{8I} species and that its concentration is relatively high. In addition, examination of Figure 4.8 (spectra of $C_{12}E_4$ in heptane) shows a noticeable shoulder at approximately 3400 cm^{-1} which may well be due to the intramolecular H-bonded fourteen membered ring. Though these bands are visible, the behaviour of their frequency maximum as function of enthalpy will be complex and not necessarily monotonic in behaviour. Also since the absorption coefficient of the various species (ring sizes greater than M_{8I}) are unknown, calculation of their concentration is not possible (band fitting procedures are of little use since there is considerable overlap).

The high concentration spectra of $C_{12}E_1$ in heptane (Figure 4.5) show a third band to appear at 3505 cm^{-1}. This peak is due to intermolecularly associated species.

For higher $C_{12}E_N$ homologues, the associated band also seems to appear at this frequency since it is this part of the spectrum which increases in intensity with concentration. Dodecanol (Figure 4.4) shows the most interesting behaviour, since it has two well defined hydrogen bonded bands (both intermolecular) at 3545 and 3350 cm^{-1}. These bands have been assigned in the literature as the dimer and tetramer, respectively.[30] In addition the concentration of the dimeric species

is relatively small at higher dodecanol mole fractions. Comparison of the frequency maximum for the tetrameric species and that of the associated bands in $C_{12}E_N$ surfactants suggests that hydrogen bonding in the former is much stronger.[68] Also, the breadth of this band suggests a greater distribution of multimeric species.[6]

4.4 Aggregation Phenomena in $C_{12}E_N$-Heptane Systems

4.4.1 The Behaviour of $C_{12}E_N$ Monomers with Total Concentration

The procedure which has been used to calculate monomer levels is described in Section 4.3.1. In this section we will discuss the results obtained, their sources of error and also possible implications.

As far as the error is concerned, one may distinguish between the following sources:

(a) Sample handling and preparation generates a small but finite error. The major contribution arises from sample preparation since only gram quantities are used. The error is ±0.0001g in weighing out the surfactant sample, thus for a 1% solution the maximum discrepancy is 2%. The inaccuracy will decrease as the concentration is increased.

(b) The effects of moisture has been a subject of some controversy in the past.[71] It is known that this water competes, with the terminal -OH group, for the ether oxygens on the oxyethylene chain.[71] This will alter the intramolecular H-bonding equilibrium which is expected, from ideal solution theory, to have a small effect on the association properties.

The $C_{12}E_4/CCl_4$ spectra of Figure 4.35 show evidence for this. Though the samples contain varying amounts of water *cf.* band at ≈3700 cm^{-1} of Figure 4.35,[72] the behaviour of the monomer is little affected and a smooth curve is obtained, see Figure 4.40.

(c) Probably the largest source of error comes from estimating the monomer absorbance using the deconvolution method described in Section 4.3.1. The error increases with concentration, particularly with the higher $C_{12}E_N$ homologues. The error originates from measuring the monomer absorbance where it overlaps with the bound band. By taking maximum and minimum values we have calculated this contribution to be no more than 5% and 10% for dodecanol and $C_{12}E_1$-$C_{12}E_8$, respectively.

(d) In our calculation of monomer concentration we have made the assumption that monomer levels may be estimated from absorbances of the M_{I5} species. In thermodynamic terms this means that the equilibrium constants for this and the other major species (M_{I8}) with that of the associated molecule is equal. Ideal solution theory assumes that at low concentrations, the interaction of molecules with each other is small and that their chemical potentials will be equal. At higher concentration where association is observed one may therefore assume that all species will be effected to the same extent. A comparison of our i.r. data with that obtained by VPO[67] (Figures 4.18 and 4.20) show reasonable agreement, thus qualifying our assumption (the VPO technique measures the number of solute particles, therefore M_{I5}, M_{I8}, *etc.* are treated collectively).

Figure 4.14 shows a typical curve of monomer *versus* total concentration of surfactant from dodecanol. The diagram

FIGURE 4.14 THE BEHAVIOUR OF DODECANOL MONOMER AS A FUNCTION OF CONCENTRATION IN HEPTANE AT 30°C.

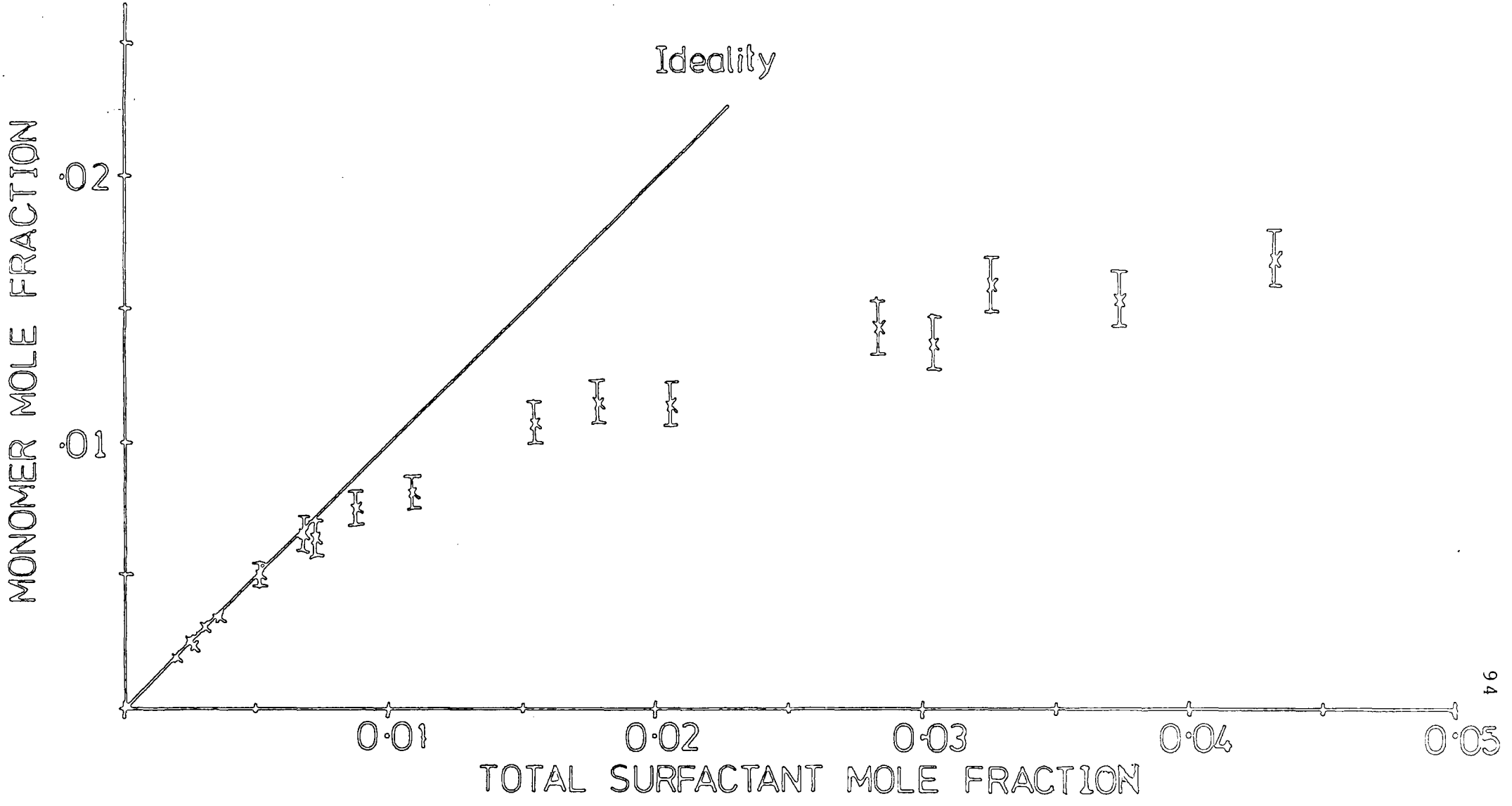

illustrates that at low mole fractions the behaviour follows ideality and no association is observed. As the concentration is increased aggregation begins and the curve deviates from linearity. The extent of this deviation is thus directly proportional to the magnitude of the aggregation process. For dodecanol the deviation becomes visible (from the monomer curve) at approximately 0.0050 mole fraction (0.035 M) though some association (as the dimer) is detected at 0.0031 mf (0.021M). This value is in agreement with that obtained by Aveyard *et al*[30] using a similar technique.

Analogous curves obtained for the oxyethylene surfactants are shown in Figures 4.15 to 4.20. All the curves exhibit the familiar deviation, but to slightly differing extents. In particular $C_{12}E_1$-$C_{12}E_5$ all show similar behaviour to each other with a gradual decrease in the slope of the curve. However, for $C_{12}E_8$ (Figure 4.20) the graph shows a more abrupt deviation from ideality. In addition the curve levels out to a plateau with the monomer concentration staying almost constant. We can draw a number of conclusions from this behaviour. Firstly that association is a gradual process and generally stronger for the larger oxyethylene chain length.

If we compare the curves of Figures 4.14 to 4.20 (Figure 4.21) we see a surprising result in that dodecanol shows behaviour between $C_{12}E_4$ and $C_{12}E_8$. This indicates that hydrogen bonding cannot be the <u>major</u> driving force for aggregation in these surfactants. This conclusion may be reached if one realises that a reduced H-bonded interaction (probably due to inductive effects) will occur for <u>all</u> the $C_{12}E_N$s (more so for $C_{12}E_8$, it has the most oxyethylene units) and dodecanol should

FIGURE 4.15 THE BEHAVIOUR OF $C_{12}E_1$ MONOMER AS A FUNCTION OF CONCENTRATION IN HEPTANE AT 30°C.

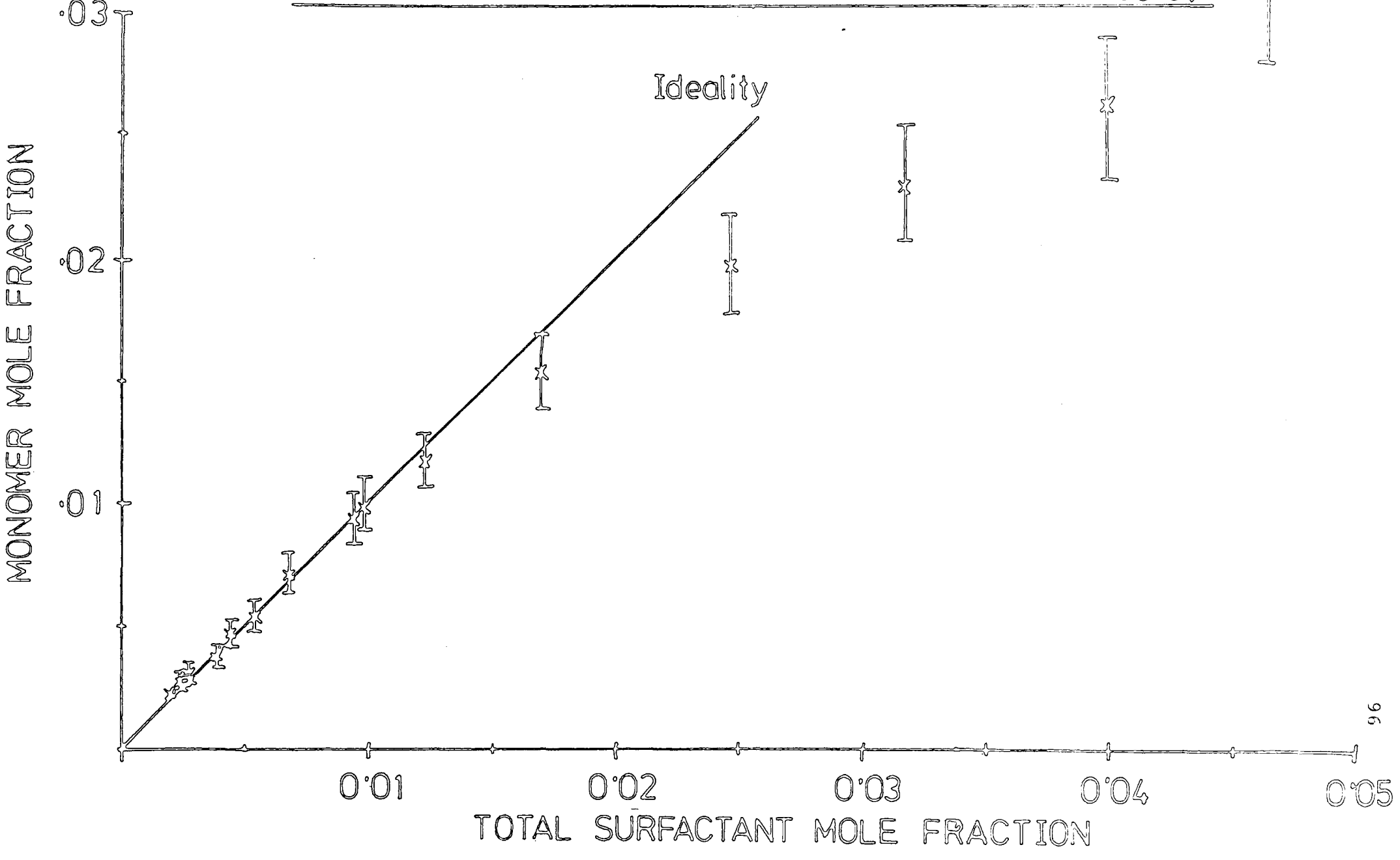

FIGURE 4.16 THE BEHAVIOUR OF $C_{12}E_2$ MONOMER AS A FUNCTION OF CONCENTRATION IN HEPTANE AT 30°C.

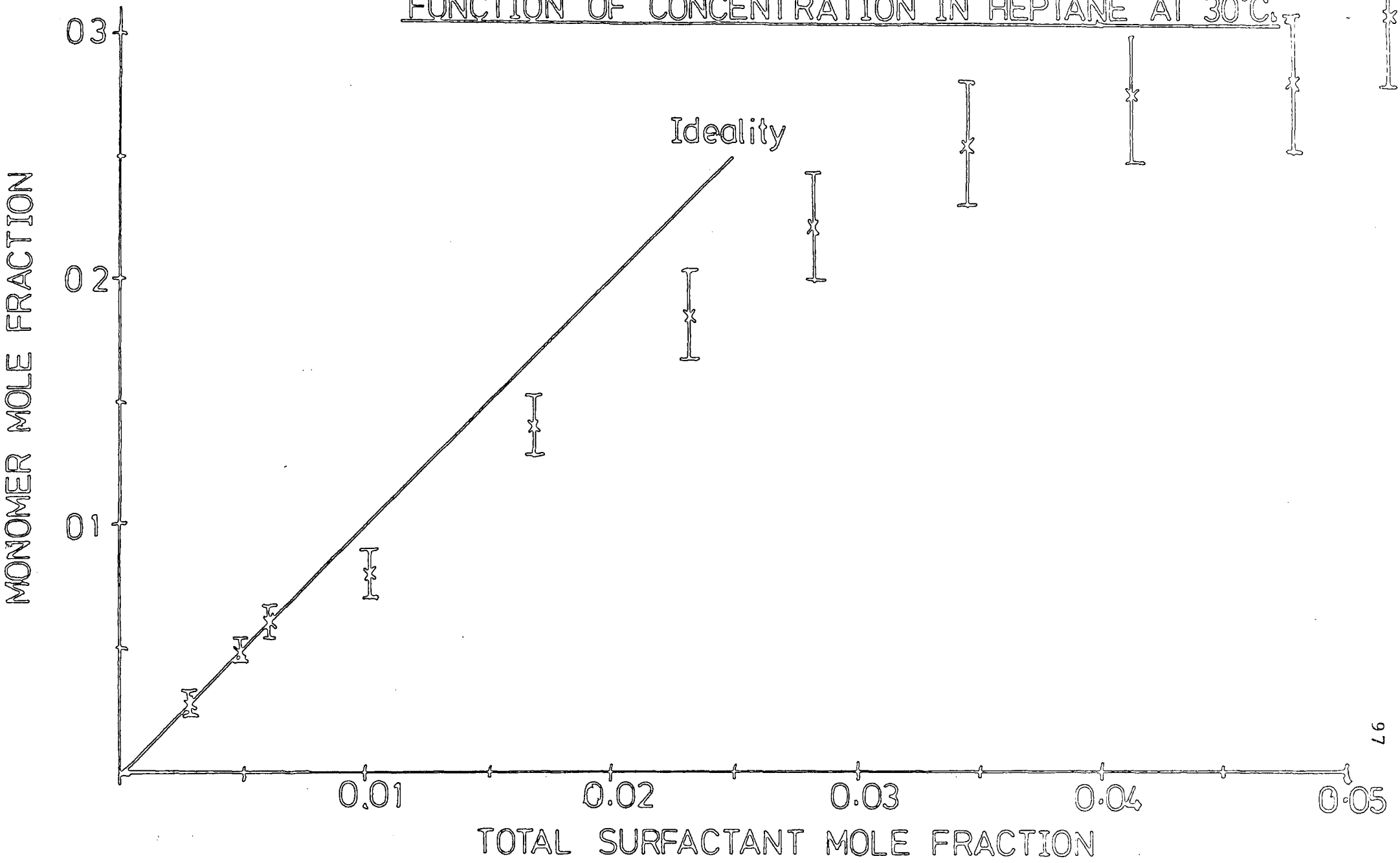

FIGURE 4.17 THE BEHAVIOUR OF $C_{12}E_3$ MONOMER AS A FUNCTION OF CONCENTRATION IN HEPTANE AT 30°C.

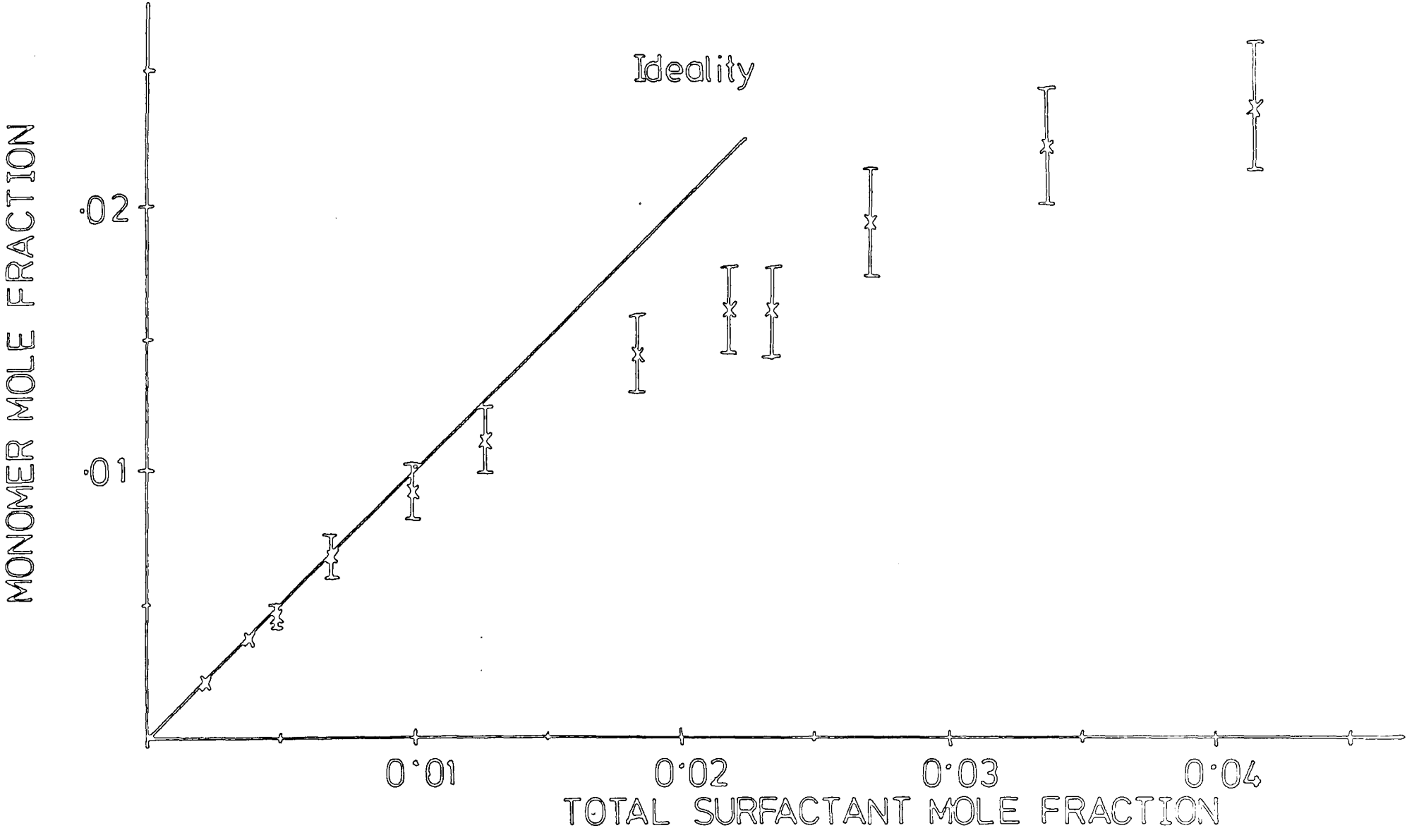

FIGURE 4.18 THE BEHAVIOUR OF $C_{12}E_4$ MONOMER AS A FUNCTION OF CONCENTRATION IN HEPTANE AT 30°C

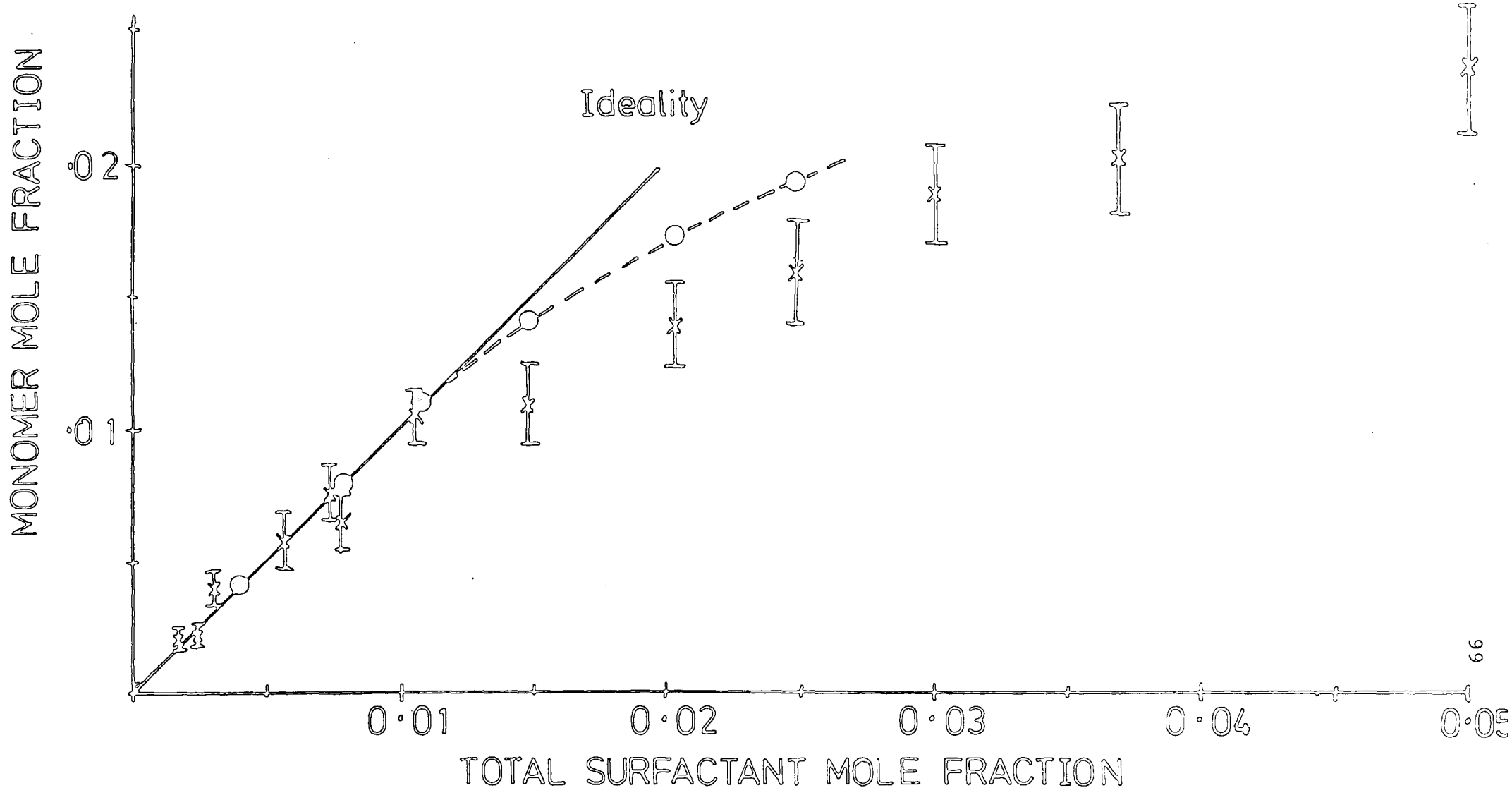

FIGURE 4·19 THE BEHAVIOUR OF $C_{12}E_5$ MONOMER AS A FUNCTION OF CONCENTRATION IN HEPTANE AT 30°C

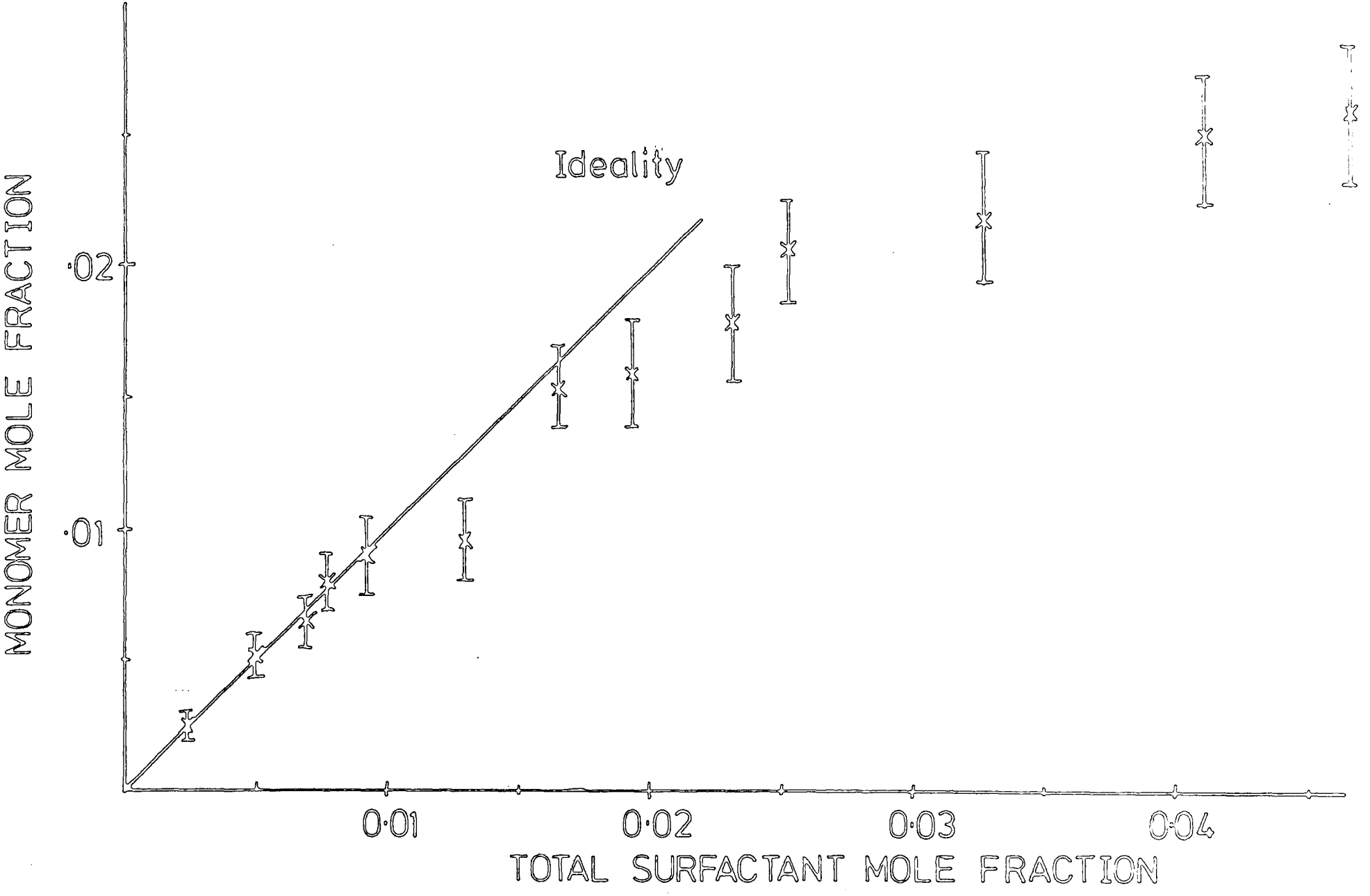

FIGURE 4·20. THE BEHAVIOUR OF $C_{12}E_8$ MONOMER AS A FUNCTION OF CONCENTRATION IN HEPTANE AT 30°C.

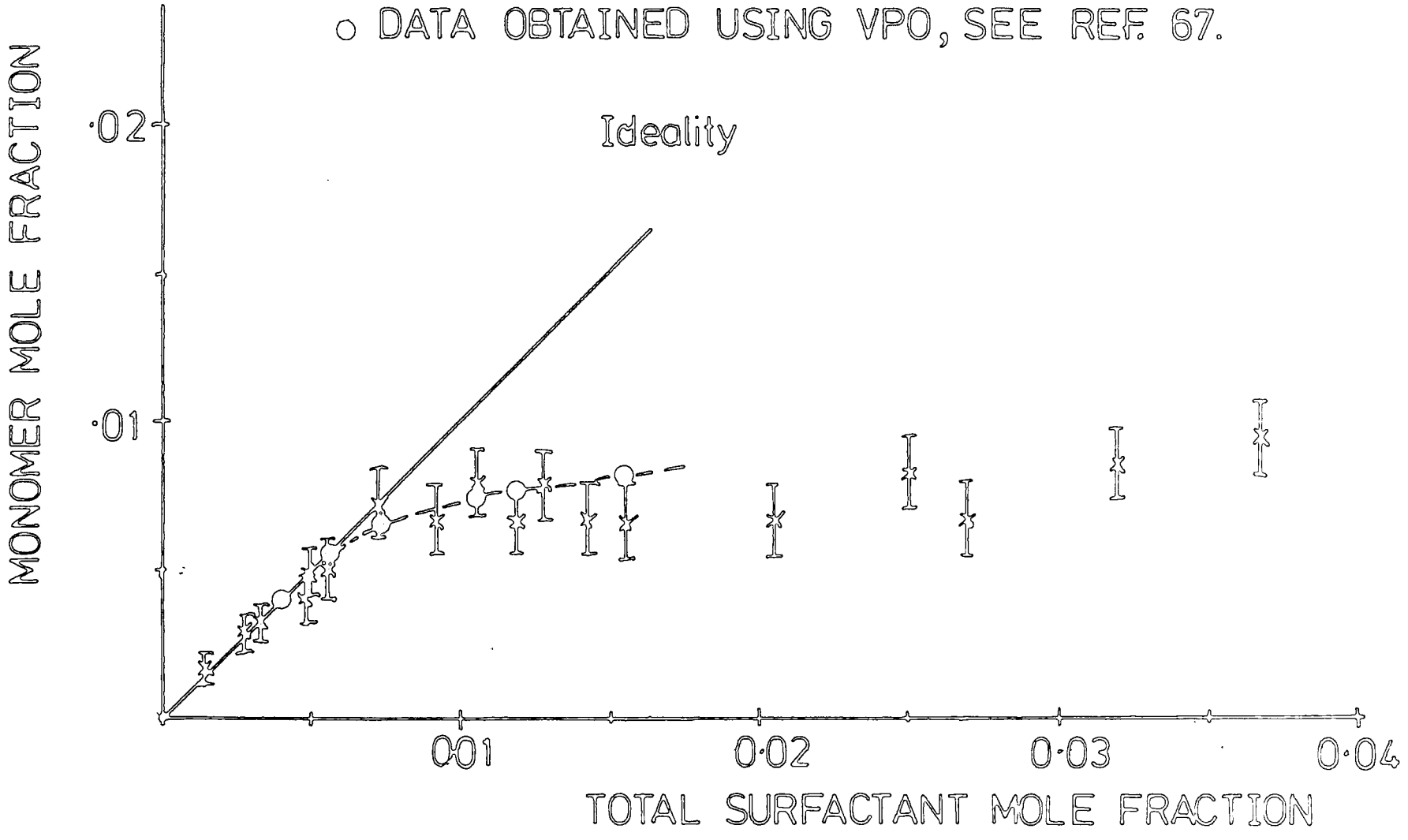

FIGURE 4·21 A COMPARISON OF $C_{12}E_N$ MONOMER BEHAVIOUR IN HEPTANE.

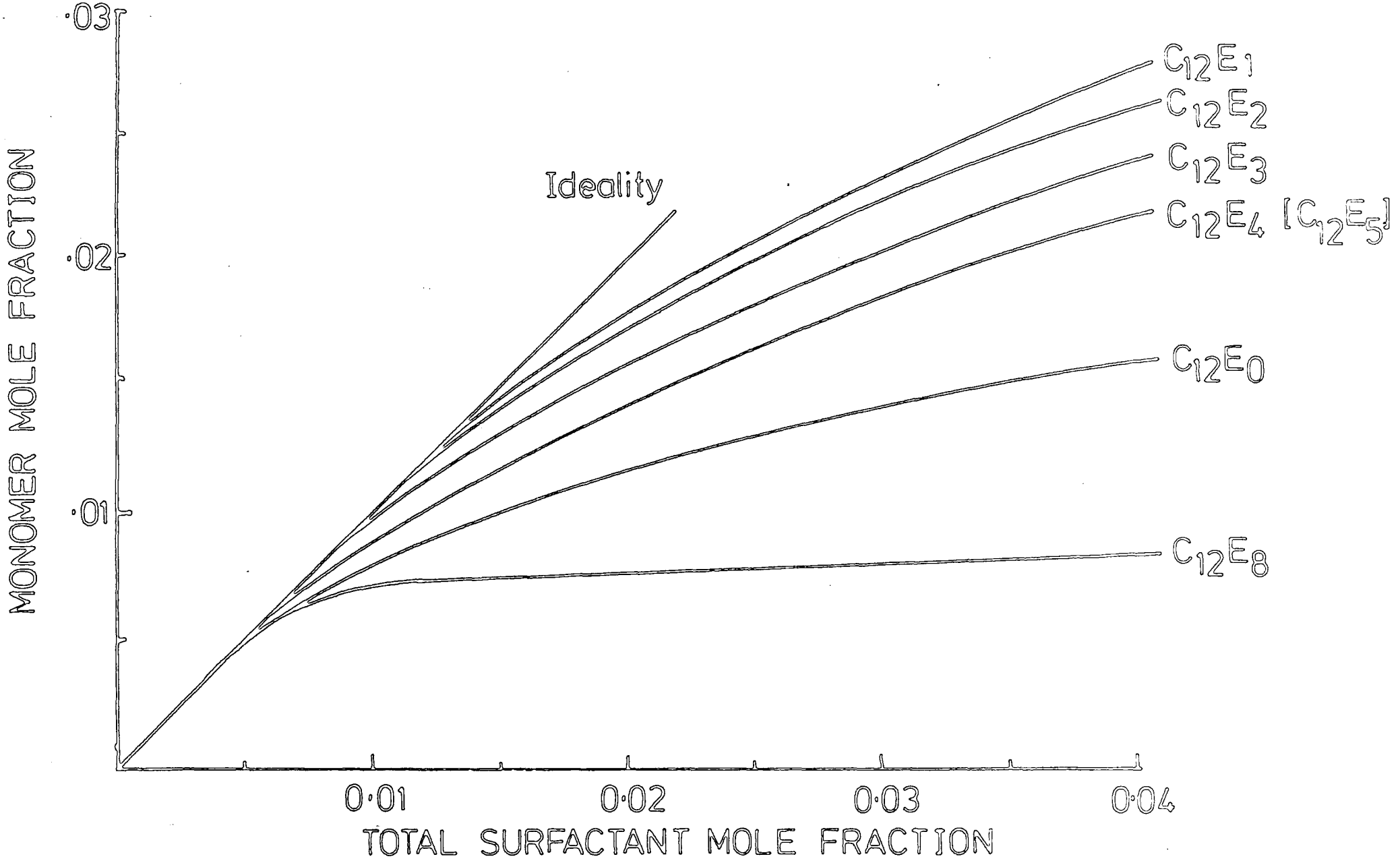

therefore aggregate more strongly than $C_{12}E_8$. The obvious conclusion is that other interactions must also be involved. Consideration of the molecular structure of an oxyethylene head group leads to several other possibilities:[93]

(i) The interaction energy between a permanent dipole and a dipole induced by it in another molecule. This dipole-induced dipole interaction is dependent on the inverse sixth power of the intermolecular separation (R) and is therefore considered as a short range effect. It depends on the polarizability of the affected molecule.

(ii) The energy of interaction between permanent dipoles which are again short range and dependent on R^{-6}.

(iii) The dispersion interaction between electrically neutral atoms or molecules such as that found in the inert gases. As with (i) and (ii), Londons dispersion forces are dependent on R^{-6} and thus relatively short range acting over several Å's. Figure 4.22 below shows the form of the potential which two surfactant molecules may experience.[70]

Figure 4.22 Intermolecular Potential Diagram for a Typical Molecule

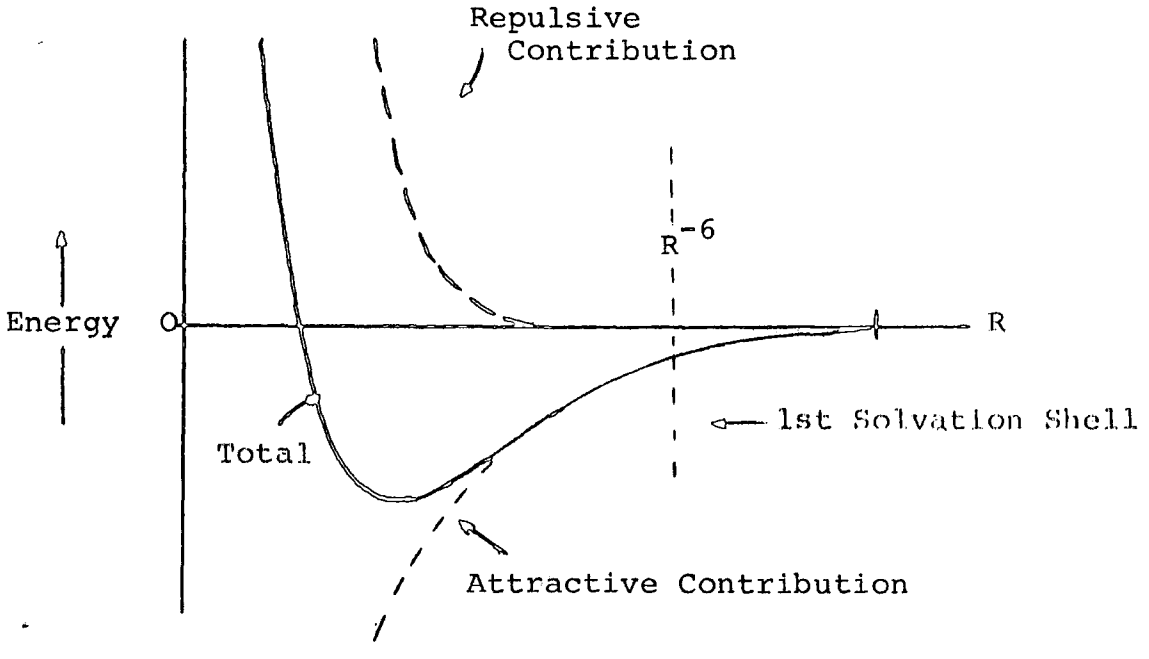

It is likely that the intermolecular potential energy diagram will be comprised of contributions from all the above interactions. Though we may only speculate here, it would seem likely that the major influences will originate from dipole-dipole and H-bonded interactions. For example there are several permutations for these interactions.

Figure 4.23 Some Possible Interactions Experienced by Oxyethylene Surfactants

(i) 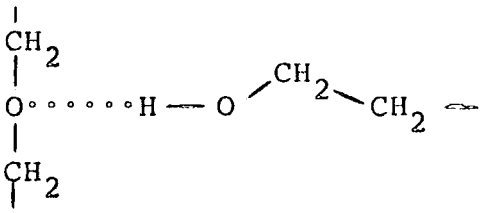 H-bonded

(ii) 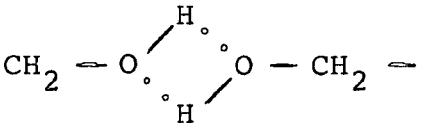 H-bonded

(iii) 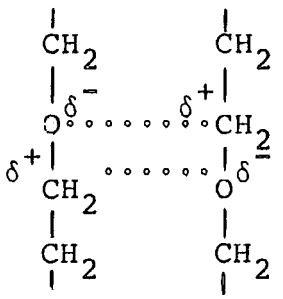 dipole-dipole

Figure 4.23 shows some of the possibilities available. It is obvious that as the headgroup increases in size then so does the number of different ways the molecules may interact. It seems likely that the magnitude of (iii) also becomes increasingly important in these systems. The overall contribution may be thought of as a "stickiness" of the head groups, acting over microscopic distances. One must realise that entropy considerations have been omitted in the above discussion. In general,

the greater the molecular freedom allowed by a particular interaction the greater likelihood of it occurring (for a given enthalpic attraction). Finally in addition to the above contributions, there will be a short range closed shell repulsion term for when the head groups approach too closely.[53]

In summary, therefore, one can say that polyoxyethylene surfactants form aggregates as a result of a number of possible contributions including, H-bonding, dipole-dipole, dipole-induced dipole and London's dispersion interactions. As the length of the oxyethylene chain increases then so does the magnitude of the above contributions. Association in dodecanol follows an entirely different mechanism with hydrogen bonding being the only likely interaction. The strength of the interaction follows the order,

$$C_{12}E_1 \lesssim C_{12}E_2 \lesssim C_{12}E_3 \lesssim C_{12}E_4 = C_{12}E_5 < C_{12}E_0 < C_{12}E_8$$

with hydrogen bonding being approximately equivalent to the interaction of <u>six</u> oxyethylene units.

The heats of solution of these compounds[51] show interesting behaviour in that a discontinuity is observed at low concentrations, of the order of 10^{-5} mol. ℓ^{-1}. They have assigned this discontinuity to the formation of micelles. We believe this data to be incorrect since our own findings show that the monomer behaviour follows ideality to concentrations several orders of magnitude higher.

4.4.2 The Determination of Aggregation Numbers

As mentioned in Chapter Three one can relate the total and monomer surfactant concentration with the number average aggregation number, $\bar{N}_A$ as:

$$\bar{N}_A = \frac{\partial[\ln(x_T - x_M)]}{\partial(\ln x_M)} \qquad \text{(eqn. 4.18)}$$

Thus the slope of a plot of $\ln(x_T - x_M)$ *versus* $\ln x_M$ will give the aggregation number. Though $\bar{N}_A$ may be calculated at any point, we have chosen 0.03mf since there will be some aggregation occurring at this concentration.

Figure 4.24 shows a typical plot for dodecanol at 30°C. At low concentration, where $\ln(x_T - x_M)$ approaches large values the slope of the curve approaches 1. As the mole fraction increases the slope increases gradually up to what seems a constant value. This increase in slope and hence aggregation number up to a value of 4.8±1.0 (at 0.03mf) agrees with what is generally accepted in the literature as being the tetramer.[30] Though the dimer is known to exist it is present in such small concentrations that it is not detected by this method *cf.* C≤2%.[30] The curve at higher concentrations then has a constant slope and hence a constant aggregation number. Similar results have been previously determined for both dodecanol and octanol.[30] The error in the data and that of the subsequent $C_{12}E_N$ curves have been calculated from minimum and maximum slopes at ≃0.03 m.f. The scatter in the data originates from the 5-10% error in monomer concentration calculated at high mole fractions.

The behaviour of the $C_{12}E_N$ surfactants is, not surprisingly, quite different to that of dodecanol. For $C_{12}E_1$ to $C_{12}E_5$ the

FIGURE 4.24 DETERMINATION OF AGGREGATION NUMBER FOR DODECANOL IN HEPTANE.

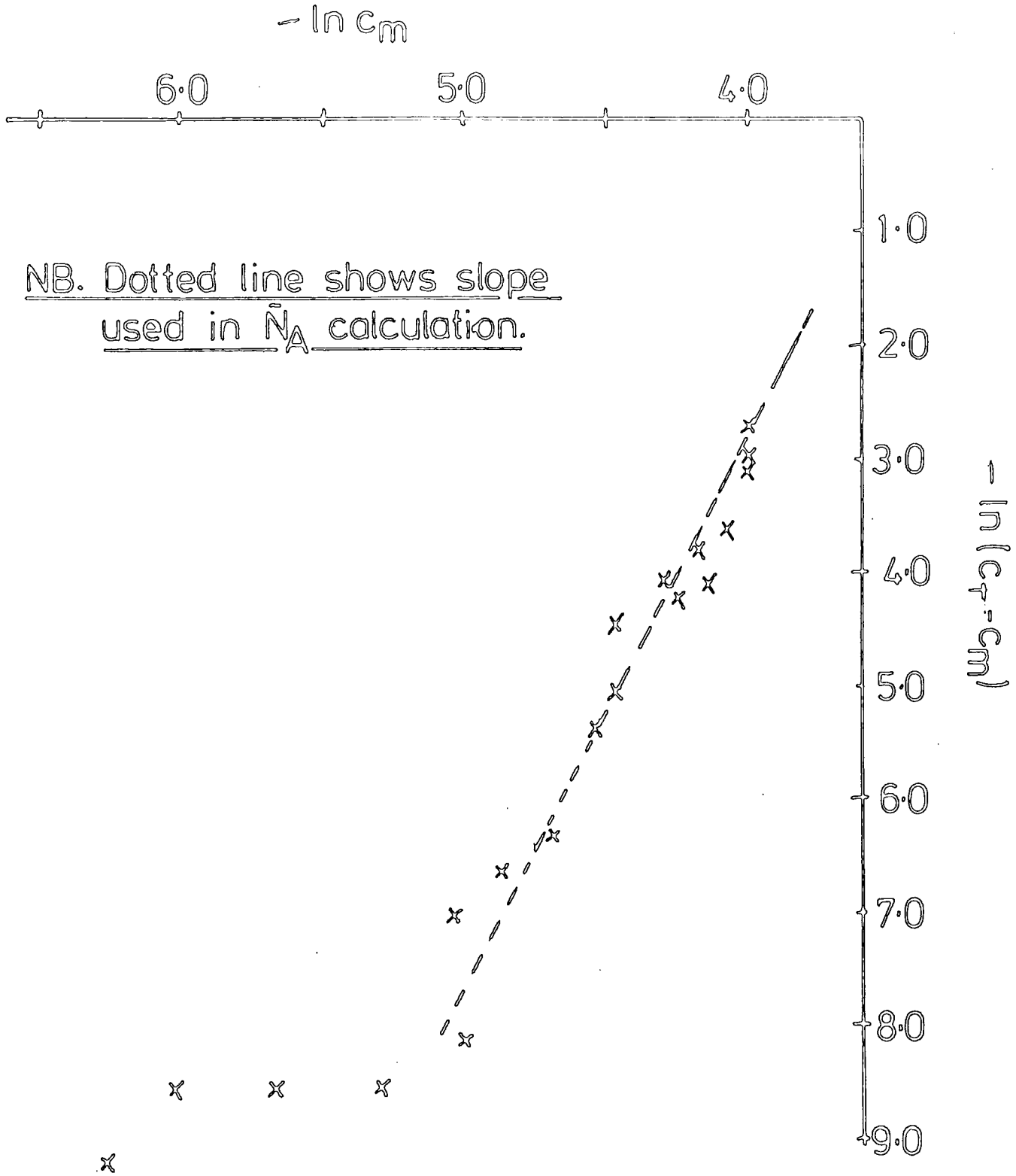

aggregation numbers seem to be constant at approximately 3 (at 0.03 mf). Table 4.4 shows the values while Figures 4.24-4.30 illustrate the curves from which the aggregation numbers were calculated. The first thing to note is that for $C_{12}E_1$ - $C_{12}E_5$ the curves are very similar but the slopes not as sharp as that for dodecanol.

TABLE 4.4 Aggregation Numbers for some Oxyethylene Surfactants at 30°C

Surfactant	$\bar{N}_A$ (at 0.03 mf)	Literature
$C_{12}E_0$	4.8 ± 1.0	4 (30)
$C_{12}E_1$	3.5 ± 0.6	-
$C_{12}E_2$	2.8 ± 1.0	-
$C_{12}E_3$	3.7 ± 1.0	-
$C_{12}E_4$	2.9 ± 0.3	6 (20°C) (53)
$C_{12}E_5$	3.9 ± 1.0	-
$C_{12}E_8$	8 ± 4	8 (67)

Unfortunately the data does not extend high enough in concentration to be able to say whether the aggregation number remains constant. The data of $C_{12}E_8$ is quite difficult to interpret since the scatter is quite large. However inspection of the slope at high concentrations suggests that aggregates are larger than in the other amphiphiles. Data obtained using vapour pressure osmometry and light scattering give the same value of $\bar{N}_A = 8$ for $C_{12}E_8$.[67] For the other surfactants there seems to be a reasonable agreement with the values obtained using other techniques. The work of Ravey *et al*[53] shows that

FIGURE 4·25 DETERMINATION OF AGGREGATION NUMBER FOR $C_{12}E_1$ IN HEPTANE.

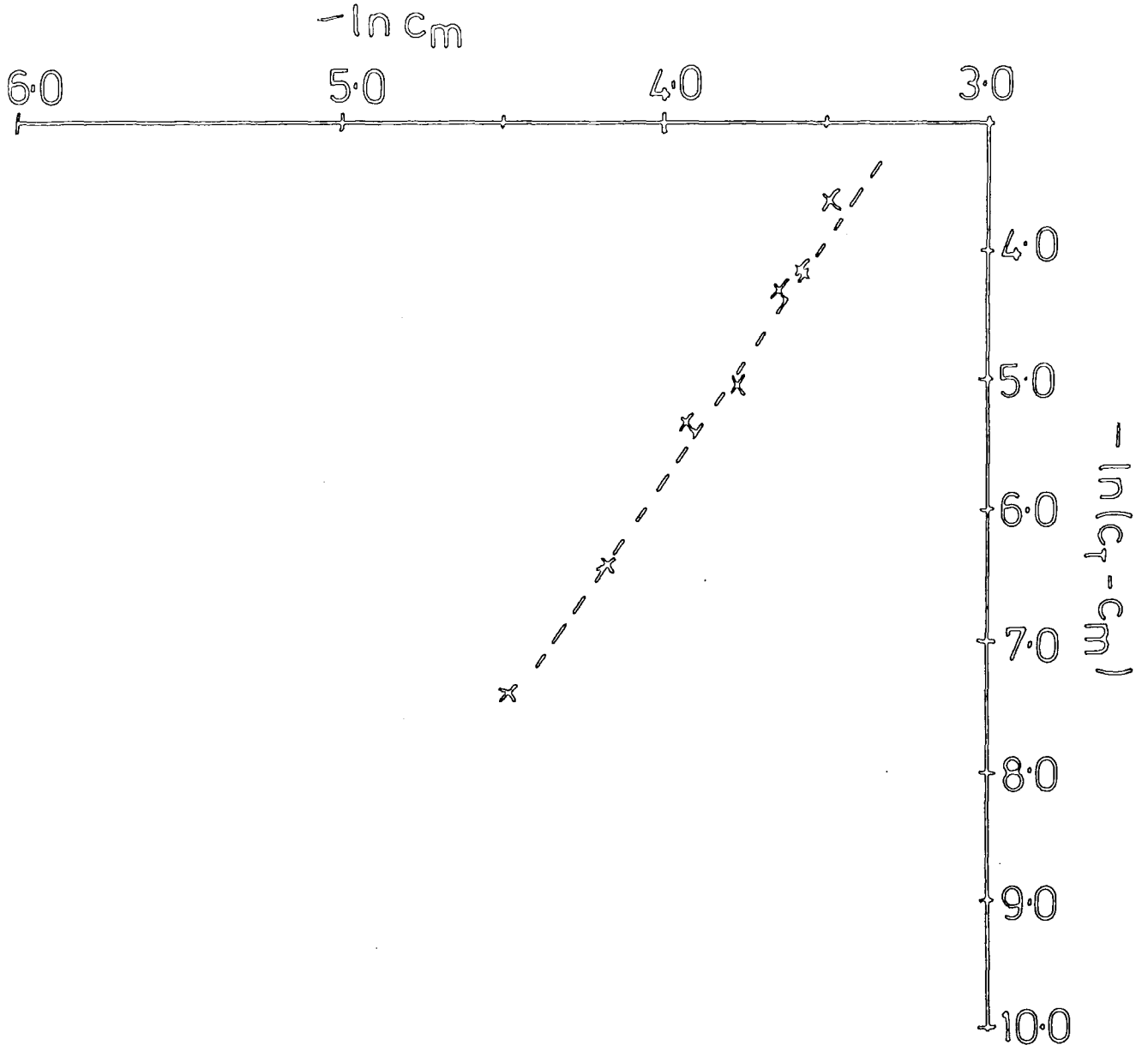

FIGURE 4·26 DETERMINATION OF AGGREGATION NUMBER FOR $C_{12}E_2$ IN HEPTANE.

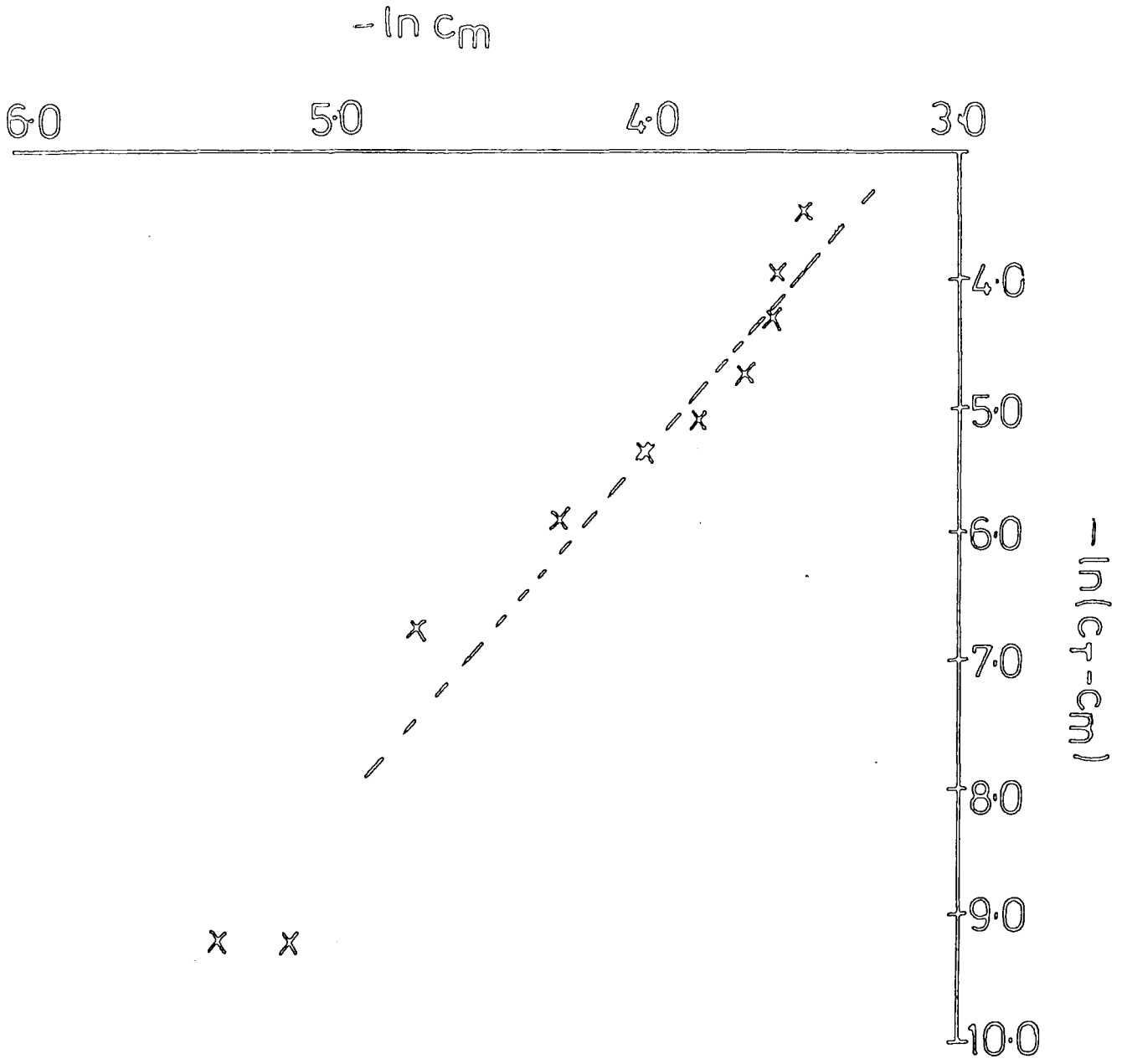

FIGURE 4.27 DETERMINATION OF AGGREGATION NUMBER FOR $C_{12}E_3$ IN HEPTANE.

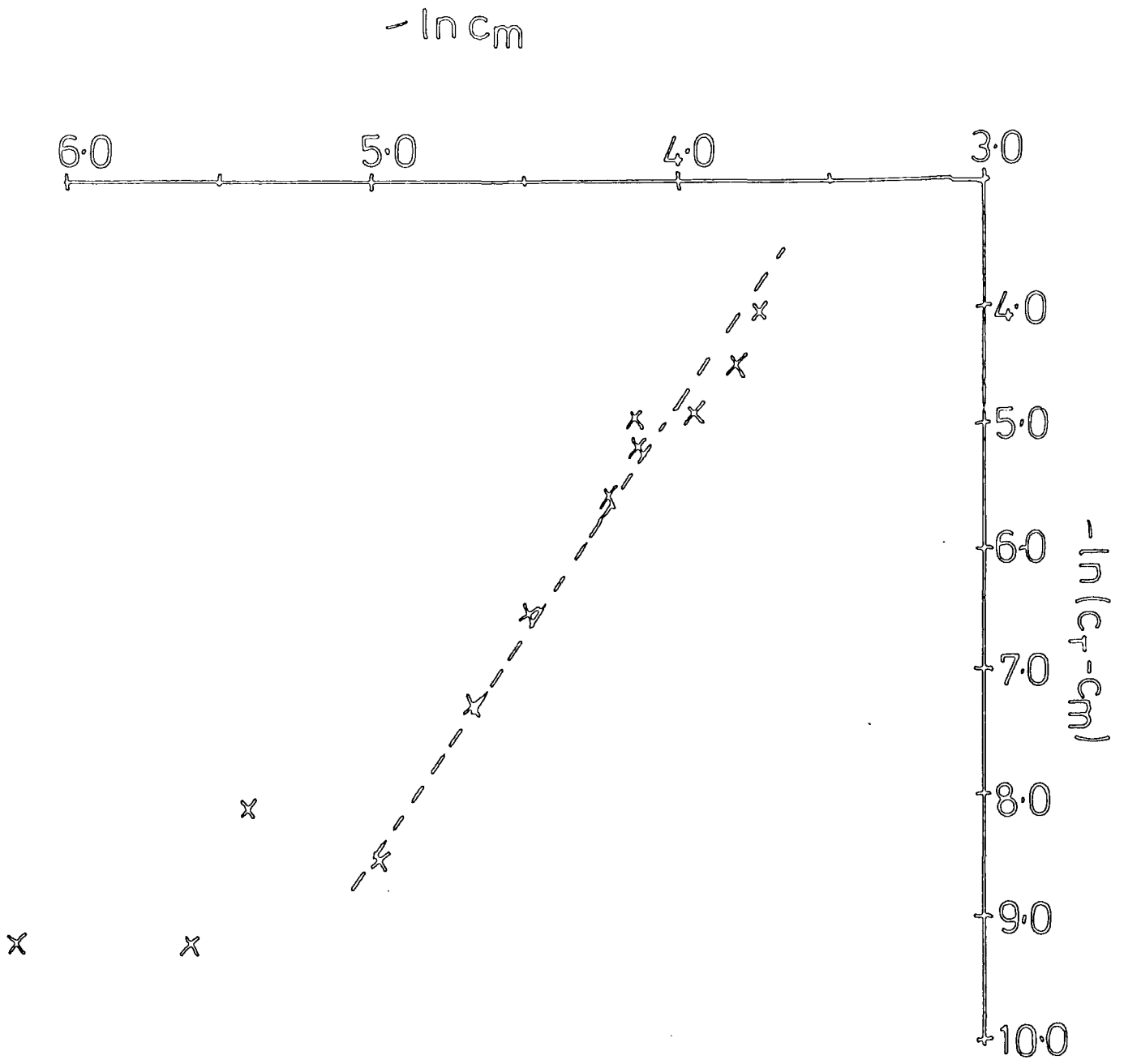

FIGURE 4·28 DETERMINATION OF AGGREGATION NUMBER FOR $C_{12}E_4$ IN HEPTANE

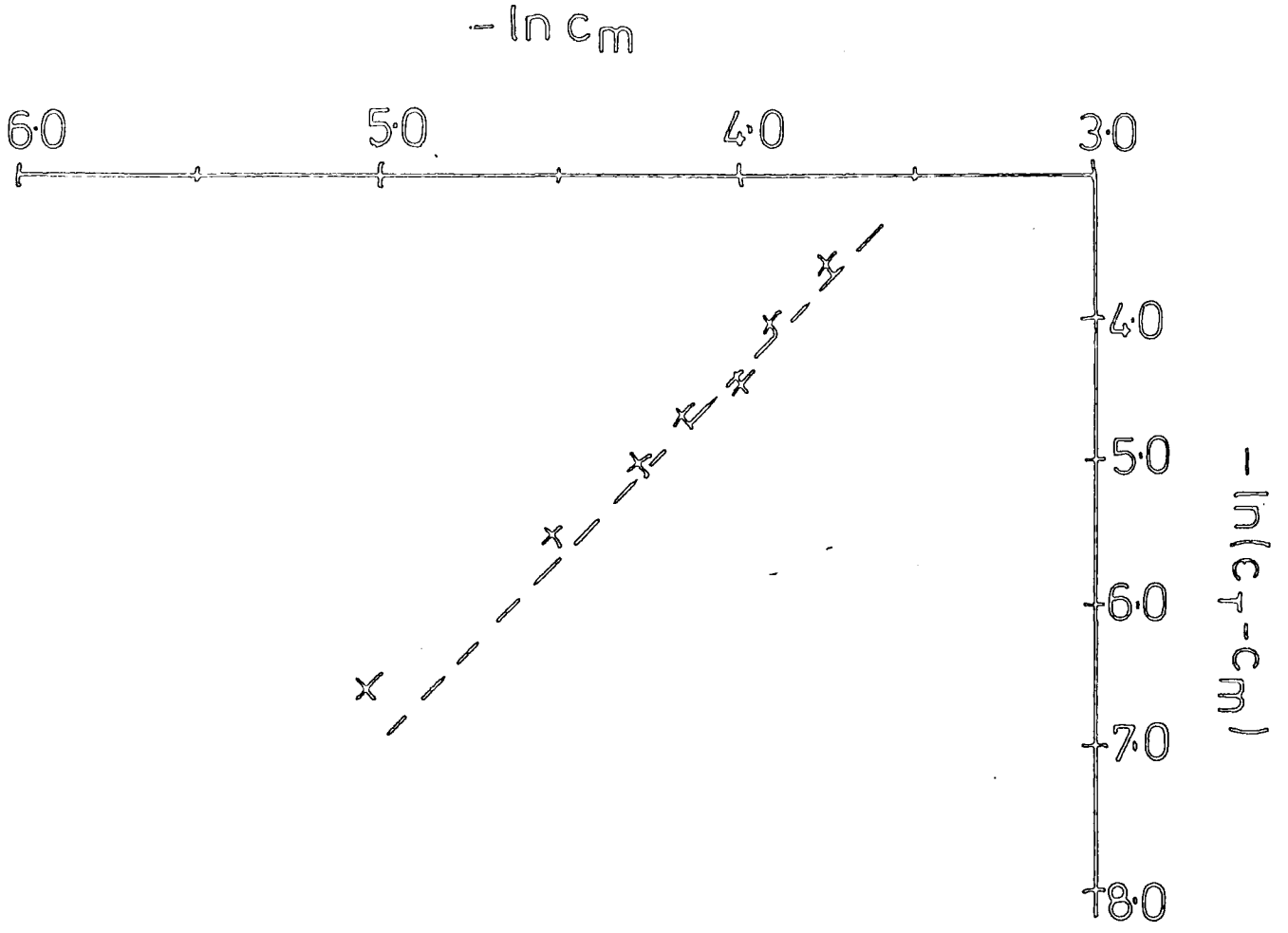

FIGURE 4.29 DETERMINATION OF AGGREGATION NUMBER FOR $C_{12}E_5$ IN HEPTANE.

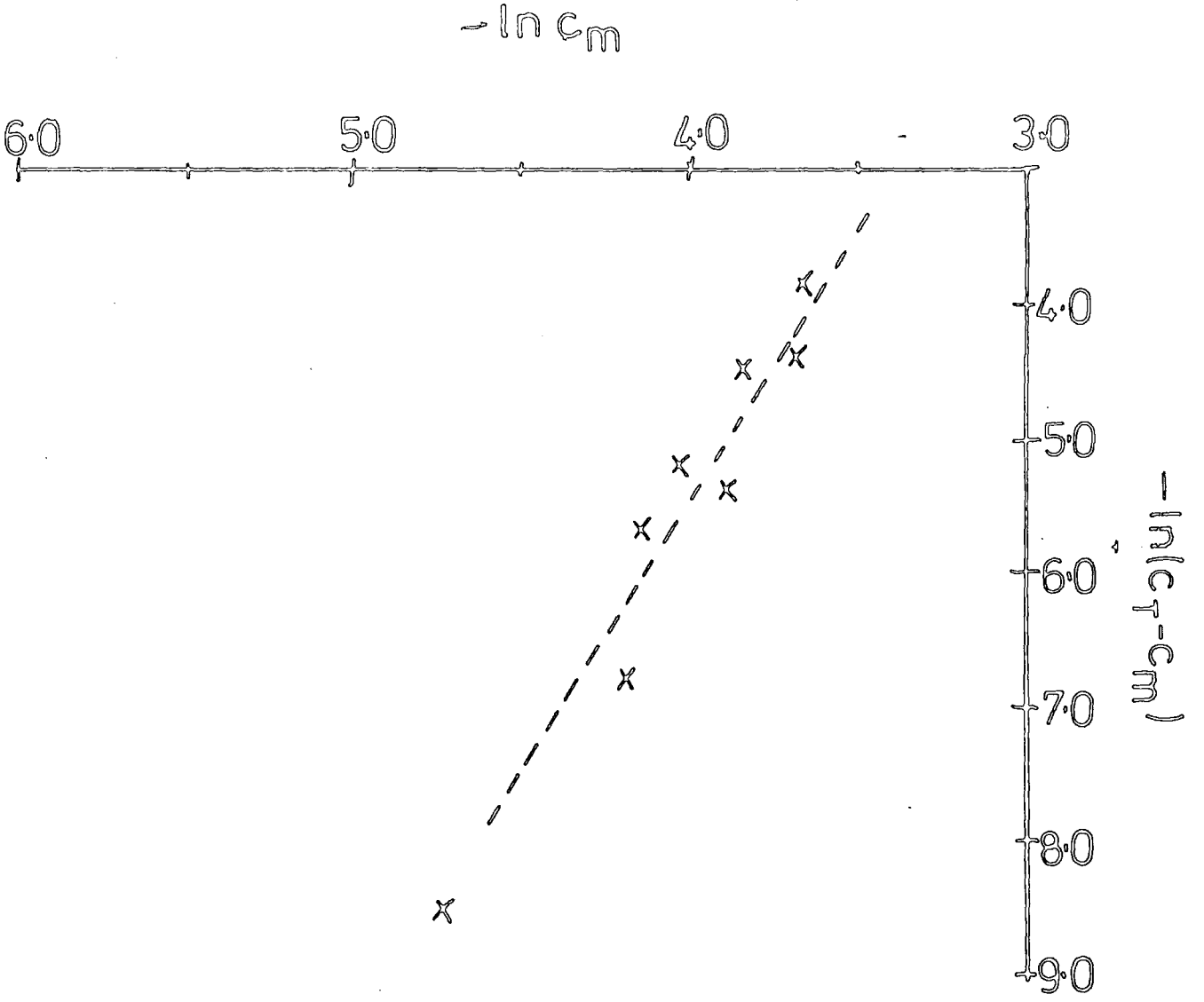

FIGURE 4.30 DETERMINATION OF AGGREGATION NUMBER FOR $C_{12}E_8$ IN HEPTANE.

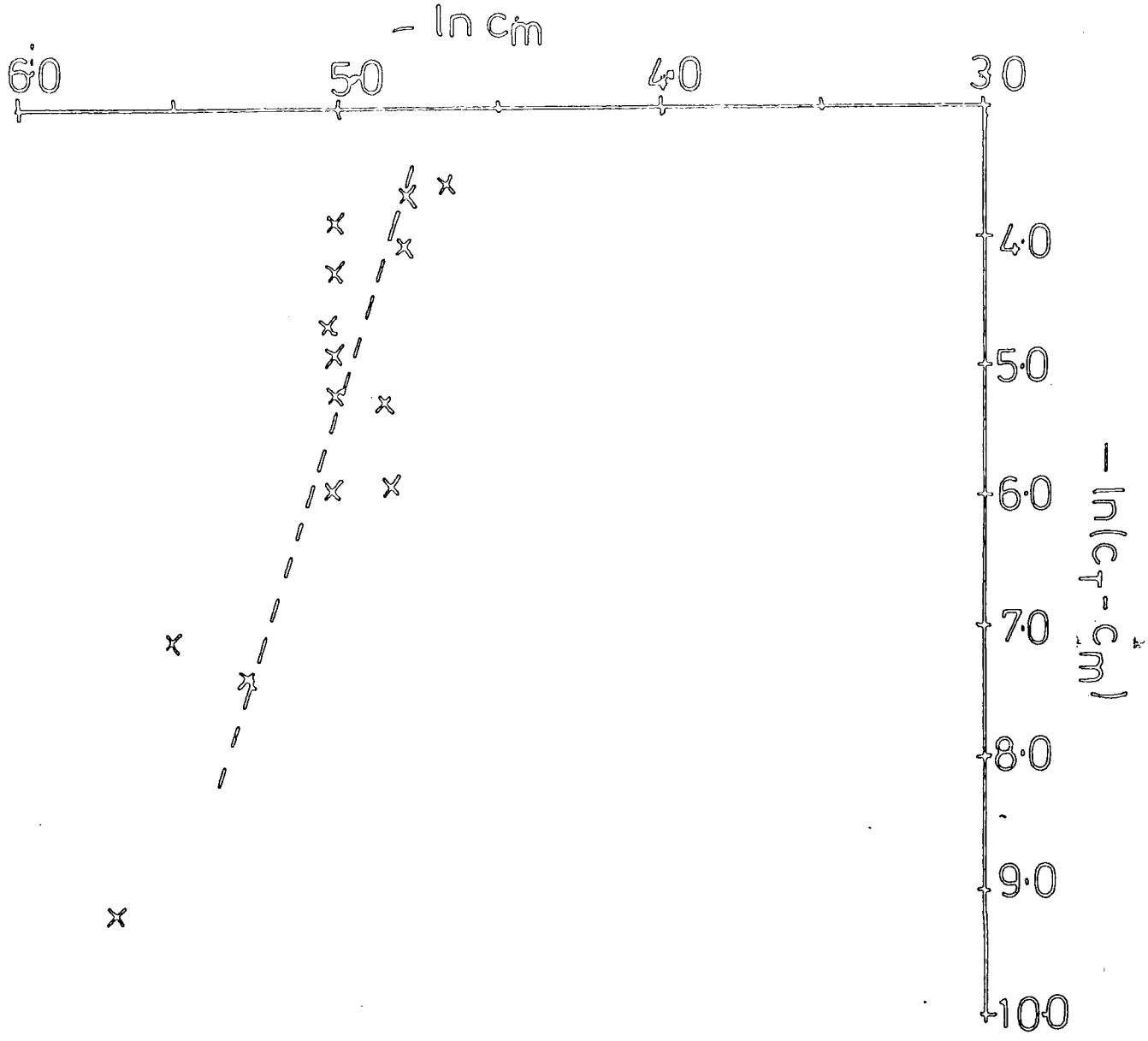

the aggregation number only increases slowly once the association has begun. It is interesting to note that their technique (small angle neutron scattering) is able to distinguish between two aggregate types, the lamella and the Hank-like aggregate depicted below in Figure 4.31.

Figure 4.31 Two Types of Aggregate Geometry found in $C_{12}E_N$ Systems (reproduced from reference[53])

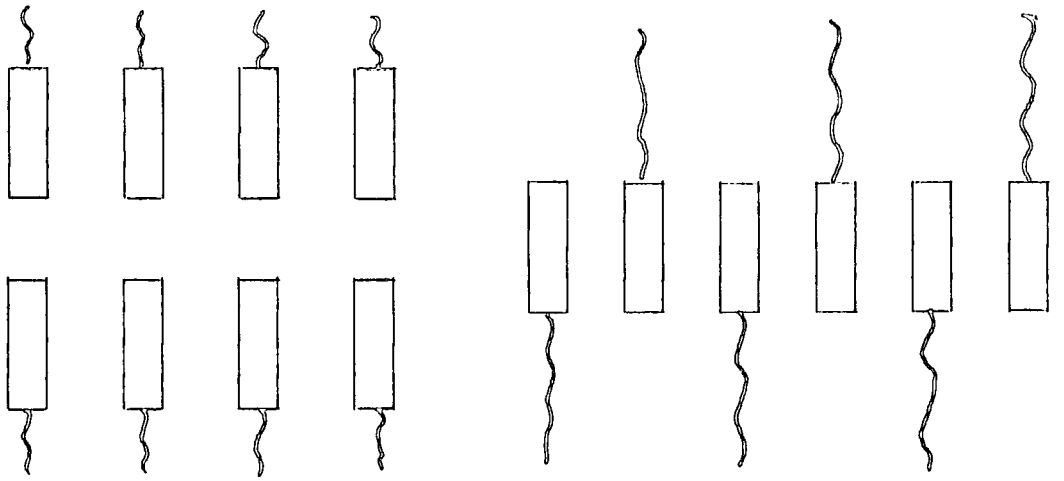

Lamella Hank-like

Disc-shaped aggregates are thought to be preferred since this geometry maximises the various interaction energies. In addition their work gives important information concerning aggregation in the different solvents but this will be discussed in the next section.

Since aggregation numbers have been calculated it is possible to determine the average free energy of aggregation $\bar{G}^{\theta}$ for the equilibrium:

$$A(C_{12}E_{\square}) \rightleftharpoons^{K} (C_{12}E_N)_A \qquad \text{(eqn. 4.19)}$$

using the standard relationship:

$$\Delta G^{\theta} = -RT\ln K \qquad \text{(eqn.4.20)}$$

Table 4.5 gives the results of these calculations.

TABLE 4.5 Free Energy of Aggregation for some $C_{12}E_N$ Surfactants in Heptane at 30°C

Surfactant *	$\bar{N}_A$	$\Delta\bar{G}^\theta$ (KJ mol^{-1})
$C_{12}E_0$	5 ± 1	-24 ± 6
$C_{12}E_1$	3.5 ± 0.6	-9 ± 3
$C_{12}E_2$	2.8 ± 1.0	-9 ± 5
$C_{12}E_3$	3.7 ± 1.0	-14 ± 5
$C_{12}E_4$	2.9 ± 0.3	-10 ± 2
$C_{12}E_5$	3.9 ± 1.0	-17 ± 6
$C_{12}E_8$	8 ± 4.0	-59 ± 32

* All values calculated at ≈0.03 mf.

The average standard free energies of aggregation calculated above show that at 0.0300 mole fraction the association is a spontaneous process (in the thermodynamic sense). The errors of the above values largely arise from the prior determination of the aggregation numbers.

4.5 Aggregation Phenomena of $C_{12}E_4$ in various Solvents

4.5.1 The Spectroscopy of $C_{12}E_1$ and $C_{12}E_4$ in Apolar Solvents

As well as enabling us to determine monomer concentrations, spectra of $C_{12}E_1$ at low mole fractions provide a wealth of qualitative information. The spectra obtained show significant changes in both spectroscopic properties and the

internal monomer equilibrium. Table 4.6 below shows these parameters for the M_{I5} band of $C_{12}E_1$ as a function of solvent.

TABLE 4.6 Spectroscopic Properties of $C_{12}E_1$ in some Apolar Solvents

Solvent	Molar Volume ($cm^3.mol^{-1}$)	$\nu_{max}(M_{I5})$ cm^{-1}	$\Delta\nu_{1/2}(M_{I5})$ cm^{-1}	$B^{\dagger}(M_{I5})$ $\ell.mol^{-1}.cm^{-1}$
Heptane*	147	3607 ± 2	18 ± 2	1050 ± 10
Decane	195	3607 ± 2	18 ± 2	1030 ± 10
Decalin	156	3605 ± 2	20 ± 2	1190 ± 40
CCl_4	97	3600 ± 2	35 ± 2	1680 ± 60
Benzene	89	3595 ± 2	38 ± 2	2680 ± 350
$CDCl_3$	80	3600 ± 2	58 ± 2	2570 ± 30

*At 30°C †B is the integrated molar absorption coefficient.

Of the solvents studied, the aliphatic hydrocarbons show little change relative to each other. A slight increase in the absorption coefficient (B), width at half maximum intensity and frequency maximum is however observed for decalin as the solvent. Such a change would not be entirely unexpected from consideration of differences in the molecular geometry. Though the molar volumes of decane and decalin are 195 and 156 $cm^3.mol^{-1}$, respectively, the value of 147 $cm^3.mol^{-1}$ for heptane suggests that some other affect is observed. However, further examination of Table 4.6 shows that there is some gross relationship between the molar volume and the above spectroscopic properties. From such behaviour one may anticipate differences in the fluctional head group equilibrium ($M_{NB} \rightleftharpoons M_{I5}$), thus possibly altering the magnitude of some vibrational relaxation mechanisms.

Figures 4.32,a,b and c show the low concentration $C_{12}E_1$ spectra in heptane, decane and decalin. The spectrum obtained in CCl_4 is significantly different from those in the above hydrocarbons yet it, too, is also a relatively "inert" solvent. In this case the perturbations are likely to arise from a combination of molar volume (97 $cm^3.mol^{-1}$) and surrounding electric fields. This latter contribution will have an effect on the electron distribution and hence on $\left|\frac{\partial \mu}{\partial q}\right|^{2.75}$.

The behaviour of the M_{I5} hydrogen bonded bands in benzene and deuterochloroform are more complex. It is known that strong interactions exist between the ether oxygen and these molecules.[53,71,76] The M_{NB} band is more noticeable in deuterochloroform and its increased relative intensity (see Figure 4.32f) suggests that there is some stabilization of this species. The corresponding band in benzene is less noticeable, probably because the M_{NB} and M_{I5} species absorb at approximately the same frequencies. This result suggests that intramolecular H-bonded interactions in benzene are small (*e.g.* due to solvent polarity) and would explain the large absorption coefficients which occur for these two solvents.

Inspection of the low concentration spectra of $C_{12}E_4$ in these solvents (Figures 4.33-37) reveal little concerning the intramolecular equilibria. In general all the spectra at low concentrations show the M_{I8} band at 3505 cm^{-1} with the notable exception of $CDCl_3$. Also the width of this band increases in the order Heptane $\cong$ Decane $\cong$ Decalin $\cong$ CCl_4 < Benzene $\cong$ $CDCl_3$, varying from 55 to 90 cm^{-1}. It is not possible to draw conclusions concerning the internal equilibria with higher ring

FIGURE 4.32 SPECTRA OF $C_{12}E_1$ BETWEEN 3800-3400cm^{-1} IN SOME APOLAR SOLVENTS.

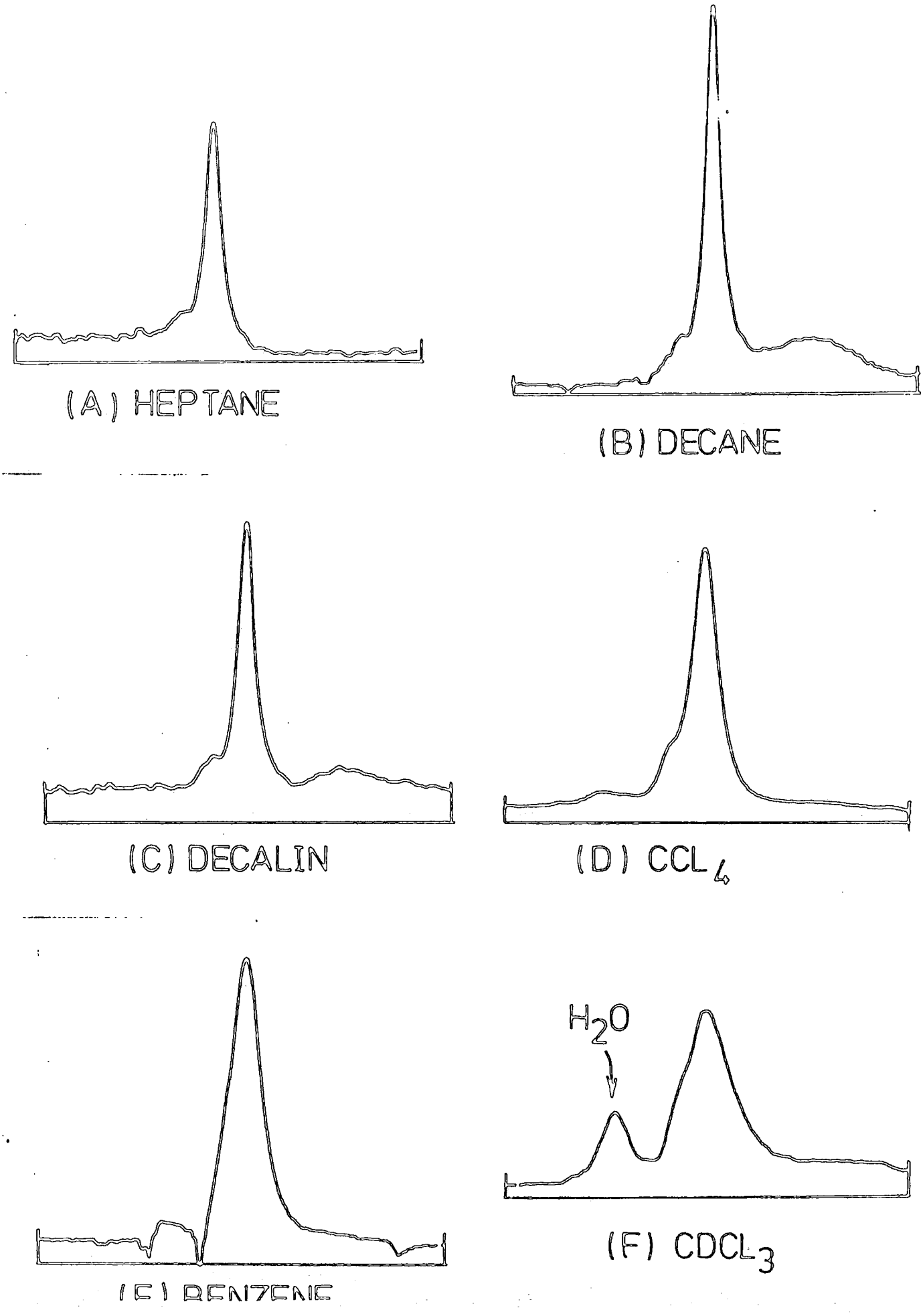

FIGURE 4·33 SPECTRA OF $C_{12}E_4$ IN DECANE.

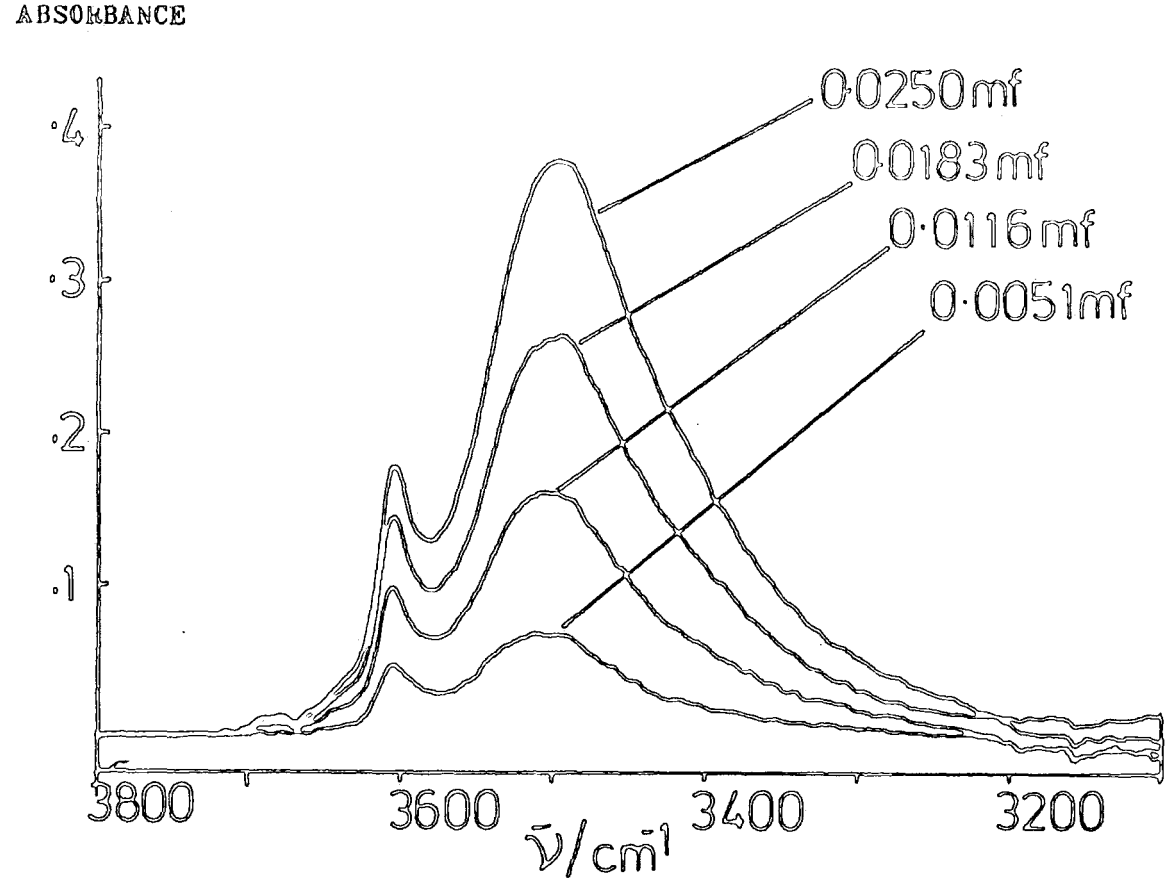

FIGURE 4·34 SPECTRA OF $C_{12}E_4$ IN DECALIN.

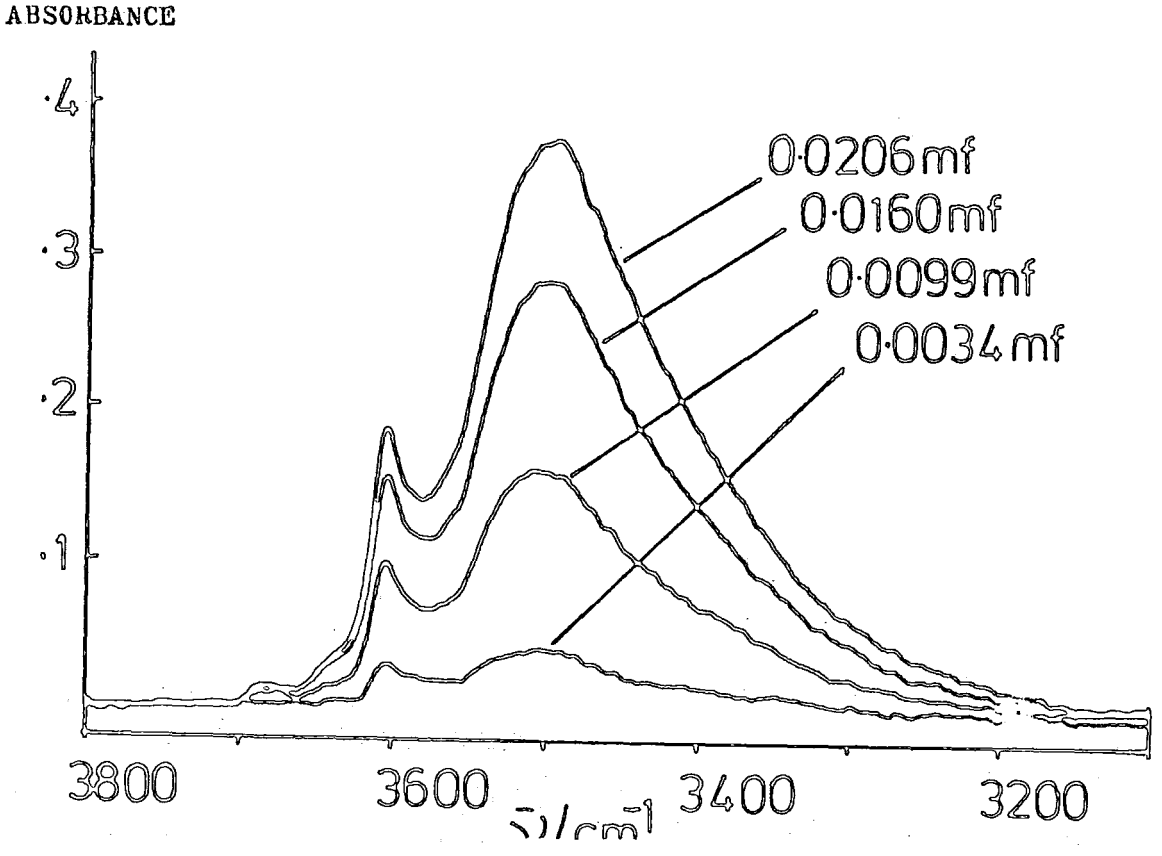

FIGURE 4·35 SPECTRA OF $C_{12}E_4$ IN CCl_4

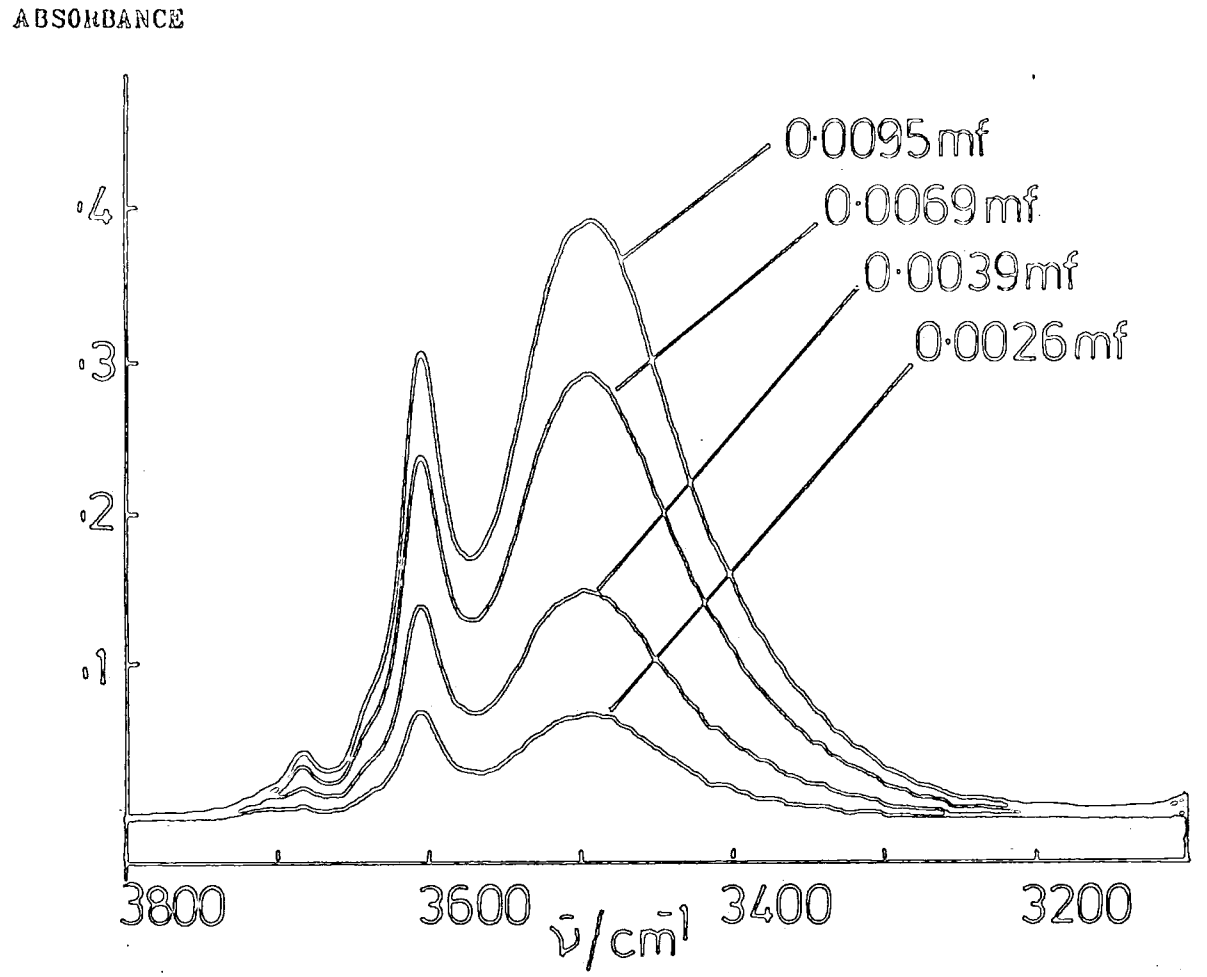

FIGURE 4·36 SPECTRA OF $C_{12}E_4$ IN BENZENE

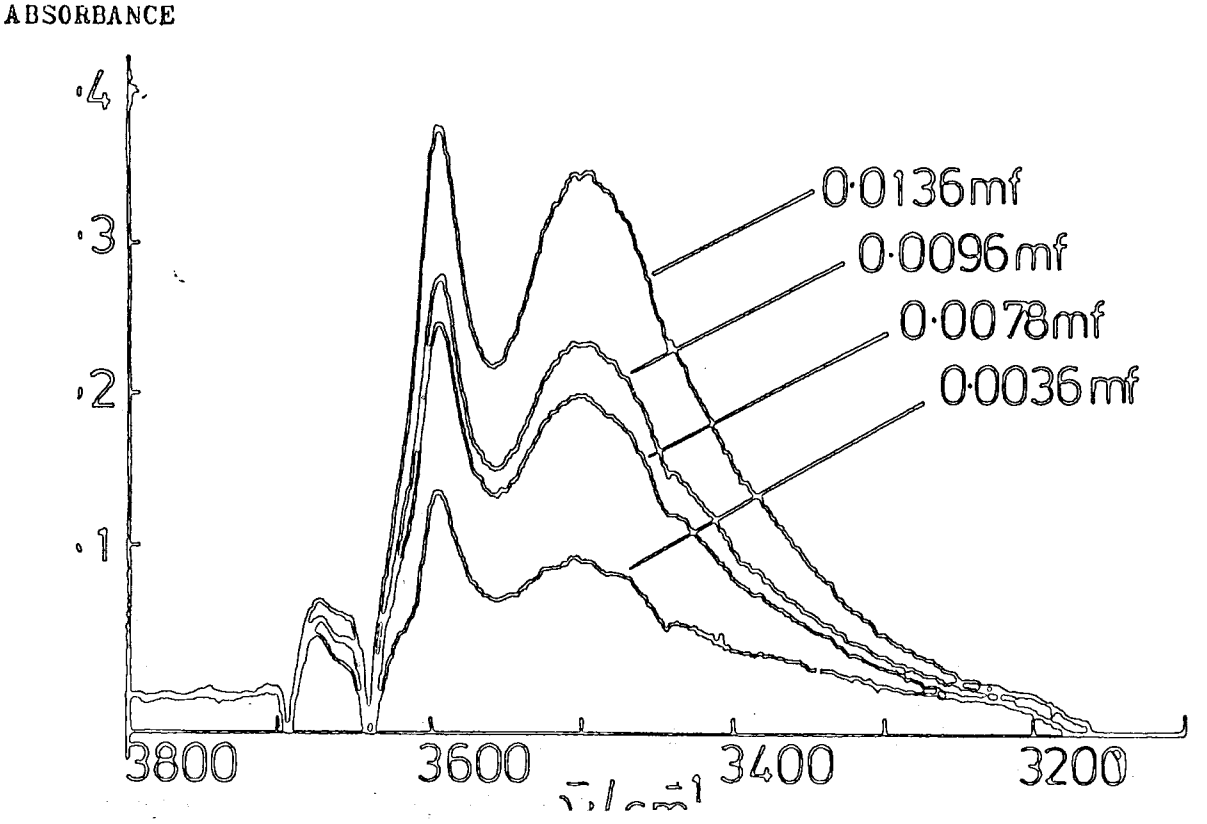

FIGURE 4·37 SPECTRA OF $C_{12}E_4$ IN $CDCL_3$.

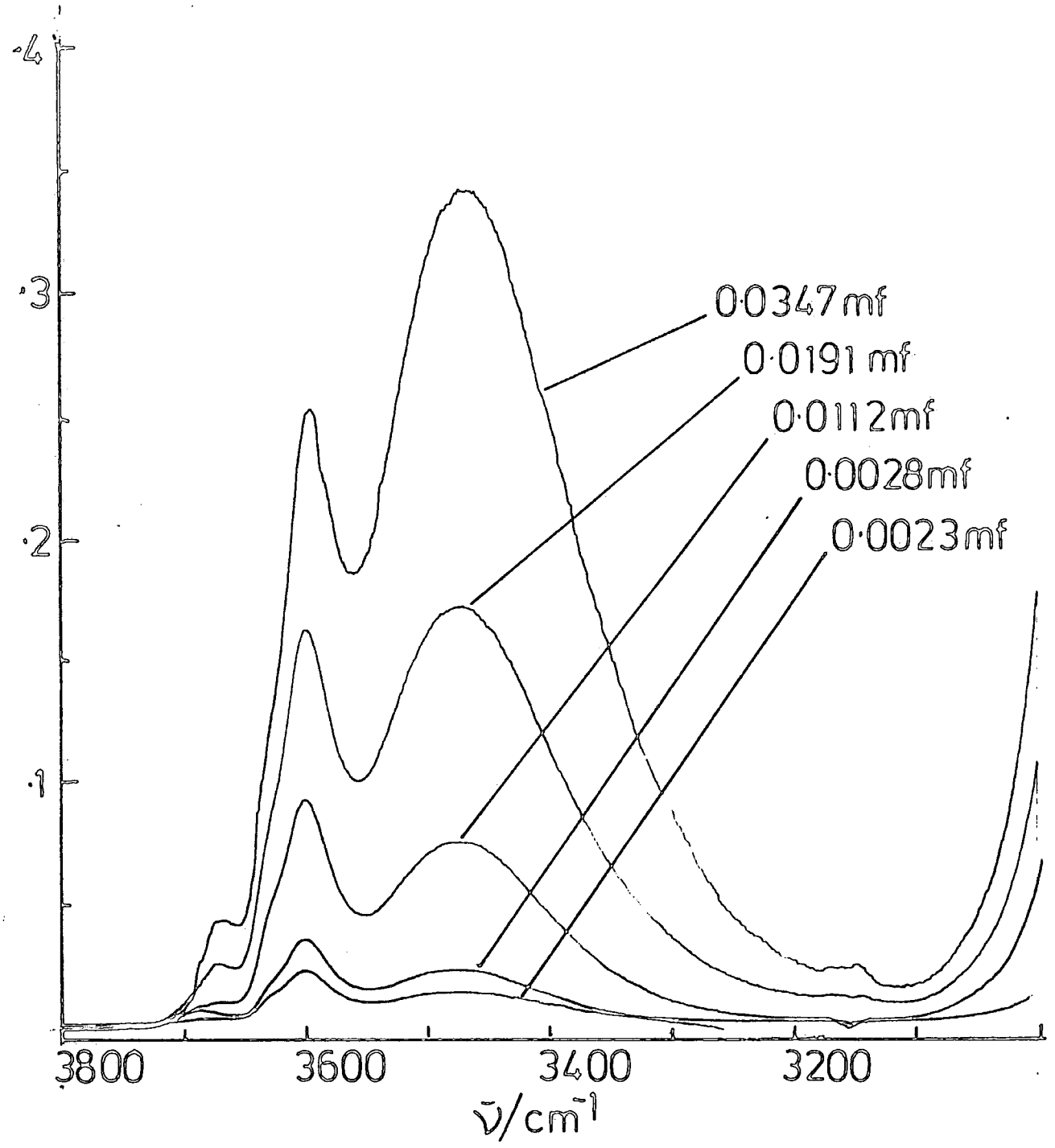

sizes because of the changes in width observed in the M_{I5} band previously. It was thought that similar perturbations would be experienced by these higher analogues. The spectra at higher concentrations showed a shift of ≈15 cm^{-1} for $C_{12}E_4$ in all solvents indicating stronger hydrogen bonded interactions.

4.5.2 The Behaviour of $C_{12}E_4$ Monomers in Apolar Solvents

Earlier in this chapter we discussed the possible driving forces for surfactant association in apolar systems. In this section we present further evidence to support our earlier conclusions by studying the association process in various solvents. In addition to $C_{12}E_4$ in heptane (at 30°C) we have studied this ampliphile in n-decane, decalin, carbon tetrachloride, benzene and deuterochloroform. The experimental procedure adopted in this section is identical to that used in the earlier work (see Section 4.2) though the temperature used was 35°C and special care was taken to reduce the water in these systems. In some cases (deuterochloroform) a slightly different normalizing region was chosen for solvent subtraction. In all cases low concentration of spectra $C_{12}E_1$ were recorded so as to calculate the absorption coefficient for the M_{I5} species. The half widths determined in these spectra were applied in the determination of the M_{I5} absorbance. The significance of this procedure requires only the height to be determined in the $C_{12}E_4$ spectra (the half width seems to remain constant with increasing concentration). Also, the assumptions discussed in Section 4.3.1 have also been used here.

The monomer curves for $C_{12}E_4$ in the various solvents have been plotted individually in Figures 4.38-4.42. A comparison

FIGURE 4·38 THE BEHAVIOUR OF $C_{12}E_4$ MONOMER IN DECANE AT 35°C.

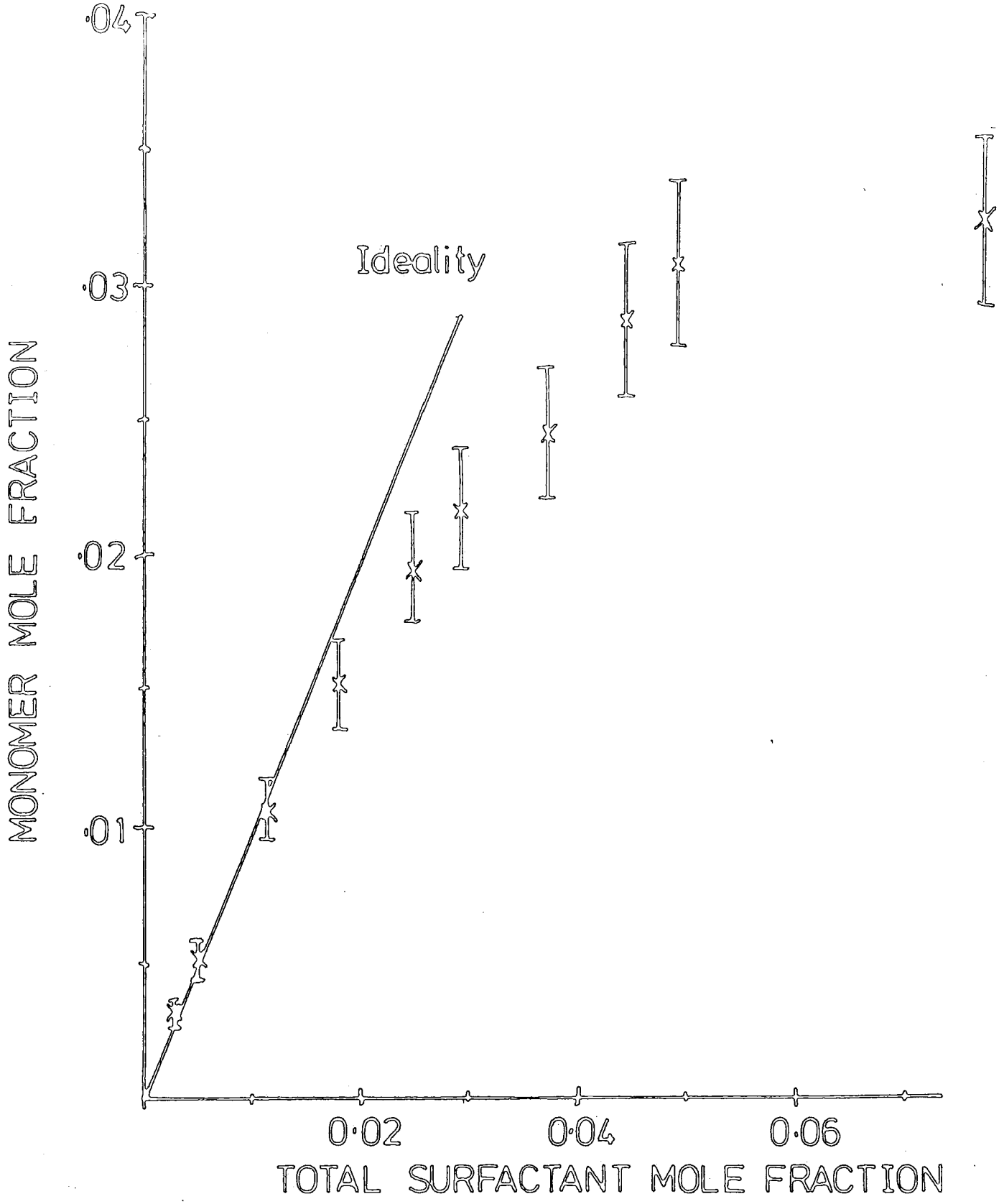

FIGURE 4·39 THE BEHAVIOUR OF $C_{12}E_4$ - MONOMER IN DECALIN AT 35°C.

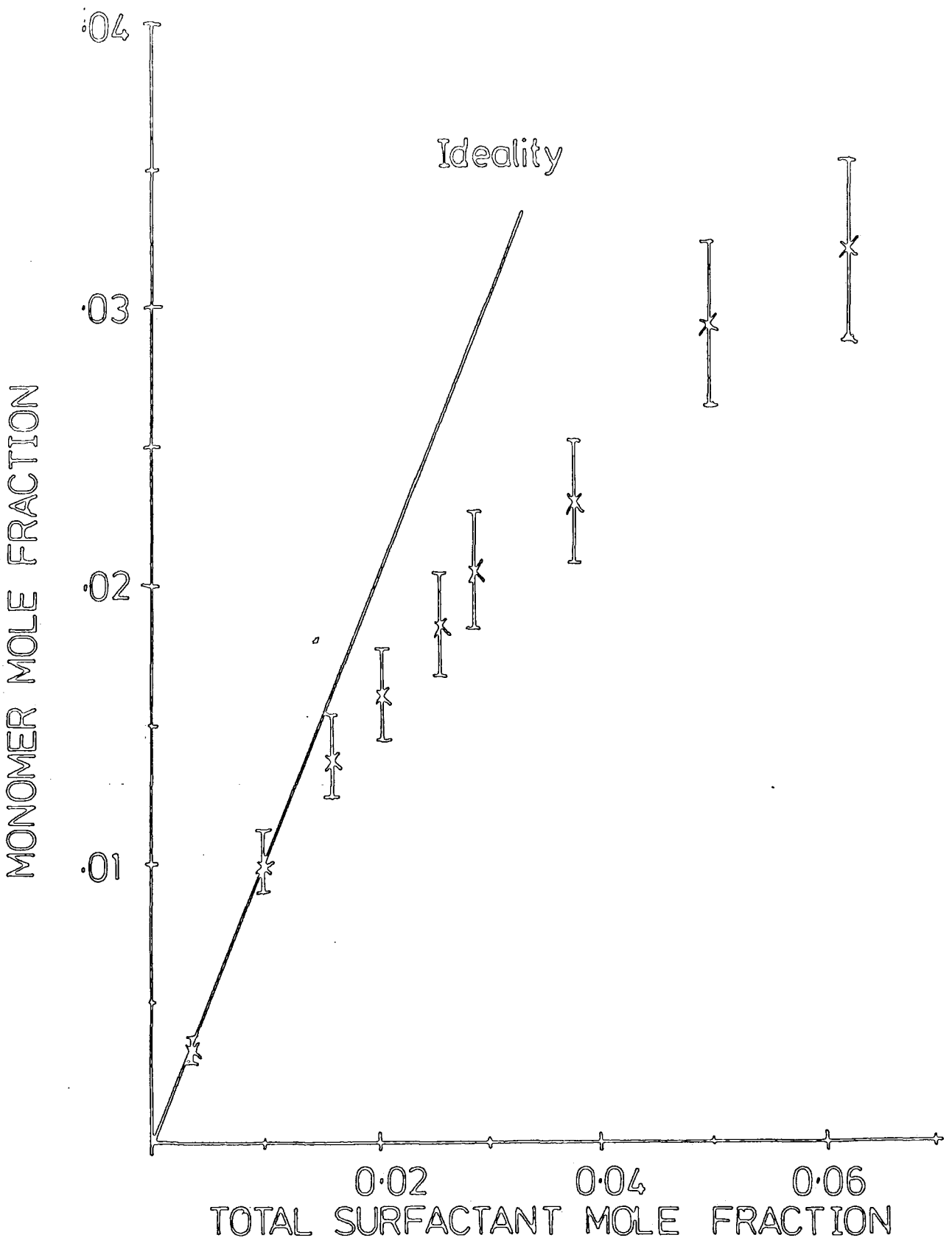

FIGURE 4·40 THE BEHAVIOUR OF $C_{12}E_4$ MONOMER IN CCl_4 AT 35°C.

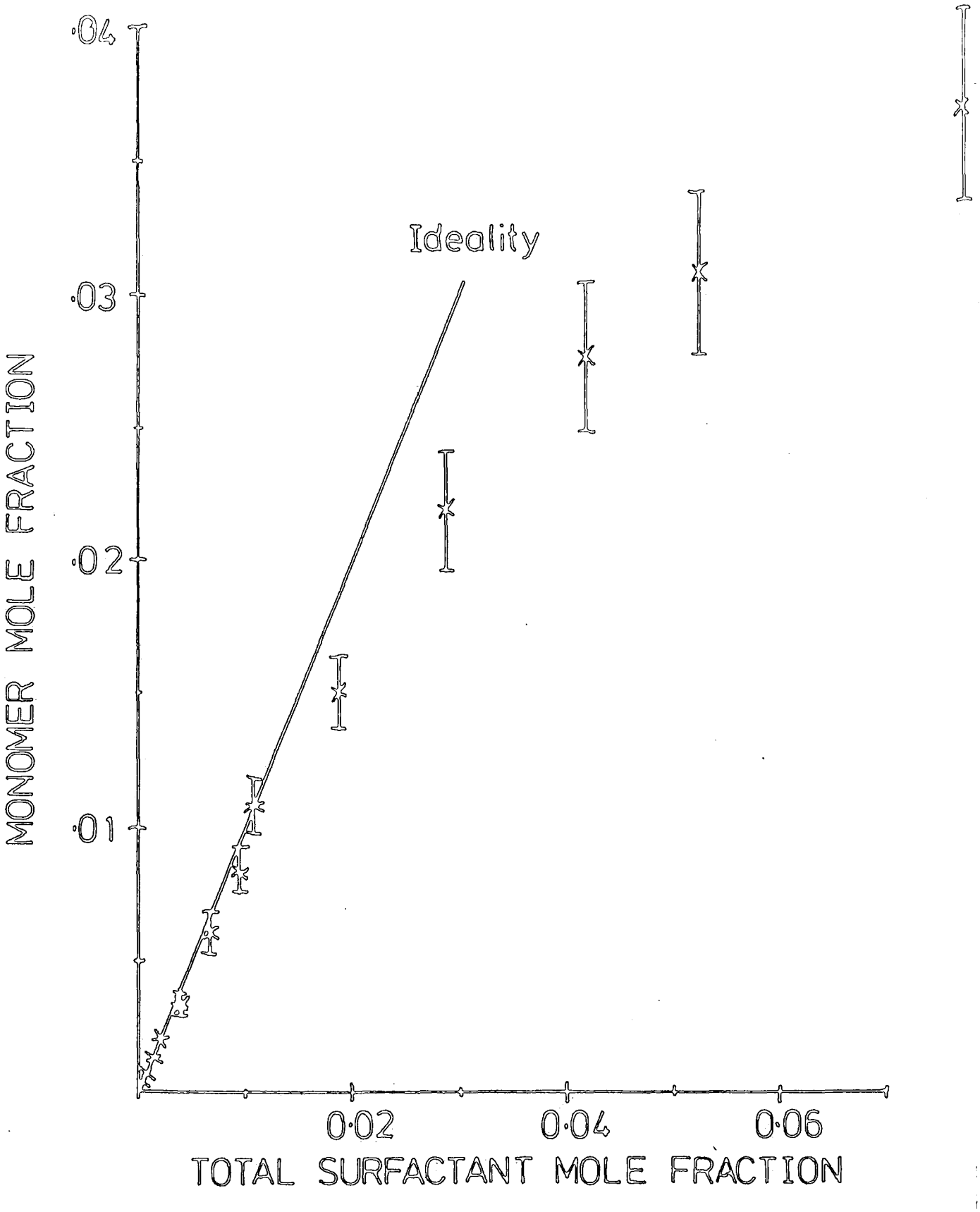

FIGURE 4.41 THE BEHAVIOUR OF $C_{12}E_4$ MONOMER IN BENZENE AT 35°C

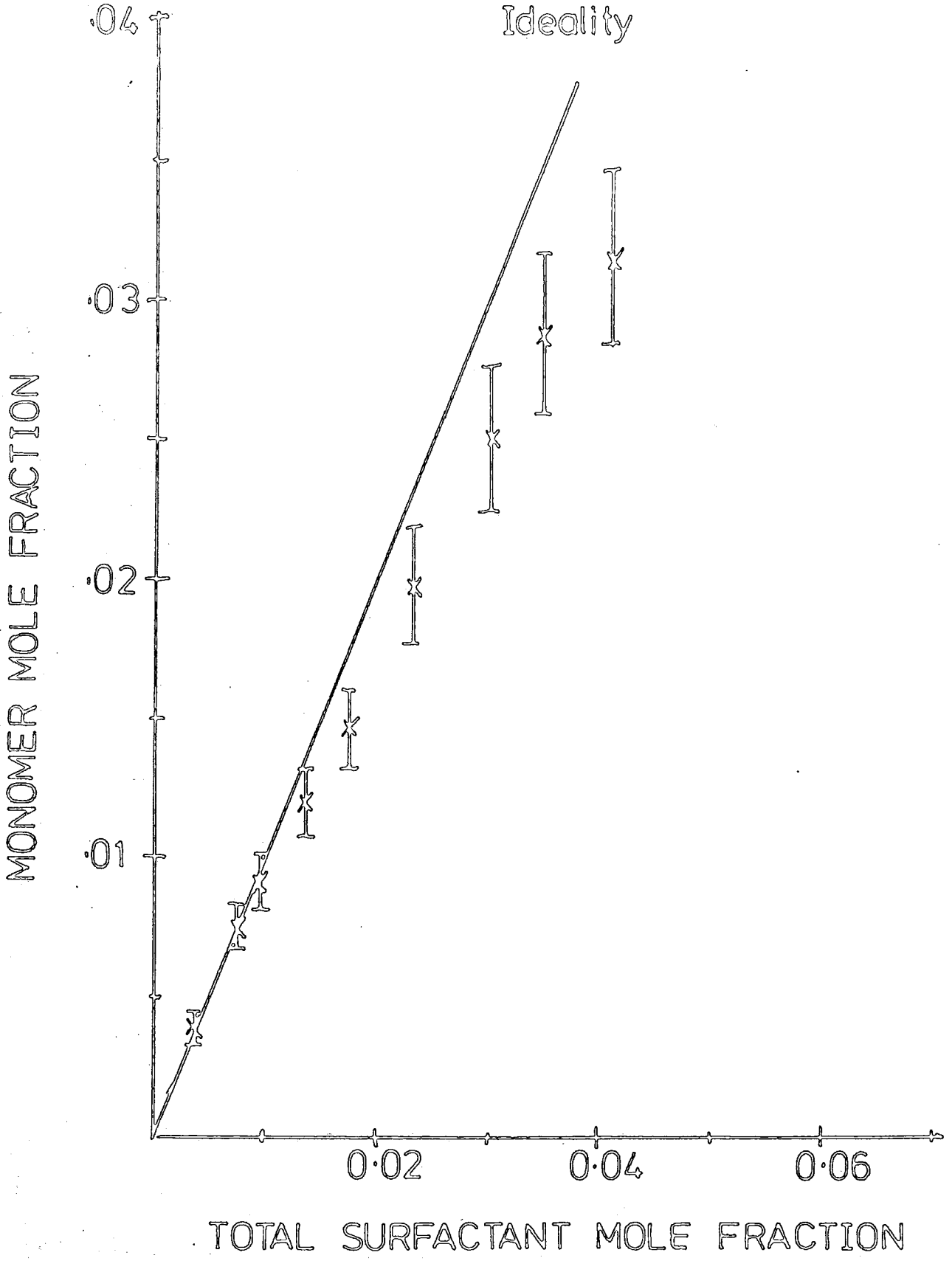

FIGURE 4·42 THE BEHAVIOUR OF $C_{12}F_4$ MONOMER IN $CDCl_3$ AT 35°C.

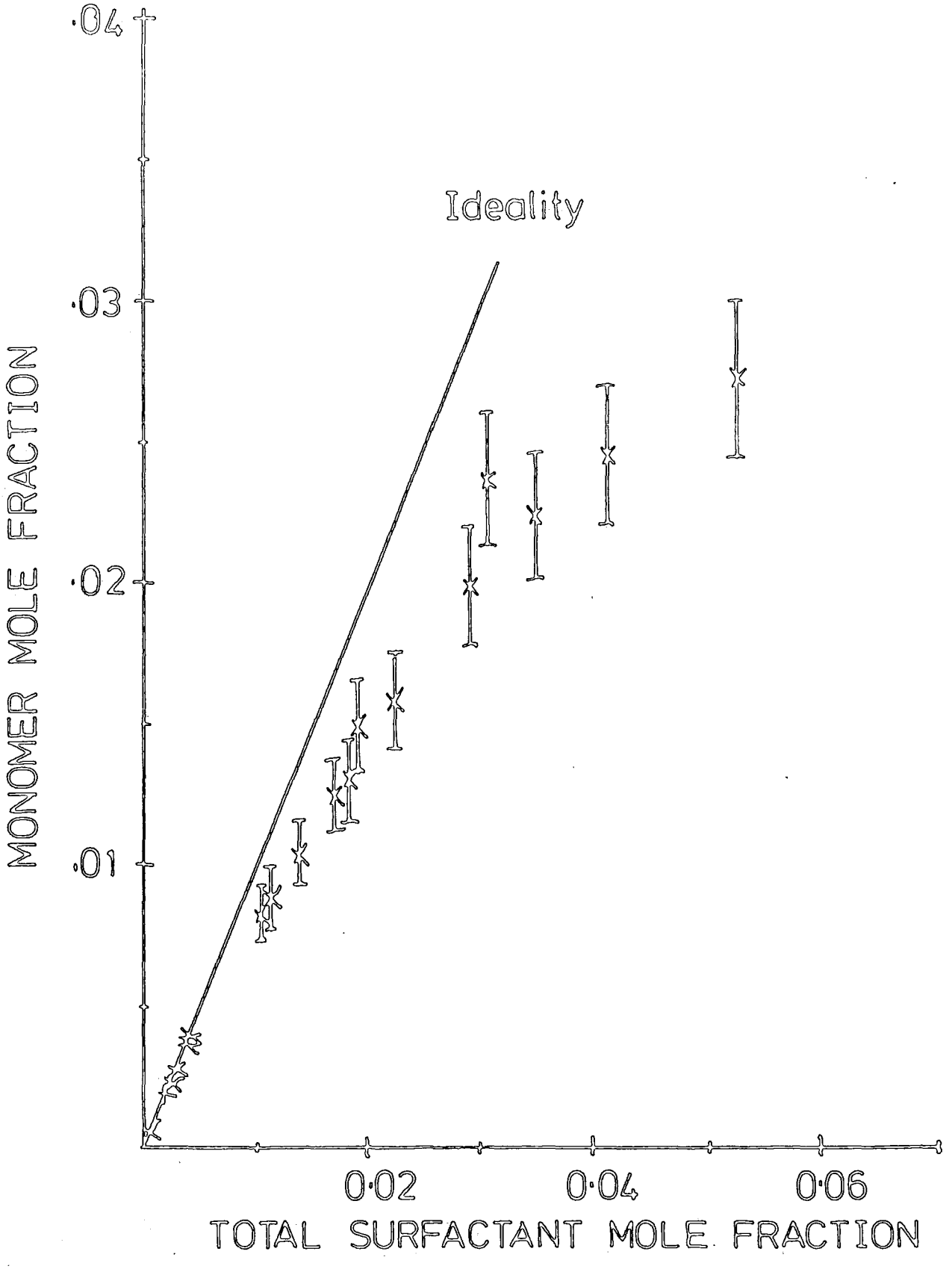

is shown in Figure 4.43. The most obvious feature of this graph is the curve for $C_{12}E_4$ in benzene which shows only a small deviation from linearity. This indicates that association in this system is small as compared with, *e.g.* decane. The result is not entirely unexpected since it is known that benzene rings solvate the ether oxygens.[76] As far as the association process is concerned this "shielding" will result in a decreased intermolecular interaction. The same conclusions have been obtained recently by Ravey *et al*[53] using small angle neutron scattering. As well as the curve shown in Figure 4.41 the aggregation number has been calculated and is shown in Table 4.7 below.

TABLE 4.7 Average Aggregation Number and Average Free Energy of Aggregation for $C_{12}E_4$ in various Solvents at 0.04 mf. and 35°C

Solvent	$\bar{N}_A$	$\bar{N}_A$ from ref. 53	$\Delta\bar{G}^\theta$ (kJ mol^{-1})
Heptane*	2.9±0.3	5 (20°C)	-10±2
Decane	4±1	9 (20°C)	-13±5
Decalin	3±1	3 (Cyclohexane) at 20°C	-8±4
CCl_4	3.0±0.5	-	-5±1
Benzene	1.6±0.4	1 (20°C)	+1.3±1.1
$CDCl_3$	2.5±0.3	1 (20°C)	-

* At 30°C.

The value of 1.6 calculated implies that the molecule exists as the monomer with a small concentration of dimers. In addition the free energy change for the process is unfavourable, the only positive value among the systems studied.

FIGURE 4.43 A SUMMARY OF $C_{12}E_4$ MONOMER BEHAVIOUR IN VARIOUS SOLVENTS.

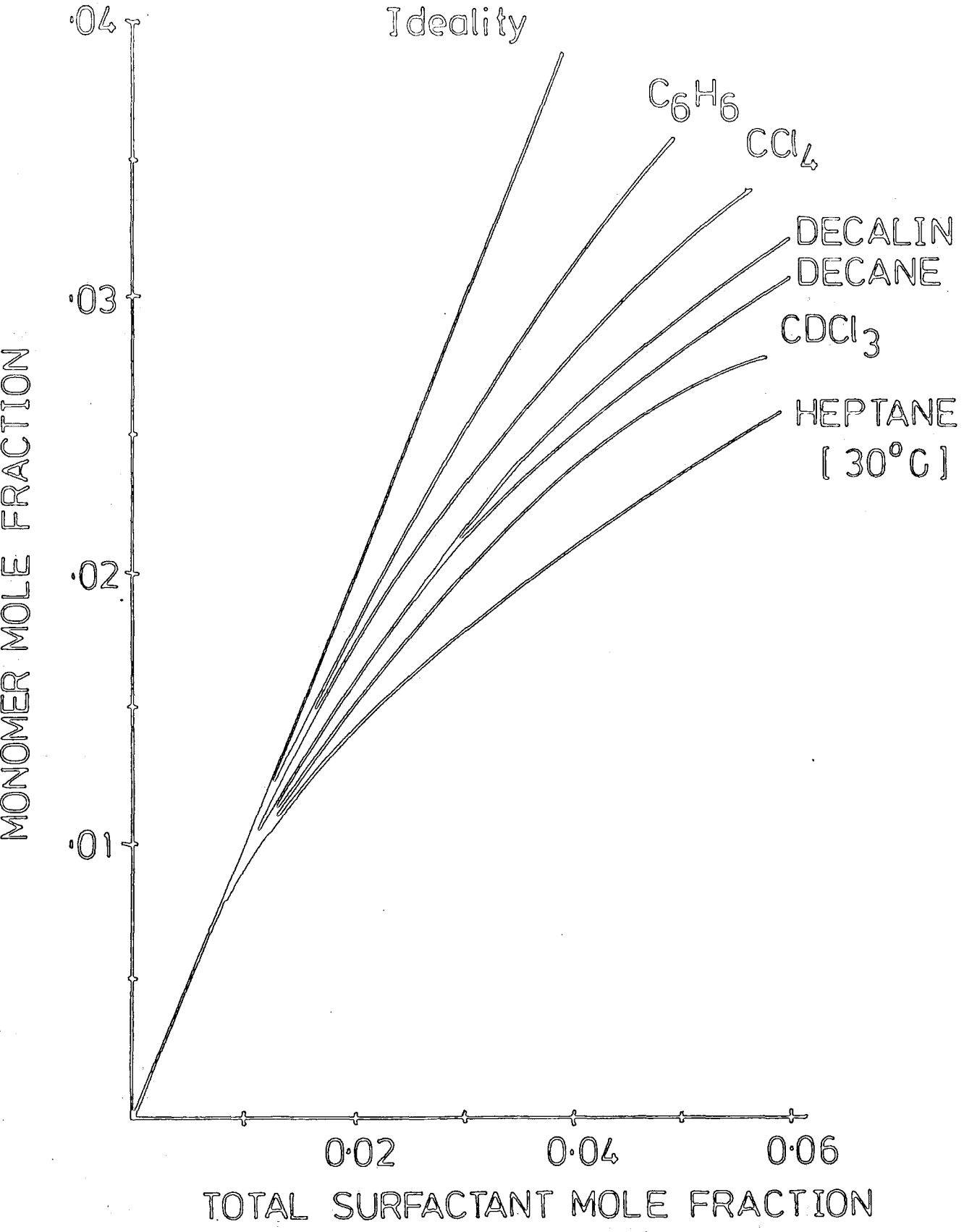

The curves for decane, decalin and carbon tetrachloride are all similar and all give aggregation numbers of about 3 (trimers) at 0.04 mole fraction (Figures 4.38 - 4.40 and 4.43). The results for heptane were recorded at 30°C and were expected to show similar behaviour to decane (to within the error). The aggregation numbers calculated agree favourably with those of Ravey and coworkers[53] except in the cases of decane and deuterochloroform. The high value observed by Ravey for $C_{12}E_4$ in decane was obtained at a lower temperature though no simple explanation for the behaviour of $C_{12}E_4$ in deuterochloroform is immediately available. With the exception of deuterochloroform our results indicate that an increase in solvent polarity has an affect of reducing the aggregation process in these systems. This observation supports our earlier ideas as to the cause of the association process since the solvent in effect reduces the "stickiness" of the head group, *i.e.* dielectric constants for benzene and, *e.g.* decane are 2.28 and 1.99 respectively.[132]

The most unexpected result is obtained for $C_{12}E_4$ in deuterochloroform. This solvent, as with benzene, is known to solvate the ether oxygens. Indeed the spectrum of $C_{12}E_1$ in $CDCl_3$ (Figure 4.32f), shows a relative increase in the M_{NB} species as compared with M_{I5}. Examination of Figures 4.42 and 4.43 show a considerable deviation from linearity, normally associated with relatively strong aggregation. In addition the deviation is noticeable at quite low concentrations ($C \ll 0.0050$ mole fraction). Ravey and coworkers[53] have established that no aggregation occurs in chloroform implying that moisture may be present in our system. Though this is known

to be the case (the spectra show a small peak at ≈3680 cm^{-1} known to be due to water) the quantities are small (less than a fraction of a per cent) and vary with little or no effect on the ν_s (M_{I5}) spectra. It is difficult to understand the behaviour of $C_{12}E_4$ in $CDCl_3$ and further experiments with this system are required.

In Section 3.5.3 we noted the linear relationship of aggregation number with the Hildebrand solubility parameter (δ) for some ionic surfactants. No such dependence is observed for $C_{12}E_4$ with the solvents used here though the spread of δ values is small. One would expect a more complex dependence and it seems doubtful that one single parameter can quantitatively account for all the possible solute solvent and aggregate-monomer interactions.

4.6 Conclusions

Though vibrational spectroscopy has long been used as a tool for quantitative analysis it has never found application in complex amphiphile systems such as those studied here. The results show that the technique has been successful in quantifying the aggregation process of polyoxyethylene surfactants in non aqueous solvents. In doing so we have established that hydrogen bonding, dipole-dipole, dipole-induced dipole and dispersion interactions have large favourable contributions to the free energy of aggregation. Thus one finds that association increases in the order:

$$C_{12}E_8 > C_{12}E_0 > C_{12}E_5 \geqslant C_{12}E_4 \geqslant C_{12}E_3 \geqslant C_{12}E_2 \geqslant C_{12}E_1$$

The above sequence demonstrates that the larger the oxyethylene head group, the greater the "stickiness" between molecules,

which become equal in magnitude to hydrogen bonding at about $C_{12}E_6$.

In addition to oxyethylene chain length we have found that solvent has a profound effect on the aggregation process. In particular, that benzene solvates the ether oxygens thus effectively shielding them from neighbouring molecules. This results in a much reduced interaction and decreases the association of these molecules. A study of the intermolecular ν_s(O-H) association bands in these solvents ($\simeq$3500 cm^{-1}) has shown that aggregation, particularly with small oxyethylene chains, is a gradual process and begins at low mole fractions. Indeed, the absorption coefficient of the above species is such that it may be detected at concentrations lower than by other techniques such as vapour pressure osmometry and light scattering.

Though the association process is of most interest, we have observed the presence of intramolecular H-bonded monomer species.

CHAPTER FIVE

THE BEHAVIOUR OF SURFACTANT-WATER SYSTEMS AT HIGH AMPHIPHILE CONCENTRATIONS. THE FORMATION OF LIQUID CRYSTALS

5.1 Introduction

The term "liquid crystal" is often used to describe systems which possess both solid and liquid properties. In general the molecules in such systems have long range order of crystalline materials yet also displaying some rotational and translational mobility. They may be formed by simply heating, in which case they are termed "thermotropic", or secondly, by the addition of a liquid. It is this latter class of liquid crystalline systemswhich interests us here. They are referred to as "lyotropic liquid crystals".

In Chapter Three we saw that the hydrophobic effect was responsible for the formation of surfactant aggregates in water known as micelles. The addition of further surfactant, such that the hydrated micellar volume fraction exceeds a critical value, causes a transition to a liquid crystalline phase. For cylindrical micelles the transition is always to a hexagonal mesophase, with the rods in parallel and arranged in a hexagonal array (see Figure 5.2). Similarly spherical micelles usually form isotropic mesophases with a cubic structure (see Section 5.2). Further increases in concentration, or the addition of a third component, may cause the formation of other types of liquid crystals. The mechanism thought to describe such phase transitions is discussed in Section 5.3.

The phase behaviour of surfactants and water as a function of concentration and temperature is most conveniently expressed in the form of a phase diagram. Figure 5.1 shows one such diagram of the $C_{12}E_8$/water system,[87] The lines re-

Figure 5.1 The Phase Diagram of the $C_{12}E_8$/Water System over the temperature range 0-100°C

(reproduced from ref.[87])

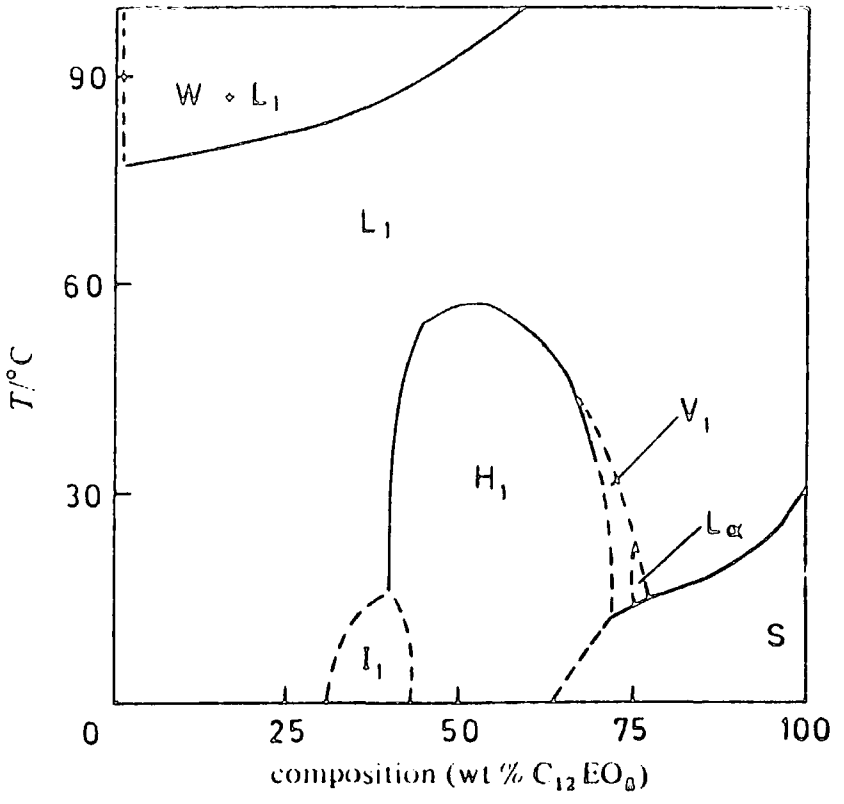

N.B. W is defined as a very dilute surfactant solution.[87]

present phase boundaries, which as the diagram shows, are sensitive to temperature and concentration. Similarly tertiary systems may be expressed on triangular phase diagrams, but only at a single temperature. The representation of phase behaviour in such a manner is of great importance in the detergent industry where certain phases are to be avoided for their viscosity.

The law governing such heterogeneous equilibria, first applied by Gibbs many years ago, relates the number of components (C), the number of degrees of freedom (F) and the number of phases (P) as:

$$F + P = C + 2 \qquad \text{(eqn. 5.1)}$$

The above relationship is known as the Gibbs Phase rule.

The degrees of freedom are intensive variables and under normal conditions may be one or more of the quantities; temperature, pressure or composition. The phase rule assumes that the influence of other variables such as magnetic and electrical fields are negligible. If such influences do affect the equilibrium they are simply included as another degree of freedom. The phase rule is of much use when diagrams similar to the one illustrated in Figure 5.1 are determined. They help to make sense of sometimes complicated phase boundaries and tell us where to expect regions of coexisting phases. Such areas arise where two or more phases are in equilibrium with each other, and occur between microscopically homogeneous phase boundaries. Indeed for a phase transition to be first order one usually observes a coexisting region between them.

5.2 The Structure of Liquid Crystalline Phases

Above the Krafft boundary (see Chapter Three) at high surfactant concentrations one finds that micelles order themselves in a fixed array. The structure of this micelle array or "mesophase" depends on the concentration and on the surfactant itself. Various structures have been determined, some of them equivocal and many well established.

5.2.1 The Hexagonal Phase

It is generally believed[79] that there are two mesophases with a hexagonal structure found in lyotropic systems There are the "normal" and "reversed" hexagonal phases, which according to the nomenclature of Tiddy[80] have been designated as H_1 and H_2, respectively. The H_1 phase is composed of normal cylindrical micelles packed in a hexagonal array within a water continuum as shown in Figure 5.2. Generally speaking the diameter of the rods is between 10% and 30% less than twice the surfactant length, with a water separation of 8-50Å depending on the concentration.[79] The phase is quite common and because of anisotropy is birefringent when observed between crossed polars. Under the polarizing microscope it often exhibits an "angular" or "fanlike" texture.[81] A Photomicrograph of the hexagonal phase found in hexadecyltrimethyl ammonium chloride (C_{16}TACl) is shown in Chapter Seven.

The reversed hexagonal structure, though not as common, generally occurs at high amphiphile concentrations, particularly with surfactants having two alkyl chains on a small head group. Unlike the H_1 phase the hydrocarbon "tails" are directed towards the sides of the cylinders as shown in

Figure 5.2 The "Normal" Hexagonal Phase

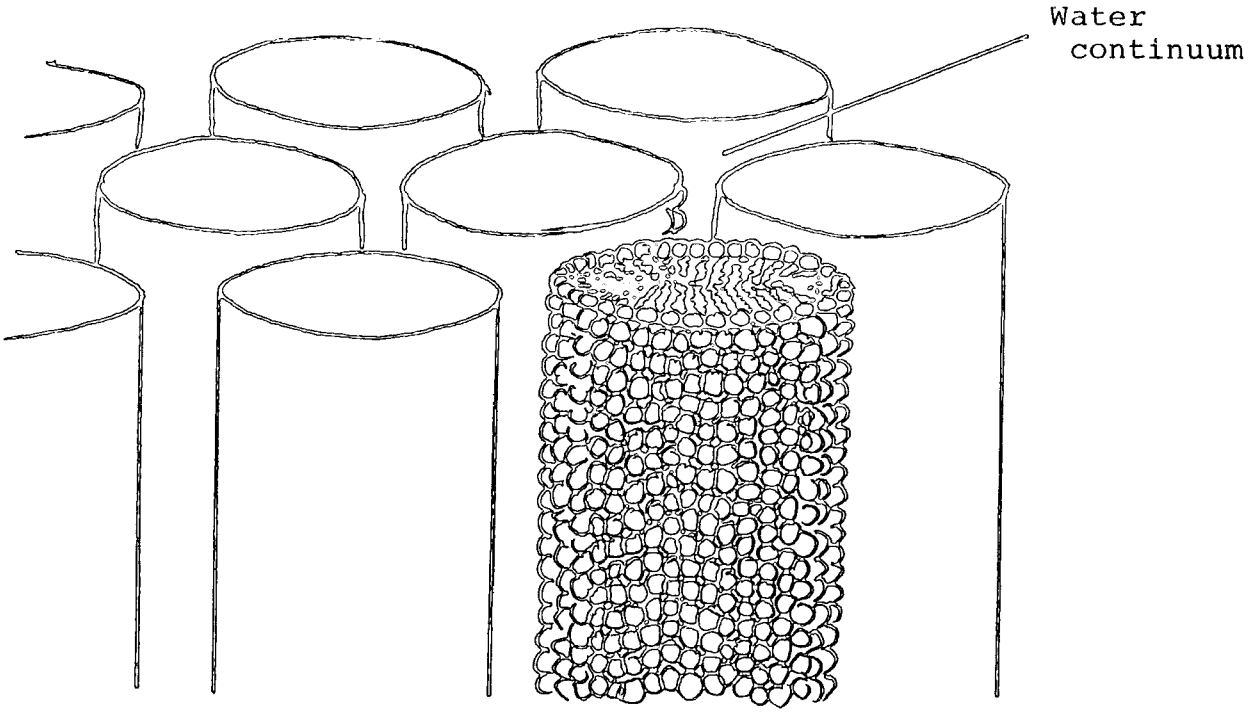

Figure 5.3 The "Reversed" Hexagonal Phase

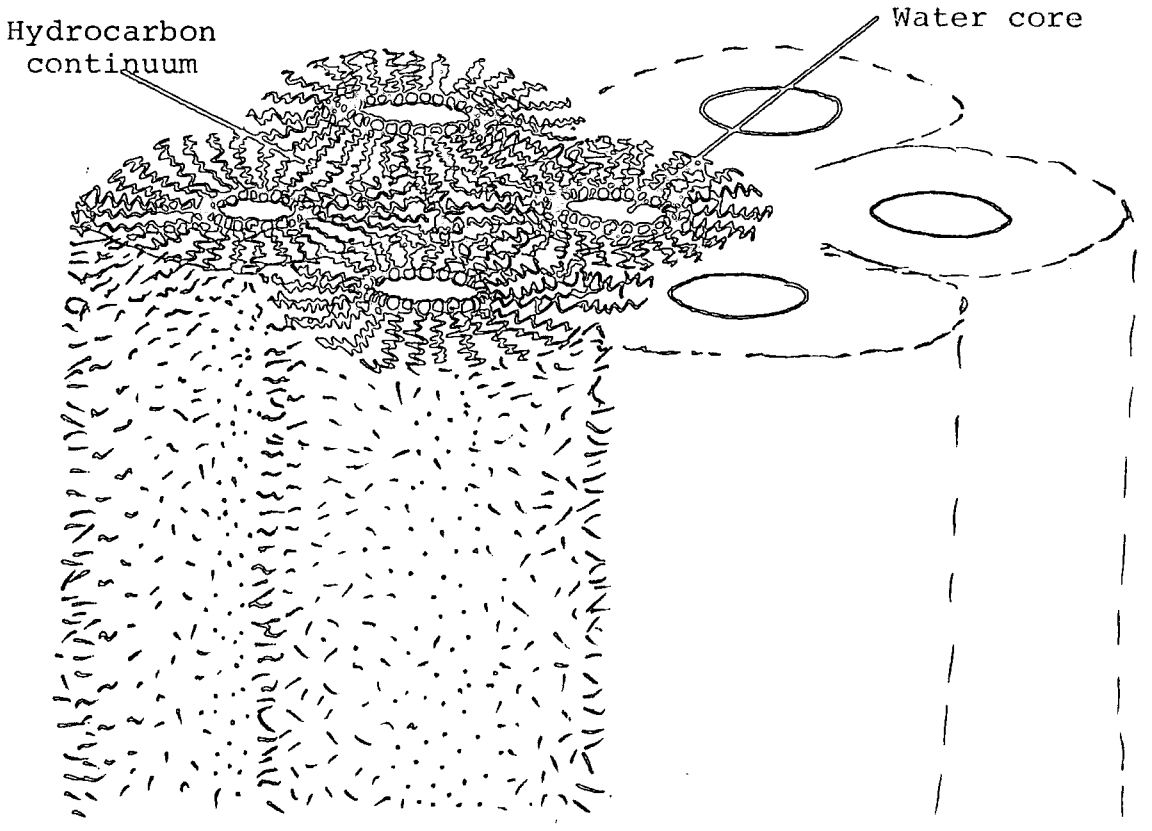

Figure 5.3. If water is used as the solvent, the water cylinder diameter is generally between 10 and 20Å.[79] The H_2 phase shows similar texture to the "normal" structure under the polarizing microscope. The viscosity is also similar, typical values of between 20-45P (a stiff gel) are observed.[77]

A third hexagonal phase, though not as well established as the previous structures, is the deformed hexagonal, H_{1d} phase[82] shown in Figure 5.4. This phase, which occurs in sodium dodecyl sulphate, is thought to arise from a "structuring" of water as the concentration of surfactant is increased. The result is a minor change in cylinder position of alternate layers.

Though other more equivocal hexagonal phases may exist such as the complex hexagonal H_C of Ekwall,[77] the structures have not been well established.

Figure 5.4 The Deformed Hexagonal Phase
(reproduced from ref.82).

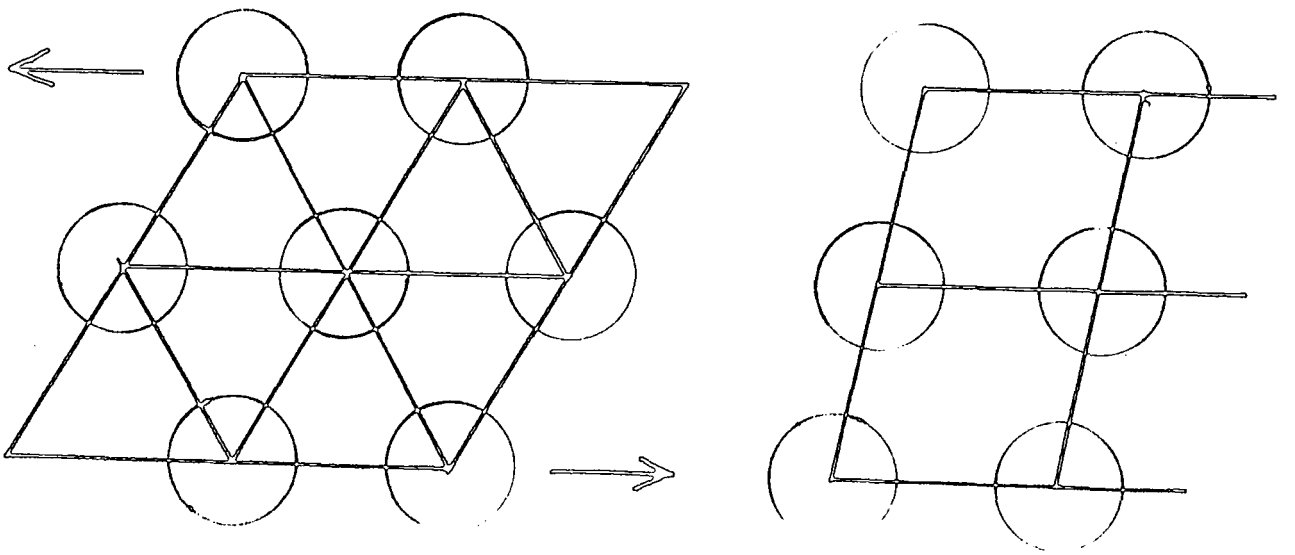

5.2.2 The Lamellar or Neat Phase

This mesophase is probably the most common and well known because of its similarities with biological membranes.[80] Typically in binary aqueous systems the lamellar phase occurs at high concentration, generally between 70-90% surfactant. In a few cases the lamellar phase (L_α) may form without water, but this is rare and normally a certain minimum amount is required. For anionic surfactants the value is quite large and is believed to be due to the prerequisite of counter-ion hydration (for Na, K soaps),[77] (2-6 moles of water per mole of amphiphile). For cationics however much less water is required, 0.88 moles for dodecyl trimethyl chloride at 60°C.[77] The nature of water in these systems is not well understood, though some discussion of this subject will be reserved for Chapters Six and Seven.

Figure 5.5 shows a schematic diagram of the neat phase illustrating the alternating bilayers with intercalated water sheets. The dimensions of the phase may vary significantly but generally the water thickness is between 8 and >100Å with bilayers 10-50% thinner than two all trans chain lengths.[79] Like the hexagonal phase, the L_α phase is anisotropic thus exhibiting birefringence when observed between crossed polars. Under the polarizing microscope it is described as having a "mosaic" or "oily streaks" texture[81] coupled with its very low viscosity (1-10P),[77] and its microscopy, this phase is generally easily identified (see Chapter Seven).

Figure 5.5 The Neat or Lamellar Phase (L_α).

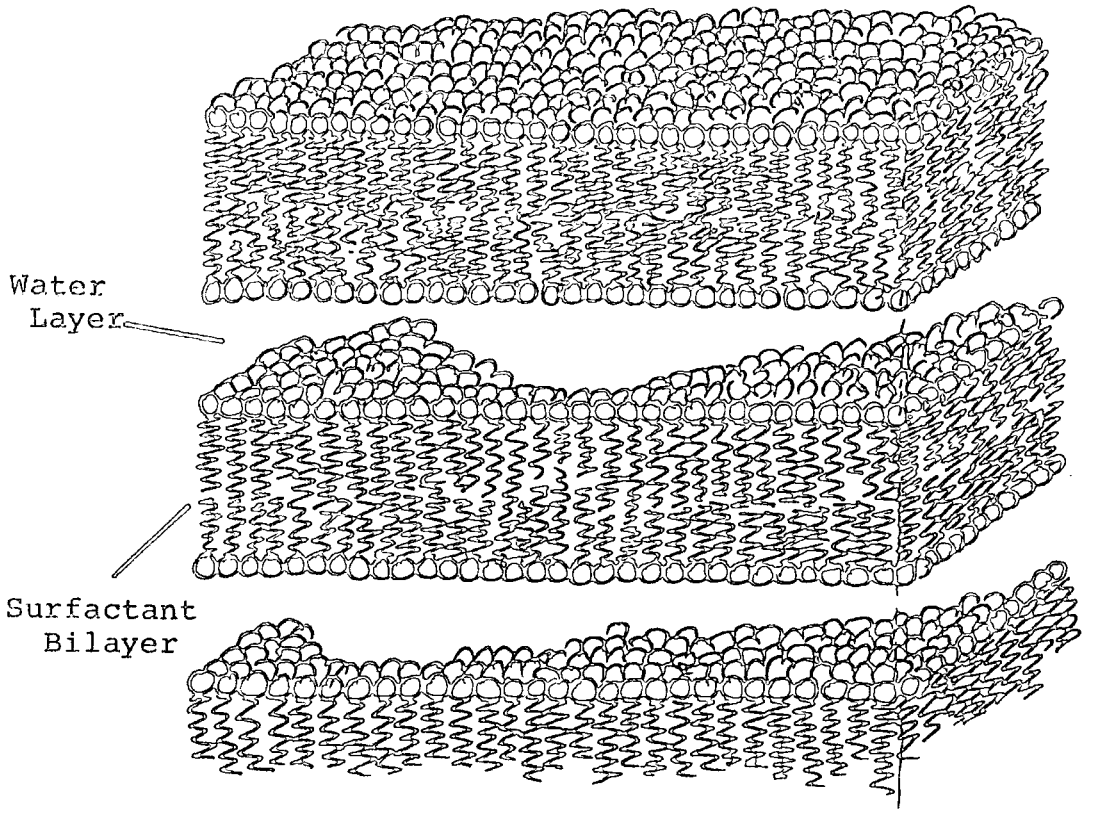

5.2.3 Isotropic Liquid Crystalline Phases

According to the current literature, there are believed to be four different types of isotropic mesophase. From X-ray diffraction studies,[83] these mesophases have a cubic structure and again as with the hexagonal phase may be further divided into "normal" and "reversed".

The first type of cubic mesophase is the I_1 form which often occurs between micellar solution and H_1 phase (see Figure 6.1). It is made up of spherical micelles packed together in a face centered or body centered cubic

array (Figure 5.6,a). Again at high concentrations the cubic structure may occur with reverse micelles as shown in Figure 5.6,b. This latter phase is designated the I_2 phase according to the Tiddy nomenclature.[80] The dimensions of the micelles are similar to those found in solution with water spacings between them varying from 10 to 20Å (equivalent to that in the H_1 phase).[79]

The second class of isotropic mesophases are often referred to as the "bicontinuous" cubics (V_1, V_2) and consist of surfactant and water continuous regions. Although their structure has not been well established, one of the possible geometries is shown in Figure 5.7. No differences are observed between the I_1 and V_1 under normal light conditions or when viewed between crossed polars, *i.e.* both completely transparent and showing no birefringence. However, the V_1 may be distinguished by N.M.R. since it has faster translational diffusion.[84] Both cubic phases are extremely viscous which reflects on the relative difficulty of displacing individual micelles. In general they are far more viscous than either lamellar or hexagonal phases.

5.2.4 The Gel Phase

In some systems there is a complication at the Krafft boundary due to the formation of a "gel phase". Usually this occurs at high concentrations where lamellar phase is known to exist, but on cooling the gel phase appears before the crystalline surfactant. The structure is intermediate to that of the neat and crystalline phase. It is

Figure 5.6 Face Centered Cubic Structures of the I_1 and I_2 Phase.

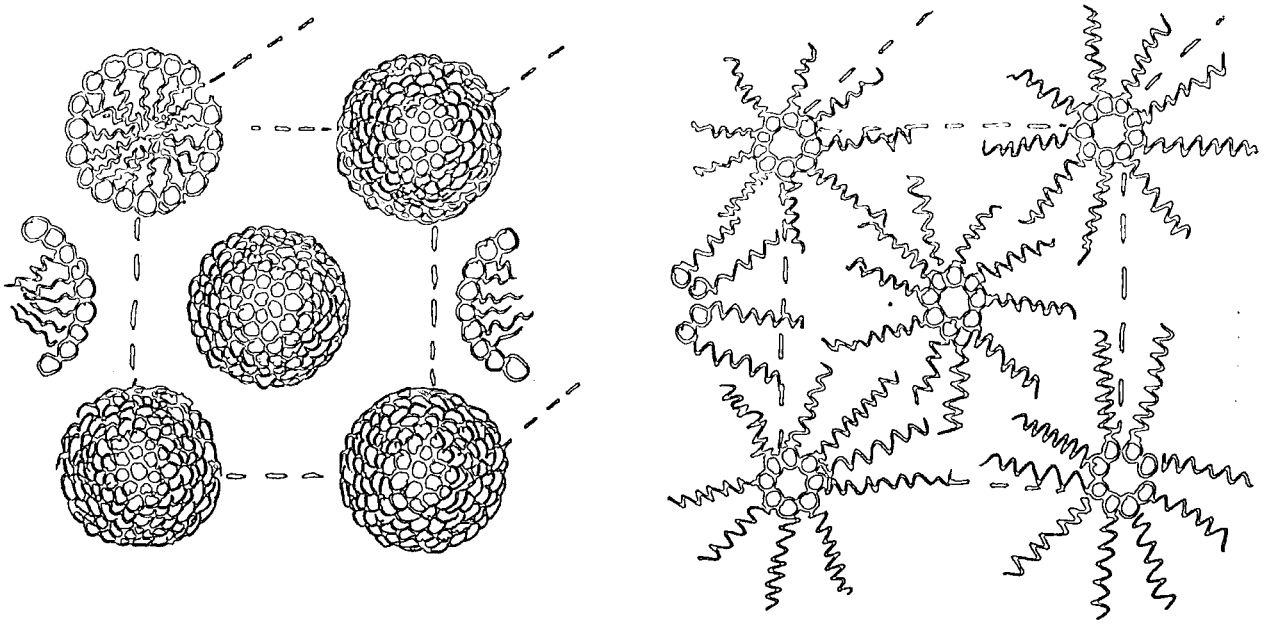

(a) (b)

Figure 5.7 The Viscous Isotropic Phase (reproduced from ref.52)

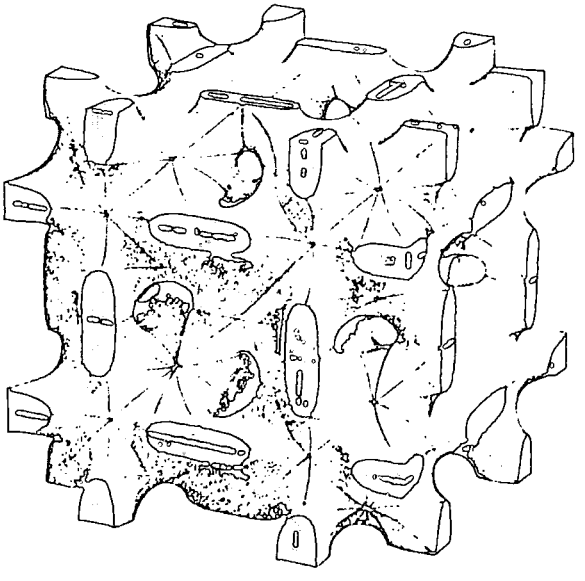

thought to be composed of interdigited surfactant molecules with rigid all-trans hydrocarbon chains as shown in Figure 5.8. Water is found between the monolayers, but in some cases between bylayers (*c.f.* Figure 5.8,b). As with the lamellar phase the anisotropy causes gel phase samples to be birefringent. Plate 7.4 shows a photomicrograph of the gel phase found in the C_{16}TACl-water system, (see Chapter Seven).

Figure 5.8 Two Possible Structures of the Gel Phase

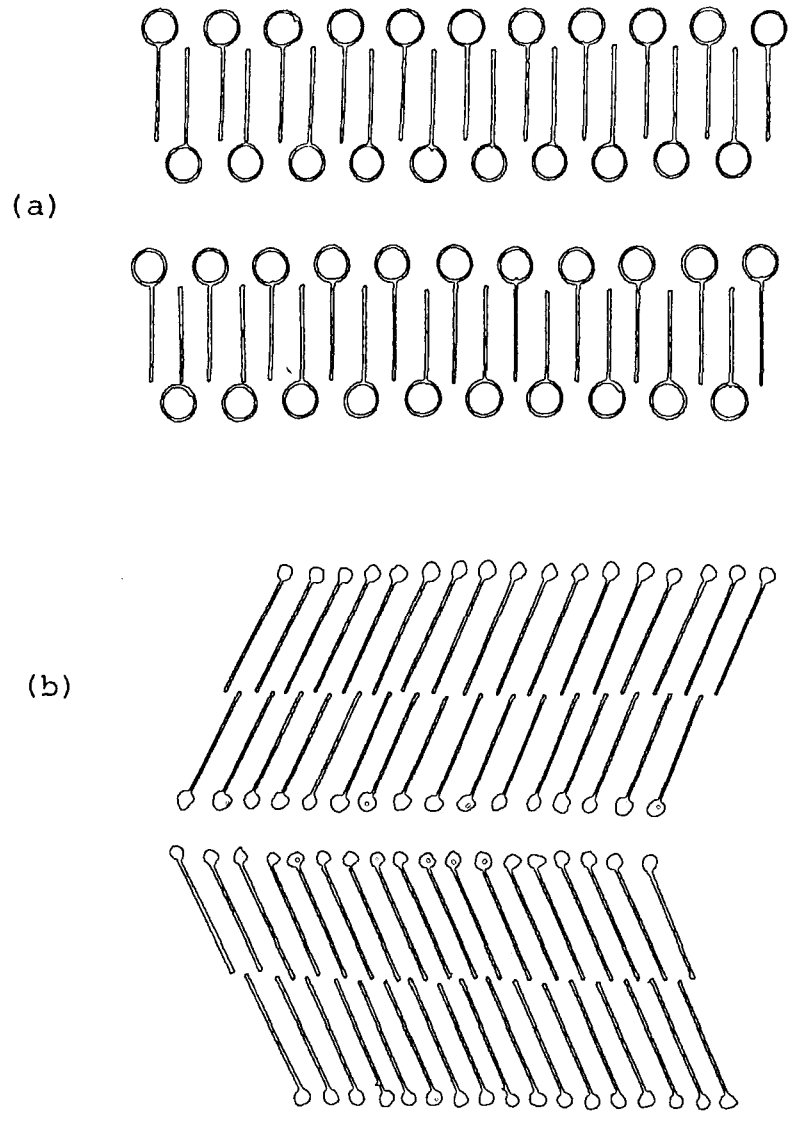

5.2.5 "Intermediate" Phases

Until fairly recently the nature of "intermediate" phases was a matter of much discussion.[82,85] It is now fairly well established that these phases occur between normal hexagonal and lamellar phase regions, where one would expect to observe the V_1 cubic. In general amiphphiles of small hydrocarbon chain (C_n <10) form the V_1 phases, while the higher homologues tend to formthese new structures. In two anionic systems studied by Tiddy[82,85] (SDS/water and Na alkanoate/water) the deformed hexagonal phase mentioned in Section 5.2.1 is formed. It has a parallelogram as the repeat unit in the hexagonal rods distorted by interstitial water.[82] However in the sodium laurate/water system a second intermediate phase is believed to be formed having a structure akin to the lamellar phase with thin bilayers.[85]

Cationic surfactants show similar behaviour in their formation of such phases. It is interesting to note however that this effect is observed with higher alkyl homologues than that in the anionics. For example alkyl trimethyl ammonium chlorides show only a V_1 phase with C_n=12 whereas C_n=16 homologue shows two intermediate phases.[86] This higher crossover point at $C_n \simeq 14$, *c.f.* anionics $C_n \simeq 10$, coupled with the fact that nonionics and zwitterionics do not form such phases, may be interpreted in terms of inter- and intramicellar forces[25,26] (see Section 5.3). A point worthy of mention concerns one of the intermediate phases of cetyl trimethyl ammonium chloride, C_{16}TACl. It is thought that the structure of the first intermediate is that of a

"rectangular phase" as shown in Figure 5.9.[77] However further discussion of this subject will be postponed until Chapter Seven.

These intermediate phases are birefringent with a texture not far removed from that of the hexagonal phase. They do differ, however, in their rheological properties, the former for example showing a higher viscosity.

Figure 5.9 The Rectangular Phase

(reproduced from reference[80])

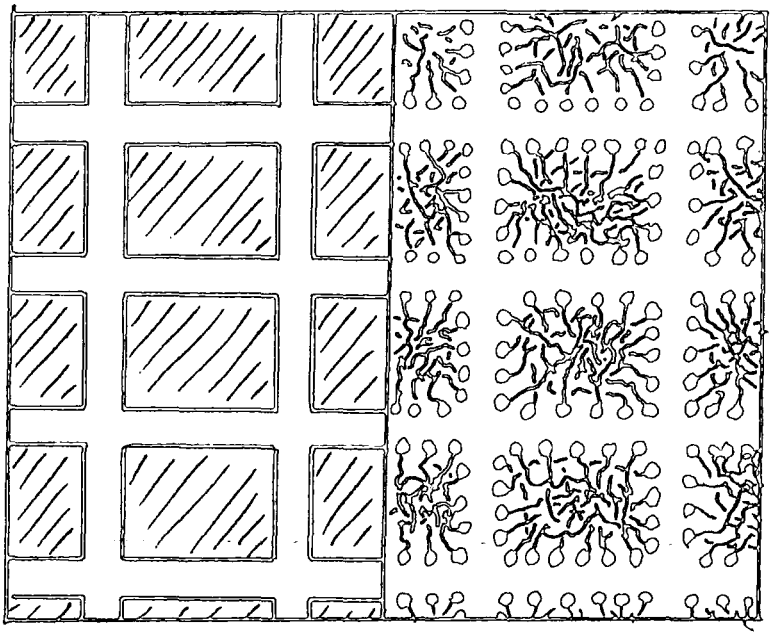

5.3 The Interactions Responsible for Mesophase Formation

The formation of micelles and liquid crystals in water is a cooperative process between the hydrophobic effect and other electrostatic and steric interactions. Ultimately the system will minimise its chemical potential by achieving a mutual balance between all contributions. In this section we will discuss these interactions, initially considering the intramicellar contributions which dominate micelle shape and subsequently the behaviour at higher concentrations where intermicellar interactions play an important role.

5.3.1 Intramicellar Interactions

As mentioned in Chapter Three, one can distinguish between several micelle geometries: there being spheres, rods and discs which all differ in their average surface curvatures. In this current treatment the micellar shape may be determined semi-quantitatively for both ionic and nonionic surfactants in terms of simple packing constraints and interactions imposed by the head groups, the hydrophobic chain and the solvent (water in this case). The work of Israelachvili, Mitchel and others[25,26] considers intramicellar interactions in terms of four variables. These are the 'Bulk', 'Surface', 'Curvature' and 'Packing' terms:

(i) The Bulk Term arises from the change in chemical potential on removing the hydrophobic surfactant tails from an aqueous environment.

(ii) The Surface Term allows for water contact between portions of the hydrophobic tail close to the head group.

(iii) The Curvature Term is included in ionic systems where it is important as an electrostatic consideration.

(iv) The Packing Term assumes that the hydrophobic tails are fluid like and not compressable. Consideration of these variables embraces thermodynamics, geometry and interaction energies in order to explain rod and disc micelles (which could not exist under thermodynamic considerations alone).

For a spherical micelle one can relate the volume of the surfactant chain (V) with the micelle radius generally taken to be less than or equal to, the all trans chain length, (l_t), and the surface area per molecule (a):

$$\text{(spheres)} \qquad V = \frac{a l_t}{3} \qquad \text{(eqn. 5.2)}$$

similarly for rods and discs one has

$$\text{(rods)} \qquad V = \frac{a l_t}{2} \qquad \text{(eqn. 5.3)}$$

$$\text{(discs)} \qquad V = a.l_t \qquad \text{(eqn. 5.4)}$$

These three equations set out packing constraints for a particular surfactant with twelve C atoms such that:[79]

$$\text{(spheres)} \quad a \geqslant \frac{3V}{l_t} = 70\text{Å}^2 \qquad \text{(eqn. 5.5)}$$

$$\text{(rods)} \quad a \geqslant \frac{2V}{l_t} = 47\text{Å}^2 \qquad \text{(eqn. 5.6)}$$

$$\text{(discs)} \quad a \geqslant \frac{V}{l_t} = 23\text{Å}^2 \qquad \text{(eqn. 5.7)}$$

Thus, as the surface area per molecule decreases then so does the possibility of the various geometries. For example a molecule having a surface area of 50Å may only form rod or disc shaped micelles. Given that there are two geometries possible, the resulting shape will depend on the surface curvature which is a balance of intramicellar forces acting

at the micellar surface. Figure 5.10 below shows schematically the origin of these forces which generally act in the planes denoted by x, y and z.

Figure 5.10 Schematic diagram of a micellar surface (reproduced from ref.87).

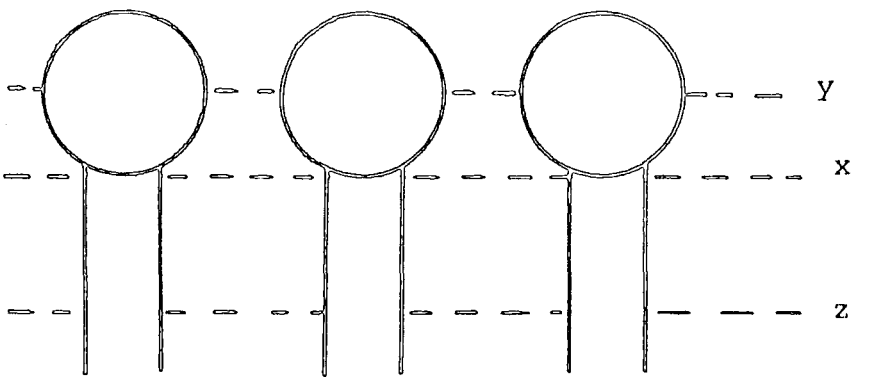

The interactions along a plane denoted by y in the above diagram, are generally due to head group repulsions caused by either electrostatic or steric factors and will increase 'a', the surface area per molecule. The hydrophobic effect results in an attractive force in the plane x such that the hydrocarbon-water contact is minimized, resulting in a smaller value of a. Finally an interaction originating from decreased molecular freedom of the hydrocarbon chain may result along the z-plane. This repulsion is thought to depend on the micellar shape and is thought to be small except for low values of a, *i.e.* $a<47\text{Å}^2$.[87] Finally, to be able to calculate the actual curvatures, some knowledge of the chain length is required. Previously we have assumed that all trans chain length (l_t), but as the hydrocarbon tail gets larger the probability of gauche conformers increases which results in smaller values of l_t. Thus in summary, high head

group repulsions (and hence curvatures) favour spherical micelles, a gradual decrease in curvature results in transitions to rod, disc and finally reverse phases (where the curvature is inverted). An extension of the hydrocarbon chain length (for a particular value of 'a') results in a decrease in curvature.

5.3.2 Intermicellar Interactions

Though intramicellar forces are important just above the CMC, other factors dependent on intermicellar interactions, become evident at higher concentrations. For example, there may be a change in the micellar shape either due to restrictions imposed by a and l_t as the concentration is increased or by "soft sphere" repulsions between micelles. Thus these "shape transitions", *i.e.* sphere→rod may appear in the L_1 phase or at concentrations where liquid crystals are found. The repulsions between micelles mentioned above are actually responsible for the formation of liquid crystals. Above a certain volume fraction these repulsions will cause packing of the micelles in an ordered array. Thus the point at which mesophases first form have been termed order/disorder transitions, with there being no change in micellar shape, *i.e.* spheres→I_1 phase, rods→H_1 phase and discs→L_α phase. In addition to this "soft sphere" repulsion there is also an interaction from water molecules bound to the head group. This force is repulsive in nature and arises from contact of adjacent water networks and may decrease the point at which the liquid crystalline phase occurs.[119,120,130]

Further increases in concentration lead to the formation of larger micelles. In principle such an increase in micellar size should cause a decrease in curvature. This will occur provided that the chain length remains constant. Thus a point will be reached where the curvature cannot sustain a particular geometry and so a shape transition is observed. Thus from spherical micelles one may usually observe the following phase behaviour:

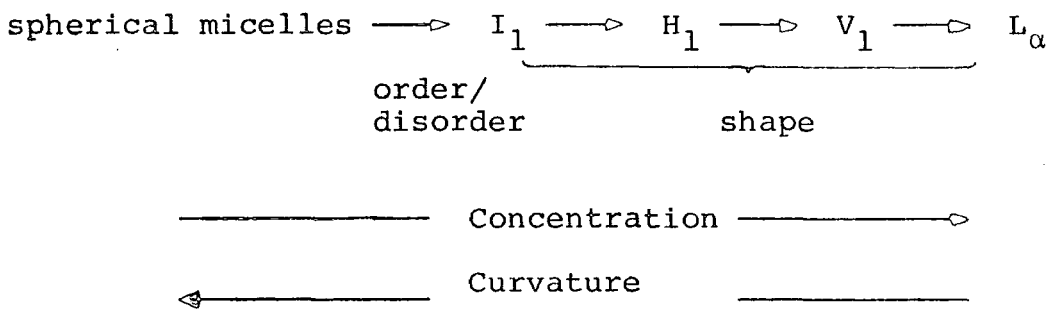

For a fixed chain length each phase transition occurs at a particular value of the surface area per molecule, the curvature thus decreasing from left to right.

Figure 5.11 shows a schematic diagram of typical mesophase behaviour as a function of concentration and micellar curvature.

In cases where one observes very little curvature even at low concentrations, reverse phases are encountered. Such behaviour is observed when:

(i) the size of the head group is small;

(ii) the hydrocarbon chain is long or if two chains exist on the same molecule.

Figure 5.11 Mesophase Behaviour as a function of Curvature and Volume Fraction of Amphiphile (modified from ref. 87).

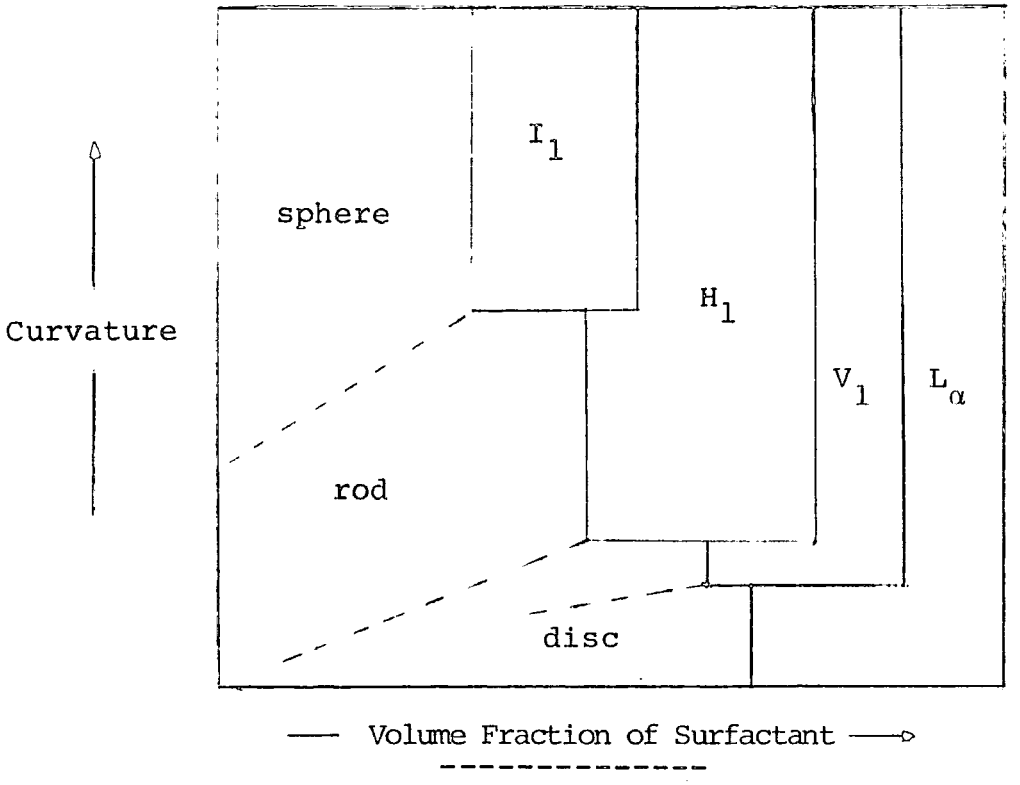

The small values of 'a' give rise to disc micelles at low concentrations with an order/disorder transition to the lamellar phase occurring when the micelles begin to experience intermicellar repulsions. An increase in concentration results in a "reverse curvature" which may lead to a shape transition. These will usually occur in the order:

$$\text{discs} \longrightarrow L_\alpha \longrightarrow V_2 \longrightarrow H_2 \longrightarrow I_2 \longrightarrow L_2$$

5.4 Counter Ion Binding in Lyotropic Liquid Crystals

The distribution of counter ions in mesophases are of paramount importance since they reduce the effective charge density at the micelle surface. In the past, much work has been applied into the development of a Poisson-Boltzmann type treatment for counter ion distributions.[89,90,94-97] The PB equation describes the ion distribution as an electrostatic continuum such that;[94]

$$\varepsilon_r \varepsilon_o \nabla^2 \phi = \bar{\rho} = -\sum_i n_i \exp(-Z_i e\phi/kT) \qquad \text{(eqn. 5.8)}$$

where ε_r and ε_o are the relative permittivity and permittivity in a vacuum, respectively, ϕ is the electrostatic potential, ρ is the charge density, $z_i e$ is the charge of ion i, k is the Boltzmann constant and T is the absolute temperature. The above equation may then be simplified by a number of boundary conditions. For the case of two charged parallel plates separated by an intervening water and counter ion medium, the boundary conditions are, by symmetry

$$\left.\frac{d\phi}{dx}\right|_{x=o} = 0 \qquad \text{(eqn. 5.9)}$$

and through electroneutrality[94]

$$\left.\frac{d\phi}{dx}\right|_{x=a} = \left.\frac{d\phi}{dx}\right|_{x=-a} \qquad \text{(eqn. 5.10)}$$

The situation is described in Figure 5.12 below.

The solution of the PB equation brings about an ion condensation hypothesis and a number of conclusions emerge:[94]

Figure 5.12 A Schematic Representation of a Lamellar Lyotropic Mesophase

[reproduced from ref.94]

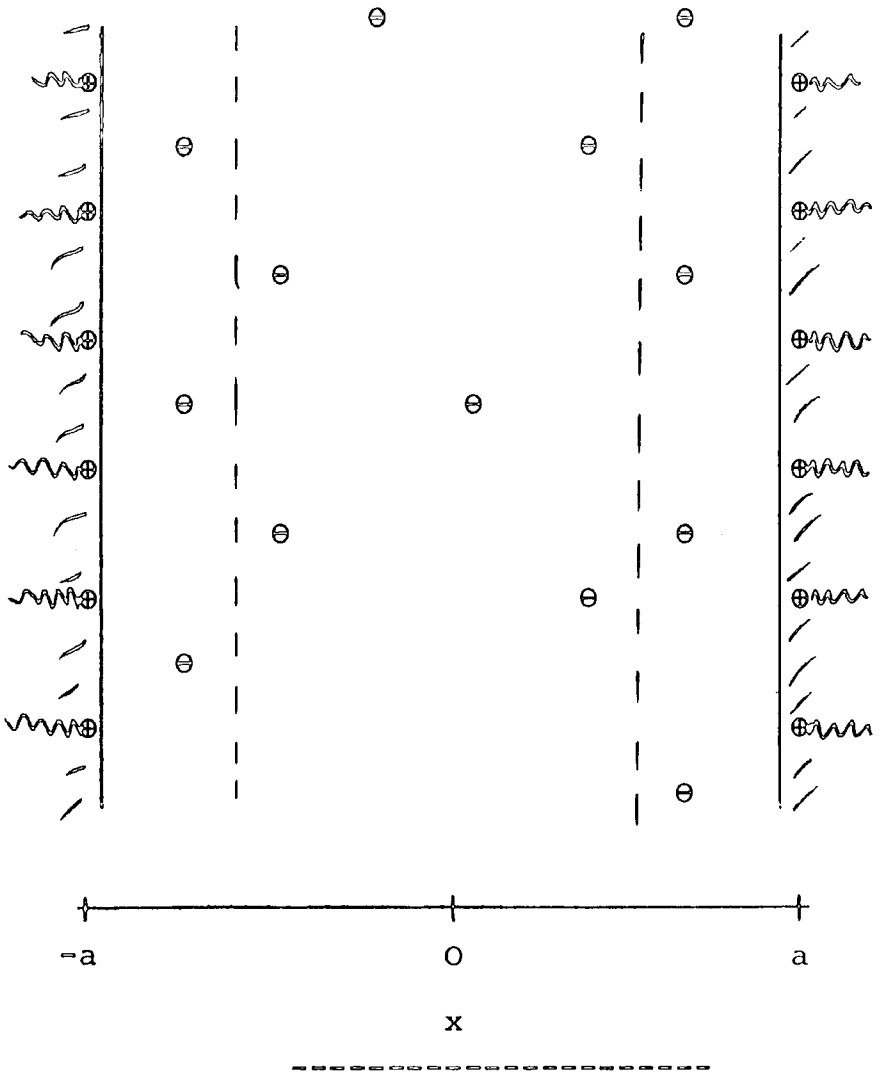

(i) When the charge density on the micelle surface is increased above a critical amount, all added counter ions are found close to the surface. In this case the concentration of counter ions far from the surface remains constant.

(ii) At a constant surface charge density the concentration of counter ions close to the surface remains constant if the distance between the plates is varied.

(iii) In the limit of infinite distance from the charged surface the counter ion distribution is unaffected by added electrolyte.

(iv) The counter ion distribution is independent of temperature.

The above model for two charged plates has been compared to results obtained by Monte Carlo simulation calculations[95] and by NMR.[89] In general the PB treatment predicts the correct asymptotic behaviour of a decrease in the relative electrostatic potential as the distance between the plates is increased. The Monte Carlo simulations[95] however give higher concentrations of ions at the surface, which are thought to be due to correlations between ions not included in the PB treatment. The NMR results of Wennerström *et al* [89] show a general agreement with the ion condensation hypothesis derived from the PB treatment.

The behaviour of rod micelles is generally found to be similar to the results obtained for two charged plates.[94] For PB type calculations of spherical micelles the "cell model" is often used. Figure 5.13 shows that one may distinguish between the ionic radius, R_a, the micellar radius, R_b, and the cell radius, R_c. The counter ions and co-ions are free to move in the space between R_b and R_c. The model assumes spherical symmetry as a boundary condition.

The results obtained by a Poisson-Boltzmann treatment of the above system is again qualitatively similar to that obtained by Monte Carlo simulations. Figure 5.14 shows the concentration profile of counter ions as calculated from the PB treatment and a simulation calculation with approximately 300 particles and 2000 configurations/particle.

Figure 5.13 The Cell Model used for a Spherical Micelle Application of the PB Treatment

[reproduced from ref.96]

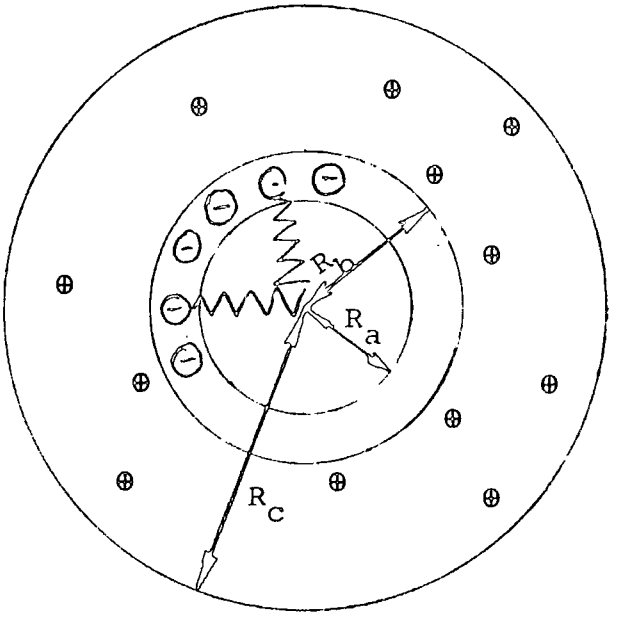

Figure 5.14 A Comparison of Poisson Boltzmann and Monte Carlo Simulation Treatments*

[reproduced from ref.96]

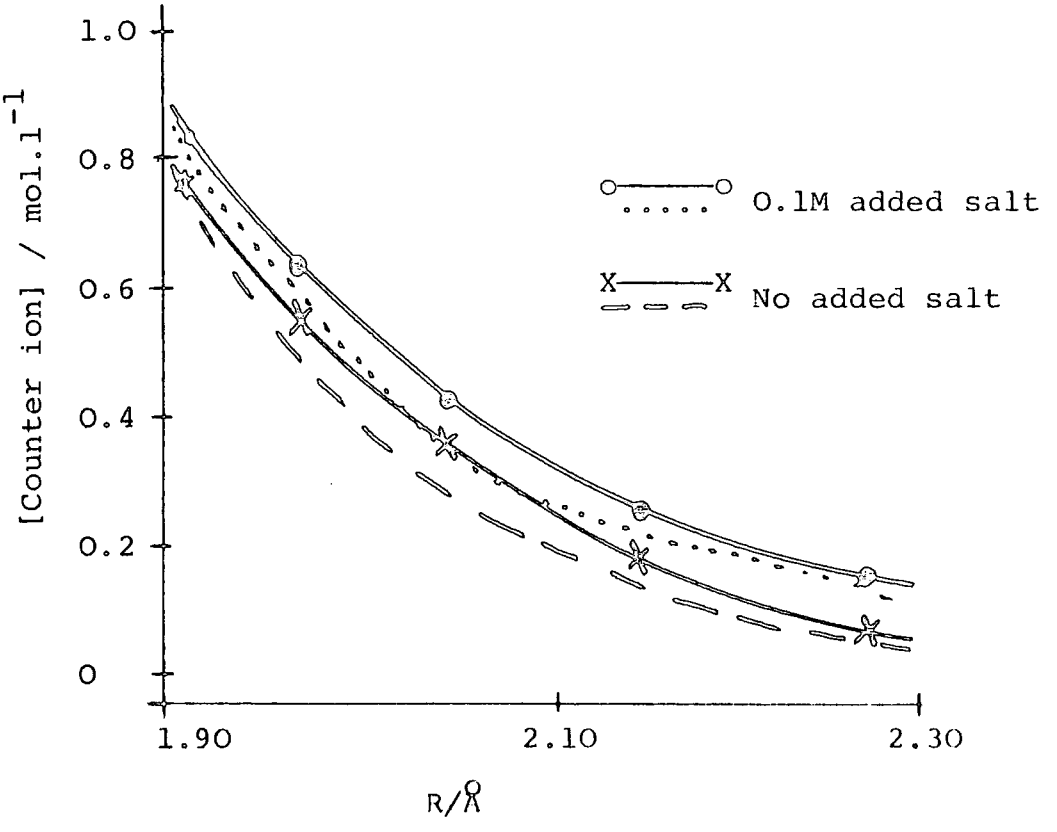

* Solid lines are for MC simulation, broken lines for PB calculations.

The curves show remarkable similarity, more so than that found in the parallel charged plate model for L_α phases. The graph shows the effect of added salt to be small at 0.1M.

There is, in most cases, surprisingly good agreement between experiment,[89] Monte Carlo simulations and the Poisson-Boltzmann treatment[90,94-96]. However, in these cases we have used only monovalent counter ions and small concentrations of added electrolyte. It is now known[97] that large deviations from the PB treatment are observed when divalent counter ions and high surface charge densities at short separations are used. Though we will not go into detail here (the reader is referred to reference 97), deviations from the standard PB treatment have two causes:

(i) Due to ion-ion repulsions, the counter ions concentrate towards the charged surface reducing the overlap between the double layers.

(ii) Fluctuations in the ion clouds of surface layers cause attractions between similarly charged surfaces.

CHAPTER SIX

A SPECTROSCOPIC STUDY OF THE DODECYL TRIMETHYL AMMONIUM CHLORIDE (C_{12}TACl)-WATER SYSTEM

6.1 Introduction

The phase behaviour of the cationic surfactant, dodecyl trimethyl ammonium chloride ($C_{12}TACl$) and water is fairly well established.[32] The phase diagram for the system (Figure 6.1) shows four liquid crystalline phases. These are the two cubic phases, a hexagonal phase and a lamellar phase, all separated by first order phase boundaries. The hexagonal (H_1) and lamellar (L_α) phases have the conventional structures described in Sections 5.2.2 and 5.2.1, respectively. The cubic phases, however, have aroused much discussion concerning their structure.[103] It is generally accepted that the isotropic cubic phase, occurring at high concentrations (V_1) (between hexagonal and lamellar regions of the phase diagram), has a bicontinuous structure,[52,103] where both surfactant and water form continuous zones. The pictorial representation of Scriven[52] is shown in Figure 5.7. The cubic phase occurring at low concentrations (I_1) between isotropic micellar solution and hexagonal phase has received much attention. Initially X-ray diffraction studies[74] had pointed at a structure consisting of "rod like cages which enclosed two micelles per unit cell". The NMR self diffusion data[84] however, were not consistent with a continuous rod structure, but for one exhibiting discrete spherical micelles (*i.e.* data showedrestricted self diffusion). These data have recently been reconciled[73] by showing that the X-ray data can also be assigned to the Pm3n space group (previously $Pm3n^2$) and believed to consist of 48 spherical micelles per unit cell.

A subject of much interest in lyotropic liquid crystal systems has been the behaviour of the water at a micellar

FIGURE 6:1

The Phase Diagram of the $C_{12}TACl$/WATER SYSTEM

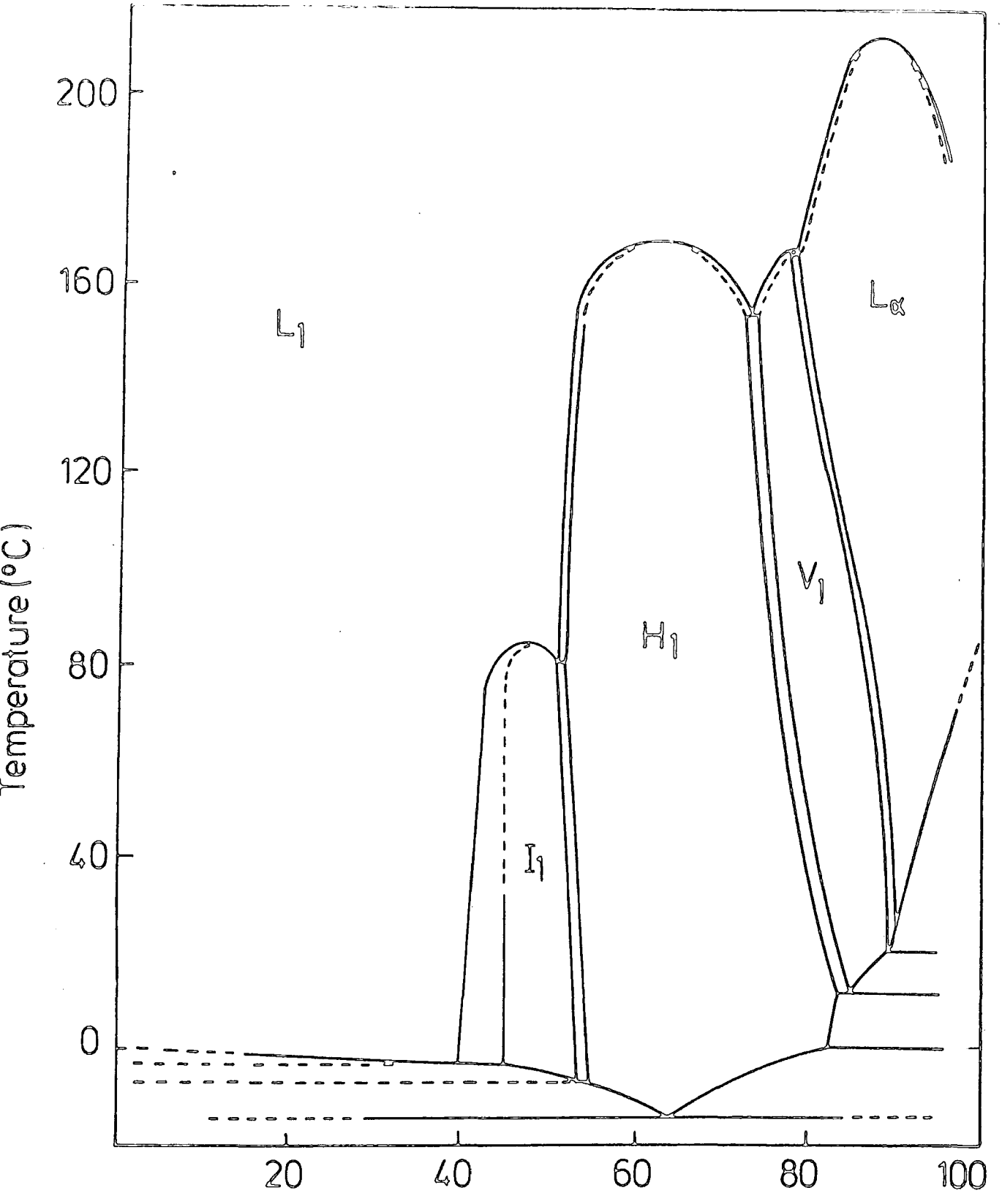

surface. In the past NMR has proved to be a powerful tool in this context.[82,101-102,104-109] The technique has shown, *e.g.* using deuteron quadrupole splitting,[107] that two types of water exist. These are water perturbed by the surfactant and water bound to itself, *i.e.* bulk water. It has been established that perturbations of water structure extend over several molecular diameters. The existence of various water species should therefore be detected using vibrational spectroscopy. In particular, a study of the various inter- and intramolecular hydrogen bonding infra red modes should provide further information concerning the state of water in these systems.

The study of water "structuring" using infra red spectroscopy has been of interest to a number of workers.[54,110-113,115] Though some of this work has been done using reverse micelles [54,55,112,113,115], the spectra reveal the presence of two distinguishable types of water molecule. As with the NMR results given above the interpretations have been based on water in the bulk solvent and water bound to the surfactant [54,112,113,115]. Sunamoto *et al*,[113] observing the ν_2 and ν_3 combination mode of water in reverse micelles, postulated that the water showed greater perturbations by the head group than the counter ion. Their data, using a range of surfactants with varying head group and counter ion, suggested that the strength of the water interaction is greater in cationic surfactants (C_{16}TACl and C_{16}TABr) than in anionics. These findings allowed them to propose two different hydration mechanisms for anionic and cationic surfactants; the former exhibiting a hydrogen bonded interaction of the type

$\{R\cdot X^{-}\circ\circ\circ\circ\circ H\text{-}O^{\prime}\}$ while the latter a coordination type $\{R\text{-}X^{+}\circ\circ\circ\circ\circ O\langle^{H}_{H}\}$. In this context therefore one would expect, as far as the ν_s stretching mode was concerned, to see greater perturbations from counter ion interactions since these lead to greater changes along the O-H normal coordinate. However, Raman data of Lucas *et al*[114] has shown that anion hydration is also important. The literature shows little work performed of water structure in lyotropic liquid crystals.

One notable investigation in this area by McDonald *et al*[111] has revealed the presence of a shoulder towards the lower frequency side of the decoupled ν_s(O-H) stretching band (see Section 6.2.1), at low water concentrations. This asymmetry has been assigned as a surfactant perturbed water. As the surfactant concentration is increased the shoulder disappears and the ν_s(O-H) band becomes symmetrical and almost identical to that in liquid water.[111]

Far infra red has been little used to study the structure of water in mesophase systems. This is surprising when one considers the sensitivity of this region to perturbations in water structure. Work by Colbow *et al*[116] of the lamellar phase in the water-lecithin system, have shown absorptions due to dipolar interactions between choline groups. Their data suggest that these dipoles lie parallel to the bilayer plane. However, the spectra are obtained up to a maximum of 120 cm^{-1} and provide little information concerning the state of water.

Raman spectroscopy has proved to be extremely productive in liquid crystal studies.[117] Though the amount of information concerning water using this technique is limited (the same conclusions can be drawn by I.R.).[117] However, the greatest wealth

of data is obtained by studying the Raman spectra of the alkyl hydrophobic chains. It is possible to determine the order and fluidity within the hydrocarbon portions of micelles and mesophases.[118] There are three regions which may be used to study the oleophillic chains, these are:

(i) The longitudinal acoustical mode which occurs in the region 100-300 cm^{-1}.[118]

(ii) An intermediate region 1000-1200 cm^{-1} giving rise to the skeletal stretching and methylene rocking modes.[118]

(iii) A high frequency region which shows a number of overlapping methyl and methylene C-H stretching modes, occurring at 2700-3100 cm^{-1}. Though this region is sensitive to temperature and composition, it shows complex behaviour which will be discussed in Section 6.5.

As with other workers who have used i.r. spectroscopy to study lyotropic liquid crystalline systems[54,110-113] we have tried to learn as much as possible about the state and organization of both water and amphiphiles. The infra red measurements in both the far and mid regions have shown perturbations in water structure that occur as a result of counter ion and head group interactions. We have tried to correlate spectral changes with known phase boundaries, the C_{12}TACl-water system, in the hope that a similar procedure may be applied to a less well known system (see Chapter Seven). In the Raman spectra, we have studied the oleophillic chain and the head group. This we hope should give information concerning the packing of alkyl chains and changes in head group conformations, respectively.

6.2 Experimental

6.2.1 Materials and Sample Handling

Cationic surfactants were obtained from Eastman Kodak and Unilever research, with both samples having been recrystallised from acetone. For the mid infra red experiments a bulk water solution was prepared containing approximately 4% v/v deuterium oxide (Fluorochem Limited, 99.83% purity), in distilled water, thus allowing a study of the decoupled ν_s(O-D) band of HDO (see Chapter Two). Samples of surfactant, previously dried over P_2O_5, were weighed out in 10mm vials. The desired mass of water solution was then added and the vial subsequently sealed with an airtight screw cap. The components were mixed by prolonged incubation at elevated temperatures (60^oC) for up to 3-5 weeks depending on sample viscosity. Periodic centrifugation at 4000 r.p.m. ensured sample homogeneity which was checked before use under a polarizing microscope. Samples for far infra red spectroscopy were generally the same as those used in the mid i.r. experiments except in some cases where distilled water was used in place of the 4% v/v deuterium oxide solution.

Before commencing any spectroscopic investigations the sample vials were inspected at room temperature. Anisotropic samples, such as that found in hexagonal or lamellar phase regions appeared slightly opaque to the eye, while isotropic samples appeared completely transparent. A comparison with the phase diagram (Figure 6.1) thus allowed an immediate check on sample composition. In cases where the exact concentration was desired, *i.e.* in the second cubic (V_1) and lamellar

phase (L_α) regions, a small portion was observed through a polarizing microscope, possessing a Koffler heating stage. This allowed the determination of an isoplethal phase transition from which one could interpolate the surfactant concentration using the phase diagram of Balmbra *et al.*[32] (*N.B.* This diagram has been shown to be correct by another laboratory).[86]

Small portions of the mesophase sample were placed between calcium fluoride windows for the mid infra red, and silicon windows for the far infra red. These were then clamped in variable temperature cells and compressed so that the entire area of the cell plate was in contact with the mesophase. Since only a central portion of the cell plates transmitted radiation, most of the water loss occurred in the outer regions of the sample not exposed to the incident beam. A further precaution was taken, in some cases, of wrapping tape around the perimeter of the cell. This again reduced water loss during heating and cooling cycles. Due to the inherent viscosity and high absorbing characteristics of these mesophase samples, path-length spacers could not be used and so several methods of quantifying the spectra were investigated. These included - measuring the cell thickness with and without the sample using a micrometer; tightening cell bolts to an approximately constant torque. The best method however, was by measuring the mesophase thickness at each corner of the windows using a reflecting microscope with a graduated scale. This allowed an average thickness to be measured with an accuracy of ±20μ. In general the samples were of the order of 50μ in thickness and so an error of 40% was expected in the absorption coefficients so calculated. The method was therefore only used in the far

infra red where fewer spectra were recorded. The results therefore only allowed a qualitative comparison.

The temperature for the infra red work (both mid and far) was controlled by a Beckman RIIC Temperature controller and varied between 30 and 70°C. For the mid i.r. experiments spectra were first recorded at 50°C and then further spectra obtained using 10°C step heating and cooling cycles as a check on hysteresis. Such a procedure allowed the 50°C spectrum to be recorded in triplicate. 50°C was chosen as the main temperature for the study because it allowed spectra of the lamellar phase to be obtained (the region of lamellar phase broadens with an increase in temperature, see Figure 6.1) with a minimum of water loss. The heating and cooling cycles also minimised water loss which was found to be 3.5% w/w for a 0.034g smear of a 74% w/w C_{12}TACl sample at 24°C exposed to the atmosphere for 10 minutes.

Samples for Raman spectroscopy were weighed out in 3mm internal diameter NMR tubes in the same way as described for mid i.r. samples. The tubes were however sealed permanently since spectra could be recorded *in situ*. As a check on concentration, samples were, in some cases, observed through crossed polars while being heated. In this way isotropic → anisotropic (and *vice versa*) phase transitions could be determined accurately.

6.2.2 Mid IR Spectroscopy

Infra red spectra were recorded between 2800 and 1500 cm^{-1} using a Perkin Elmer PE580 spectrometer (see Section 2.2) equipped with air drying facilities. This region exhibited

two bands of interest:

(i) the ν_s(O-D) decoupled stretching band of HDO at 2520 cm^{-1}. and

(ii) the $\nu_A(H_2O)$ combination band at≈2120 cm^{-1}.[5]

For each spectrum, the frequency maximum, width at half maximum intensity and any other salient features (*i.e.* shoulders, *etc*) were noted. Since the pathlength was unknown, only relative intensity changes could be obtained.

6.2.3 Far I.R. Spectroscopy

All the spectra in this region were obtained using the modified Beckman FS720 described in Section 2.3.2. Data were recorded using two detectors, a Golay cell and a helium cooled Germanium bolometer which covered the 50-350 cm^{-1} and 20-180 cm^{-1} ranges, respectively. Optimization of conditions included changes in a number of parameters and these have been tabulated below (Table 6.1). As mentioned in Chapter Two the interferometer used here employed a system of phase modulation to improve the signal to noise ratio. Such a system allows the characteristics of the background spectrum to be, to some extent, dependent on the amplitude of the oscillating mirror. This oscillation is dependent on the modulation current, and for a given amplitude, varies from one loudspeaker coil to another (see Chapter Two). During the course of our experiments this assembly was replaced and the modulation currents used were 2 and 33mA for the old and new units, respectively.

As mentioned in the previous section, spectra were recorded using silicon windows with (as a thin film) and without

TABLE 6.1 Instrumental Parameters used for Beckman FS720 Detectors

Detector	Golay Cell	Ge Bolometer
Beamsplitter	15 Gauge Mylar	25 Gauge Mylar
Modulation frequency	11-15 Hz	50-80 Hz
Frequency range	50-350 cm^{-1}	20-180 cm^{-1}
Filters	Black Polythene lens	200 cm^{-1} Cambridge and Blocking Filter
Sampling interval	10μm	20μm
Typical Gains (with sample)	0.5-5 Full Scale	10-100 Full Scale (at 60dB Bolometer setting)
Time Constants	0.4-1.25s	0.125-0.4s
Sampling speeds	1-0.3 pulses/s	3-1 pulses/s

sample such that the ratio

$$A = \log \left(\frac{I_o}{I}\right) \qquad \text{(eqn. 6.1)}$$

only included effects due to the sample. The silicon plates themselves were optically flat so that the space between them, as well as beng wedged, prevented any reasonable effects from interference fringes.

6.2.4 Raman Spectroscopy

Raman spectra were obtained using a Cary model 82 spectrometer employing a Spectra Physics Argon Ion laser tuned to the green line at 514.5nm. Before commencement of any experiments, the instrumental optics were cleaned and adjusted

for maximum power. The temperature was maintained by the use of a special cell block which allowed the circulation of water from a thermoregulated bath. The cell is illustrated in Figure 6.2. Instrument frequency calibration was performed using the 462 cm^{-1} line of CCl_4.

The scan conditions have been tabulated below.

TABLE 6.2 Raman Scan Conditions

Laser Power at Sample	200-400mW
Spectral Bandwidth	3-5 cm^{-1}
Sensitivity	500-50,000 counts s^{-1} full scale
Pen Period	2-20 seconds
Scan Speed	0.1-1 $cm^{-1}s$.
Polarization	No selection

6.3 Mid IR Spectroscopic Investigation of the $C_{12}TACl$-Water System

6.3.1 The Spectrum of Decoupled Water

Figure 6.3 shows the spectrum of a H_2O solution containing 4% v/v deuterium oxide. Four bands are observed in this region and they have been assigned as follows:[5] the decoupled ν_s(O-D) stretching band at ≈2520 cm^{-1}, the water combination band, $\nu_A(H_2O)$, occurring at ≈2100 cm^{-1}, the water bending mode, ν_2, at ≈1650 cm^{-1}, and the HDO bending mode at ≈1450 cm^{-1}.

FIGURE 6.2 CELL BLOCK USED IN RAMAN EXPERIMENTS.

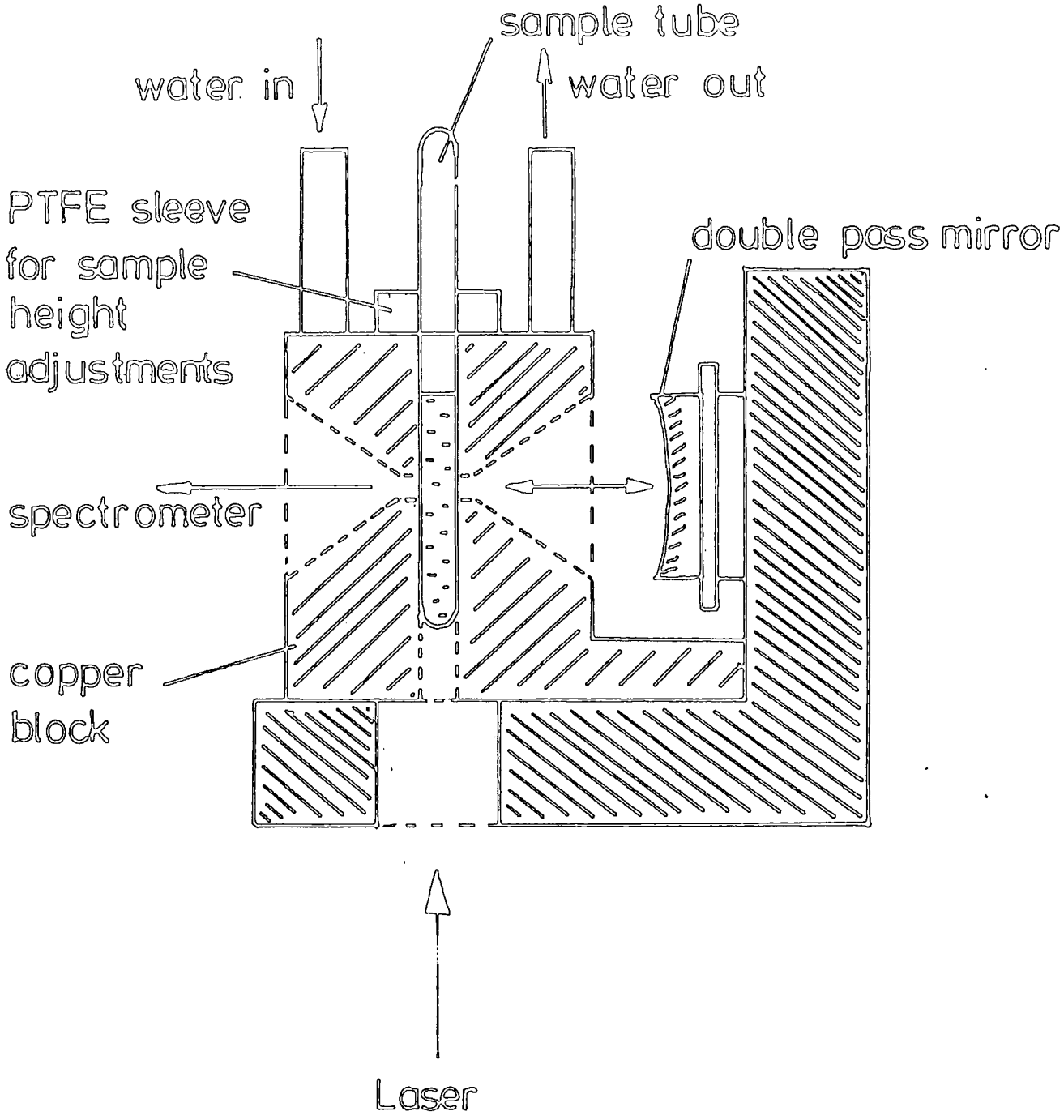

FIGURE 6.3 IR SPECTRUM OF DECOUPLED H_2O (4% v/v D_2O) AT 50°C.

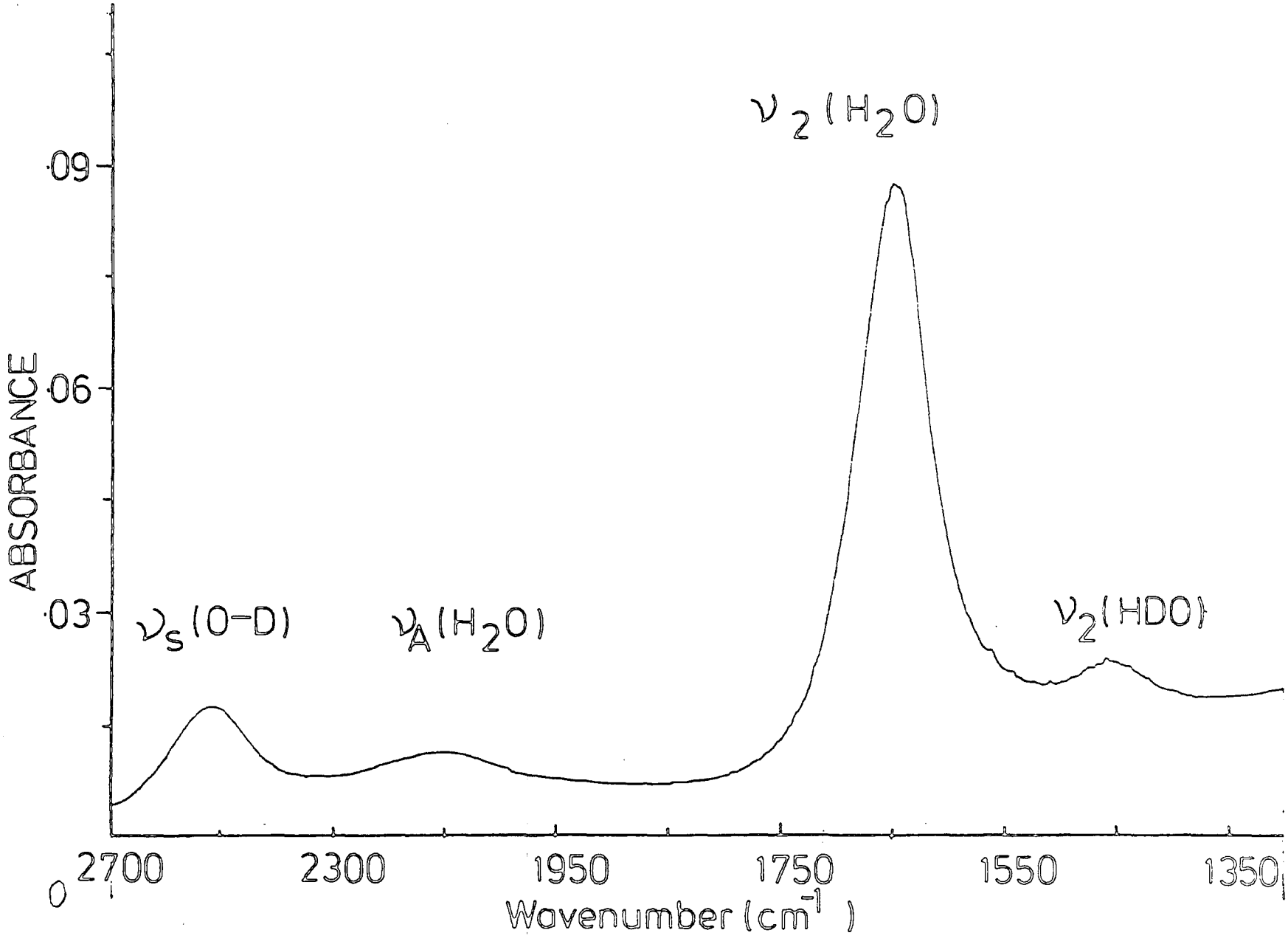

Inspection of the water spectra in the mesophases of $C_{12}TACl$ reveals that only the $\nu_A(H_2O)$ and $\nu_s(O-D)$ bands may be used in a survey of these systems. The two bending modes of H_2O and HDO overlap with the skeletal carbon-carbon bands of the amphiphile chain. Preliminary experiments with H_2O in bulk D_2O solutions show little improvement in the situation, since in this case the decoupled $\nu_s(O-H)$ of HDO overlaps with the C-H stretching bands of the amphiphile. We have measured the width at half maximum intensity and the frequency maximum for both the decoupled $\nu_s(O-D)$ and $\nu_A(H_2O)$ combination modes. These are shown in Table 6.3 below.

TABLE 6.3 Band Parameters* for the $\nu_s(O-D)$ and $\nu_A(H_2O)$ Water bands at 50°C

	$\nu_{max}(cm^{-1})$	$\Delta\nu_{1/2}$ (cm^{-1})
$\nu_s(O-D)$	2520(2500)	156(160)
$\nu_A(H_2O)$	2106(2125)	221(-)

* Literature Values in parenthesis at 25°C.[5]

A comparison with the band parameters observed in the literature shows that there is reasonable agreement considering the difference in temperatures.

6.3.2 The Behaviour of the $\nu_s(O-D)$ stretching Mode in $C_{12}TACl$ and $C_{12}TABr$ Mesophase Systems

The spectrum of HDO in a 74.8% $C_{12}TACl$ mesophase sample is shown in Figure 6.6. A comparison of this spectrum to that observed in Figure 6.4 (HDO spectra in H_2O) reveals

FIGURE 6.4 IR SPECTRUM OF DECOUPLED H_2O (4 %v/v D_2O) AT 50°C.

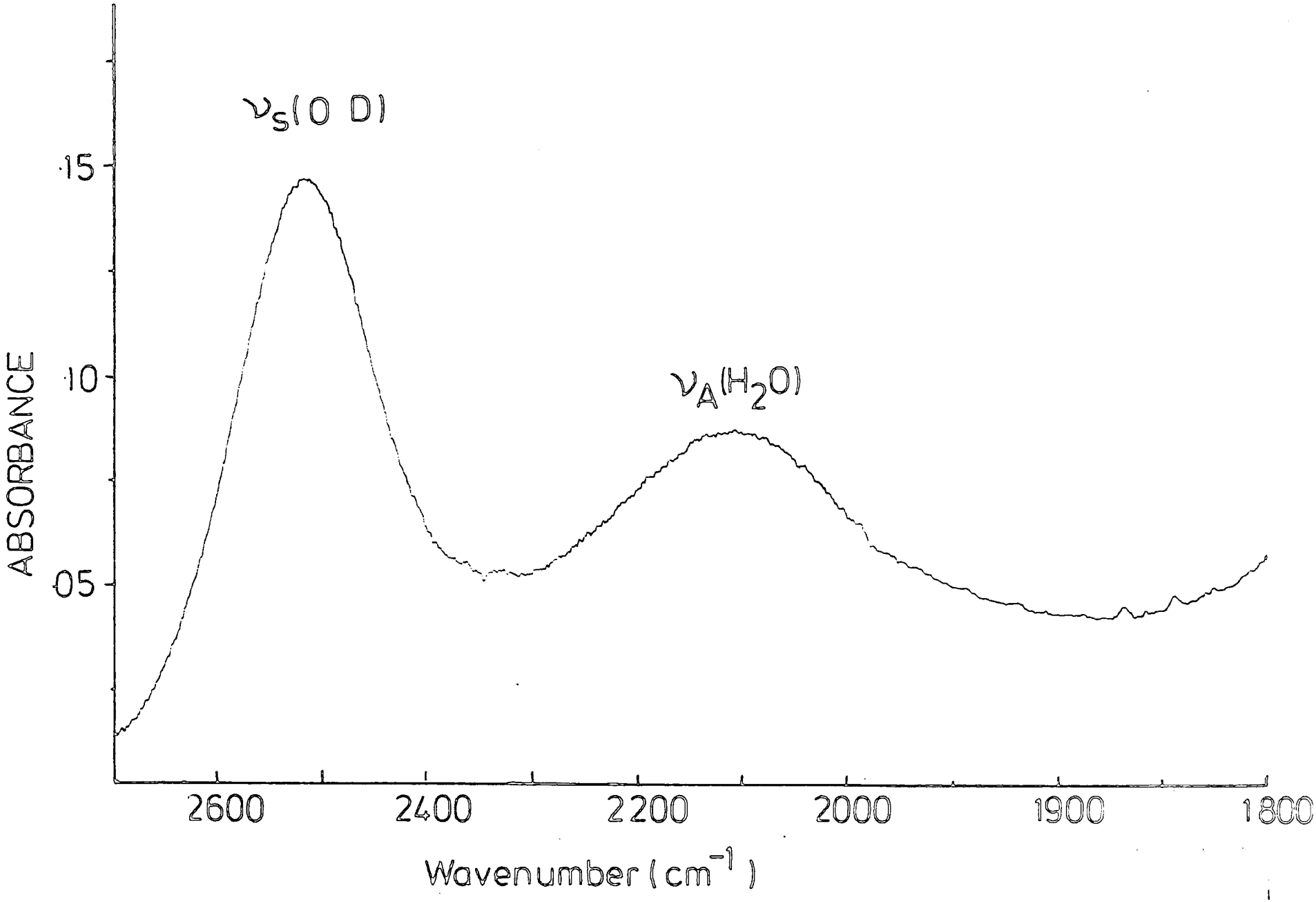

FIGURE 6·5 THE IR SPECTRUM OF A 47·4 %w/w C_{12}TACl MESOPHASE

SAMPLE AT 50°C

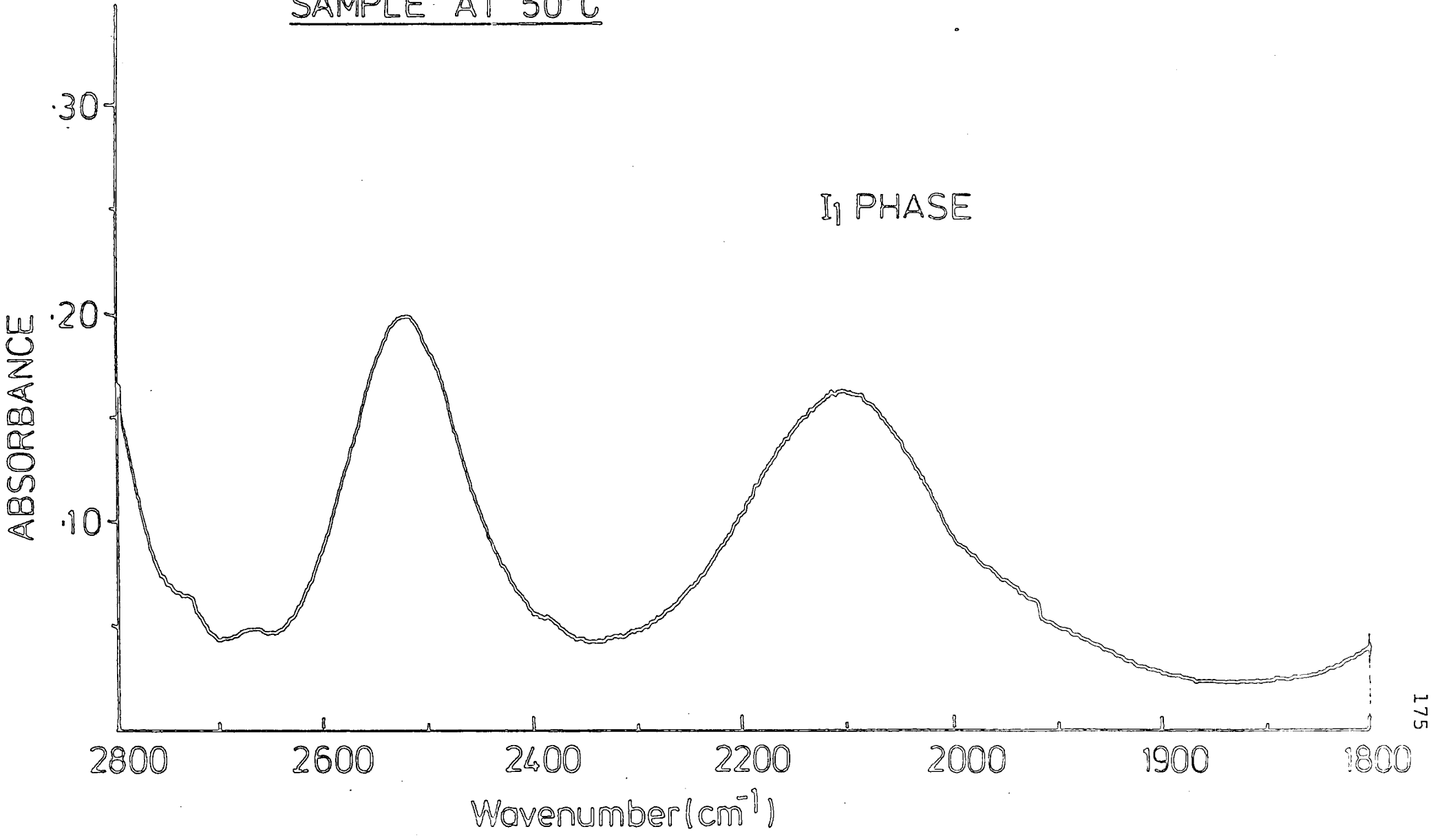

FIGURE 6.6 IR SPECTRUM OF DECOUPLED H_2O IN A 74·8 % $C_{12}TACl$ MESOPHASE SAMPLE AT 50°C.

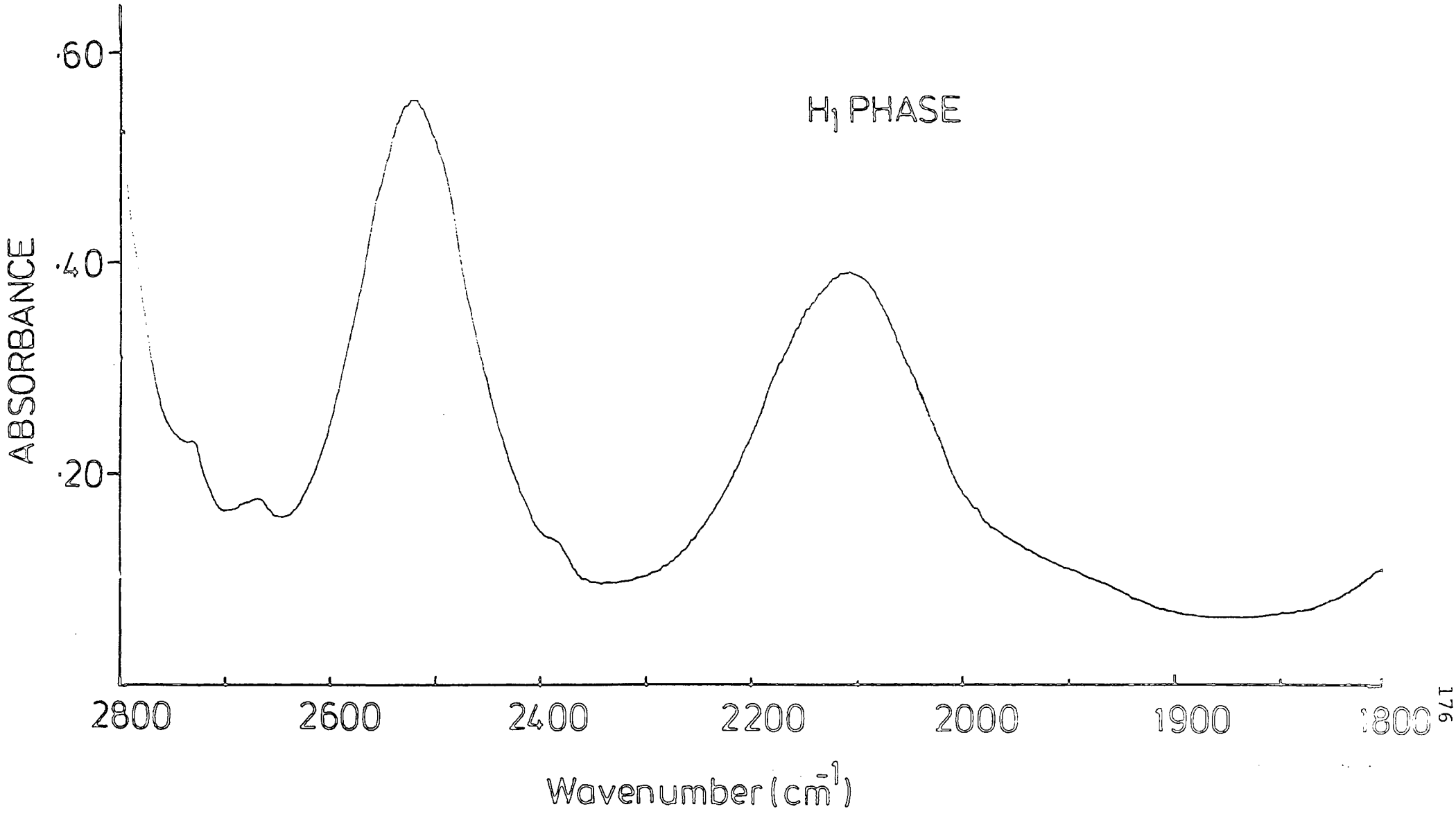

several differences. Firstly the band in the former is narrower and exhibits a shoulder towards the low frequency side (2500 cm^{-1}) of the main band at 2520 cm^{-1}. As the concentration is increased, further narrowing is observed (Figures 6.7 and 6.8) and the shoulder becomes more apparent. Similar behaviour has been observed in a spectrum of water in the lamellar phase of the undecanoin-D_2O system studied by McDonald *et al.*[111] Though their work has used the analogous decoupled ν_s(O-H) vibration of HDO, a shoulder is again apparent at high surfactant concentrations. In addition, the frequency shifted shoulder shows a marked intensity change when the orientation is altered from 0^o to 45^o about an axis perpendicular to the spectrometer beam. This dichroic effect has indicated a preferred orientation of transition dipoles, which may be interpreted as being due to water molecules bound to the bilayer surface.

Further increases in amphiphile concentration reveal the presence of fewer intense shoulders (see Figure 6.8). A comparison of such spectra, with one of the solid, shown in Figure 6.10 might suggest that these bands are due to the surfactant. The difficulty here is in deciding on the intensity of the surfactant bands in the mesophase spectra. Figure 6.9 shows two superimposed spectra of a 94% w/w C_{12}TACl mesophase at 20^o(solid + lamellar) and 50^oC (lamellar). At the lower temperature the ν_s(O-D) band is still evident but at 50^oC the band disappears completely. The absence of the ν_s(O-D) in this spectrum allows us to see that the intensity of the surfactant bands are quite small. It is difficult to imagine these small bands contributing significantly to, say, a

FIGURE 6.7 IR SPECTRUM OF DECOUPLED H_2O IN A 84·6 % $C_{12}TACl$ MESOPHASE SAMPLE AT 50°C.

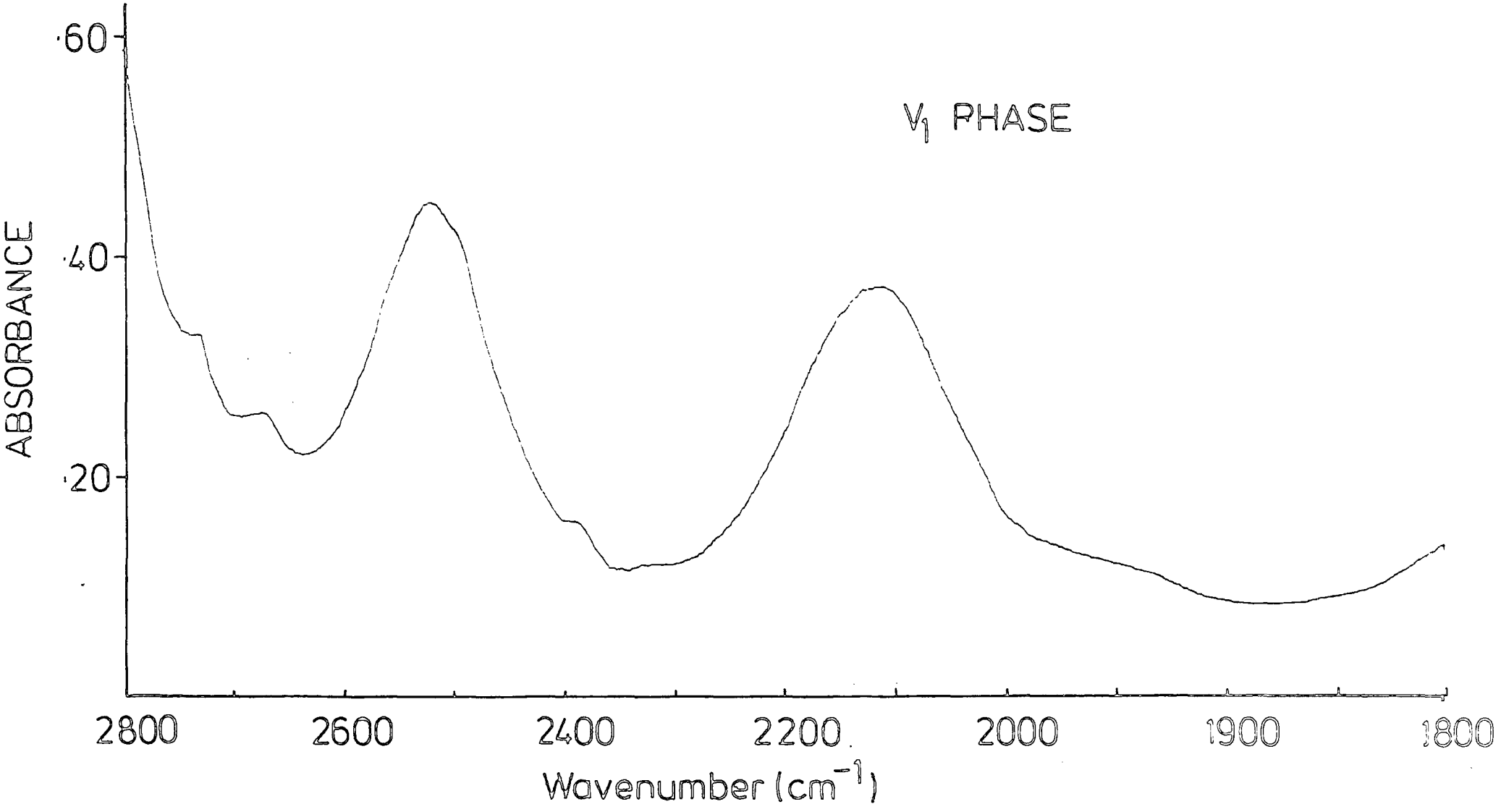

FIGURE 6.8 IR SPECTRUM OF DECOUPLED H_2O IN A 90·7% $C_{12}TAC$ MESOPHASE SAMPLE AT 50°C.

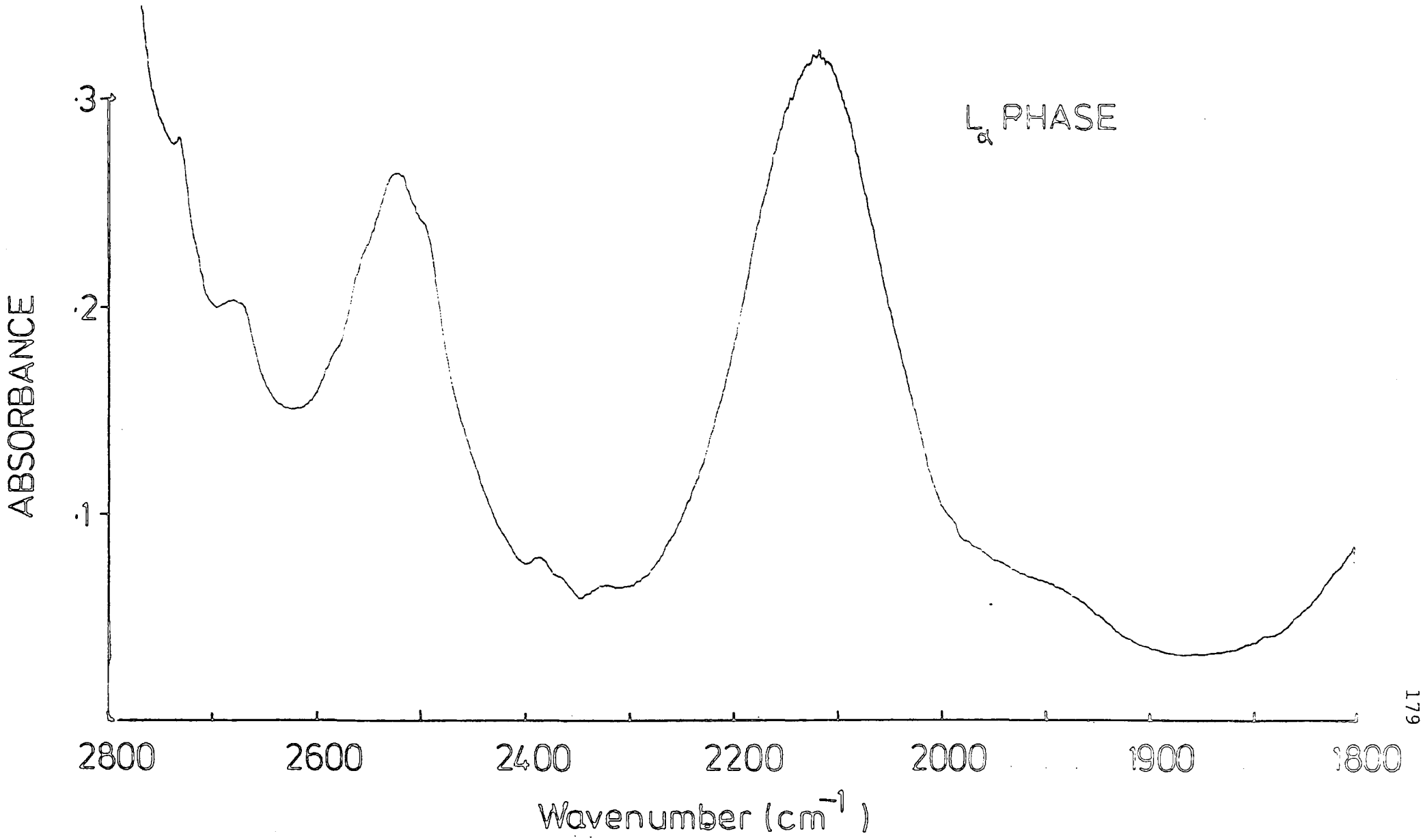

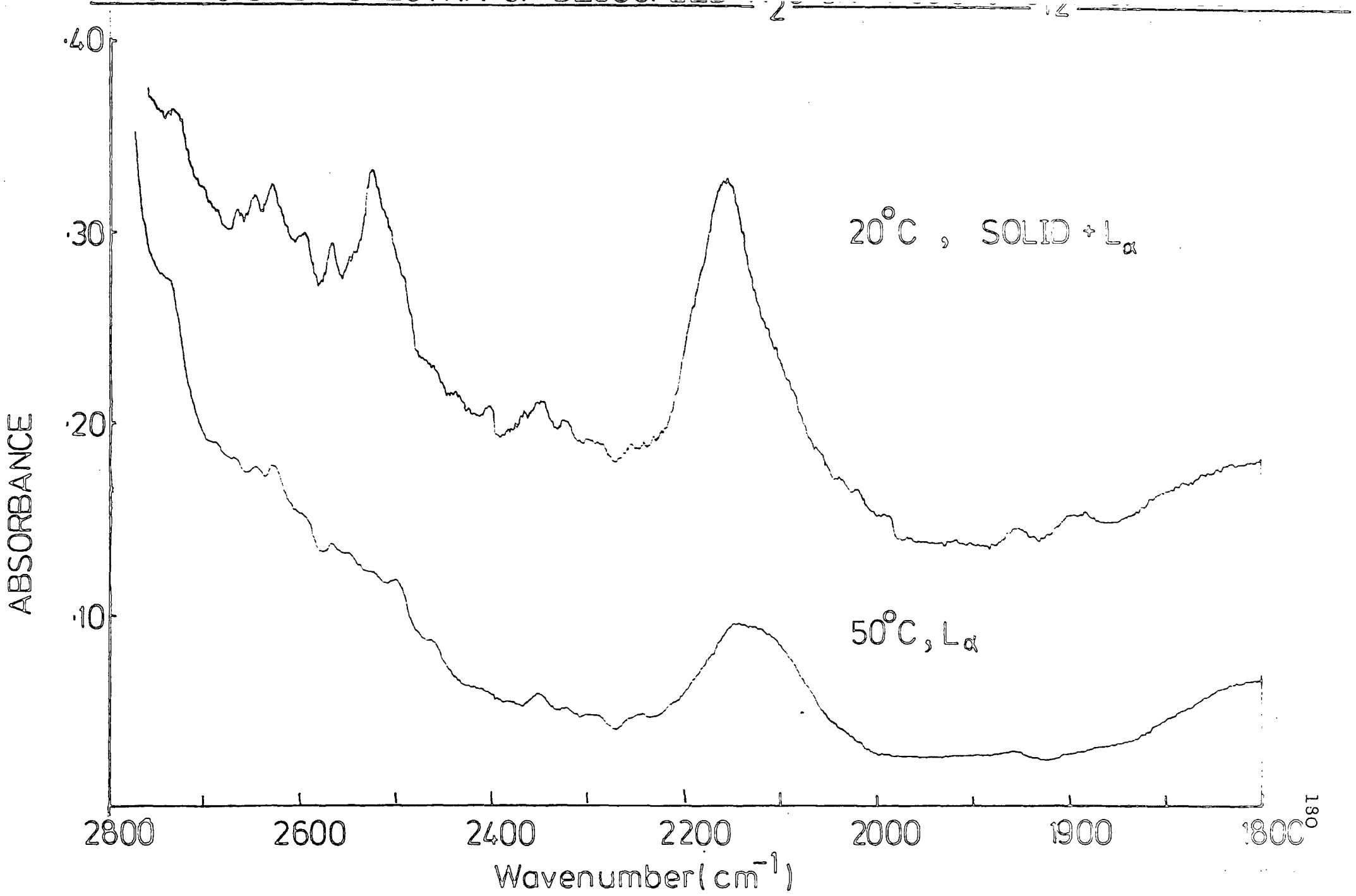
.40
.30
.20
.10
ABSORBANCE
20°C , SOLID + Lα
50°C, Lα
2800
2600
2400
2200
2000
1900
1800
Wavenumber(cm⁻¹)
180

FIGURE 6.10 DIAGRAM SHOWING A COMPARISON OF SOLID AND MESOPHASE SPECTRA IN THE 2600-2400 CM^{-1} REGION.

[N.B. Absorbance spectrum of solid $C_{12}TACl$ accumulated over 20 scans].

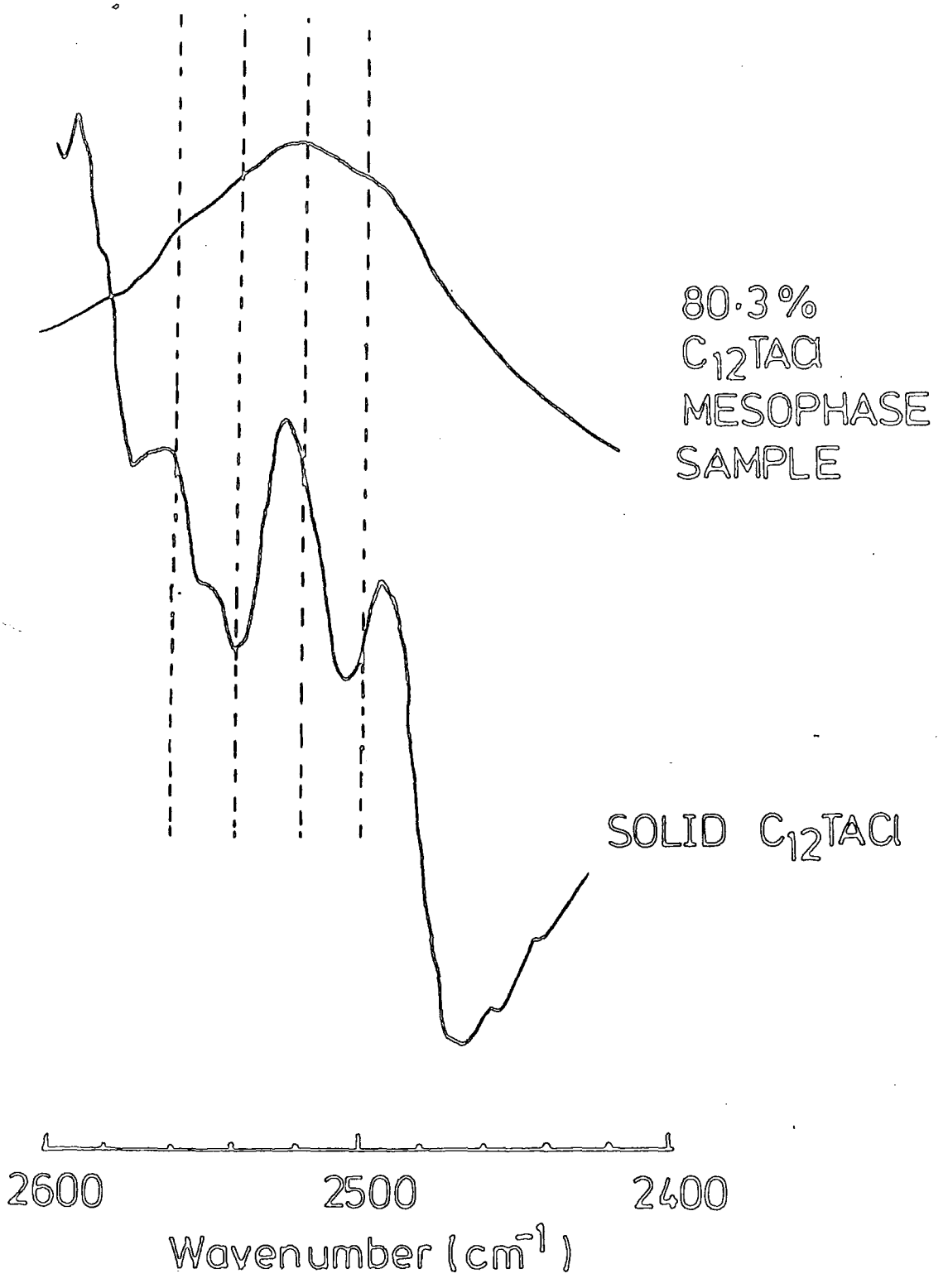

ν_s(O-D) spectrum containing 47% w/w C_{12}TACl as shown in Figure 6.5. The disappearance of the ν_s(O-D) species in Figure 6.9 poses another problem, particularly in view of the fact that the $\nu_A(H_2O)$ association band remains *ca.* 2130 cm^{-1}. There are two possibilities for this behaviour. Firstly that a species of water exists which forms the initial solvation layer of the micelle surface. This water layer, which will also be significantly affected by the counter ion, may shift from 2520 cm^{-1} to a point where it is not clearly visible in our spectral window. Secondly that this initial layer of water, by some coincidence, shows no net change in $\frac{\partial u_D}{\partial q}$ and hence disappears completely. One may not necessarily see a significant change in $\nu_A(H_2O)$ since this band, which comprises largely of ν_2, is known to be little affected in H-bonded systems. The resultant reduction in water thickness may then be enough to leave only this initial boundary water.

The literature on the subject all points to the fact that there are two water species. Wells,[115] using phosphatidyl choline reverse micelles in ether observed a surfactant perturbed $\nu_s(O\text{-}H)_{HDO}$ band 120 cm^{-1} above its natural frequency. The width, intensity and position of this band have suggested that this water displayed few H-bonded forms which were weak and far removed from either water or ice.[5] The i.r. data of McDonald[111] also demonstrates a similar result though in this case a shoulder is found to the low frequency side of the more intense band. Their work with the undecanoin-water mesophase systems showed a dichroic effect of this shoulder, thus suggesting a preferred orientation of water. (The band appearing at lower frequencies because the interaction of an

alcohol "O-H" with water is generally stronger than between "O-H" water molecules). NMR results[82,101,102,104-109] also show strong evidence for the presence of two types of water species, though the data obtained is time averaged (as a consequence of the time scale of the NMR experiment compared to the motion of the water molecules).

The general picture therefore seems to suggest the presence of a "boundary" water layer as depicted in Figure 6.11 below. Disorder-order transitions, as discussed in Chapter Five, are derived from 3-dimensional soft sphere re-

Figure 6.11 Possible Water Organization in Lyotropic Mesophase Systems

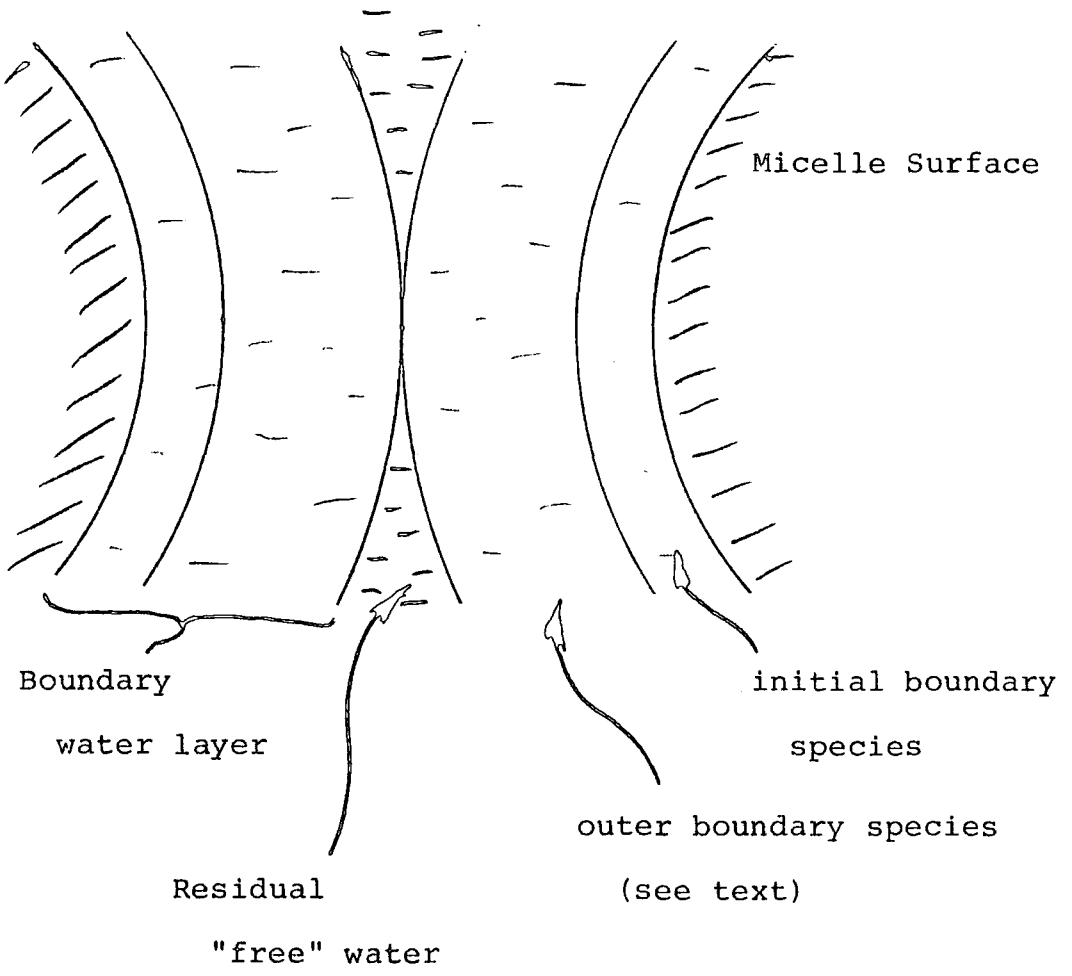

pulsions between hydrated micelles which of course may occur at low surfactant fractions, *ca.* approx. 50% $C_{12}TACl$. At these concentrations, where the mole ratio of water/surfactant is of the order of 15, one can imagine the presence of a boundary water layer, several layers thick and associated to some extent with the micelle surface. Since the literature suggests the presence of an initial boundary water layer, it might therefore be expected that the depth of the outer boundary layer decreases as the surfactant concentration is increased. If our spectra show the existence of two species, then one should observe a decrease in intensity of one relative to another. In practice (see Figures 6.5-6.8) this is not observed (*i.e.* a comparison of the 2520 cm^{-1} species and the shoulder at 2500 cm^{-1}), though this <u>may</u> in some part be due to the presence of surfactant bands.

The outer boundary layer of Figure 6.11 as mentioned earlier will be associated, albeit weakly, with the micellar surface. The data presented in the literature above[82,101,102,104-109,111,115] all show that this water species has properties very similar to ordinary "bulk" or "free" water. In this respect our results agree with these findings with ν_s(O-D) having a ν_{max} at the same frequency, 2520 cm^{-1}, as that in water. Indeed the relative intensity of this band to the $\nu_A(H_2O)$ band decreases though this point will be discussed in more detail in the next section. Ordinary bulk water, which occurs in substantial quantities at concentrations below the order-disorder transition, is expected to give a broad featureless band. This again is observed and spectra in the L_1phase are almost identical to that of pure water.

In addition to the C_{12}TACl mesophases, several dodecyl trimethyl ammonium bromide liquid crystals were prepared. The spectrum of one such sample is shown in Figure 6.12. As with the chloride, the C_{12}TABr shows two bands, at 2530 cm^{-1} and a shoulder remains at 2500 cm^{-1}, with neither of them shifting in frequency as the C_{12}TABr concentration is increased. The origins of these bands are likely to be similar to that discussed for the C_{12}TACl and hence several possibilities are available:

(i) The species at 2530 cm^{-1} and 2500 cm^{-1} are due to outer and initial boundary water species, respectively. The shift by 10 cm^{-1} being attributed to a difference in the strength of counter ion hydration, in the outer boundary solvation layer, which is expected for the larger bromide ion. The 2500 cm^{-1} species, largely influenced by the surface head groups, thus remains fixed in frequency.

(ii) The shoulder at 2500 cm^{-1} being assigned to a surfactant band, probably the surfactant chain (since no frequency shift is observed), and the initial boundary water species shifts to other frequencies not clearly observed in our spectral window. The peak at 2530 cm^{-1} belongs to the "loosely" bound water molecules which are largely influenced by the counter ion.

(iii) Same as above except that the initial boundary water molecules, occurring in the first solvation shall have a $(\frac{\partial \mu_D}{\partial q_{O-H}} = 0)$ for the O-H stretch, and the band disappears.

At low water/C_{12}TABr mole ratios (see Figure 6.13) no disappearance of the ν_s(O-D) band is observed. This evidence

FIGURE 6.12 IR SPECTRUM OF DECOUPLED H_2O IN A 79%w/w C_{12}TABr MESOPHASE SAMPLE AT 50°C.

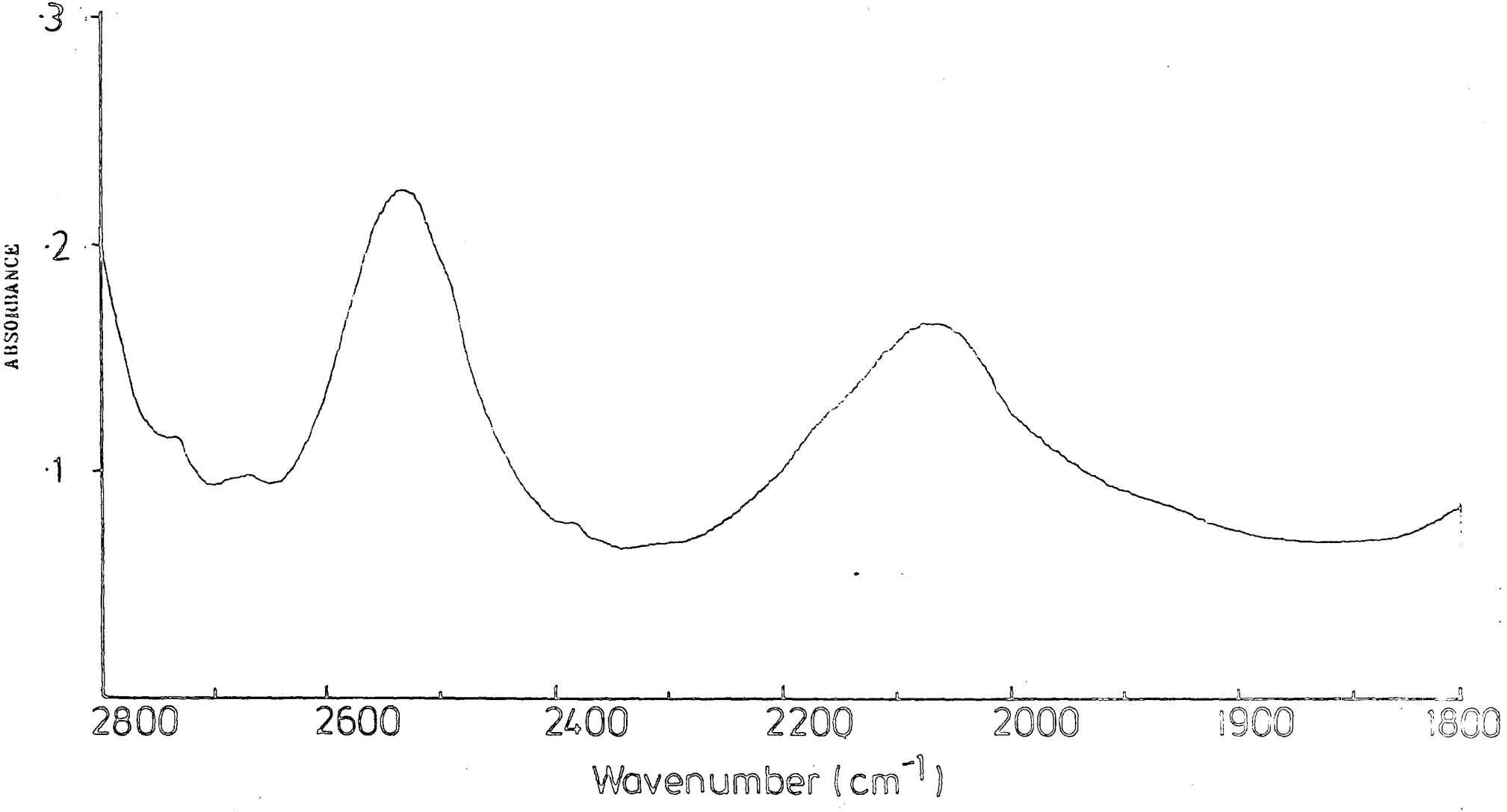

FIGURE 6·13 THE BEHAVIOUR OF DECOUPLED H_2O IN A 94%w/w C_{12}TABr MESOPHASE SAMPLE AT 70°C.

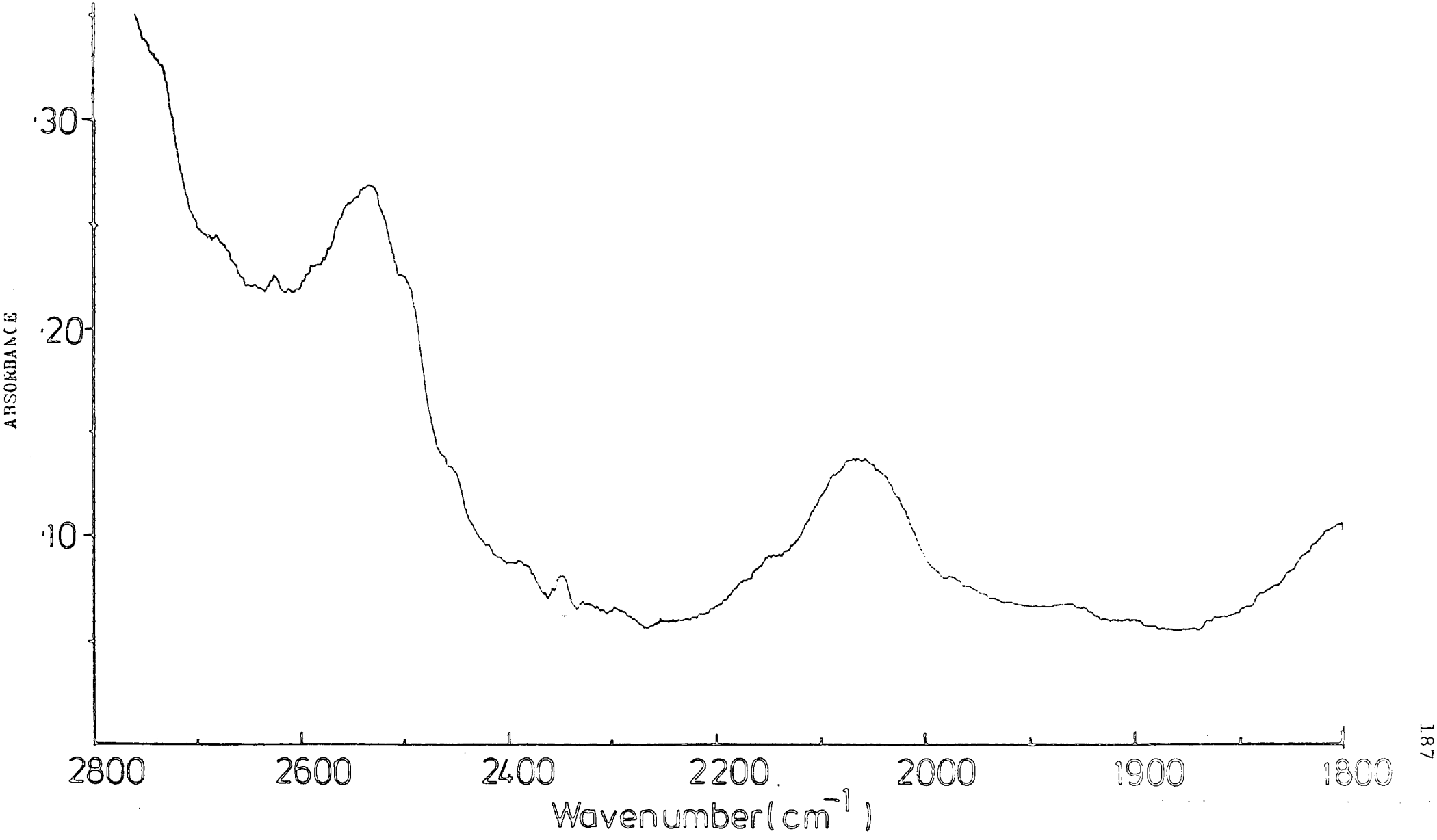

favours the first hypothesis, though (iii) may still be valid if one considers that the $(\frac{\partial \mu_D}{\partial q_{O-H}}) = 0$ situation in the chloride may now be relaxed in the bromide. The presence of this band at these high concentrations (mole ratio = 1.0) may also be due to the fact that the bromide system is different and hence requires less water for solvation. This hypothesis is however unlikely since the bromide is known to have a higher hydration number.[93]

Figure 6.14 shows a plot of the full width at half maximum intensity for the ν_s(HDO) band as a function of C_{12}TACl concentration. The graph shows a smooth curve which increases in slope as the amphiphile concentration increases. Unlike the data of Françoise,[110] who measured relative intensity changes of near i.r. water bands in some mesophases, no discontinuities across phase boundaries are observed. However, there is a general decrease in the width at half maximum intensity ($\Delta\nu_{1/2}$) as the concentration is increased. The narrowing becomes more significant at higher concentrations particularly beyond the point at which liquid crystals first form (at 45% w/w C_{12}TACl). It may be interpreted in terms of a decrease in the number of water structural forms found in the outer boundary layer mentioned earlier. The data has also been plotted as a function of the water/surfactant mole ratio and is shown in Figure 6.15. The curve is similar to that observed previously in Figure 6.14. Sunamoto *et al*,[113] using frequency maxima of bands in the near infra red to study water in reverse micelles, have found an inflection when the water/surfactant mole ratio approaches 1.0. Though an inflection is not observed in Figure 6.15 it seems possible that our data

FIGURE 6.14 THE BEHAVIOUR OF THE ν_S(HDO) WIDTH AT HALF MAXIMUM AS A FUNCTION OF CONCENTRATION AT 50°C.

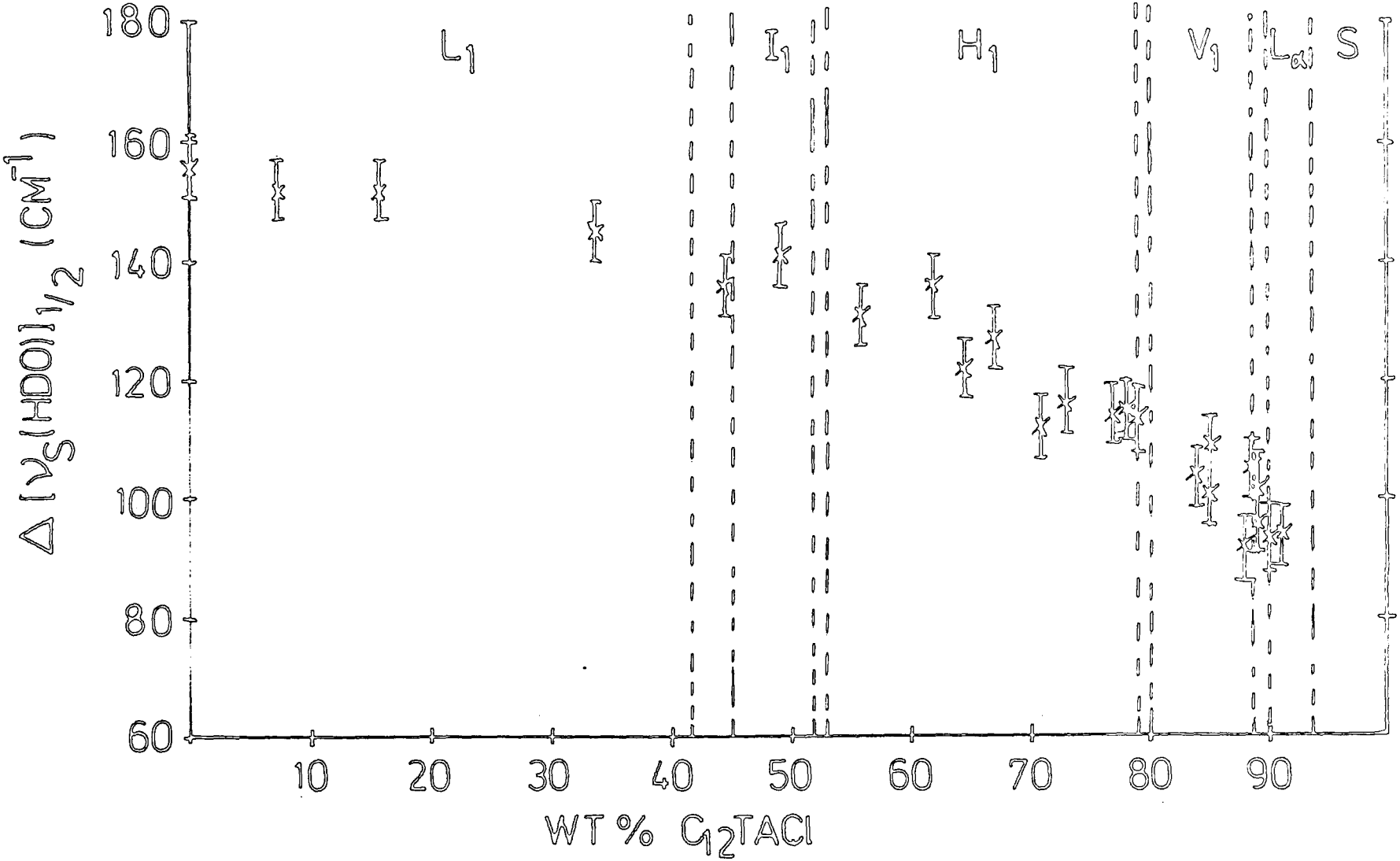

FIGURE 6·15 THE BEHAVIOUR OF $\Delta\nu_{1/2}$(HDO) AS A FUNCTION OF $H_2O/C_{12}TAC$ MOLE RATIO.

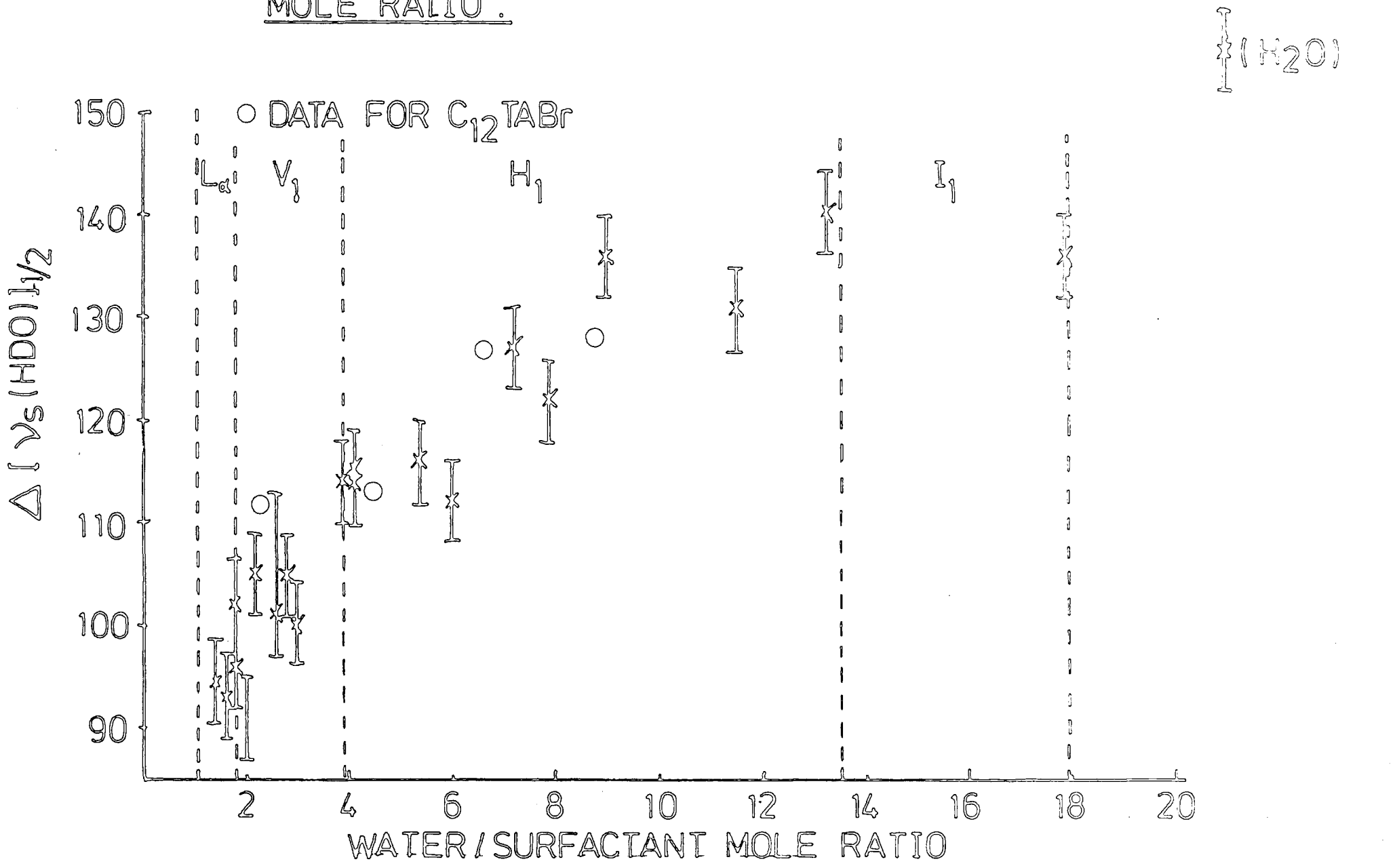

may dramatically increase in slope at this point (see Figures 6.17 and 6.19 of ν_{max} data obtained here). Sunamoto *et al*[113] have attributed their inflection as an increase in water-surfactant interaction.

Some notable publications by Parsegian, Rand and others[42,119-121,130] studying the state of water in phospholipid bilayer systems, have defined a "hydration force".[120] They have developed methods of measuring the amount of work required to remove water from the bilayers. Their results have indicated that bilayers exert strong exponential repulsions with each other and having characteristic decay lengths of approximately 3Å (size of a water molecule).[119] They have discovered that this hydration force is greater than electrostatic repulsions at separations less than 20Å, and decays very rapidly with distance.[119] This behaviour, though not measured in our spectra, is analogous since a decrease in the bilayer separation has the effect of narrowing the ν_s(O-D) band. The narrowing follows the hydration force and may therefore be indirectly related.

The data plotted as a function of mole ratio also allows us to compare the C_{12}TACl and C_{12}TABr systems directly. The filled circles of Figure 6.15 show that as far as the ν_s(O-D) band is concerned, analogous results are observed for C_{12}TABr.

6.3.3 The Behaviour of the $\nu_A(H_2O)$ Combination Mode in C_{12}TACl and C_{12}TABr Mesophase Systems

As mentioned in Chapter Two the band arising at 2106 cm^{-1} in water (50°C) is a combination mode described as

$\nu_A = \nu_2 + \nu_L - \nu_T$ by Williams.[18] As was the case for the stretching mode, this band changes in several ways when mixed with C_{12}TACl. (Examples are shown in Figures 6.4-6.9). The spectra again reveal the presence of one or more shoulders, particularly at high surfactant concentrations, occurring at 2146 cm^{-1} and possibly a component at 2050 cm^{-1}. Unlike the ν_s(O-D) band the $\nu_A(H_2O)$ combination mode exhibits a marked frequency shift as a function of surfactant concentration. This behaviour is shown in Figure 6.16.

At low concentrations the band is similar to that found in bulk water with a maximum at approximately 2100 cm^{-1} and shifting to 2120 cm^{-1} as the concentration is increased (90% w/w C_{12}TACl). This behaviour probably arises from one or both of the intermolecular components which constitute $\nu_A(H_2O)$. In particular ν_T, the translational mode will shift to lower frequencies as the hydrogen bonded interaction is reduced. Overall, this will cause $\nu_A(H_2O)$ to shift to higher frequencies, assuming ν_2 and ν_L remain unaffected.

The shoulder, found at 2146 cm^{-1} in the $\nu_A(H_2O)$ bands of Figures 6.4-6.9, does not shift with increasing surfactant concentration. However, one does observe a gradual increase in its relative intensity until a point is reached (94% w/w C_{12}TACl of Figure 6.9) when this component becomes more intense than its neighbour. This figure, showing two spectra at 20° and 50°C, also suggests that a decrease in the relative intensity of the 2146 cm^{-1} band may be linked with the disappearance of solid. Therefore, it can be deduced that there is some contribution at this frequency from the surfactant, which broadens when the mesophase is formed at 50°C.

It is likely that a second band due to water does exist at this frequency because of its presence at low $C_{12}TACl$ concentrations (*e.g.* see Figure 6.5). It is unlikely that the 2146 cm^{-1} band is due to the outer boundary water layer, which might be initially postulated, when its relative intensity decreases with bilayer thickness. However, this band has a low intensity at high water concentrations. The 2106 to 2120 cm^{-1} frequency shift observed for the low frequency component of $\nu_A(H_2O)$ may be interpreted as an increased perturbation by the counter ions suggesting a possible connection with the outer boundary water layer of Figure 6.11. As well as the two species mentioned above, a number of ν_A spectra (Figures 6.4-6.8) show asymmetry centred at approximately 2050 cm^{-1}. The intensity of this band decreases with concentration and seems to be absent at 94% $C_{12}TACl$ (see Figure 6.9). This band could be due to another water species, *e.g.* "free" water though it would be expected to peak at the value for pure water, *ca.* 2106 cm^{-1}. Though a general increase in frequency maximum (ν_{max}) is observed in Figure 6.16, several points at low concentrations, below the order-disorder transition, show a decrease. It is not clear at this stage why this should be the case, but one explanation could arise from micellar disruption of the hydrogen bonded water network. This is known to occur in electrolyte solutions where modifications of the far i.r. spectra of H_2O have been observed.[69]

The data above has also been plotted as a function of water/surfactant mole ratio and is shown in Figure 6.17. The graph shows the familiar behaviour observed for the width at half maximum intensity ($\Delta\nu_{1/2}$) data of $\nu_s(O\text{-}D)$. Results

FIGURE 6·16 THE BEHAVIOUR OF THE $\nu_A(H_2O)$ FREQUENCY MAXIMUM AS A FUNCTION OF $C_{12}TACl$ CONCENTRATION AT 50°C.

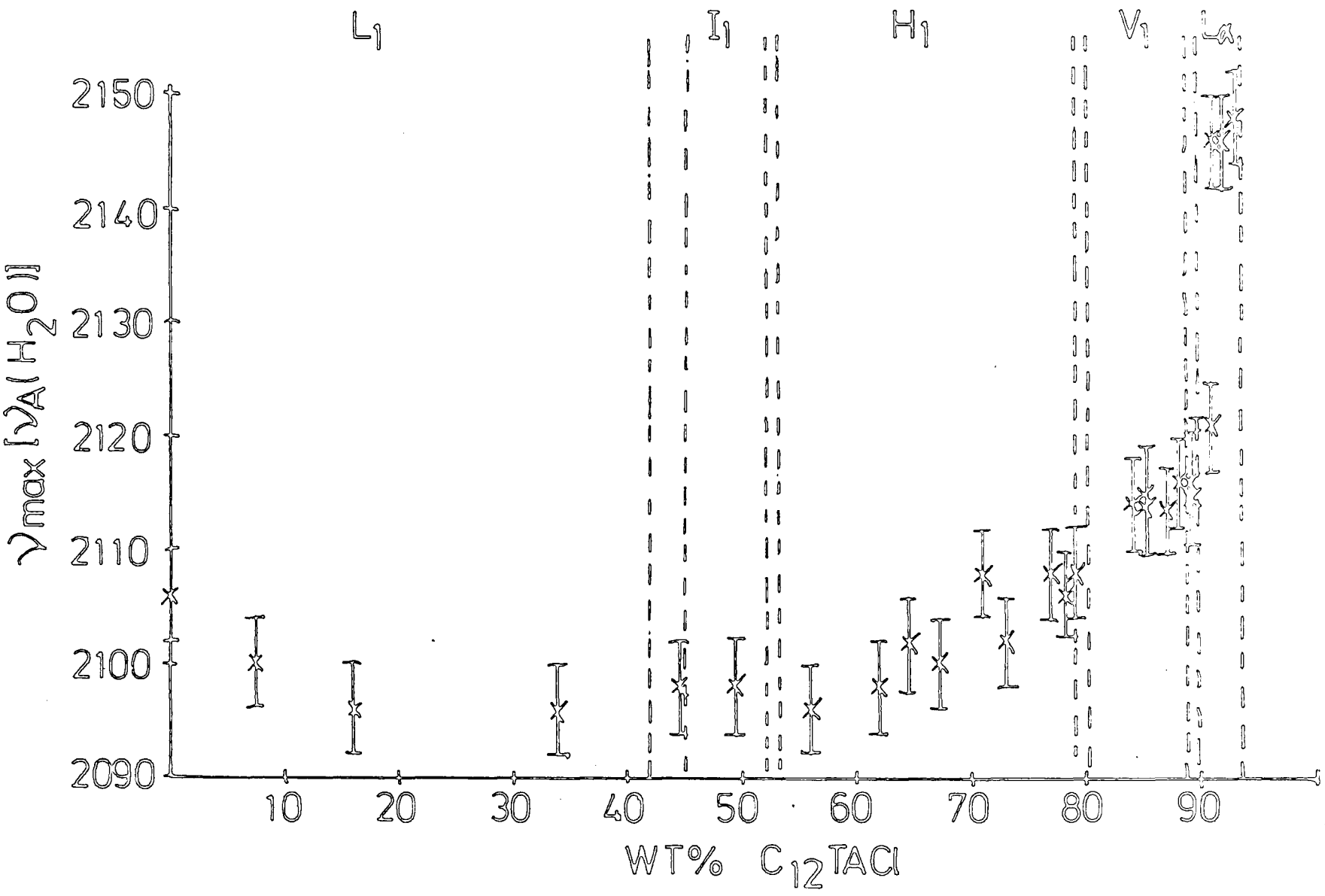

FIGURE 6·17 THE BEHAVIOUR OF THE $\nu_A(H_2O)$ FREQUENCY MAXIMUM AS A FUNCTION OF $H_2O/C_{12}TACl$ MOLE RATIO.

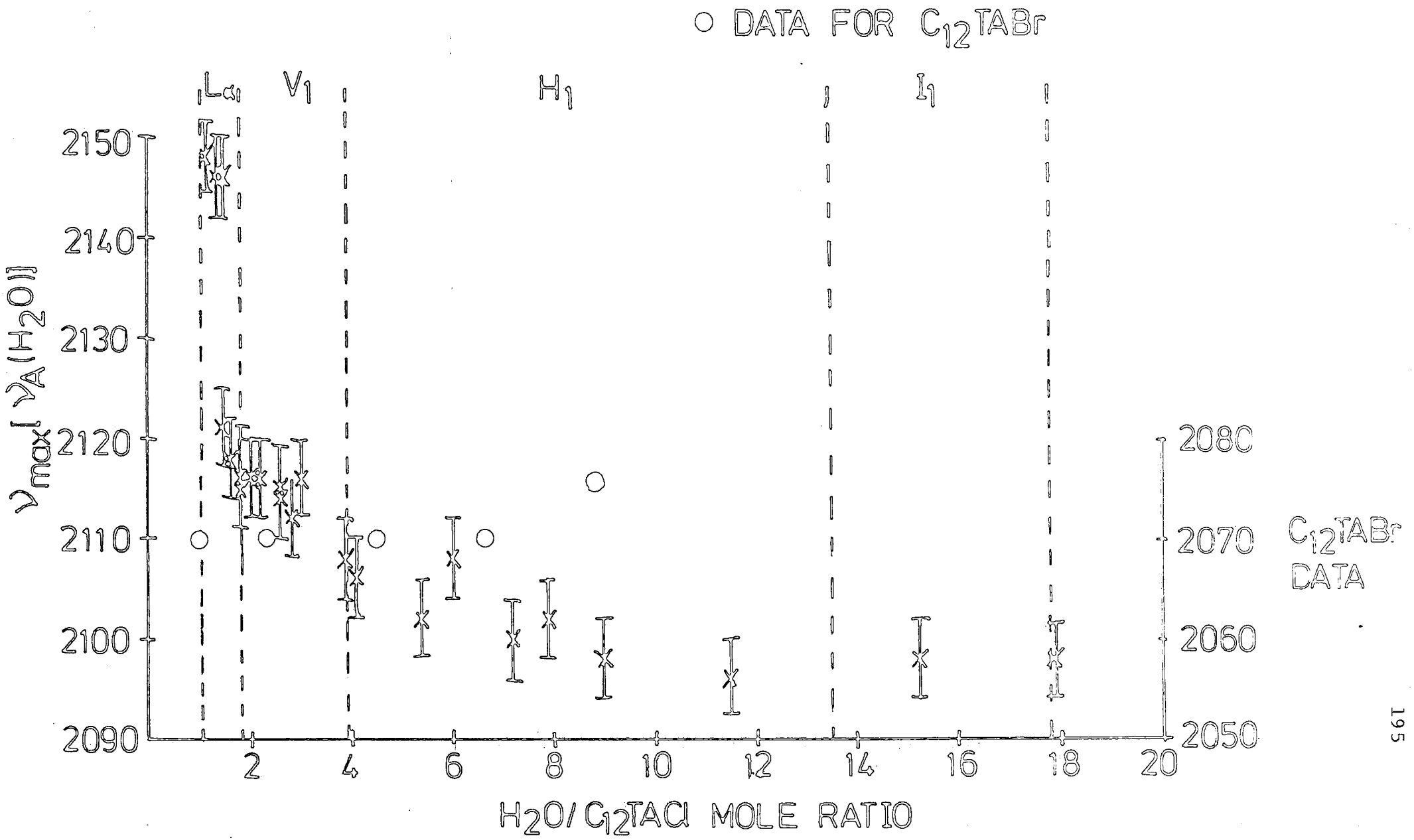

obtained from the C_{12}TABr have also been included which surprisingly show constant behaviour at frequencies 30-40 cm^{-1} lower than that of the chloride. It is thus obvious that the counter ion has a greater influence on this band which does not in this case show a shift with concentration, remaining fixed at 2072 cm^{-1} (see Figure 6.17). Since the origins of this band are fairly complex it is difficult to imagine why the above behaviour is observed. It seems likely that because of its large breadth, the band envelope probably encompasses all water interactions, and generalizations about individual shoulders is not possible. In addition, as mentioned earlier in the chapter the microenvironment of C_{12}TABr mesophase system will be different to that of the chloride. Examination of the C_{12}TABr mesophase spectra of Figures 6.12 and 6.13 shows that these samples, as with C_{12}TACl, also demonstrate the existence of a shoulder. Though this band, absorbing at 2155 cm^{-1}, is known to be a surfactant band, it is difficult as before to tell whether a true second $\nu_A(H_2O)$ water band actually exists.

As with the ν_s(O-D) stretching mode, the band width has been measured for the $\nu_A(H_2O)$ species. The results have been plotted as a function of both surfactant wt.% and mole ratio in Figures 6.18 and 6.19, respectively. The data again show no relationship with phase structure though the narrowing becoming more pronounced at high surfactant concentrations. The values for C_{12}TABr show a smaller but analogous variation as a function of mole ratio, consistent with the idea that perturbations of this band are strongly dependent on the counter ion.

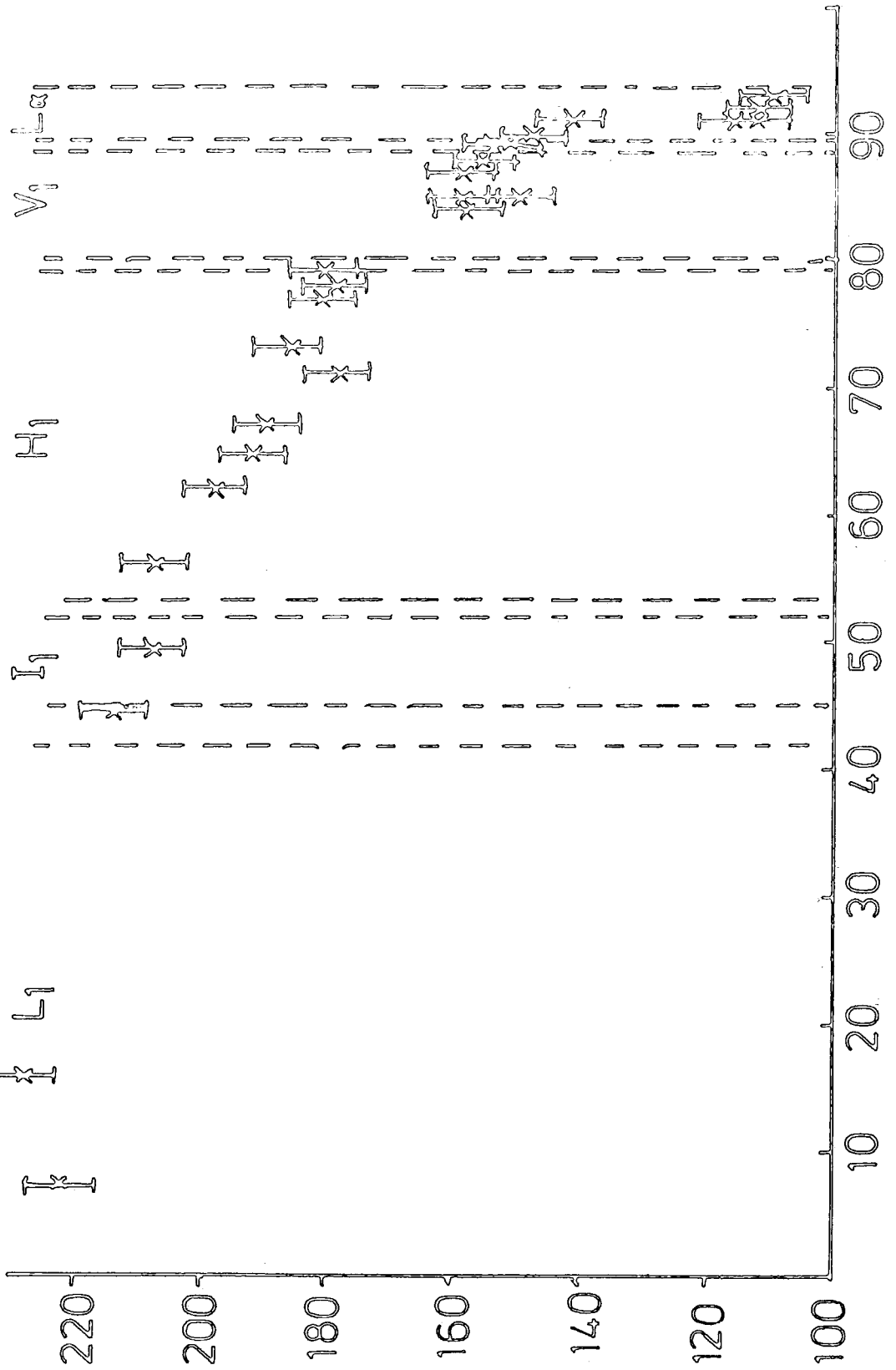

FIGURE 6.18 BEHAVIOUR OF THE $\nu_A H_2O$ BAND WIDTH AS A FUNCTION OF $C_{12}TACl$ CONCENTRATION AT 50°C.

FIGURE 6.19 THE BEHAVIOUR OF THE $\nu_A(H_2O)$ BAND WIDTH AS A FUNCTION OF $H_2O/C_{12}TACl$ MOLE RATIO.

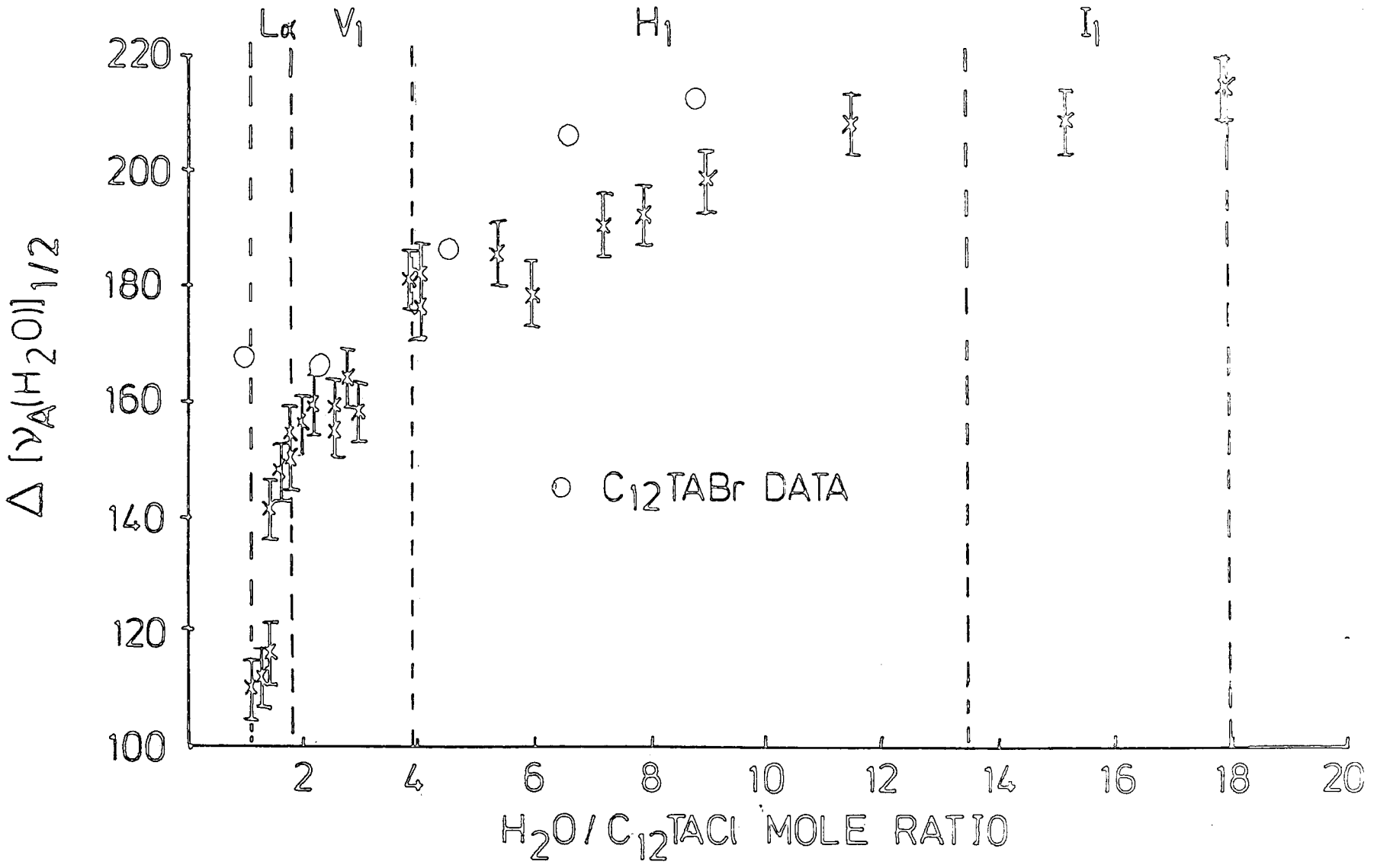

During the course of the experiments it was noticed that the relative intensity of the $\nu_A(H_2O)$ band increased relative to that of the ν_s(O-D) species. Though some moisture from the atmosphere was expected in these samples (see Section 6.2.1), it was thought unlikely to cause any consistent and/or significant effect on the spectra. For the samples studied, we have measured an absorbance ratio of $\nu_A(H_2O)/\nu_s$(O-D) which has been plotted in Figure 6.20 as a function of surfactant concentration. (The absorbances have been determined by triangulation). Again we see the familiar curved behaviour, ending with a disappearance of the ν_s(O-D) band. It seems likely that a decrease in intensity of the ν_s(O-D) band is being seen rather than an increase in the $\nu_A(H_2O)$ intensity. Further inspection of figures 6.4-6.9 and a comparison of relative intensities of the two bands with surfactant bands in their vicinity, reveals that the former conclusion is the most probable. If we make the assumption that $\nu_A(H_2O)$ includes contributions from all water species present at a particular concentration, then the above ratio could be interpreted as further evidence for the disappearance of one possible water species. In a mesophase this water is more than likely to originate from the outer boundary layers of Figure 6.11. Such a result may therefore lead us to believe that the band at 2520 cm^{-1} represents this outer boundary water layer and that a further peak due to initially bound water molecules either disappears as a consequence of the selection rules, or just shifts to other frequencies.

FIGURE 6.20 THE BEHAVIOUR OF THE $\nu_A(H_2O)/\nu_S(HDO)$ ABSORBANCE RATIO AS A FUNCTION OF CONCENTRATION.

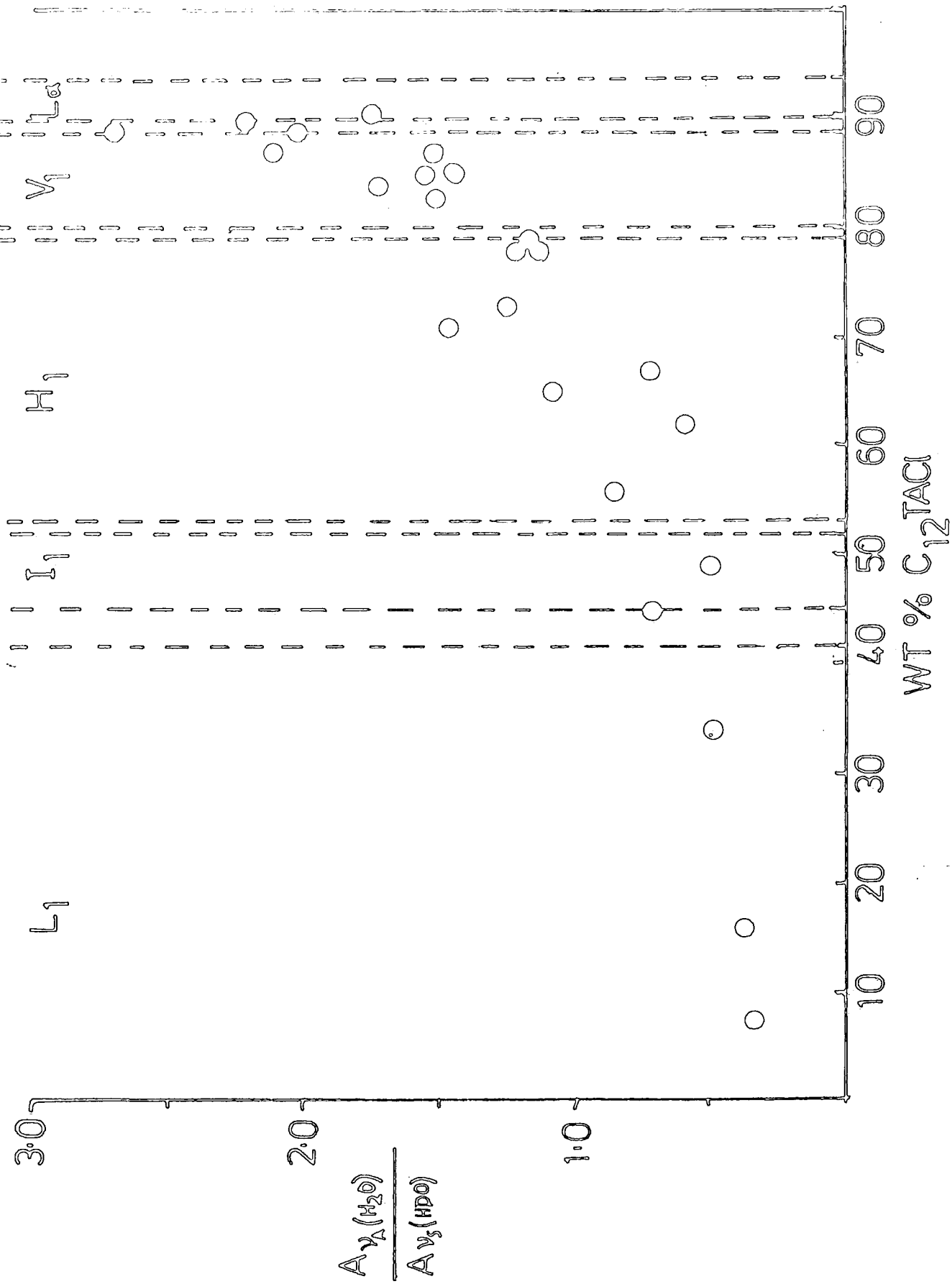

6.4 Far IR Spectroscopic Investigation of the $C_{12}TACl$-Water System

The far infra red spectrum of water has been reported by Birch *et al*[69] and is at least qualitatively comparable to the one recorded here and shown in Figure 6.21. The spectrum shows a pronounced shoulder superimposed on a sloping component which does not peak in our spectral window. The former is ν_T, the translational intermolecular mode of water, while the latter is a portion of ν_L, the librational mode which has a ν_{max} at approximately 600 cm^{-1}.[5] The poor signal to noise ratio at the spectrum shown in Figure 6.21 highlights the problems inherent in this technique, particularly when highly absorbing samples such as water are used. However it is possible to draw a line through the midpoint of the noise to get a clearer picture of the intensity profile. (*N.B.* The absorption coefficient data have been expressed in Neper. cm^{-1} units unless stated otherwise).

The addition of relatively small quantities of $C_{12}TACl$ seems to show little influence on the far i.r. spectrum of water. Figures 6.22 and 6.23 show the spectra of water in the L_1 phase containing 26.3 and 38.0% w/w $C_{12}TACl$. The only apparent change is a shift of the ν_T shoulder to 180 cm^{-1}. At 47.4% $C_{12}TACl$ certain other changes become noticeable. The spectrum of this cubic I_1 sample displayed in Figure 6.24 shows that both ν_T and ν_L are narrowing, with the former showing again a small shift to lower frequencies (now at 173 cm^{-1}). In addition, comparison of this spectrum and those of Figures 6.22 and 6.23 indicate a gradual increase in relative intensity of a second species centred at approximately 110-120 cm^{-1}.

FIGURE 6·21 THE FAR IR SPECTRUM OF H_2O AT 25°C

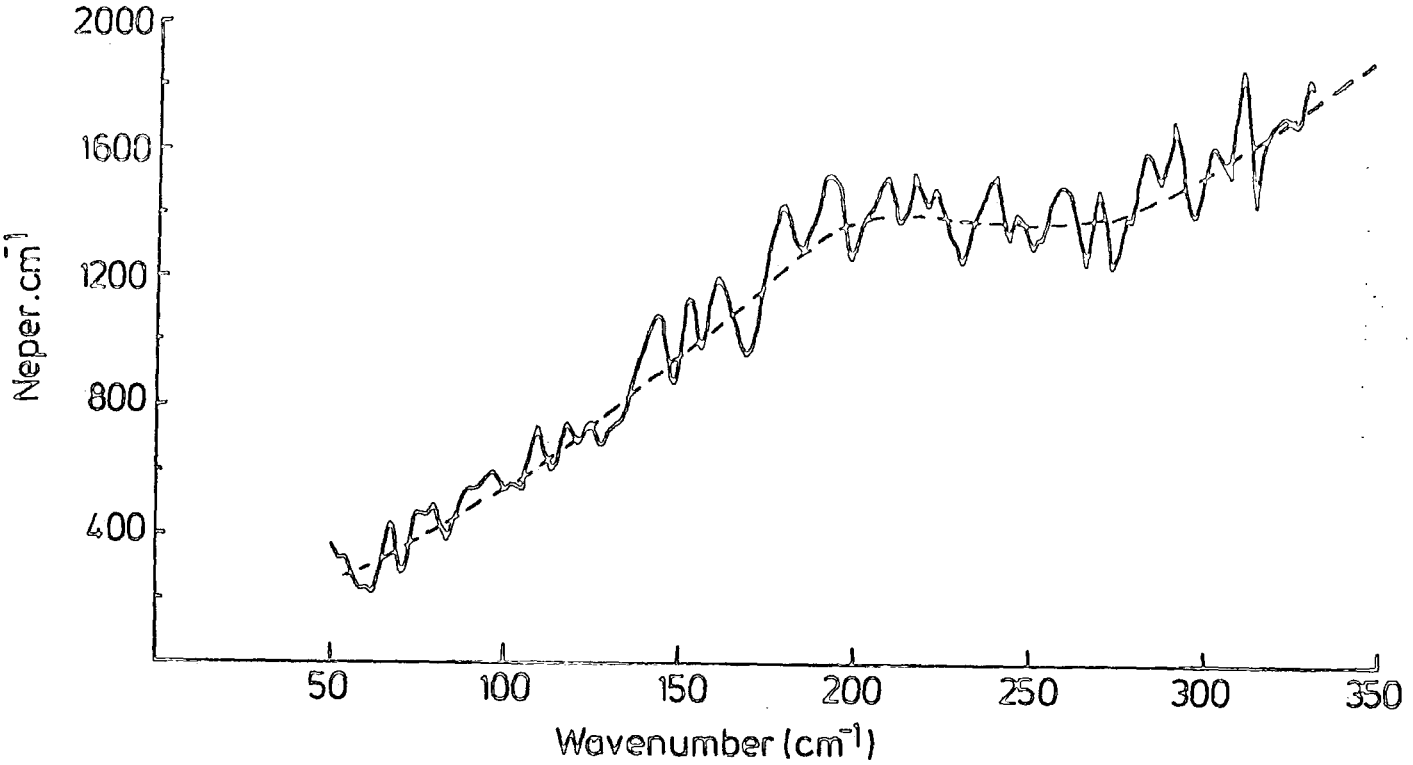

FIGURE 6·22 FAR IR SPECTRUM OF A 26·3% C_{12}TACl SOLUTION.

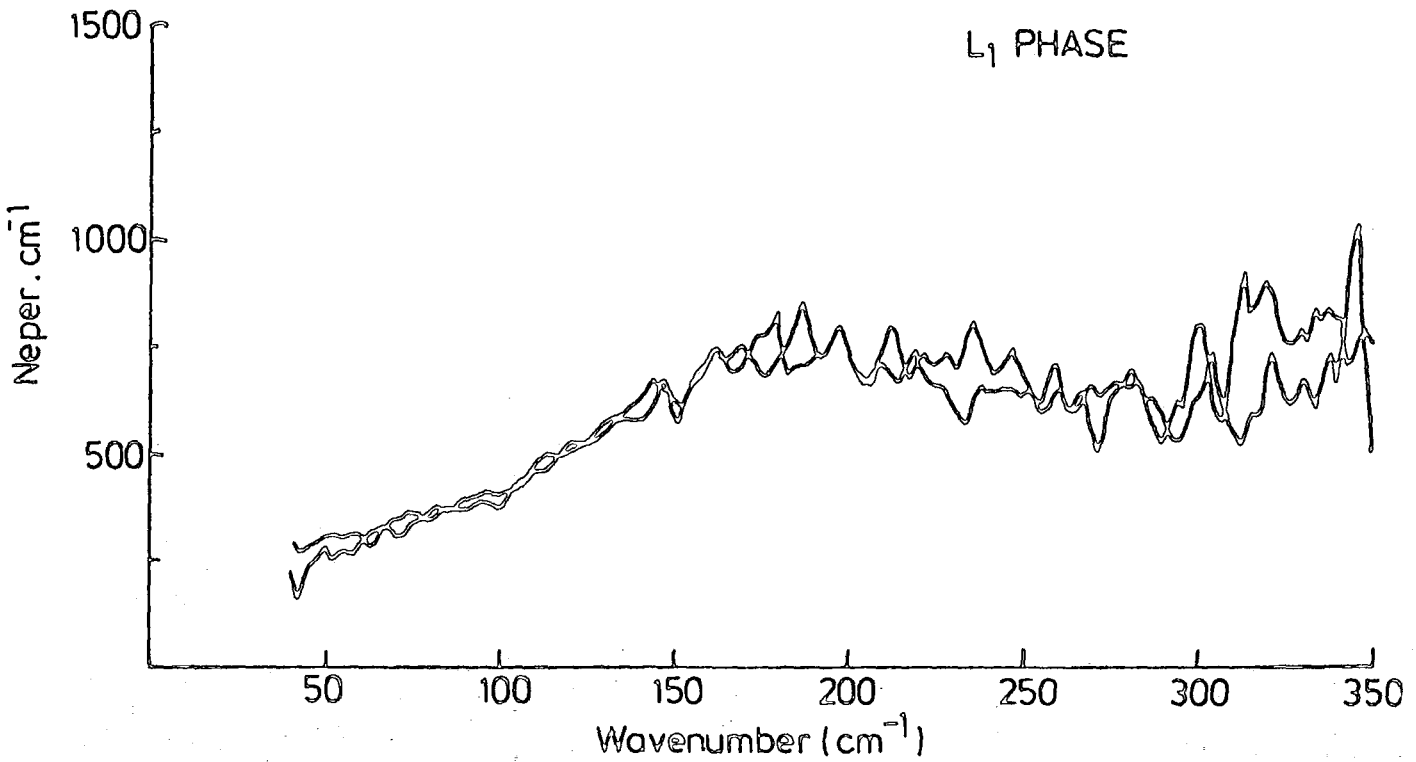

FIGURE 6·23. AVERAGED IR SPECTRUM OF A 38·0 % C_{12}TACl SOLUTION.

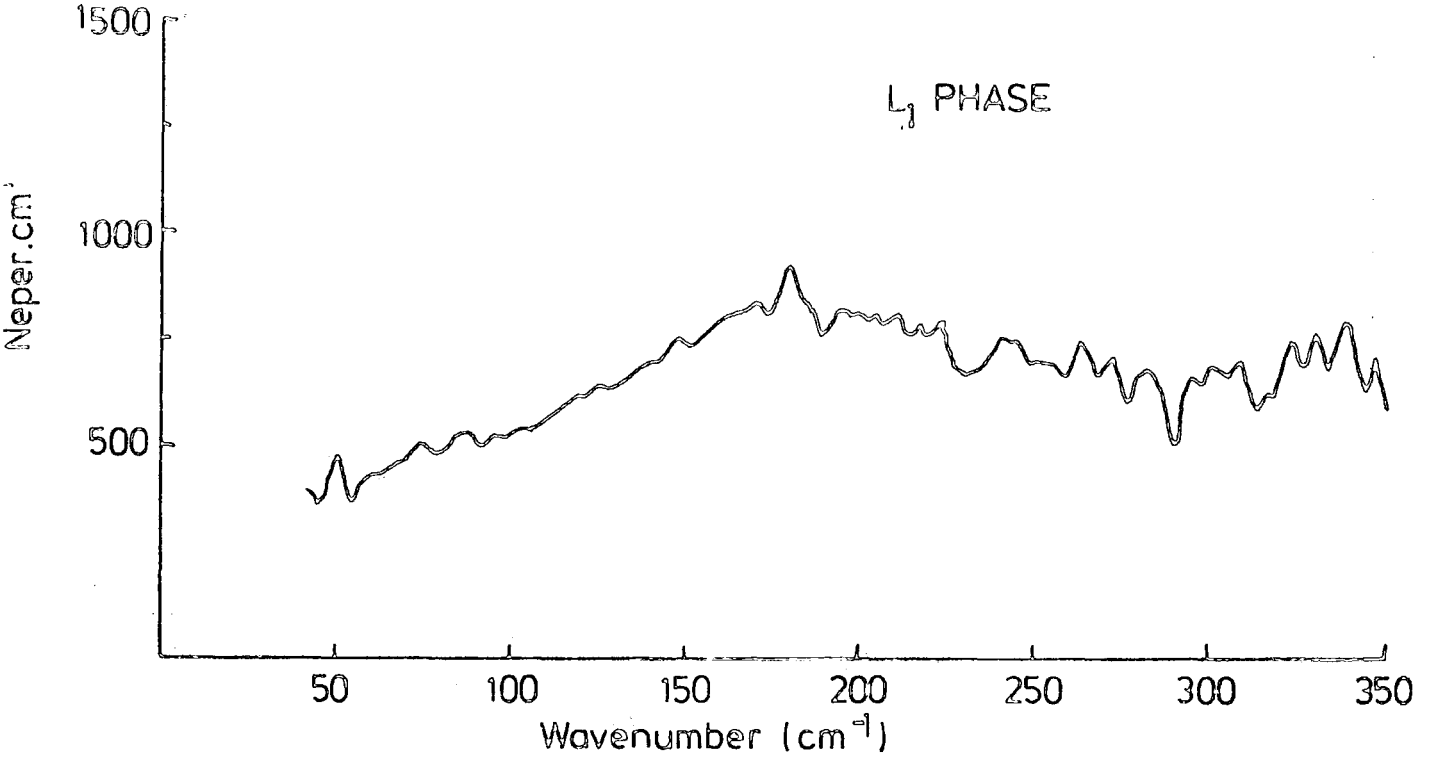

FIGURE 6·24 FAR IR SPECTRUM OF A 47·4 % C_{12}TACl MESOPHASE.

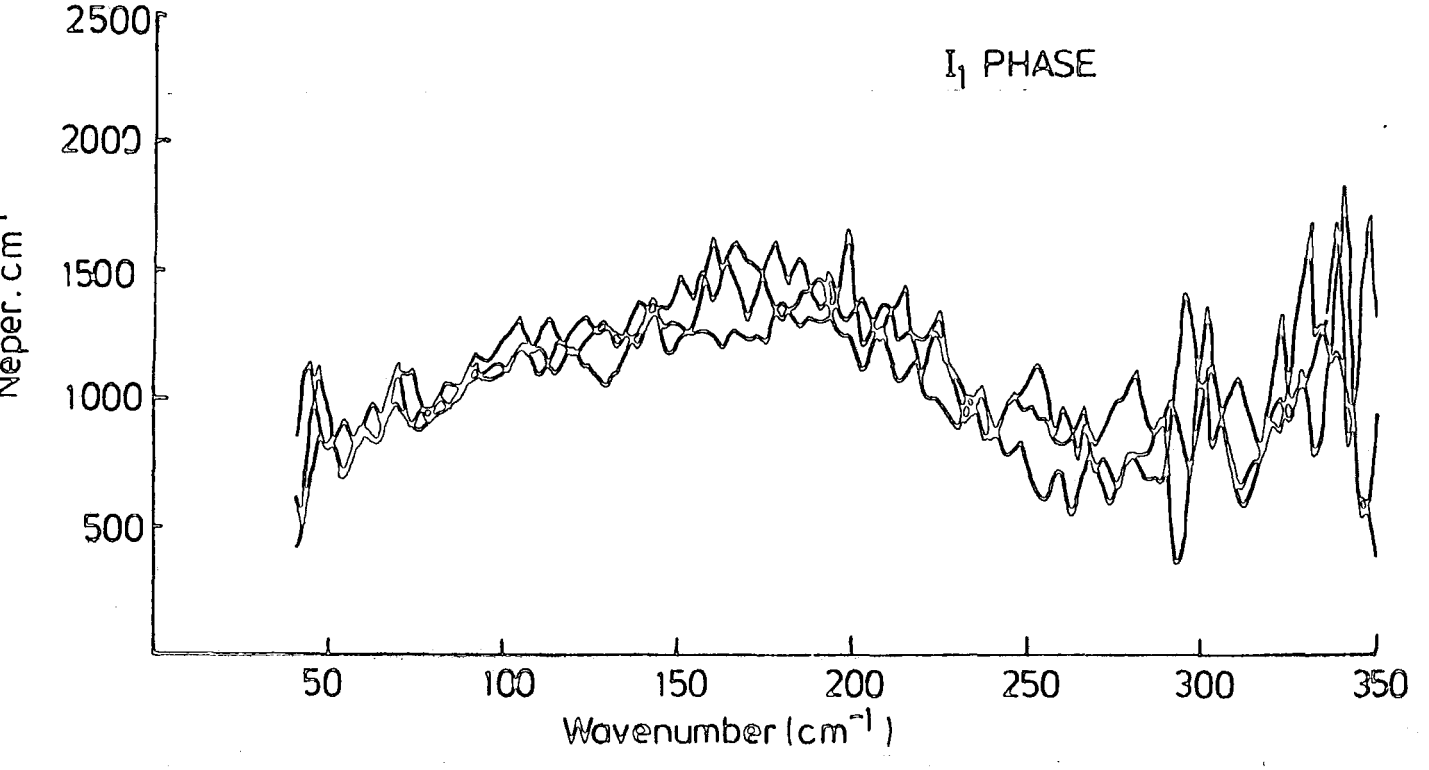

A further increase in C_{12}TACl to 56.1% (Figure 6.25) demonstrates the existence of the two species with the spectrum quite different to that of water, *i.e.* all trace of ν_L, the librational mode has now disappeared from the spectral window. The poor signal to noise of this spectrum is due to the high absorbing characteristics of these materials which are particularly viscous and difficult to mount as thin films. A second spectrum of this sample in a smaller spectral window is shown in Figure 6.26. The spectrum, recorded using a Germanium Helium cooled bolometer (golay cell used previously), clearly demonstrates the superior sensitivity of such detectors over the 2-150 cm^{-1} frequency range. Inspection of the spectrum shows the existence of a third band at approximately 65 cm^{-1} though its intensity is weak and there is some overlap with the higher frequency components. A comparison of the spectra in Figures 6.25 and 6.26 using the Golay cell and Ge bolometer, respectively, show that they are consistent below a maximum of 160 cm^{-1}. Above this frequency the latter becomes non reproducible.

A further increase in C_{12}TACl concentration to 70.7% w/w shows that the 165 cm^{-1} species is now less intense than the 110 cm^{-1} band (see Figure 6.27), with a general decrease in $\Delta\nu_{1/2}$ of the whole band envelope. Though this spectrum is of a sample in the hexagonal phase it is very similar to one in the V_1 cubic phase shown in Figure 6.28. This particular sample containing 83.1% C_{12}TACl exhibits a $V_1 \rightarrow L_\alpha$ phase boundary at 39°C. Though it is not shown here, a spectrum of the same sample at 40°C was recorded and found to be identical. This again suggests that the microstructure of interstitual water seems to be independent of phase. Figure 6.29 shows the same

FIGURE 6·25 FAR IR SPECTRUM OF A 56·1% C_{12}TACl MESOPHASE.

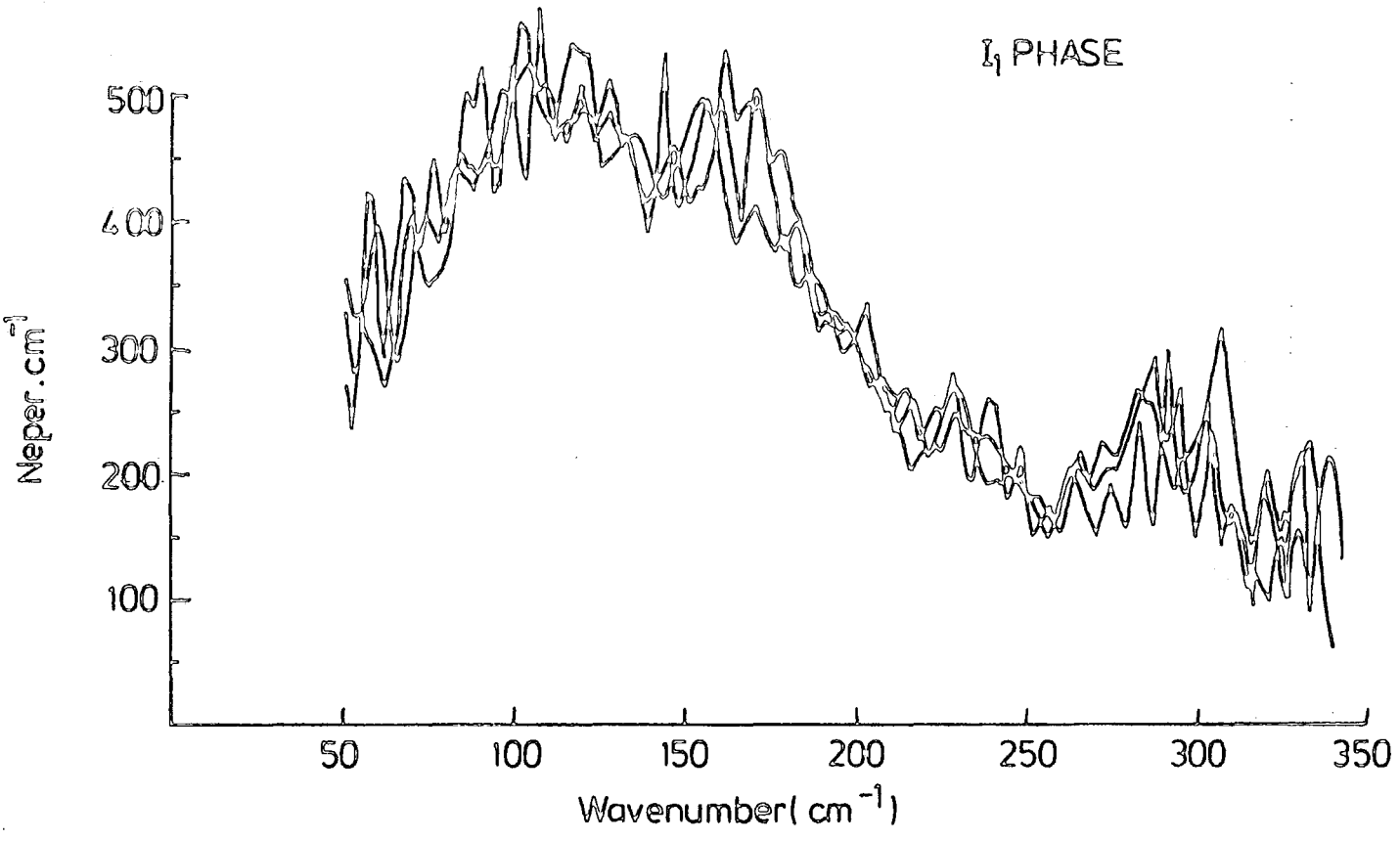

FIGURE 6·26 FAR IR SPECTRUM OF A 56·1 % C_{12}TACl MESOPHASE.

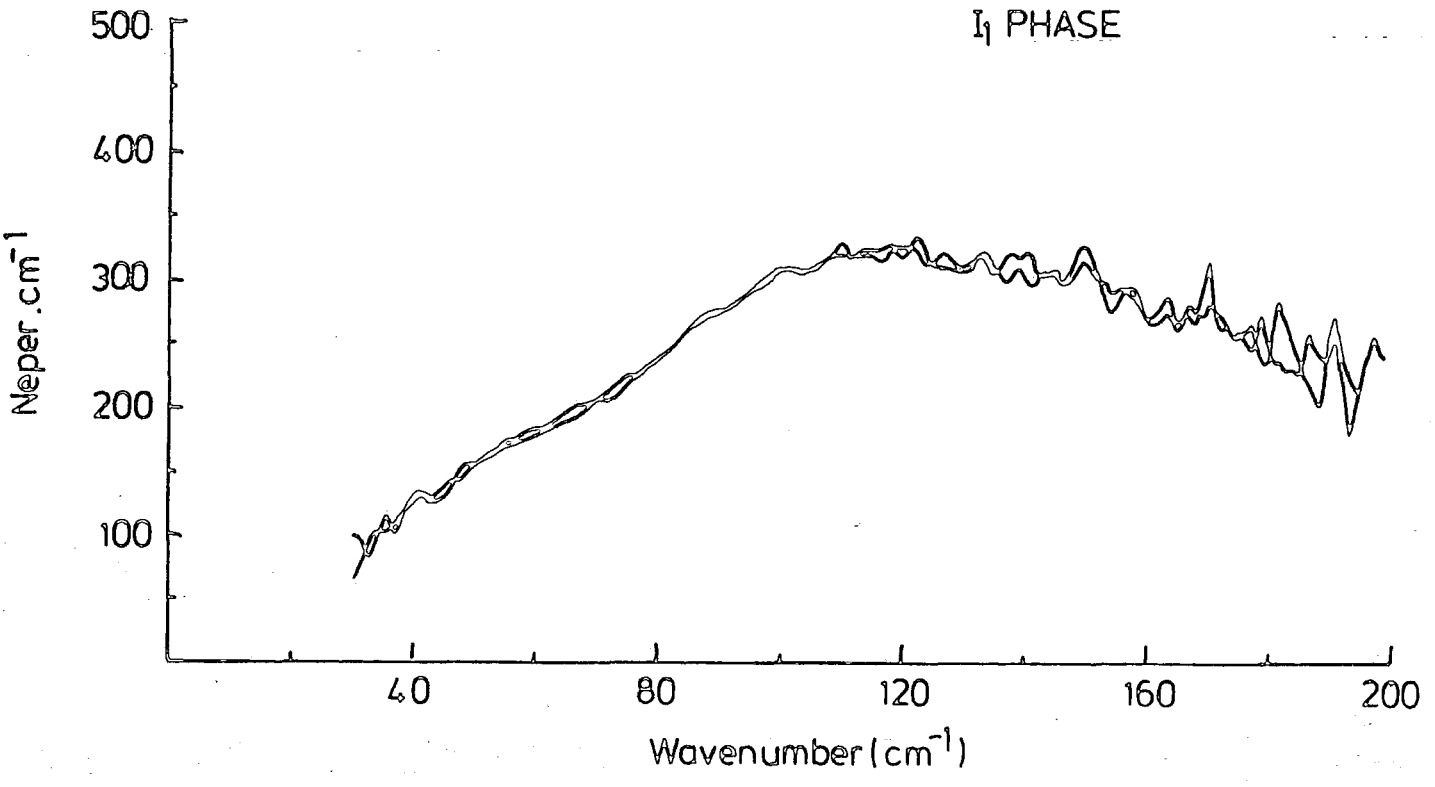

FIGURE 6·27 FAR IR SPECTRUM OF A 70·7 % C_{12}TACl MESOPHASE.

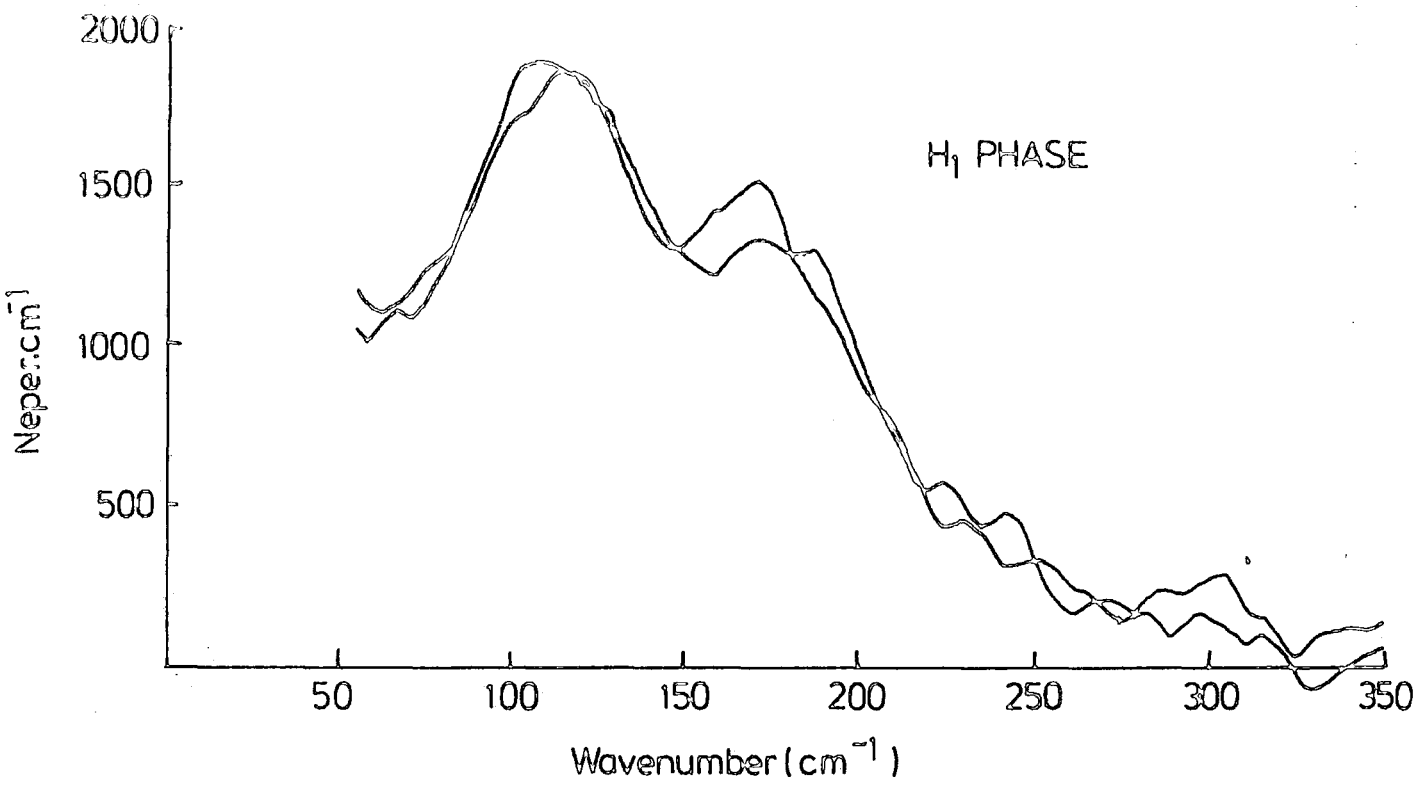

FIGURE 6·28 FAR IR SPECTRUM OF A 83·1 % C_{12}TACl MESOPHASE.

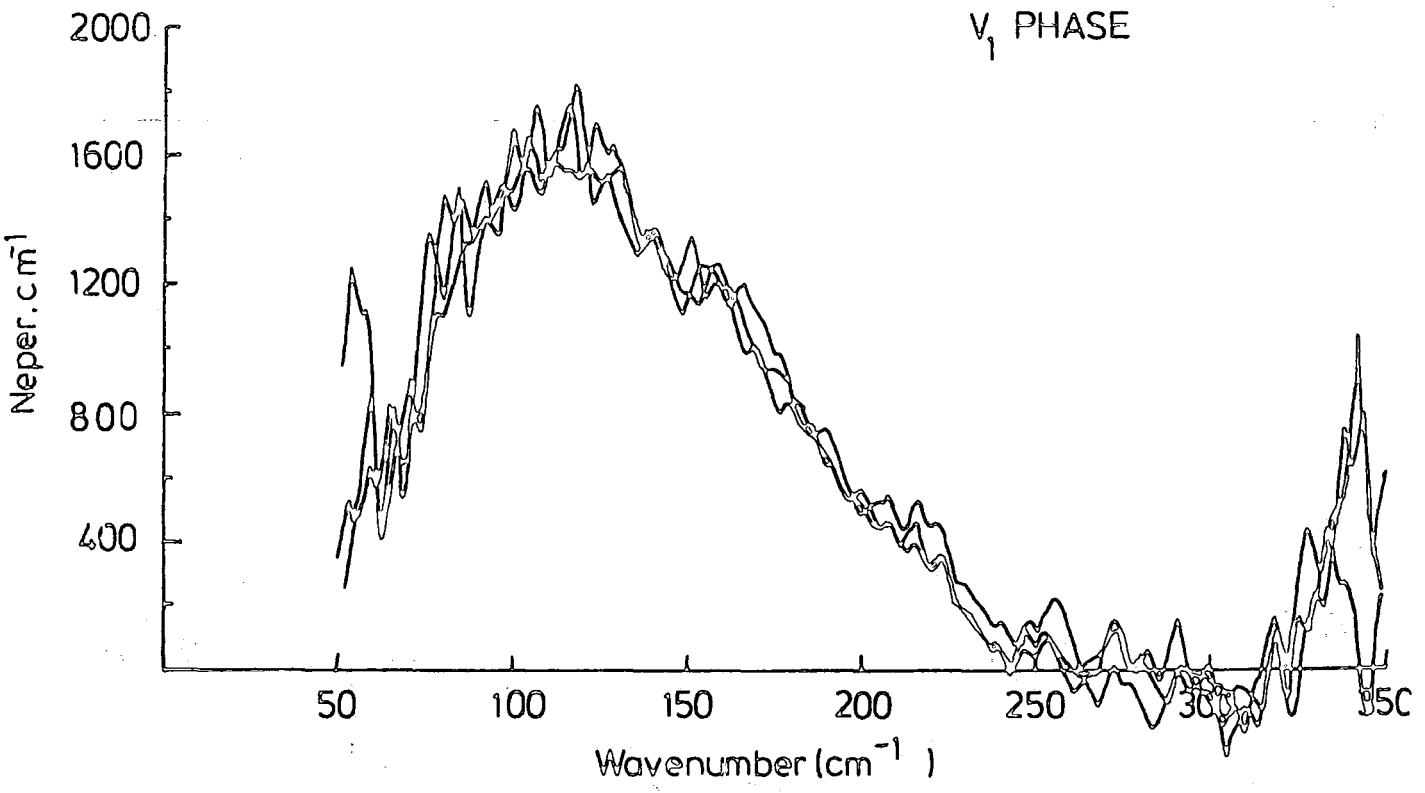

FIGURE 6·29 FAR IR SPECTRUM OF AN 83·1% C_{12}TACl MESOPHASE

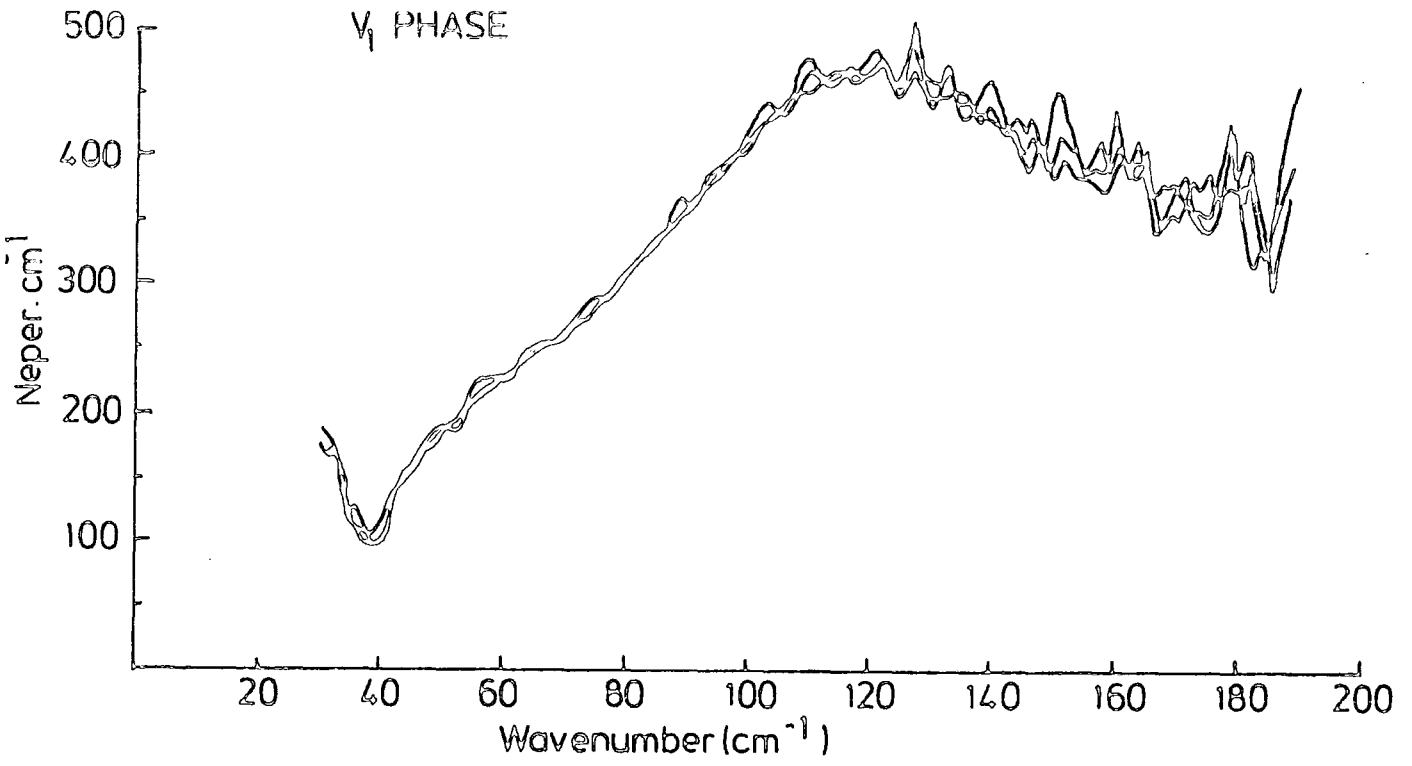

FIGURE 6·30 FAR IR SPECTRUM OF AN 88·2% C_{12}TACl MESOPHASE.

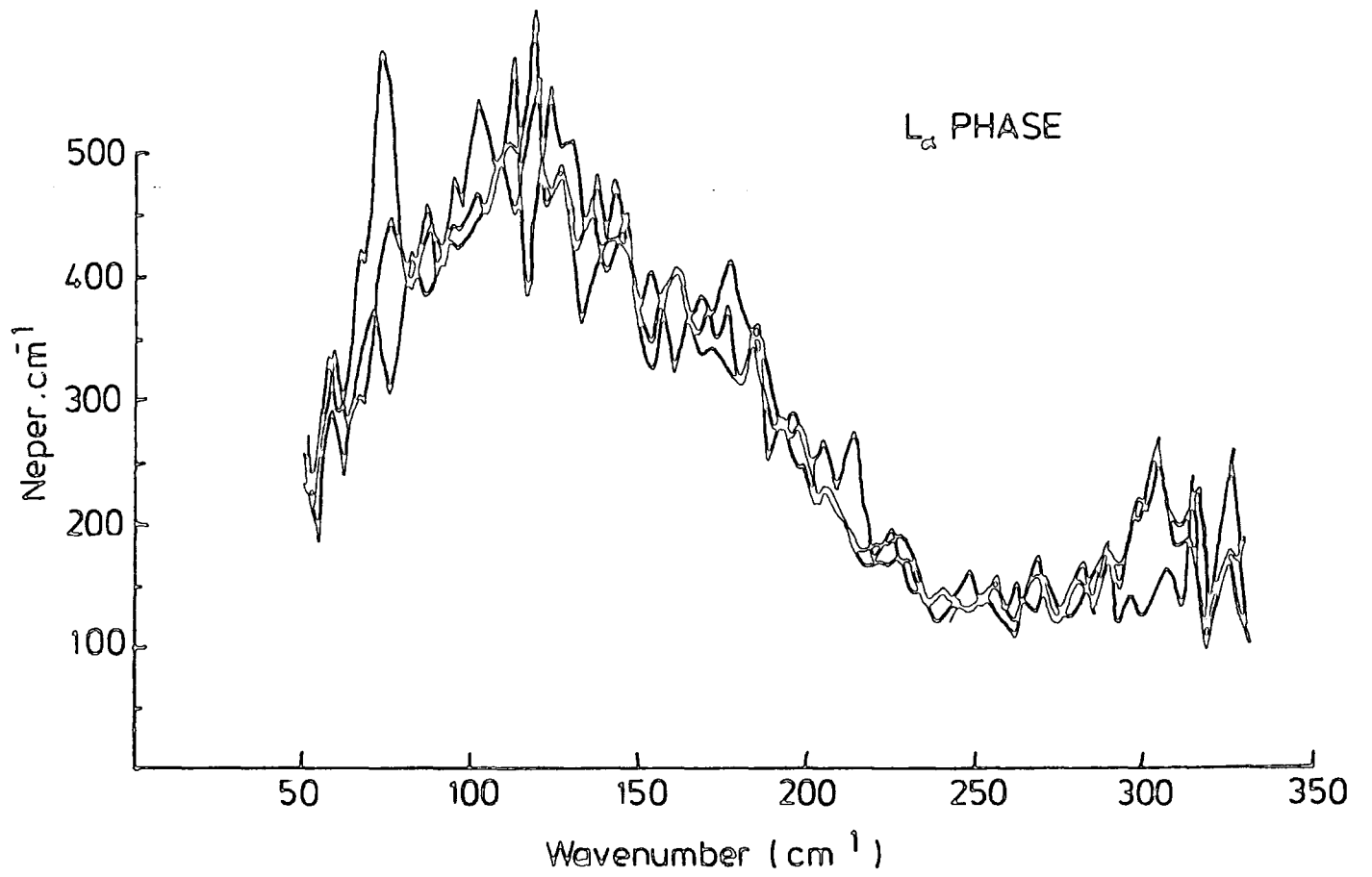

sample recorded between 20 and 200 cm^{-1} using the Ge bolometer. It again demonstrates the existence of a low frequency shoulder at around 65 cm^{-1}. Two spectra of an 88.2% w/w $C_{12}TACl$ lamellar phase sample are shown in Figures 6.30 and 6.31. They are very similar to the previous V_1 spectra. Finally, Figures 6.32 and 6.33 show far i.r. spectra of a 93.8% w/w $C_{12}TACl$ sample at room temperature and 46°C, respectively. The spectra exhibit the presence of a band at 85 cm^{-1} which decreases in intensity at the higher temperature. Investigation of this sample under a polarizing microscope has shown that at room temperature it is composed of an equilibrium mixture of solid and L_α phase which melts to the Lamellar phase at 45°C. The band seems fairly sharp and could be assigned to an $R\text{-}N(CH_3)_3^+ \cdots Cl^-$ interionic mode of the crystalline surfactant. It is not possible to say whether a species, previously observed at 65 cm^{-1} is present, though it may be hidden within the band envelope. The observations described above have been tabulated along with possible assignments in Table 6.4. The results for $C_{12}TABr$ are also given and these will be discussed later in the section.

The interpretation of the above observations seem fairly straightforward in view of the mid i.r. data discussed in the previous section. The two species observed at 110 cm^{-1} and 160 cm^{-1} (at low water concentrations) probably both originate from ν_T the translational mode. Though it is surprising that <u>both</u> these bands do not shift in frequency, it is difficult to say whether this is true for the 110 cm^{-1} species where one might expect only a small shift.

FIGURE 6·31 FAR IR SPECTRUM OF AN 88·2 % C_{12}TACl MESOPHASE.

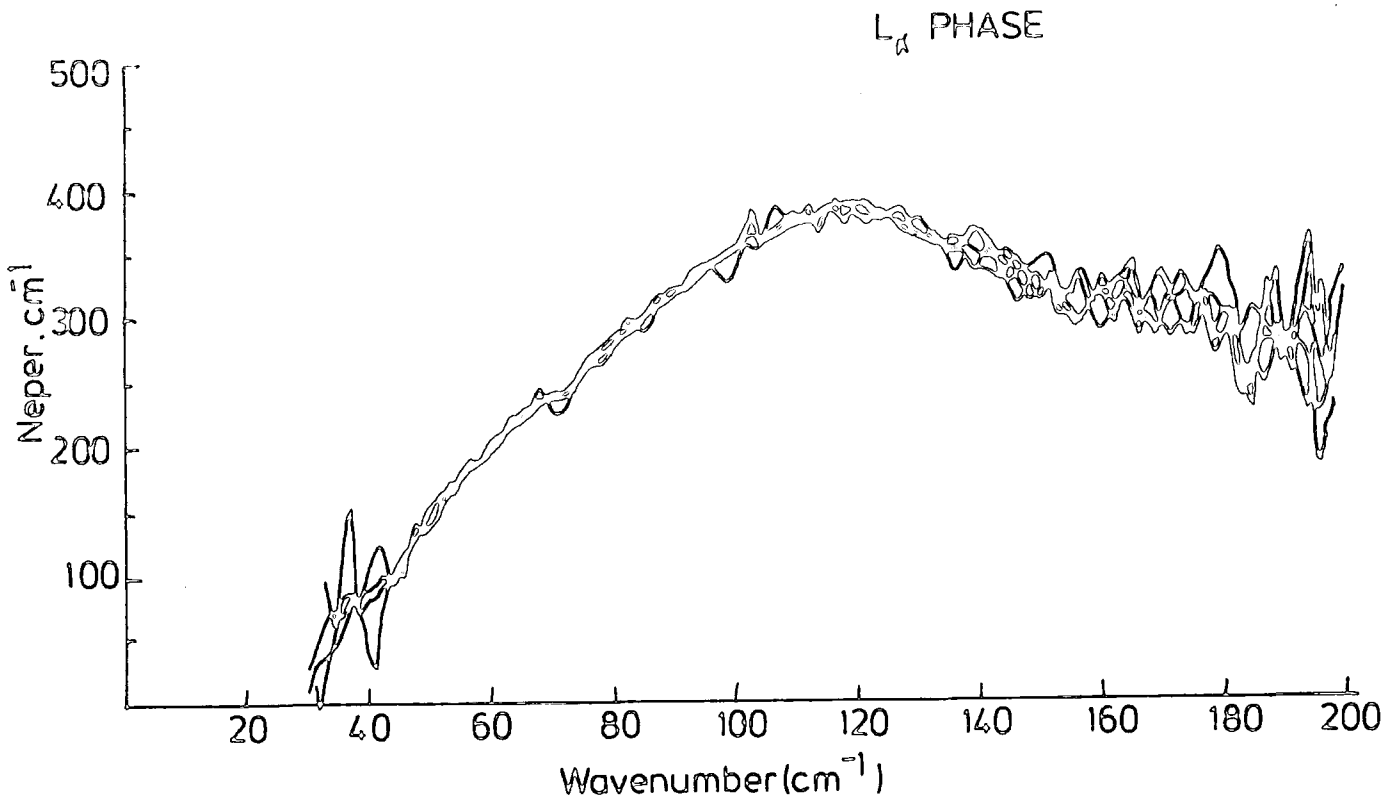

FIGURE 6·32 FAR IR SPECTRUM OF A 93·7 % C_{12}TACl MESOPHASE

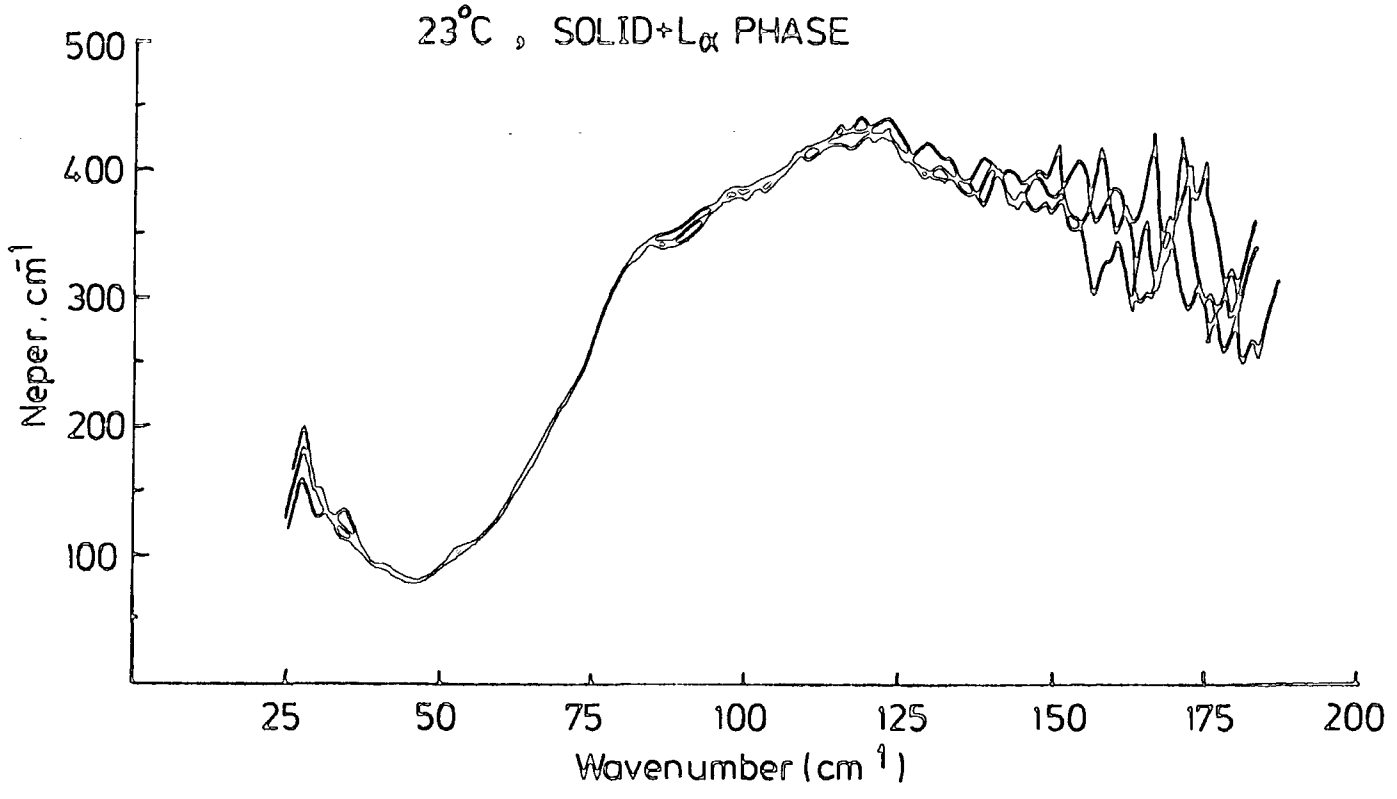

FIGURE 6·33 FAR IR SPECTRUM OF A 93·7% C_{12}TACl MESOPHASE.

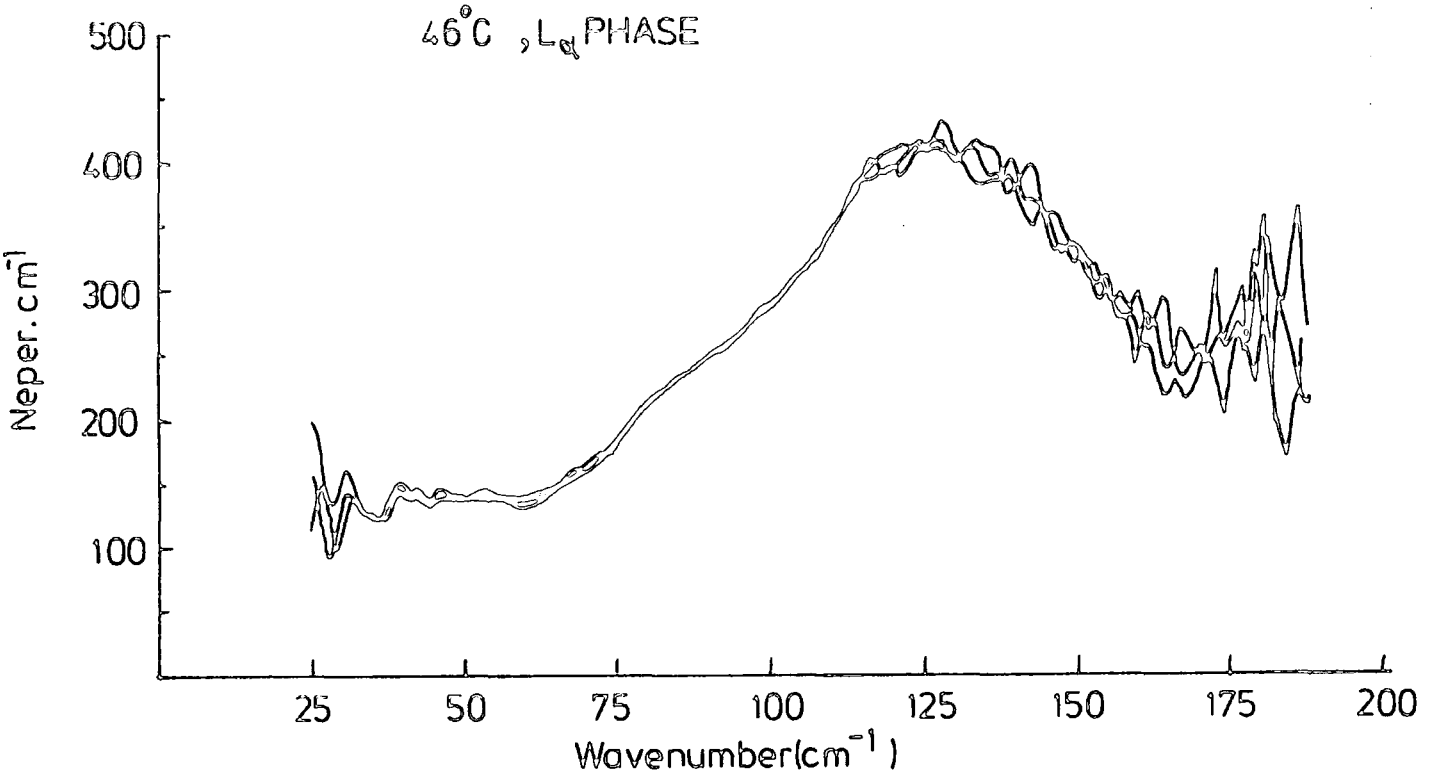

FIGURE 6·34 FAR IR SPECTRUM OF A 65·1% C_{12}TABr MESOPHASE.

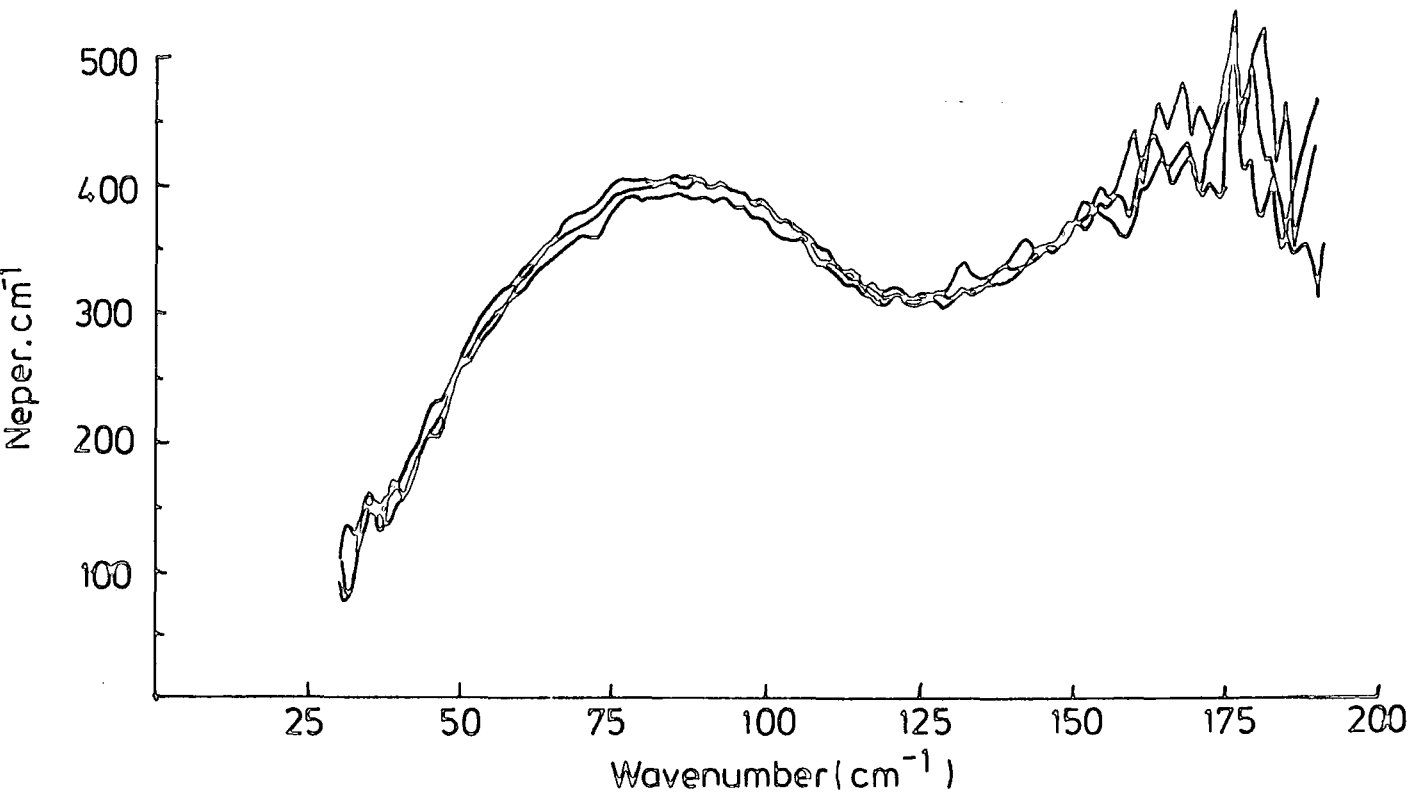

TABLE 6.4 Results obtained in the Far I.R. of some $C_{12}TACl$ and $C_{12}TABr$ Mesophases

Assignment*	$C_{12}TACl$	$C_{12}TABr$
"Free" water	200 ± 10 cm^{-1}	200 ± 10 cm^{-1}
Outer boundary water	200-160±10 cm^{-1}	200-135±10 cm^{-1}
Initial boundary water	115 ± 10 cm^{-1}	90 ± 10 cm^{-1}
Interionic mode $[R\text{-}N(CH_3)^{\oplus}\cdots X^{\ominus}]$	85 ± 5 cm^{-1}	95 ± 5 cm^{-1}
Intermolecular bending	65 ± 5 cm^{-1}	67 ± 5 cm^{-1}

* See text for discussion.

The data supports one conclusion these two bands are due to two different water species. The possibility of the 110 cm^{-1} band being a surfactant band is also not difficult to imagine since its intensity increases with $C_{12}TACl$ concentration. Though at high concentrations some direct interaction between head group and counter ion will exist, the presence of large amounts of water in, *e.g.* H_1 samples will cause hydration in preference to a direct $R\text{-}N(CH_3)_3^{+}\cdots Cl^{-}$ contact. In addition, the spectra of figures 6.32 and 6.33 (94% $C_{12}TACl$ at 23 and 46°C) show the interionic mode to occur at approximately 85 cm^{-1}. The high probability of the two above species being assigned to water species reinforces the hypothesis, made in the previous section, that two water bands must exist in the mid i.r. Also, the shift of the higher frequency band from 200 to ≈160 cm^{-1} is consistent with the shift observed for $\nu_A(H_2O)$ in the mid i.r. As far as intermolecular

modes are concerned, a decrease in frequency is evidence for a reduced hydrogen bonded interaction which will occur as the concentration of counter ions increases.

In summary therefore, the data presented suggests the presence of at least three water types. The first identified as "free" water is identical to that found in bulk water. The concentration of this species decreases as does the broad and intense bands constituting the unperturbed ν_T and ν_L vibrations. At the disorder-order transition the far i.r. spectra show that nearly all the bulk water has now disappeared, and the spectra bear no resemblamce to previous features observed in the L_1 phase. Instead, a band that shifts to lower frequencies is visible which may be due to the outer boundary water of Figure 6.11. This species though having some interaction with the head groups, is probably strongly associated with the counter ions, *i.e.*

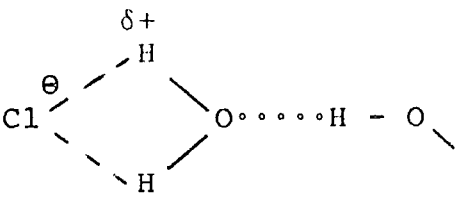

As the concentration is increased this band shifts to lower frequencies and the intermolecular mode becomes weaker as expected. In addition the presence of further species at 110-115 cm^{-1} becomes evident. Further increases in the amphiphile fraction causes an increase in this latter absorption relative to the previous band which has again shifted slightly. The obvious interpretation is that this peak may belong to a water layer at the surfactant head group. Though one might expect there to be only a small electron redistribution in an

intermolecular mode of the type

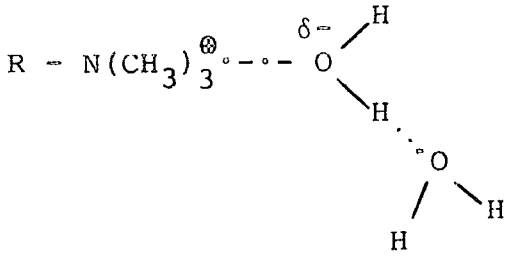

one must remember that there will also be counter ions at this boundary and so perturbations will be greater than for simple cation hydration. The frequency of this initial boundary water species (see Figure 6.11) seems not to change, though one might expect at least some shift. As well as the interionic mode occurring at 85 cm^{-1} some of the spectra exhibit a low frequency shoulder at ≈65 cm^{-1}. This energy of vibration is very small and is unlikely to originate from a stretching mode of any description. A possible assignment could be to some intermolecular rotation of water molecules.

In addition to the C_{12}TACl samples some bromide samples were also studied in this region. The first of the spectra from these mesophases are shown in Figure 6.34. Obtained with the bolometer, it shows the presence of a species at 90 cm^{-1} and possibly one at 180 cm^{-1} which seems to be slightly more intense. Increasing the concentration from 65% w/w to 71.6% w/w C_{12}TABr broadens and shifts the band slightly to higher frequencies (see Figure 6.35). This behaviour is puzzling but may be understood if the 180 cm^{-1} band shifted to lower frequencies forming what appeared to be a single broader contour. A spectrum recorded with a Golay cell of a sample containing 79% w/w C_{12}TABr is shown in Figure 6.36. It shows a relatively sharp absorption at just below 100 cm^{-1} with some residue of a band at about 180 cm^{-1} (though its intensity is very small).

FIGURE 6·35 FAR IR SPECTRUM OF A 71·6% C_{12}TABr MESOPHASE.

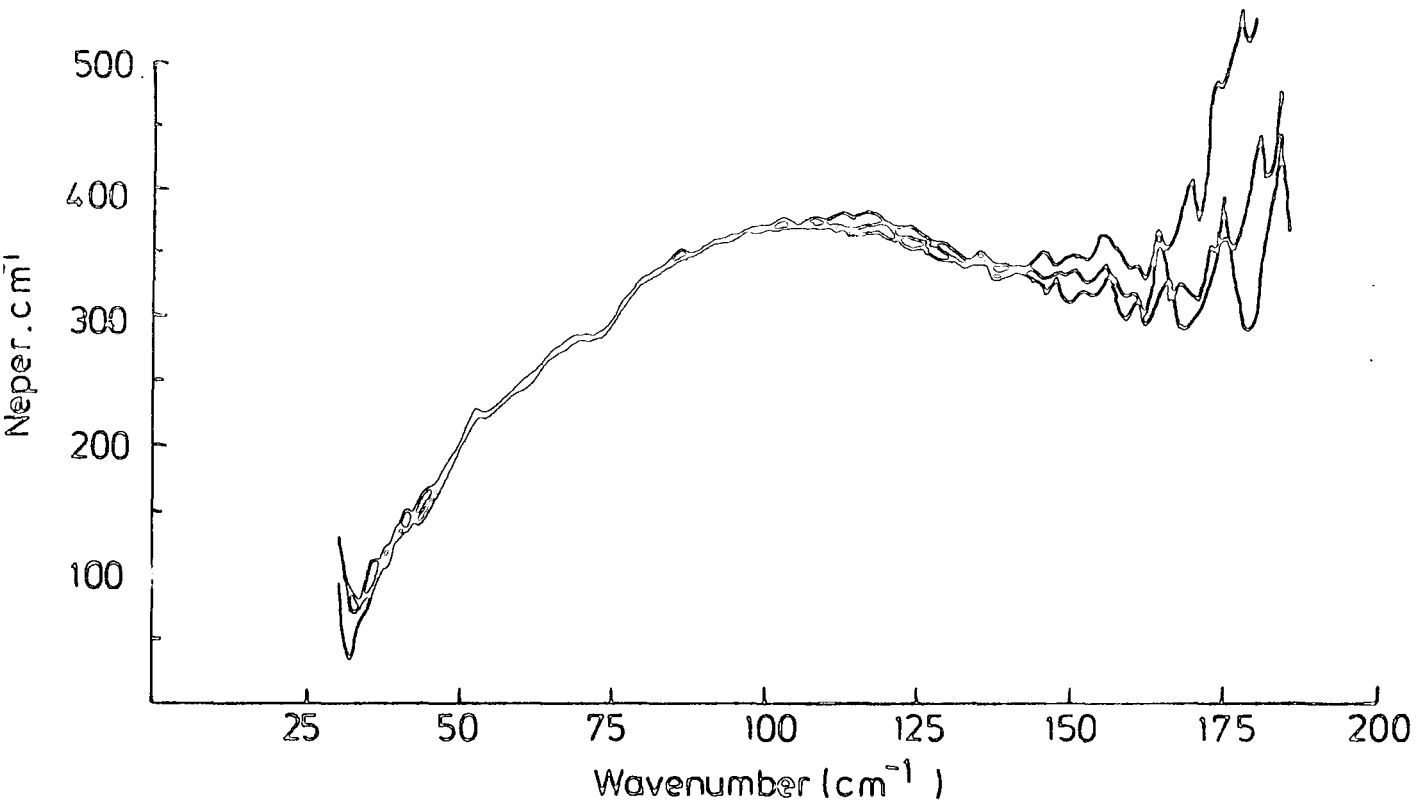

FIGURE 6·36 FAR IR SPECTRUM OF A 79·3 % C_{12}TABr MESOPHASE.

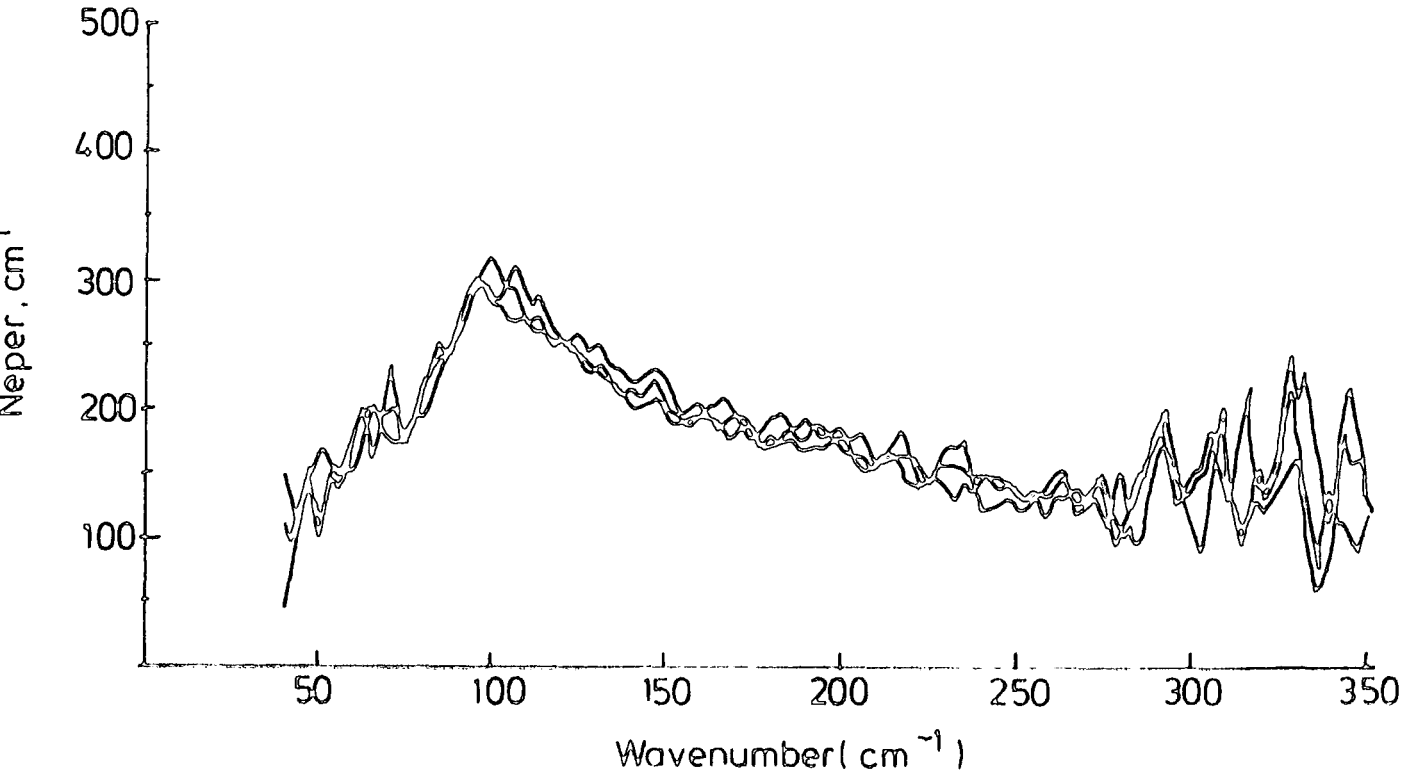

A more detailed picture of the 30-160 cm^{-1} region of this sample is shown in Figure 6.37. The sharp peak is centred at 94 cm^{-1} with an additional band at 67 cm^{-1}. This latter absorption almost certainly belongs to the same species as that found in the chloride. Its vibrational energy is such that any change in counter ion will not be easily detected. Since this sample contains some solid surfactant it is possible that the 94 cm^{-1} band is attributed toan interionic mode. An alternative interpretation is that it belongs to the initial boundary water species discussed earlier. Figures 6.38 and 6.39 show two room temperature spectra of an 88% C_{12}TABr sample. Again a sharp peak is observed at about 94 cm^{-1}, a shoulder at 67 cm^{-1} and possibly something at about 150 cm^{-1}. Microscopic examination of this sample indicates that it was a biphasic mixture of solid and lamellar phase which melted to a homogeneous liquid crystal phase at 55°C. A spectrum of the same sample was thus recorded at 60°C and is shown in Figure 6.40. The peak at 98 cm^{-1} has disappeared leaving a band at 94 cm^{-1} and a shoulder at ≈135 cm^{-1}. (It is difficult to tell whether or not a band exists at 67 cm^{-1} for this spectrum).

The above spectra suggest that the surfactant $RN(CH_3)_3^{\oplus}\cdots Br^{\ominus}$ mode occurs at about 95 cm^{-1}. There are two reasons for this, firstly that the absorption is narrow and secondly that it disappears when the solid melts. However, this generates an inconsistency since the corresponding mode in C_{12}TACl occurs at 85 cm^{-1}. From a simple consideration of Hooke's law (see Chapter Two) we would expect both the increased mass and a smaller force constant (the $R\text{-}N(CH_3)_3^{\oplus}\cdots Cl^{\ominus}$ bond will be stronger because of its charge/size ratio) to decrease the

FIGURE 6·37 FAR IR SPECTRUM OF A 79·3 % C_{12}TABr MESOPHASE.

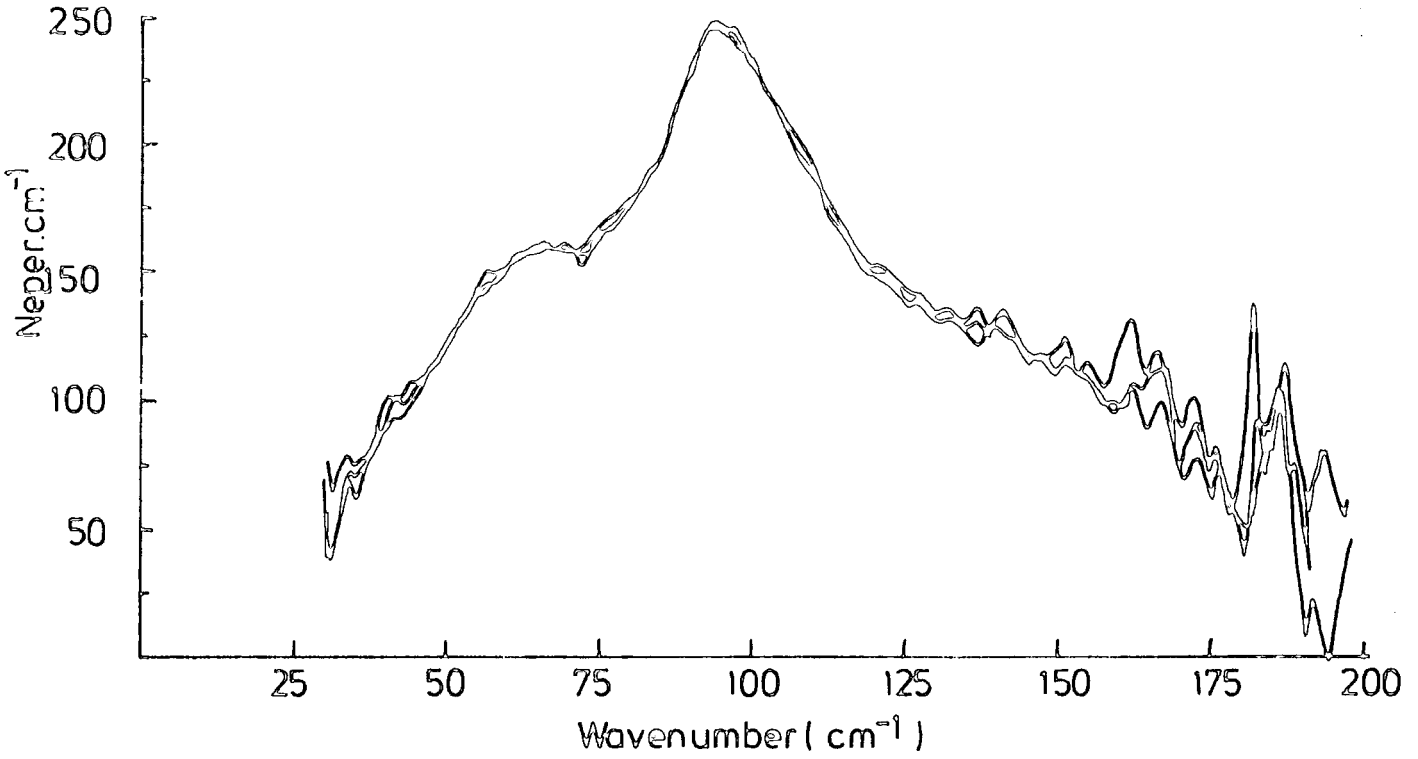

FIGURE 6·38 FAR IR SPECTRUM OF AN 88·1 % C_{12}TABr MESOPHASE.

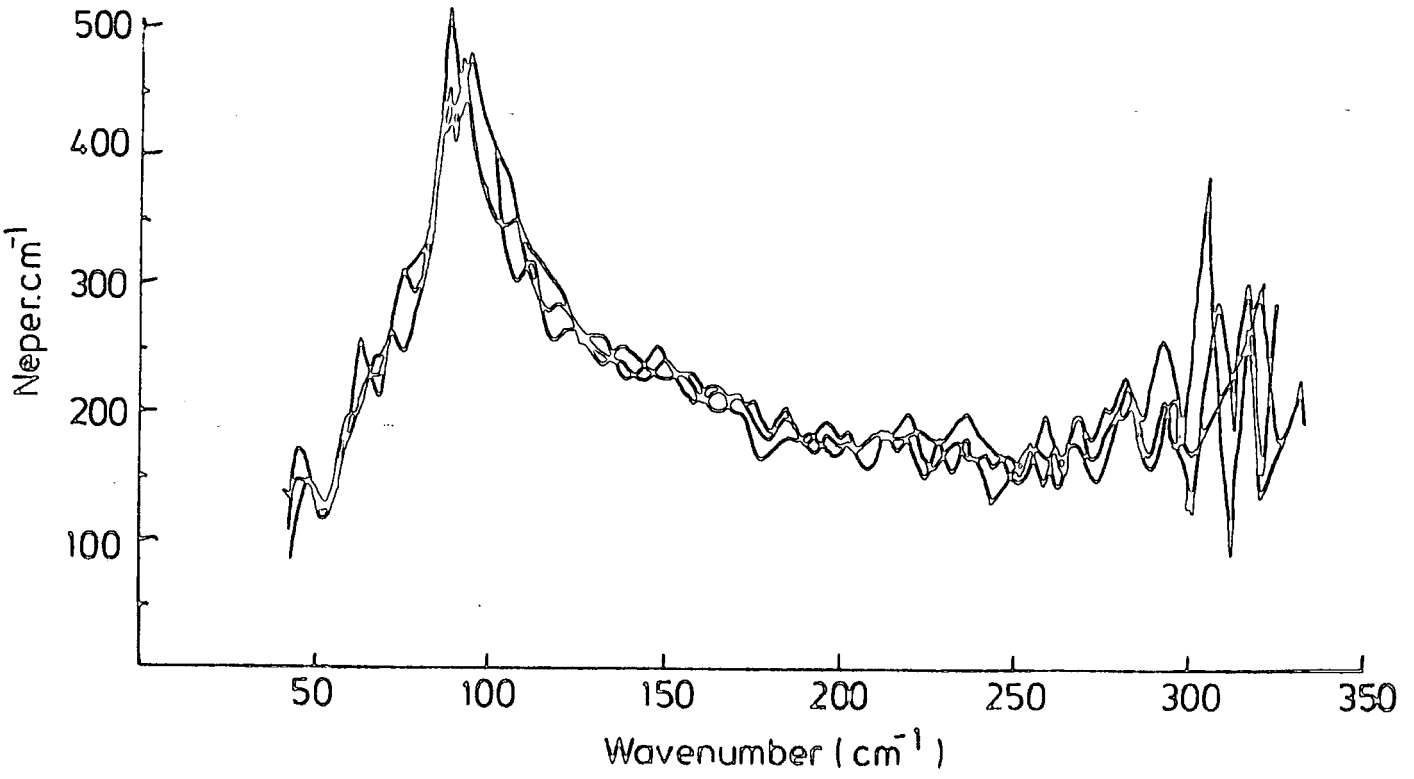

FIGURE 6·39 FAR IR SPECTRUM OF A 88·1% C_{12}TABr MESOPHASE.

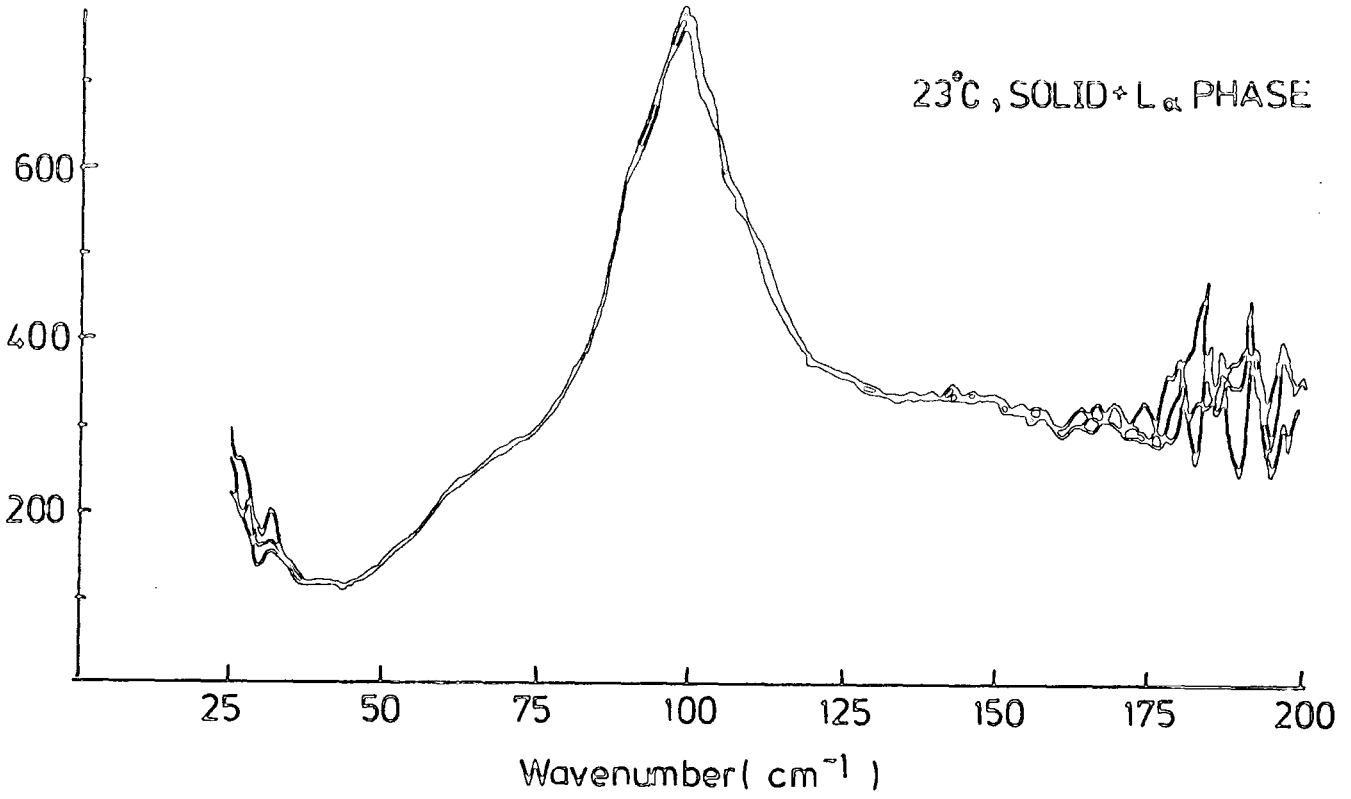

FIGURE 6·40 FAR IR SPECTRUM OF A 88·1% C_{12}TABr MESOPHASE.

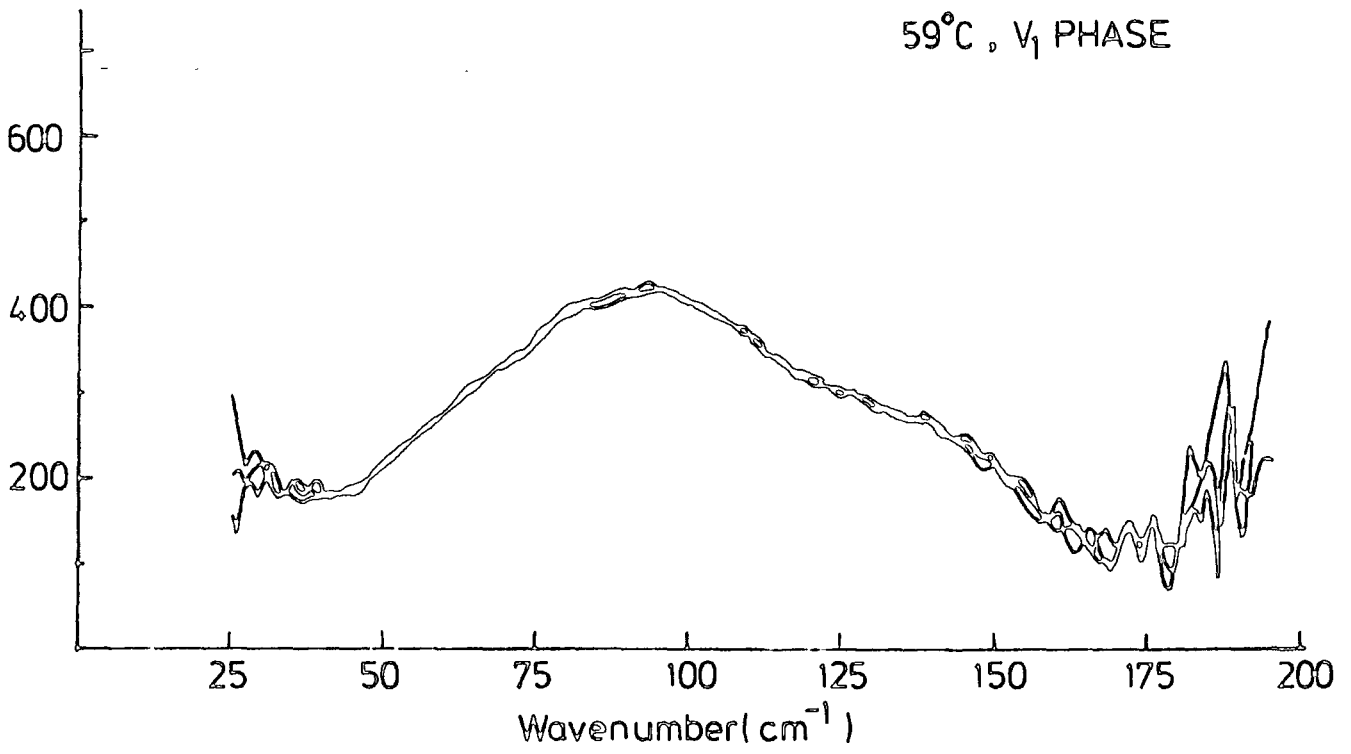

vibrational frequency of the bromide. It is therefore likely that some other influence such as water of crystallization in the chloride or differences in crystal structures is causing the discrepancy. The results obtained for the C_{12}TABr samples have been summarized in Table 6.4.

A comparison of the frequency maxima for the initial boundary water species found in the C_{12}TACl and C_{12}TABr samples demonstrates a further inconsistency. The bromide species absorbs at 90 cm^{-1} while the chloride analogue occurs at 115 cm^{-1}. If our assignment of this band is correct, the result suggests that C_{12}TABr has a greater influence on water structure than C_{12}TACl. In fundamental terms this higher frequency observed for C_{12}TACl mesophases suggests that the interaction enthalpy of the surfactant with water is less, and that hydrogen bonded interactions between water molecules is greater than in C_{12}TABr mesophases. The reason for this behaviour is not clear at present and further more detailed experiments are required.

6.5 Raman Spectroscopy of C_{12}TACl Mesophases.

6.5.1 Introduction

Raman spectroscopy of biological membranes and liquid crystals is not a new field of research. It has long been known that this technique may be used to study conformations, molecular packing, order and mobility of the amphiphillic chain [122-128] using this technique. As mentioned in Section 6.1 three regions may be used for such studies. These include the longitudinal acoustical mode region (100-300 cm^{-1}), the

skeletal mode region (1000-1200 cm^{-1}) and the C-H stretching region (2700-3100 cm^{-1}).[118] In the work described here we have studied the latter two regions in each mesophase of the C_{12}TACl-water system. The data obtained has been semi-quantitative and gives some insight into the behaviour of the amphiphile chains.

The C-C skeletal region is particularly sensitive to chain conformation.[128] At low temperatures (30°C) for the solid three bands are observed in this region (see Figure 6.41), occurring at 1060 cm^{-1}, 1080 cm^{-1} and 1130 cm^{-1}.[123] These bands are strongly intramolecularly coupled and, hence, sensitive to chain geometry.[122] As the temperature is raised, such that we might expect an increase in the number of gauche conformers, there is an increase in intensity of the 1130 cm^{-1} band relative to the 1080 cm^{-1} band. Pink *et al*[123,124] have discussed the quantitative implications of this behaviour in terms of the gauche-trans equilibrium. Though their investigations largely indicate that the 1080 cm^{-1} band originates from gauche species and the 1130 cm^{-1} to the trans species, they conclude that the behaviour is nonlinear and that the intramolecular coupling complicates the results. Mendelsohn *et al*[122] however did show that measurement of the I(1130 cm^{-1}/1080 cm^{-1}) ratio could at least be used to study gel to lamellar phase transitions. A further elaboration by Pink *et al*[123,124], for monitoring phase changes and for qualitatively comparing conformational order between systems, suggested measurement of the intensity of the 1130 cm^{-1} band relative to a temperature invariant band, *i.e.* C-N stretching mode of phosphatidylcholine at 718 cm^{-1}. Their treatment however, still assumed that the

FIGURE 6.21 RAMAN SPECTRUM OF CRYSTALLINE C12TAC AT 30°C.

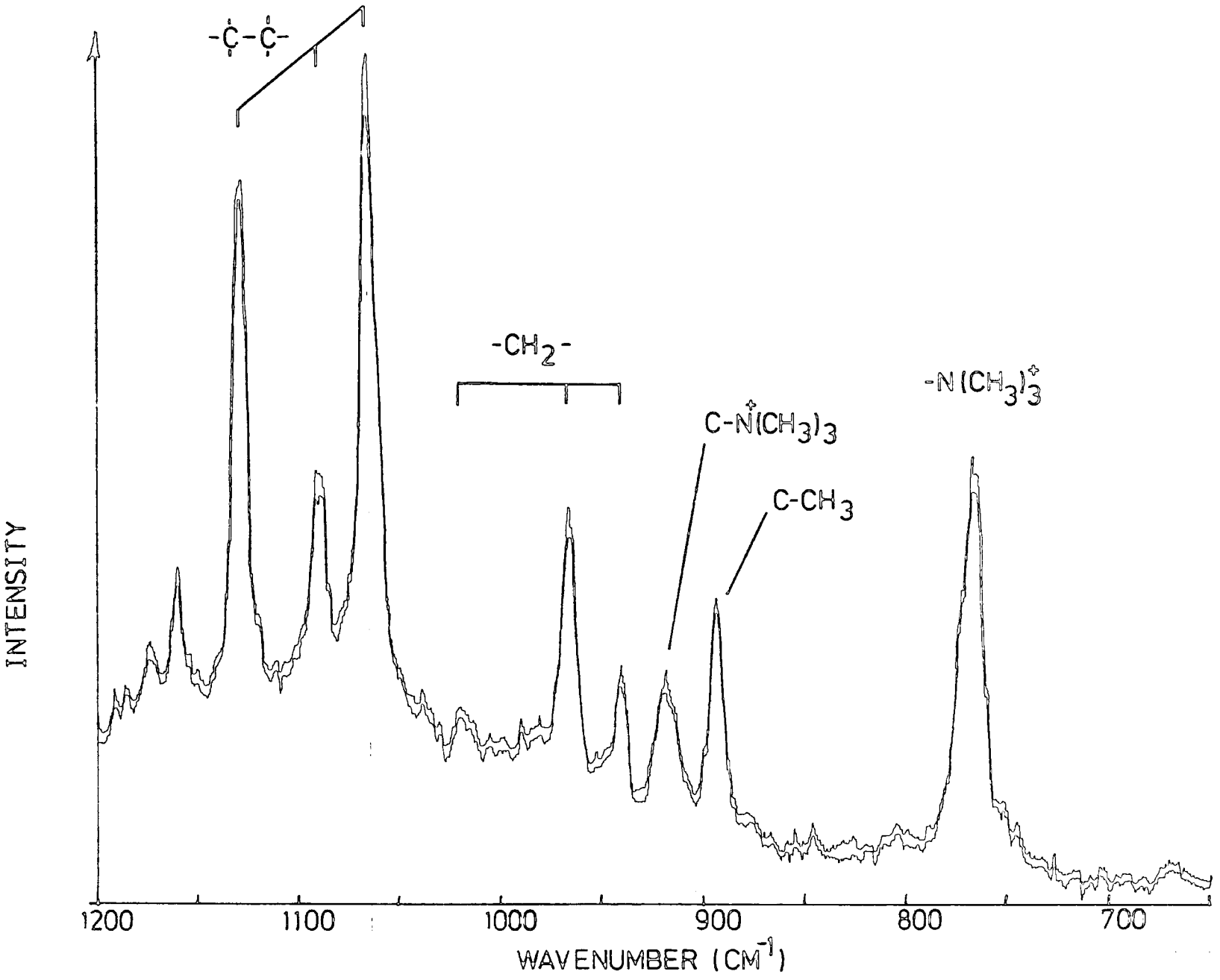

1130 cm^{-1} band originated from trans C-C bonds.

As with the skeletal region the C-H stretching part of the Raman spectra also shows complex behaviour. Some spectra are shown in Figures 6.43-6.45. The bands of most interest lie at 2850 cm^{-1}, 2880 cm^{-1} and 2930 cm^{-1} and have been assigned as $\nu_s(CH_2)$, the symmetric methylene C-H stretch, $\nu_a(CH_2)$, the antisymmetric methylene C-H stretch and $\nu_s(CH_3)$ the symmetric methyl C-H stretch, respectively. The interpretation of the relative peak heights of these bands has been a subject of some controversy. At one time it was believed that the measurement of the ratios I(2880 cm^{-1}/2850 cm^{-1}) and I(2930 cm^{-1}/2850 cm^{-1}) could be used as an indication of the gauche-trans equilibrium and environmental polarity of the amphillic chain, respectively.[118,133] The above assignments though fundamentally correct cannot be taken at face value due to intensity contributions from other sources. In particularly, Fermi resonance between the methylene antisymmetric stretch and with a continuum of the overtone bending modes (at approx. 1450 cm^{-1}) generates a broad band centred at about 2880 cm^{-1}.[122-128] This Fermi resonance may originate from two sources:[125]

(i) Intramolecular, involving interactions of the bending modes parallel to the chain axis and may be observed in completely isolated amphiphile chains.[126]

(ii) Intermolecular, involving perpendicular (lateral) interactions of the bending mode and is crystal structure dependent.[125] Thus the I_{2880}/I_{2850} ratio for a long chain hydrocarbon can be interpreted as arising from:[127]

(a) A residual intensity (*i.e.* that of the liquid).

(b) The difference between the liquid and the all trans isolated chain.

(c) A lateral contribution arising from vibrational coupling between adjacent chains.

The interpretation of the above ratio thus rests on being able to distinguish between (b) and (c), while I(2930 cm^{-1}/ 2850 cm^{-1}) generally includes a further term dependent on chain environment, and will not be discussed further here.

In addition to studying the oleophillic chain one may also observe changes in the head group bands. The strongest of the head group bands, the $N(CH_3)_3^+$ rocking mode at 760 cm^{-1} [41] in Figure 6.41 may be investigated for changes in, *e.g.* band width and frequency maximum.

6.5.2 Raman Spectra of C_{12}TACl Mesophases in the Skeletal Mode Region

Examination of the C-C skeletal modes in the 1000-1200 cm^{-1} region of these mesophases shows little or no change in therelative intensities of any of the bands in this portion of the Raman spectrum (see Figures 6.42, a,b and c). It is therefore logical to assume that the trans-gauche ratio in these liquid crystals does not undergo any dramatic changes. The spectra of Figure 6.42 may be compared to the skeletal stretching modes in the solid shown in Figure 6.41. In this spectrum the intensity of the 1130 cm^{-1} band is much larger with respect to the 1080 cm^{-1} species and therefore to a first approximation one may assume a greater proportion of trans bonds. This is expected in the crystalline surfactant where it is known that the hydrocarbon chain exists in an all trans configuration.[41]

FIGURE 6·42 RAMAN SPECTRA OF SOME C_{12}TACl MESOPHASES.

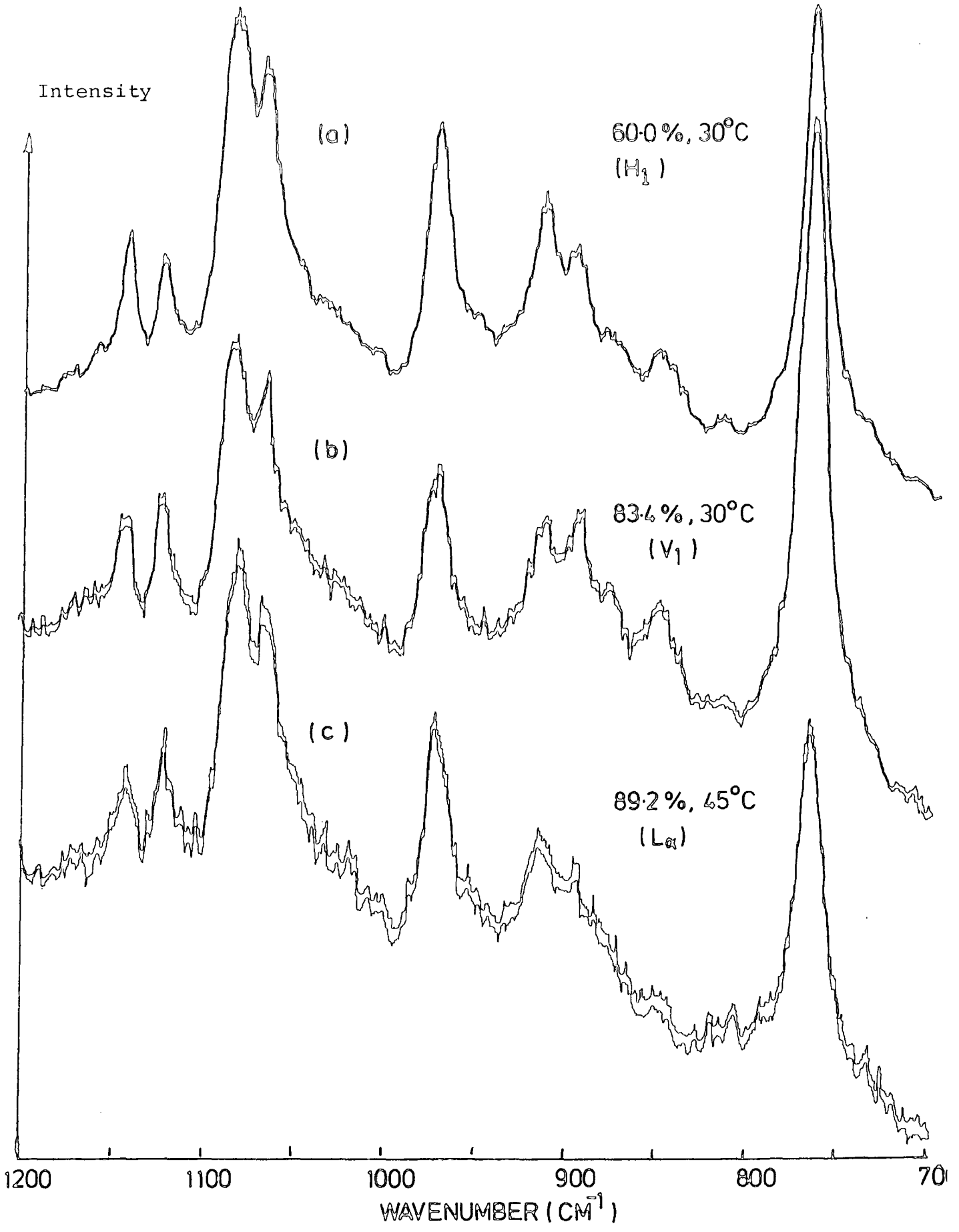

Some other interesting results using C_{16}TABr, of electrolyte-induced (NaBr) sphere to rod shape transition, have shown a slight decrease in the I_{1080}/I_{1130} ratio.[41] This data has been interpreted in terms of an increase in microviscosity of the hydrocarbon core. Unfortunately the above observations have only been performed with micellar solutions and so it is not possible to say whether or not another change, in the opposite direction, occurs at a shape transition to "spherical" symmetry. Our data have shown that this is not expected and that the above results follow a monotonic change.

6.5.3 Raman Spectra of C_{12}TACl Mesophases in the C-H Stretching Region

We have examined the 2880 and 2850 cm^{-1} profiles in each phase of C_{12}TACl across the concentration range at both 30°C and 45°C. To get a quantitative expression for the behaviour of these two bands we have measured their ratio as reported by other workers.[118,133] Spectra of the 2800-3100 cm^{-1} region are shown in Figures 6.43-6.45. The spectra of each phase are shown and exhibit unusual behaviour in that all the isotropic samples (L_1, I_1, V_1) show the intensity of the 2880 cm^{-1} band to be significantly less than that of the 2850 cm^{-1} (*i.e.* with an $\frac{I_{2880}}{I_{2850}}$ ratio of about 0.80 from peak heights). With the anisotropic samples (H_1, L_α) and the solid the opposite behaviour is true and the I_{2880}/I_{2850} ratio is greater than 1.0. The ratios have been plotted as a function of concentration in Figure 6.46 and 6.47. The results are entirely consistent and indeed, crossing a boundary between

FIGURE 6·43 RAMAN SPECTRA OF $C_{12}TAC$ MESOPHASES IN C-H STRETCHING REGION.

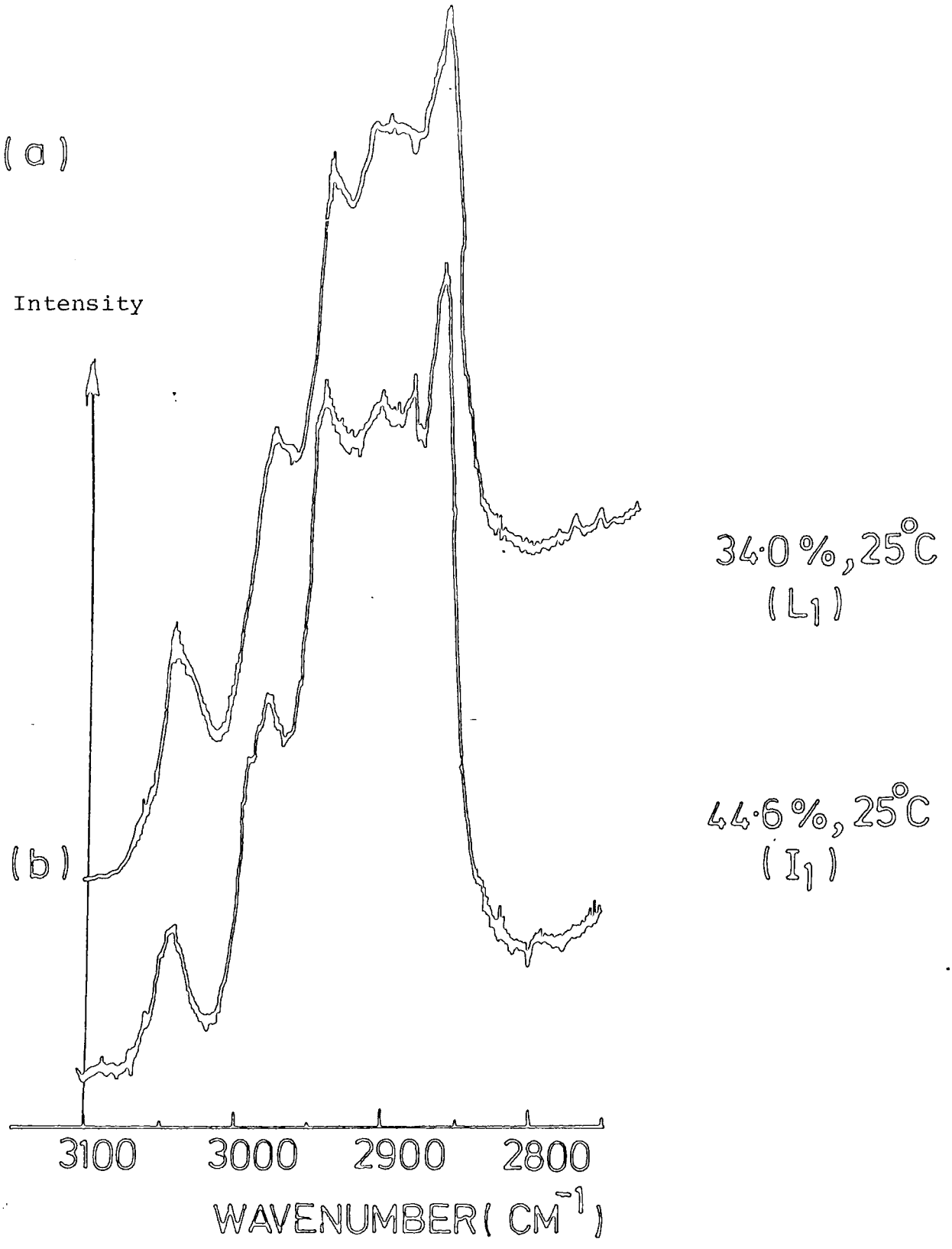

FIGURE 6.44 RAMAN SPECTRA OF SOME $C_{12}TACl$ MESOPHASES IN THE C-H STRETCHING REGION.

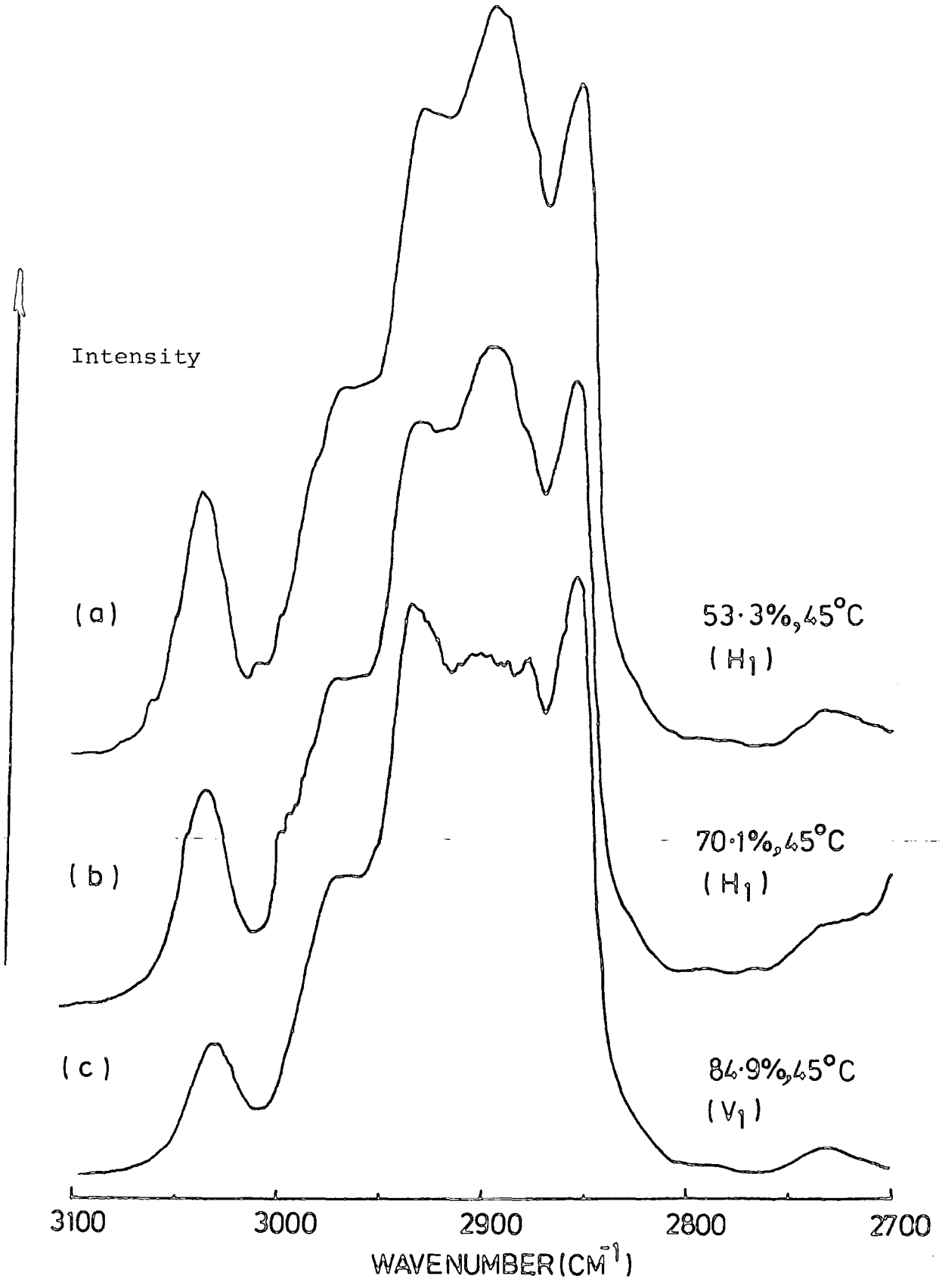

FIGURE 6.45 RAMAN SPECTRA OF SOME C_{12}TACl MESOPHASES IN THE C-H STRETCHING REGION.

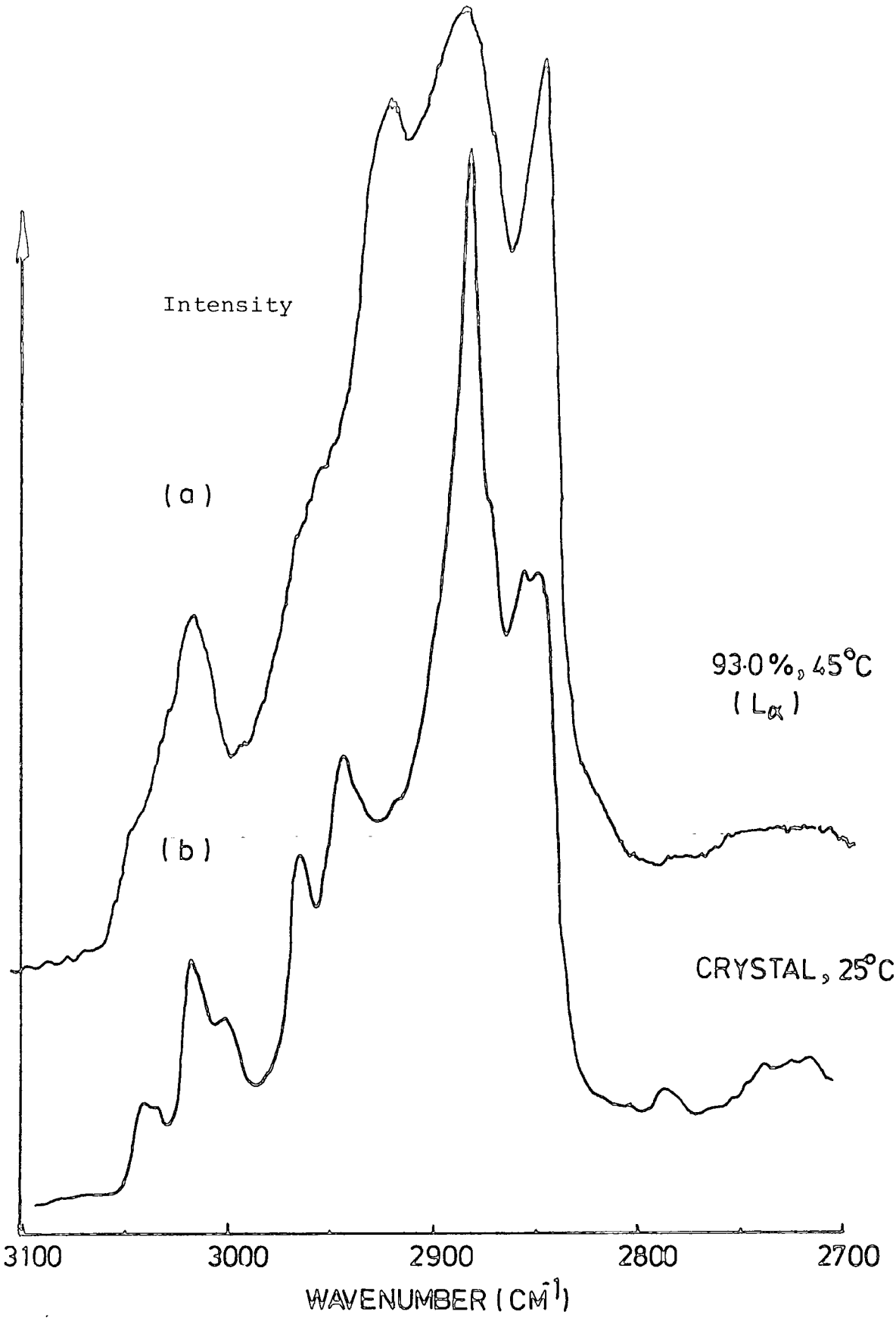

FIGURE 6·46 THE BEHAVIOUR OF THE I_{2880}/I_{2850} RATIO FOR C_{12}TACl AT 30°C.

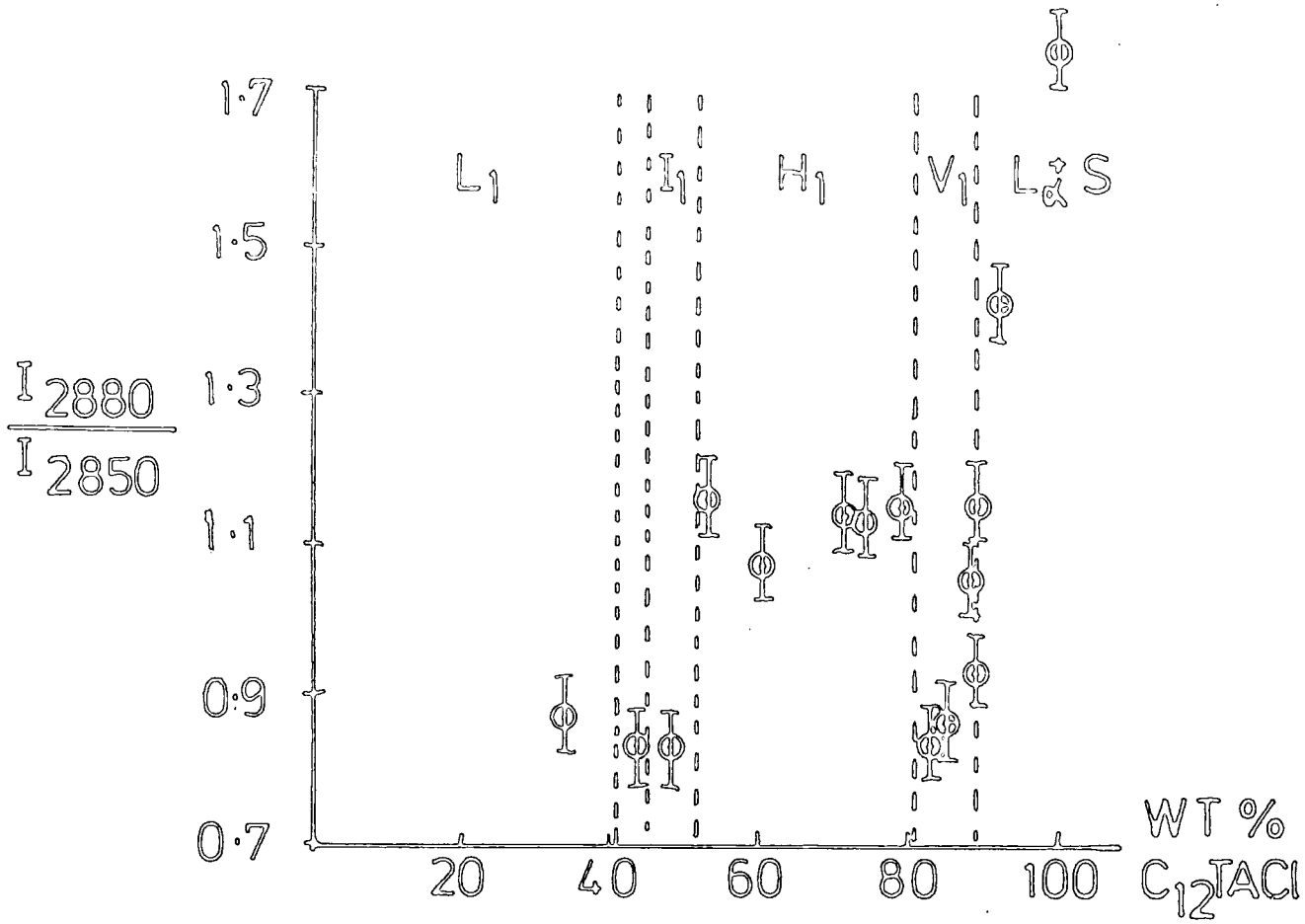

FIGURE 6·47 THE BEHAVIOUR OF THE I_{2880}/I_{2850} RATIO FOR C_{12}TACl AT 45°C.

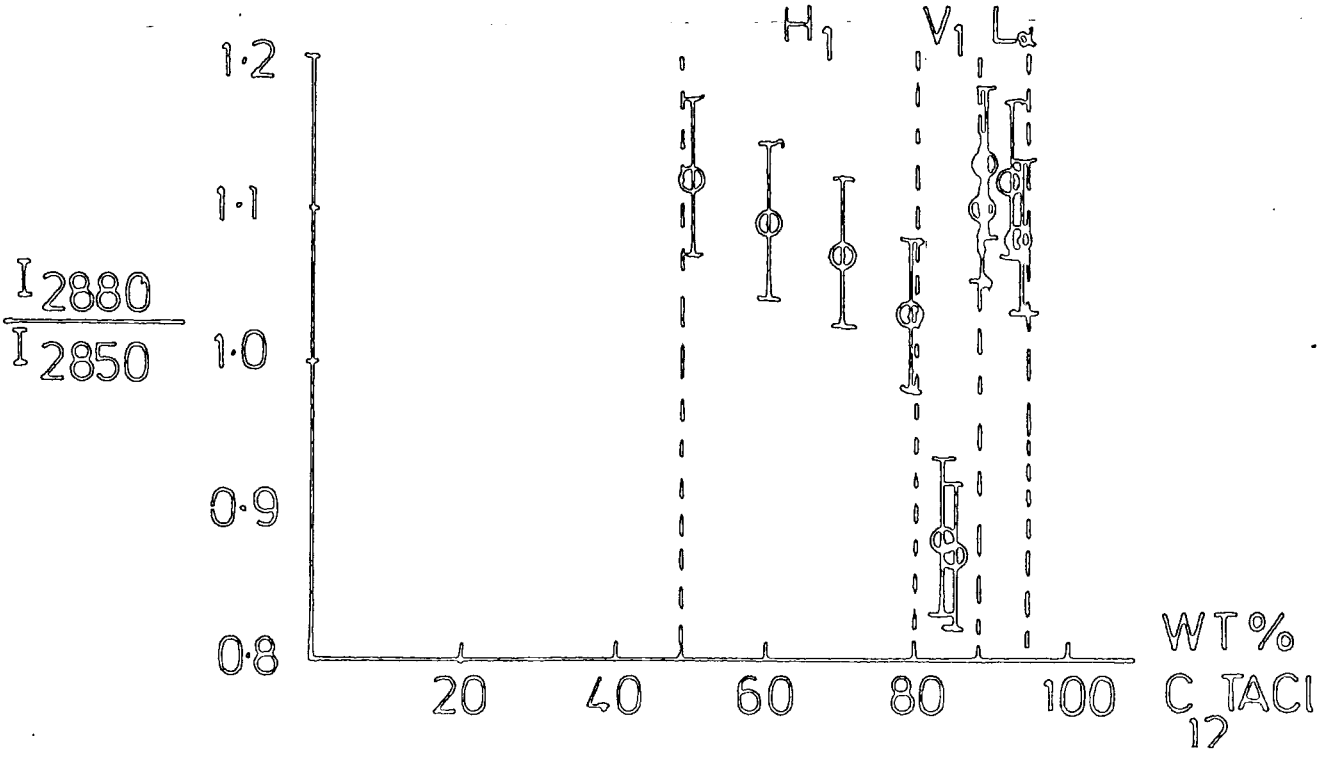

isotropic and anisotropic phases produces the increased 2880 cm^{-1} intensity. This behaviour is quite surprising since one would expect that a gradual decreased micellar surface curvature (as occurs when the concentration is increased) would result in a monotonic increase in the trans/gauche ratio, and not the "stepped" behaviour observed here. However, we have seen that there is no change in the skeletal mode region from Section 6.5.2. To a good approximation, we may therefore assume that there is no dramatic change in the trans/gauche ratio in these systems. In our introduction to this section we mentioned several possibilities which may contribute to the intensity of the 2880 cm^{-1} band. If the trans/gauche ratio remains constant then we may interpret the above data in terms of an increased lateral interaction between neighbouring chains which suddenly changes when an isotropic-anisotropic phase boundary is crossed. It therefore seems likely that there is some rearrangement in packing on crossing such a phase boundary. Without further evidence it is difficult to specify exactly the cause of such behaviour. The isotropic phase spectra found in this region are not unlike those found with dodecane in the liquid state.[41] The similarity may suggest an increase in hydrocarbon chain fluidity in these phases. This seems unlikely as mentioned previously, since no dramatic changes are observed in the skeletal region.

6.5.4 The Behaviour of the R-$N(CH_3)_3^+Cl^-$ Head Group Vibration of $C_{12}TACl$

We have, in addition to the hydrocarbon line shapes, studied the behaviour of one of the head group bands. In

particular, the CH_3 rock from the $-N^+(CH_3)_3$ group.[41] The results, across the concentration range, show no change in either the band width or the frequency maximum. This suggests that no motional or conformational changes are occurring and that the head group environment is not influenced by phase structure. Alternatively, any effects which may occur are not detected by Raman spectroscopy.

6.6 Conclusions

The results in this chapter have given us a new insight into the microstructure of mesophase and micellar systems. In particular far and mid i.r. have shown that one may distinguish between four types of water molecule. These have been described as, "free" water, outer boundary water which is associated with the micelle, and two types of strongly perturbed water, one more so than the other:* both of the latter belonging in the first solvation shell of the micelle surface. The counter ions are more evident, in the spectra of the outer boundary water layer, from the shifts that are observed. The data above are similar to the results obtained by measuring the "hydration force" of Parsegian *et al*[119-121,130] and those observed by Sunamoto.[113] The work with C_{12}TABr has shown that the interactions are qualitatively similar. The results have been summarized in Figure 6.48. One aspect of our results which has been of some confusion is the idea of several types of water species when the water/surfactant mole ratio has been small (*i.e.* approaching unity). We have therefore assumed

* [N.B. The stronger of these associated species only occurs at high surfactant concentrations, see figure 7.13].

FIGURE 6·48 SUMMARY OF THE VARIOUS POSSIBLE WATER LAYERS FOUND AS THE WATER CONC^{N} IS DECREASED.

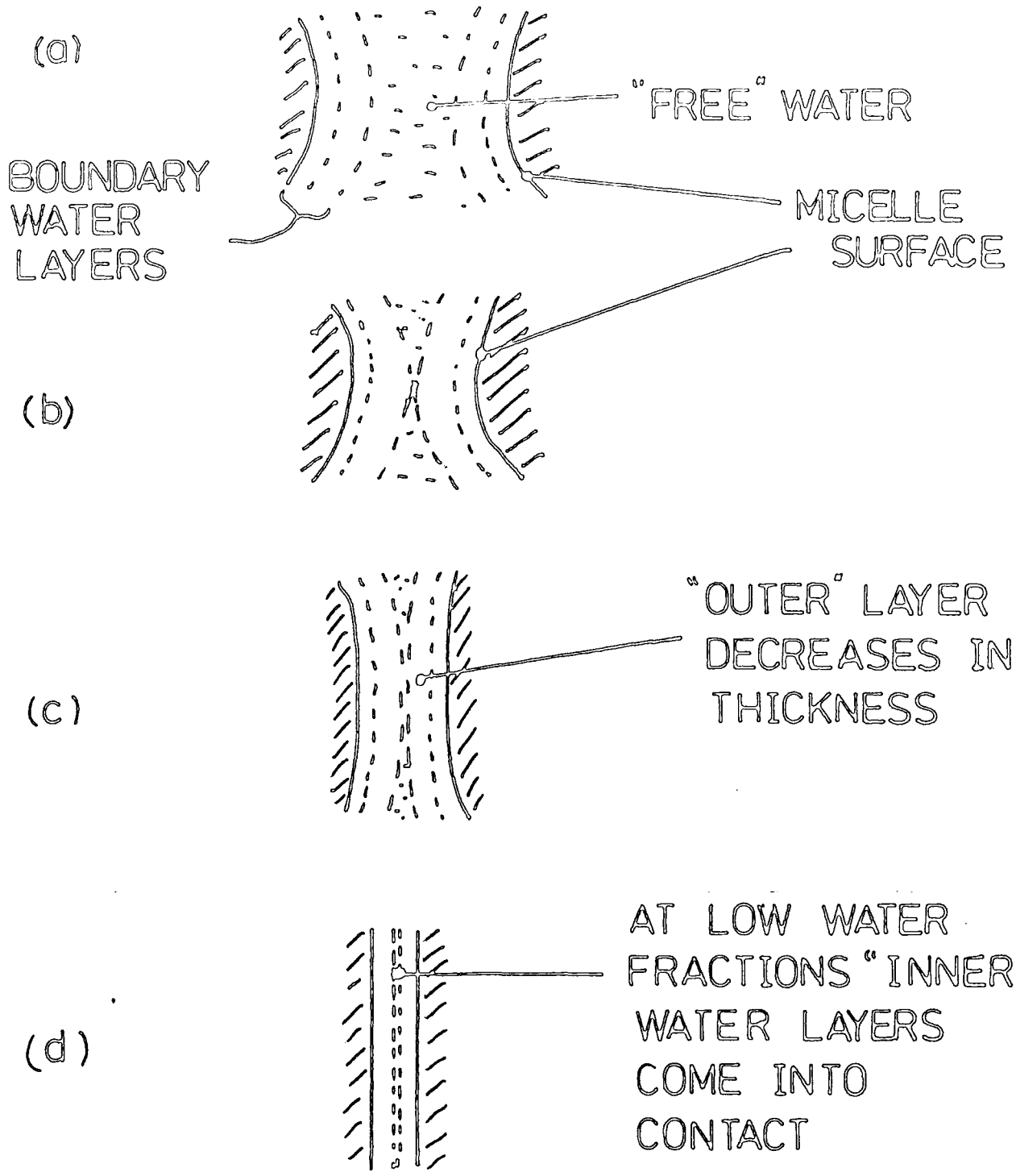

that the organization of water and surfactant molecules is more complex than can be imagined with a "one to one" type situation.

It is known that the hydration number of $C_{12}TACl$ is approximately 5 (measured from diffusion and viscosity data)[129] though we believe that all the water above about 40% w/w $C_{12}TACl$ will, in some way, be influenced by the surfactant. Indeed some of the mid I.R. data have shown an increased deviation from the behaviour of pure water (*e.g.* see Figure 6.17) at this point. The far i.r. data also suggests that at these high surfactant concentrations the structure of water is completely different to that in its normal state.

The Raman results have shown an interesting increase in the lateral interactions of anisotropic mesophases, probably as a result of some change in the packing of the oleophillic chains. This data has thus allowed us to observe phase boundaries using a novel method and at the same time giving us further information about the microenvironment of the hydrocarbon core.

CHAPTER SEVEN

A SPECTROSCOPIC STUDY OF THE HEXADECYL-TRIMETHYL-AMMONIUM CHLORIDE(C_{16}TACl)-WATER SYSTEM

7.1 Introduction

Hexadecyl trimethyl ammonium chloride (C_{16}TACl) is structurally very similar to its homologue C_{12}TACl. It might be expected that the phase behaviour of this surfactant should be comparable to that of C_{12}TACl. Though very little detailed work has been performed using C_{16}TACl-water mesophases,[86] the data available indicates that an extra four carbons in the hydrocarbon skeleton, causes quite significant differences in the phase behaviour. Data obtained by Tiddy[86] using microscopy and multinuclear NMR have indicated the presence of at least five different mesophase structures, with possibly one more also in evidence (though further work is required to prove its existence). In terms of micelle curvature, a longer hydrocarbon chain has the same effect as reducing the surface area per molecule. As discussed in Section 5.3 a reduction in this parameter may cause a decrease in possible number of micellar shapes. Inspection of Figure 7.1, showing the C_{16}TACl-D_2O phase diagram (D_2O used for NMR studies, differences from H_2O are expected to be small[86]), supports this idea and no I_1 phase (spherical micelles packed to form a cubic array) is observed. Instead the L_1 phase shows a disorder-order transition to a hexagonal (H_1) liquid crystal. As the concentration is increased to about 78% C_{16}TACl an "intermediate phase" is formed consisting of what is thought to be a biaxial structure as depicted in Figure 7.2 below. It is similar to the rectangular phase discussed in Section 5.2.

Unlike the hexagonal phase, this intermediate phase is thought to have rods with a more elliptical cross section.

FIGURE 7.1 THE MOST RECENT PHASE DIAGRAM OF THE $C_{12}TACl / D_2O$ SYSTEM

[reproduced from ref. 86]

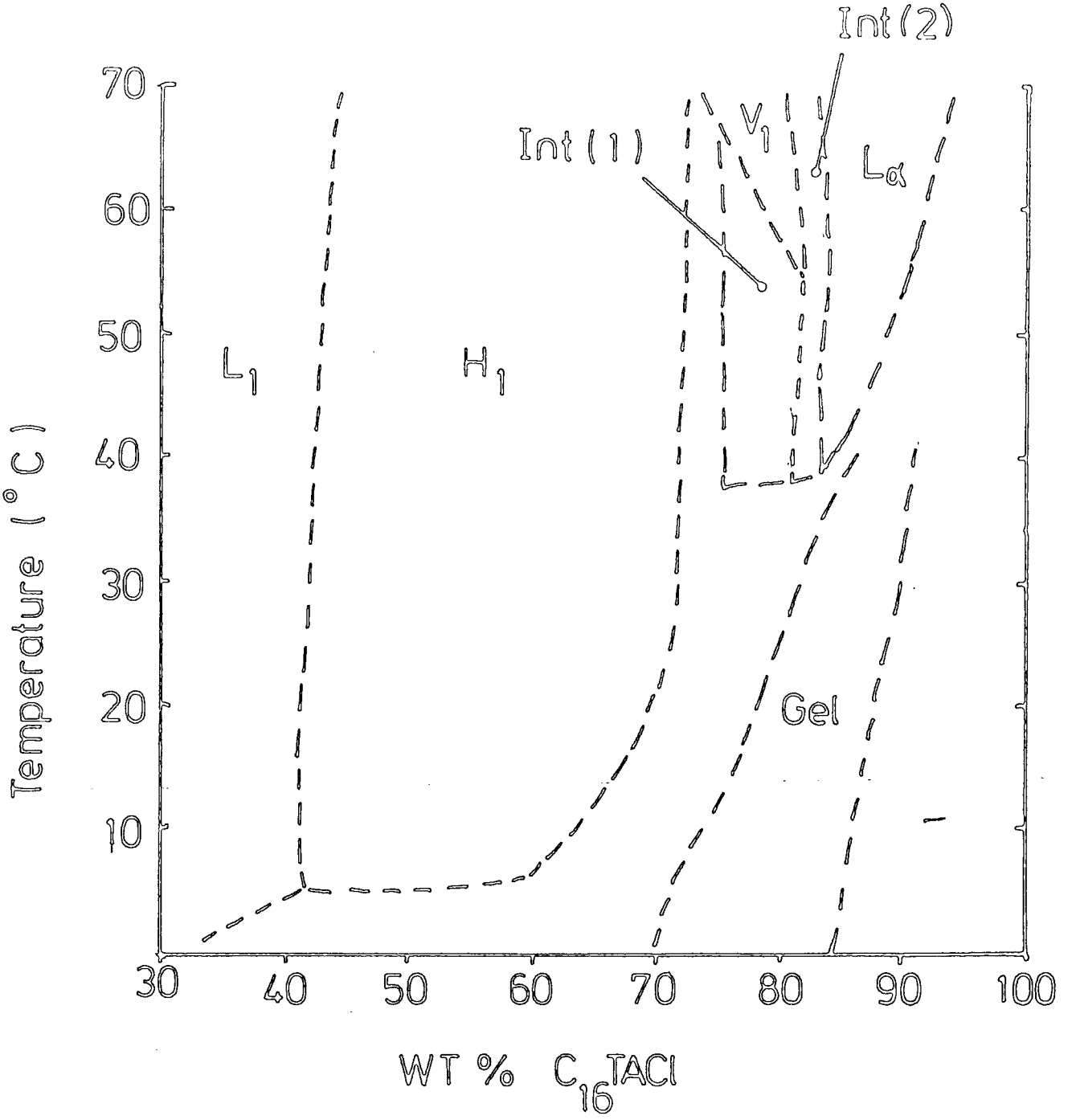

N.B. Dotted lines represent only approximate boundaries.

Figure 7.2 Schematic diagram of the First Intermediate phase formed in $C_{16}TACl$-D_2O

(reproduced from ref.80)

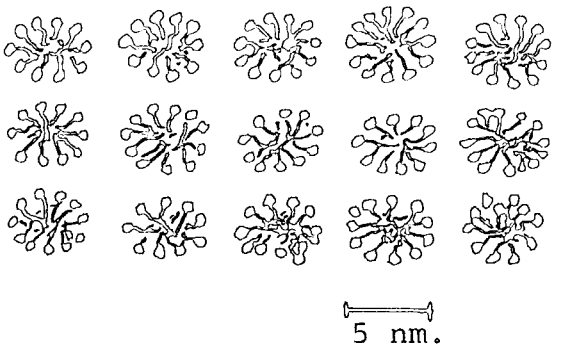

An increase in temperature results in a transition to a bi-continuous V_1 cubic phase which itself changes, on further addition of surfactant, to a lamellar phase or possibly a second intermediate phase. Though no conclusive evidence exists to date concerning this mesophase, it is thought to have a structure similar to that observed previously,[85] of a lamellar type phase with thin bilayers. At lower temperatures a gel phase exists where the surfactant molecules form inter-digited layers separated by water. Below about 45°C (at lower surfactant concentrations), the gel and hexagonal phases appear to form a large region where both are in equilibrium.

Though the structure of the majority of the above meso-phases is well understood,[77,79,80] further details, particularly concerning the microstructure of the water/counter ion environment, are less well documented. Of particular interest is the behaviour of interstitial water and counter ions when a

transition from the gel to lamellar phase occurs. Data concerning the intermediate phases are of great interest particularly for the one occurring near the hexagonal phase, where previous workers[82,85] with other systems have proposed a deformed hexagonal structure. Though such an array is not proposed here, the presence of strong hydrogen bonds (see Section 5.3.1) could be proven. Though the head groups of both C_{12}TACl and C_{16}TACl are the same it is of some interest that a direct comparison be made of the two systems. In this way the microscopic behaviour of both the water and to some extent the counter ion, in the different phases may be compared. Infra red spectroscopy provides the most convenient method of doing this since the time scale of the technique is faster than the motion of these molecules and ions (NMR only portrays an average picture of the system).

As in Chapter Six Raman spectroscopy has been used to study the oleophillic chain using both the skeletal C-C stretching modes and also the C-H stretching vibrations. Of particular interest here is whether or not the isotropic phases once more display their distinct behaviour in the 2800-3100 cm^{-1} region. In addition, it will be interesting to observe the behaviour of the intermediate phase(s) in this context.

7.2 Experimental

7.2.1 Materials, Sample Handling and Spectroscopy

Hexadecyl trimethyl ammonium chloride (C_{16}TACl) provided by Eastman Kodak was recrystallized from acetone and stored over P_2O_5. Though no accurate phase diagram was

available, penetration microscopy as used by other workers[82,85] showed phase behaviour having reasonable agreement with that of Figure 7.1. Samples for both mid and far i.r. spectroscopy were prepared in 10mm screw top vials by the method described in Section 6.2.1 and using a new 5% v/v D_2O solution. The surfactant, being less hygroscopic than C_{12}TACl was easier to manipulate and allowed a minimum of atmospheric contamination. Large batches of samples were thus prepared and unlike previously, stored at 45°C. This prevented the formation of the V_1 phase which occurs at higher temperatures and is known to supercool. A further precaution of removing the samples from the oven 24 hours before use ensured that this phase was avoided. The samples were checked by observation between crossed polars and showed good agreement with the phase diagram of Figure 7.1.

Sample handling was as described in Section 6.2.1 for mid ir, far ir and Raman spectroscopy except that three temperatures were used, 30°C, 45°C and 60°C. Similarly the spectroscopic protocol discussed in Sections 6.2.2-6.2.4 was also repeated.

7.2.2 Optical Microscopy

The C_{16}TACl-water system was examined using optical microscopy. This was done in two ways:

(i) Firstly mesophase samples of known composition were heated and photomicrographs obtained periodically.

(ii) The poor water solubility of C_{16}TACl allowed the penetration microscopy technique of Lawrence[79,80,134] to be used effectively. The first method allowed the determination

of phase transitions(though not our prime objective in this case) and also photomicrographs of homogeneous phases. The second technique allowed the determination of phase temperatures but not the concentrations at which they occurred. The method involved finely grinding dry surfactant and placing a small portion on a microscope slide. A cover slip was pressed over the surfactant powder ensuring a thin even layer and water from a dropping pipette was then allowed to permeate through to the surfactant. After a few moments a series of rings appeared at the dry surfactant-water boundary, corresponding to the various mesophases occurring across the concentration range at that temperature. Placing the microscope slide on a heating stage allows the determination of a temperature for which one observes a particular phase transition. This technique is of much value for determining new phase diagrams and also as a check on purity. Impure samples generally give non reproducible phase transitions. The phases themselves all exhibit particular optical and rheological properties. The presence or absence of birefringence, as viewed through crossed polars, could differentiate between anisotropic and isotropic mesophases.[81] The relative viscosities of each mesophase layer were qualitatively determined by pressing the cover slip and observing the flow properties. In this way a more precise assignment of phase structure could be made.[79-81]

For standard microscopy a Reichart Optical polarizing microscope was used with a Koffler heating stage. The protocol for obtaining photomicrographs was rather more complex and involved the design of an independent heating stage.

The latter was composed of heating wire sandwiched between thin flat layers of heat resistant circuit board and cemented together with epoxy resin. The temperature was controlled by a transformer and was measured using a copper constan thermocouple. The photomicrographs were obtained using a Carl Zeiss microscope and camera assembly set with automatic exposure.

7.3 A Mid IR Spectroscopic Investigation of the C_{16}TACl-Water System

7.3.1 Mid IR Spectra of Water at Three different Temperatures

As in the previous chapter two bands have been used to study the water structure in the C_{16}TACl-water system. These are the $\nu_s(O\text{-}D)_{HDO}$ stretching mode and the $\nu_A(H_2O)$ combination band which conveniently occur in the 2800-1800 cm^{-1} spectral window. Figure 7.3 shows several superimposed spectra of water in this region, each taken at a different temperature. The bands demonstrate their familiar behaviour as the temperature is increased[5], *i.e.* both bands broadening with $\nu_s(O\text{-}D)_{HDO}$ shifting up in frequency while $\nu_A(H_2O)$ shifts to lower vibrational energies. As before good agreement is observed with the literature.[5]

The broadening of these bands with temperature may be interpreted as arising from an increase in the motion of the water molecules and hence a broader distribution of H-bonded water species, while the shifts are dependent on the strengths of hydrogen bonded interactions. An increase in the H-bonded interaction, that occurs with a decrease in

FIGURE 7·3 MID IR SPECTRA OF A 5% v/v D_2O SOLUTION.

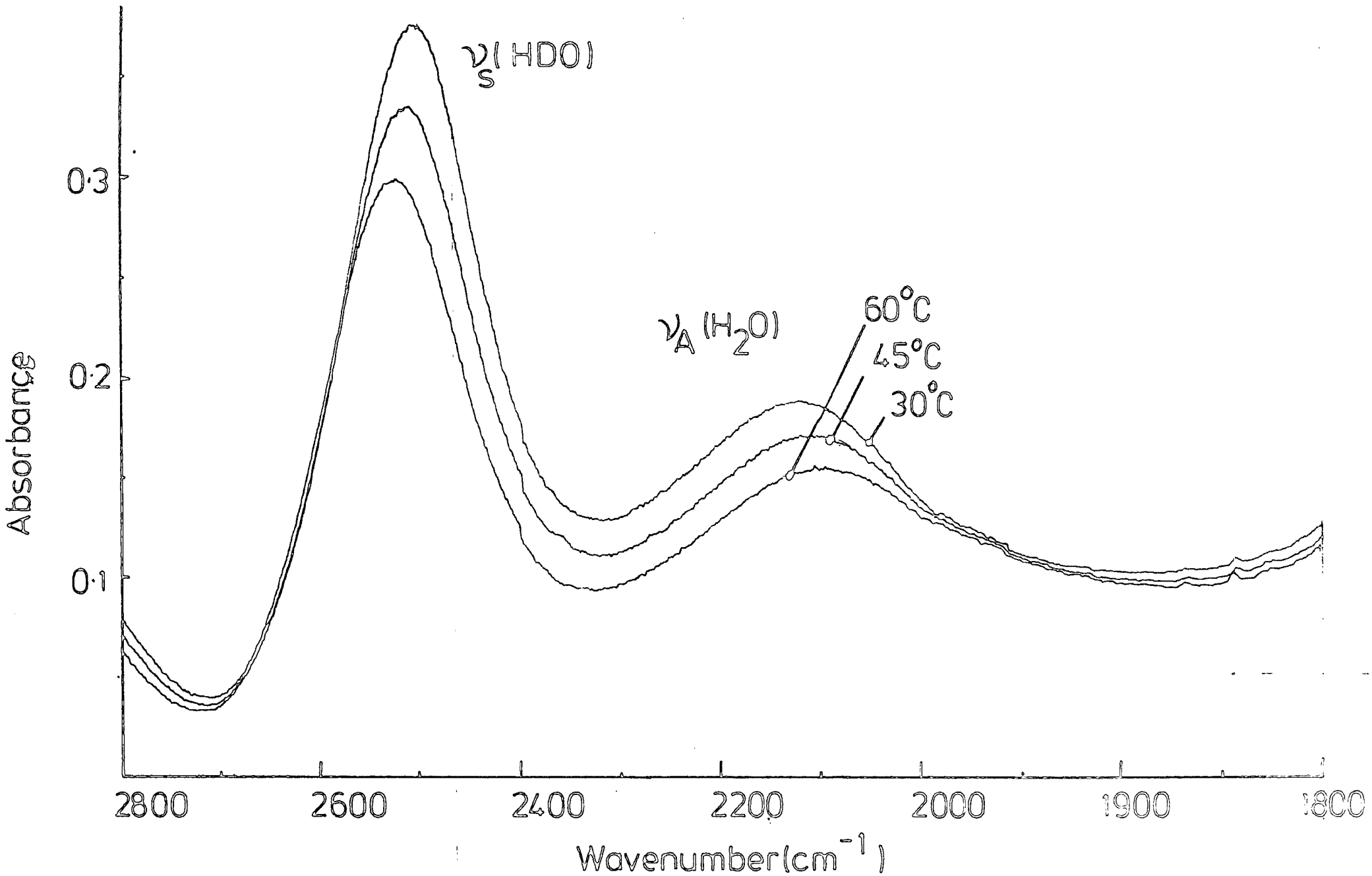

temperature, causes $\nu_s(O\text{-}D)_{HDO}$ to move to lower frequencies. However, $\nu_A(H_2O)$, which is thought to be a combination mode of $\nu_2 + \nu_L = \nu_T$,[5,18] shifts to higher frequencies with a decrease in temperature. This behaviour is difficult to explain since ν_2 is known to be only slightly affected by H-bond formation, while ν_T and ν_L will be expected to increase.

7.3.2 The Behaviour of $\nu_s(O\text{-}D)_{HDO}$ and $\nu_A(H_2O)$ as a Function of Concentration

Figures 7.4 and 7.5 show spectra obtained in the L_1 solution of micelles. The two bands do not differ in their band widths ($\Delta\nu_{1/2}$) and frequency maxima (ν_{max}), from that of the water spectra of Figure 7.3. However, it is possible to detect the presence of a shoulder in both bands, occurring to the low frequency side of $\nu_s(O\text{-}D)$ and the high frequency side of $\nu_A(H_2O)$. These shoulders become more prominent at higher concentrations above the disorder-order transition. Figures 7.6 and 7.7 show spectra of two hexagonal phases having compositions of 57.7% w/w and 70.6% w/w C_{16}TACl, respectively. The shoulders in these spectra are centred at 2500 cm^{-1} (for $\nu_s(O\text{-}D)_{HDO}$) and 2160 cm^{-1} (for $\nu_A(H_2O)$. These bands have also been observed in the C_{12}TACl system discussed in Chapter Six. Further interesting behaviour is observed as the concentration is increased to 79.2% w/w C_{16}TACl. Figures 7.8a, b and c show spectra of this mesophase at 30°, 45° and 60°C, respectively. At 30°C microscopic examination, in agreement with the phase diagram of Figure 7.1, shows that at this concentration the gel and hexagonal phases coexist. Further examination under the microscope

FIGURE 7.4 IR SPECTRUM OF DECOUPLED H_2O IN A 16.2 % $C_{16}TACl$ SOLUTION AT 45°C.

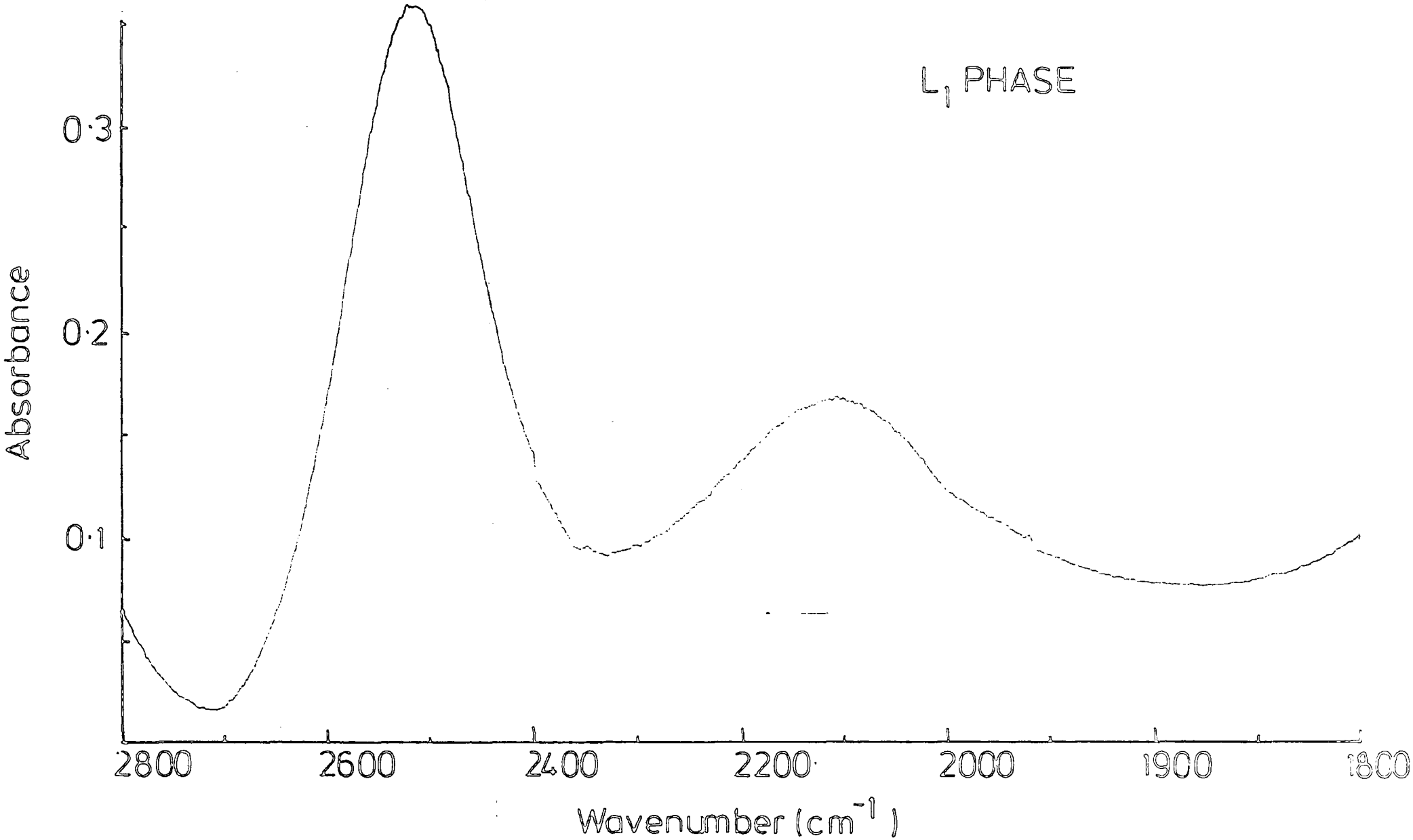

FIGURE 7·5 IR SPECTRUM OF DECOUPLED H_2O IN A 39·1 % C_{16}TACl SOLUTION AT 45°C

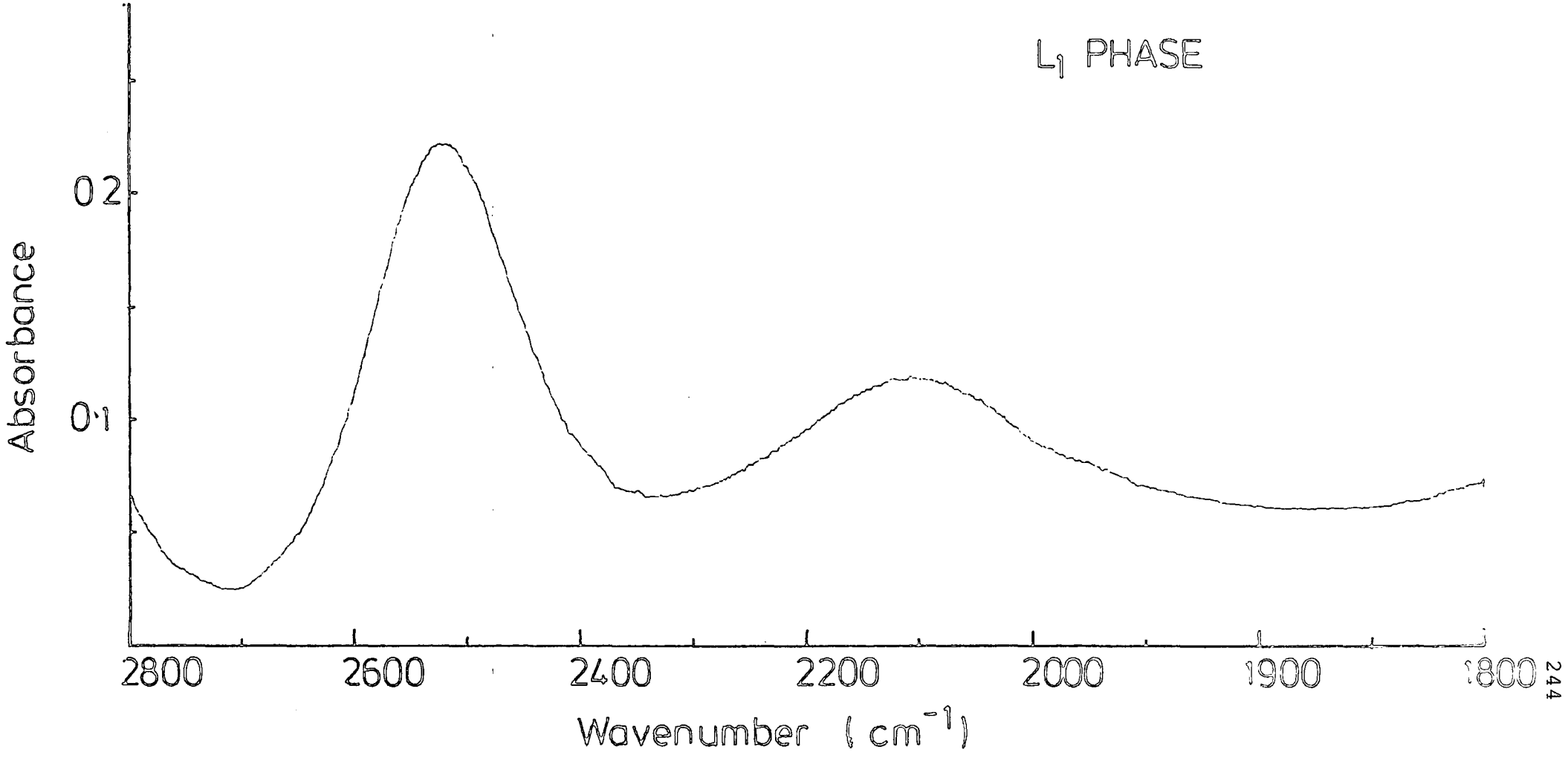

FIGURE 7·6 IR SPECTRUM OF DECOUPLED H_2O IN A 57·7 % C_{16}TACl MESOPHASE AT 45°C

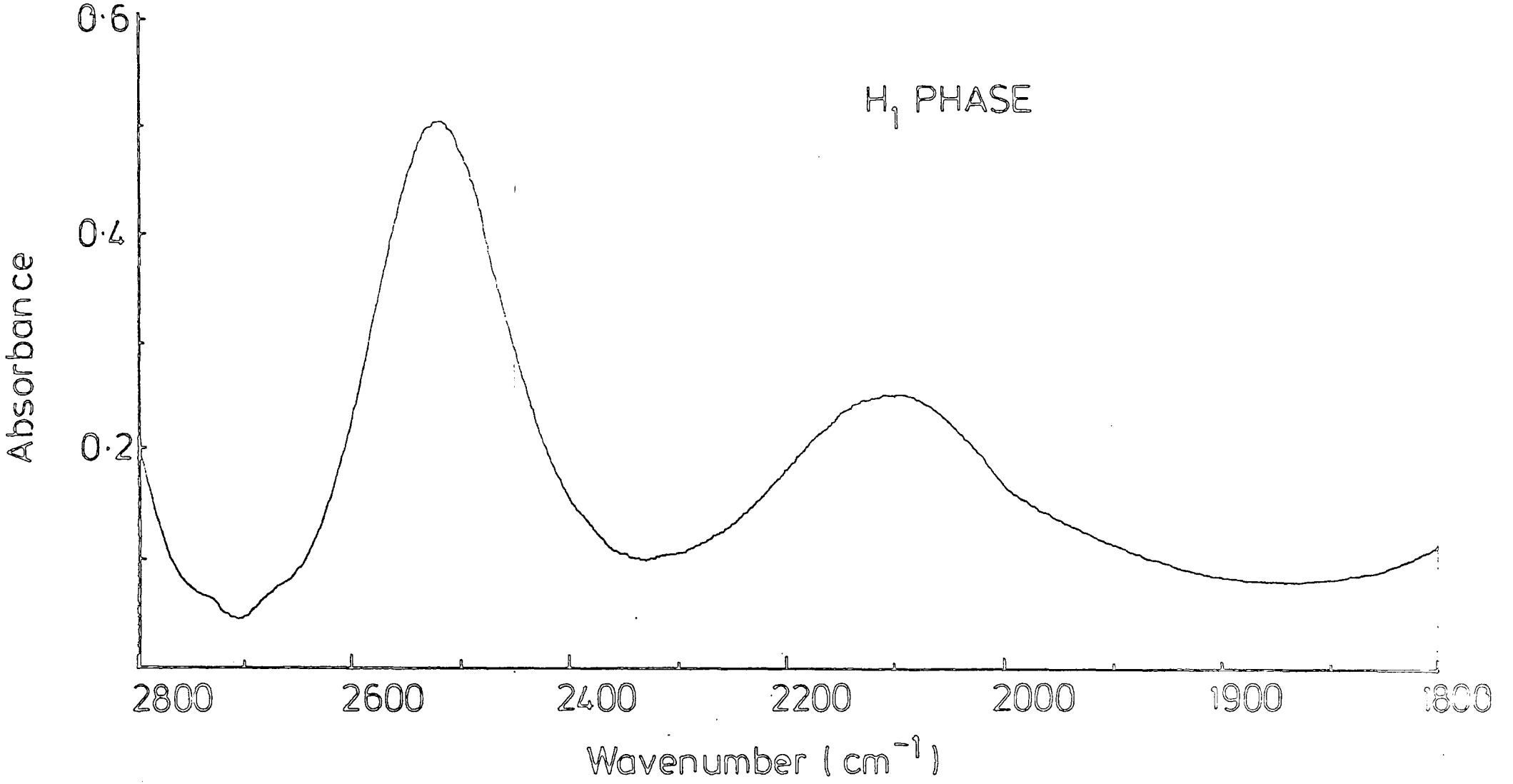

FIGURE 7·7 IR SPECTRUM OF DECOUPLED H_2O IN A 70·7% C_{16}TACl MESOPHASE AT 45°C.

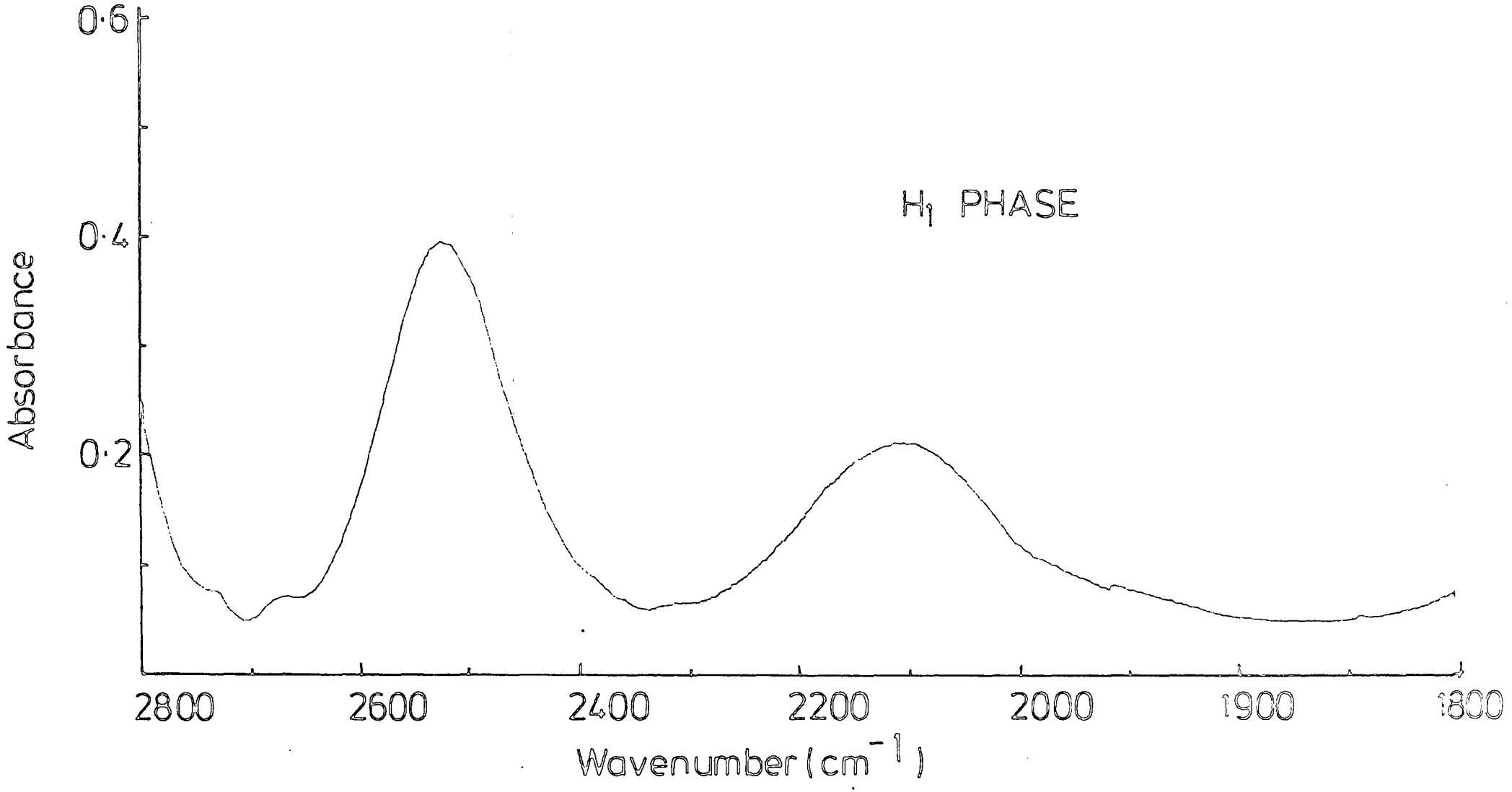

FIGURE 7·8 IR SPECTRA OF DECOUPLED H_2O IN A 79·2% C_{16}TACl MESOPHASE.

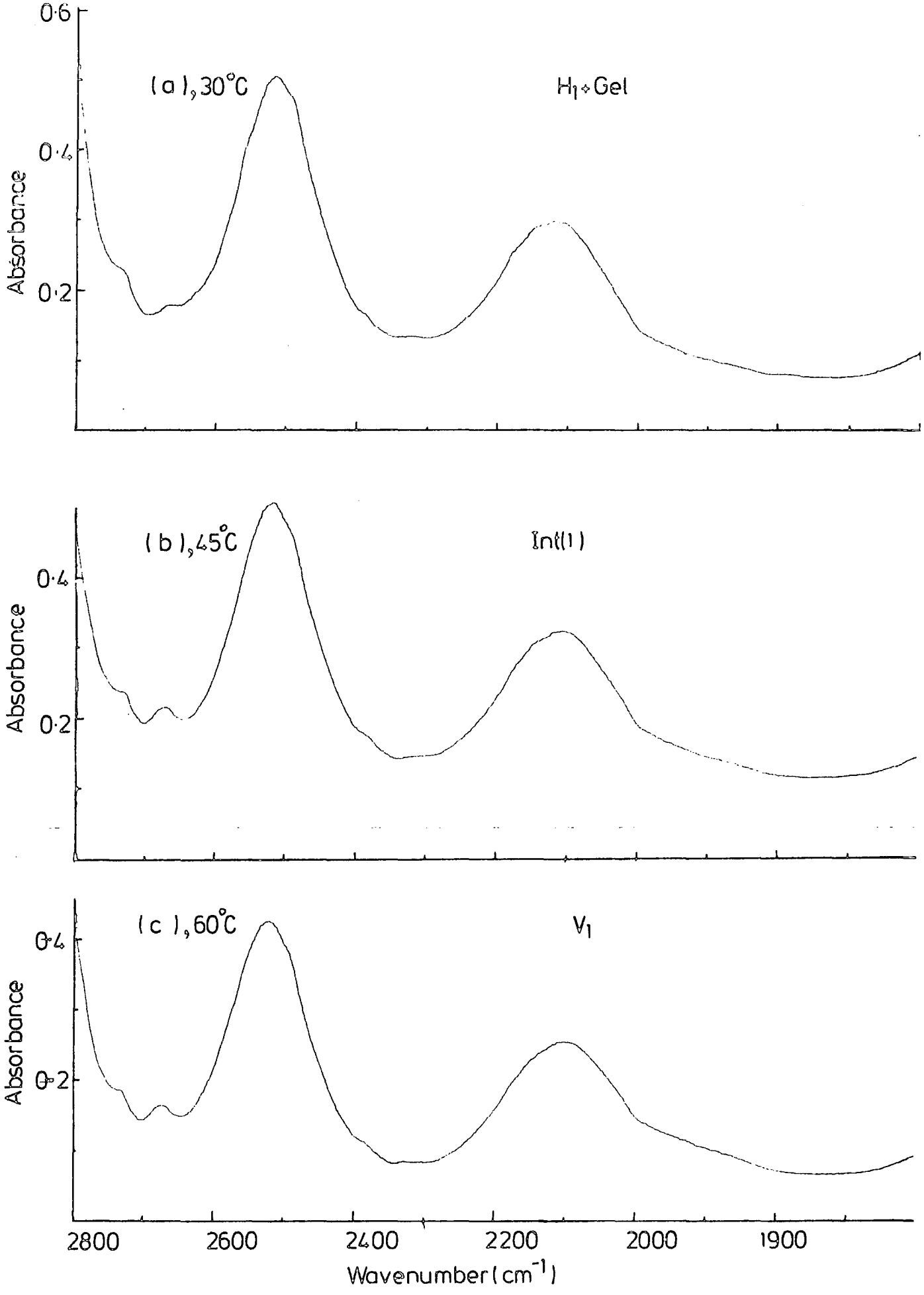

shows that two phase transitions of this sample occur. The first at 37°C, to what is believed to be an "intermediate" phase[82,85] and a second to a V_1 cubic at 55°C. The spectra of Figures 7.8a, b and c thus show ν_s(O-D) and $\nu_A(H_2O)$ in each of the above phases. These bands in Figure 7.8a (H_1+gel) show several prominent shoulders which become less pronounced as the temperature is increased to 45°C (Figure 7.8b, intermediate) and 60°C (Figure 7.8c; V_1). Figure 7.9 shows two superimposed spectra of an 84.24% w/w C_{16}TACl sample in the gel (30°C) and lamellar phases (45°C). As before, several shoulders are evident at 30°C which become less pronounced when the phase melts. Finally, another lamellar phase spectrum is shown in Figure 7.10 (89.7% w/w C_{16}TACl). Two notable features of this mesophase are that the relative intensity of the ν_s(O-D) and $\nu_A(H_2O)$ is quite different from that of water and that a small band at 2675 cm^{-1} is evident.

The features of $\nu_A(H_2O)$ and ν_s(O-D) described in the above paragraph seem to follow the same trend as that observed in C_{12}TACl previously. The assignment of the various shoulders has been discussed in great detail in Chapter Six and our results suggest that these shoulders are either due to surfactant, with there being just one water band (the other occurring at some different frequency and not easily visible) or, one or more different types of water species. Though our results are not conclusive on this issue, some of the spectra above may make the picture slightly clearer. In particular, the gel and lamellar phase spectra of Figure 7.9, which differ in that the former shows the sharp, prominent shoulders found

FIGURE 7·9 IR SPECTRA OF DECOUPLED H_2O IN A 84·2 % C_{16}TACl MESOPHASE.

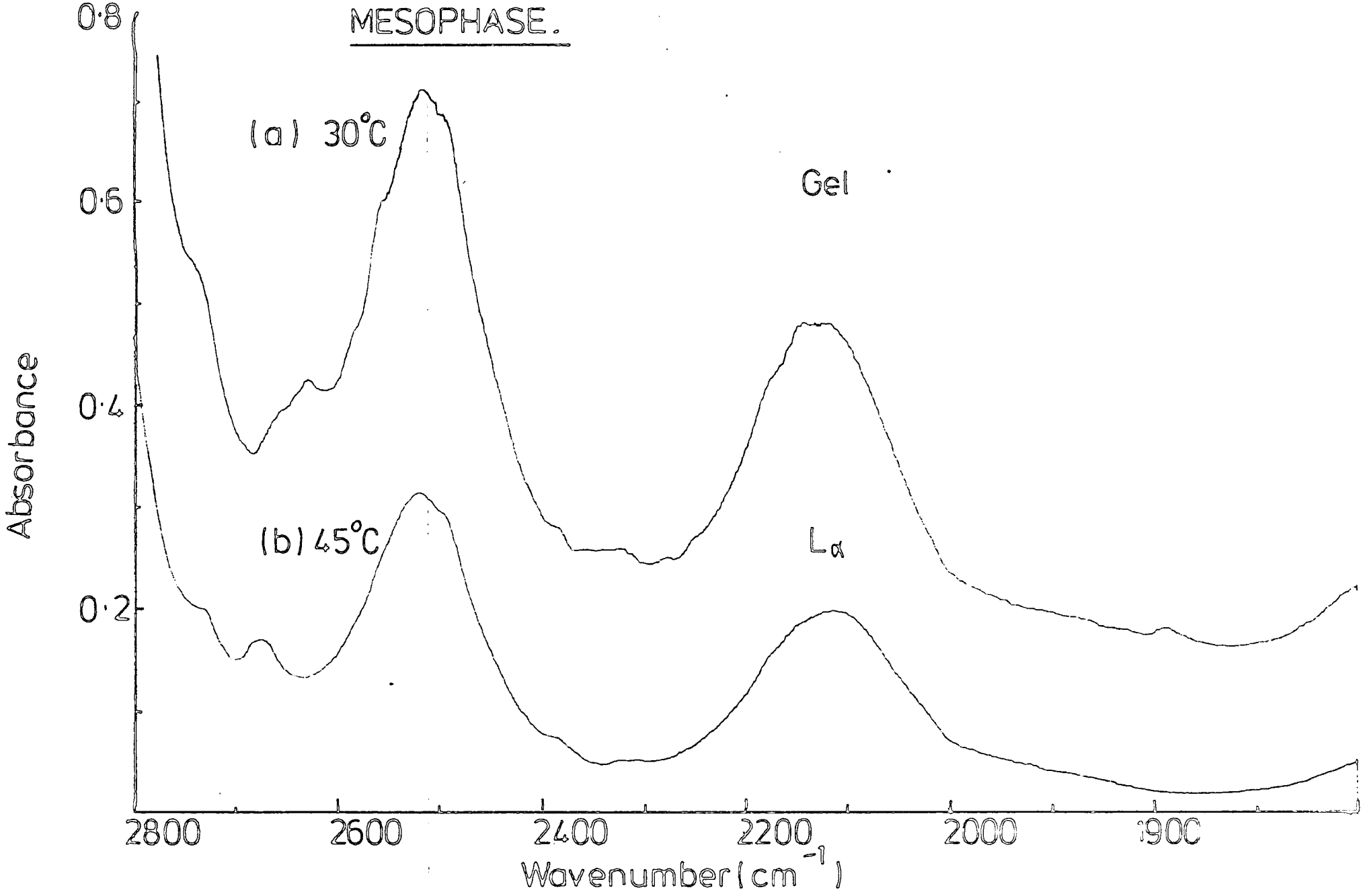

FIGURE 7·10 IR SPECTRUM OF DECOUPLED H_2O IN A 89·8% C_{16}TACl MESOPHASE AT 45°C

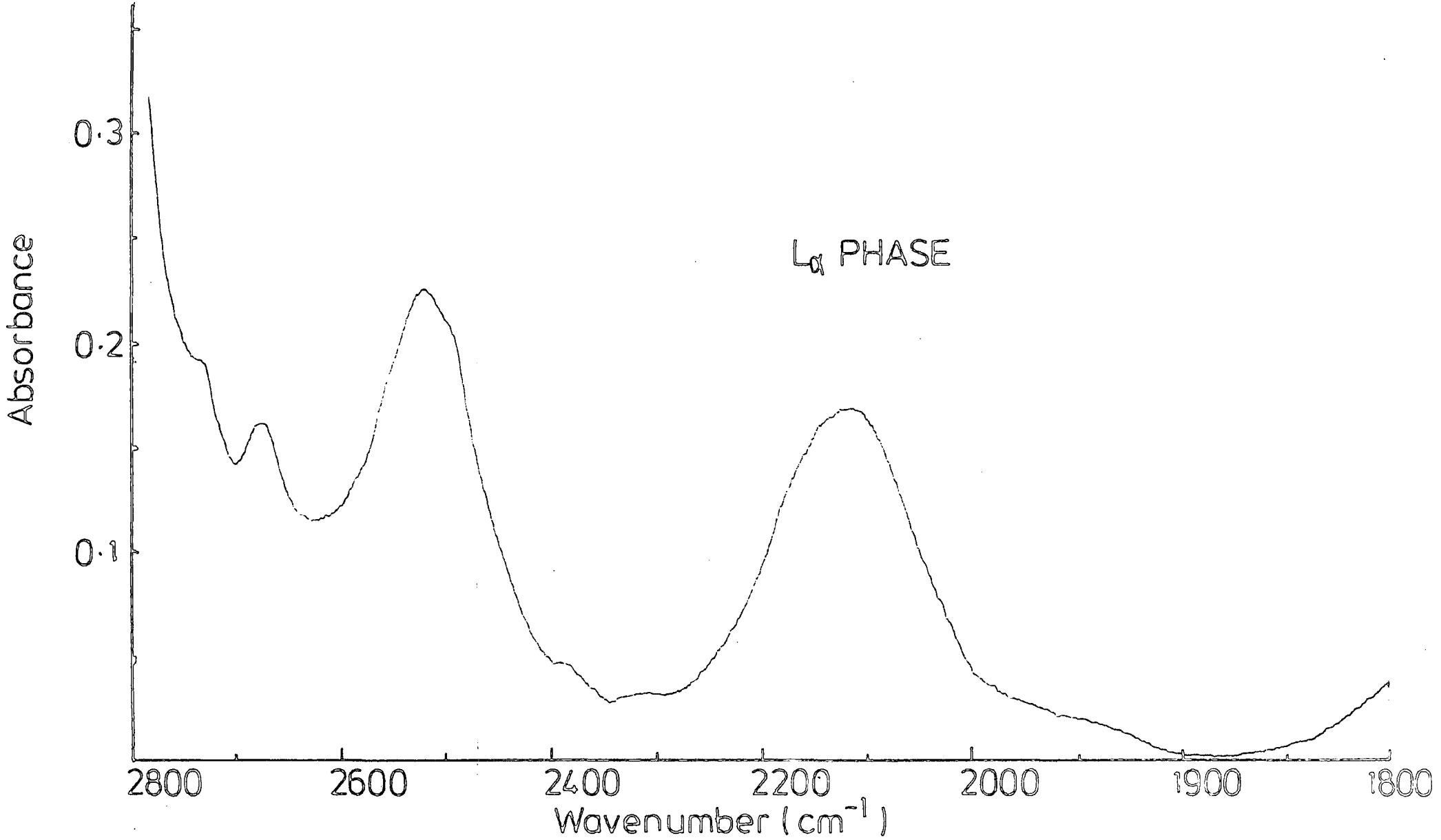

in the solid C_{12}TACl spectra in Chapter Six. Since (a) the gel and lamellar phase differ in one having an extended "solid like" hydrocarbon chain, and (b) that the solid and gel phase are similar for the same reason, one might expect these shoulders to be due to the surfactant. Though the similarity in microstructure of the water-counter ion layer in the gel and lamellar phase is a matter of contention at the moment and will be the subject of our discussion later in this section, it is expected not to change significantly. Apart from the differences in spectra on crossing the gel/lamellar phase boundary, no abrupt changes occur along the concentration range suggesting a smooth gradual perturbation of water structure.

As mentioned earlier a small band becomes quite evident at 2675 cm^{-1} in Figure 7.10. It is not observed in the low C_{16}TACl concentration spectra since the ν_s(O-D) is broad and obscures its presence. However, from about 70% C_{16}TACl (Figure 7.7), it may be measured in height relative to another band. If this peak corresponds to a water species bound at the micellar surface, and occurring at higher frequencies than "bulk" water as envisaged by Wells,[115] then its intensity relative to an internal standard, *i.e.* a surfactant band should increase. The choice of such a band is difficult in this case since no well defined surfactant absorptions occur in our spectral window. It is therefore not possible to decide whether this band is due to surfactant or not.

Figure 7.11 shows the $\Delta\nu_{1/2}$ data for $\nu_s(O\text{-}D)_{HDO}$ as a function of C_{16}TACl concentration at 30°, 45° and 60°. As the concentration is increased above about 45-50% w/w

FIGURE 7.11 THE BEHAVIOUR OF THE ν_s(HDO) BAND WIDTH AS A FUNCTION OF CONCENTRATION.

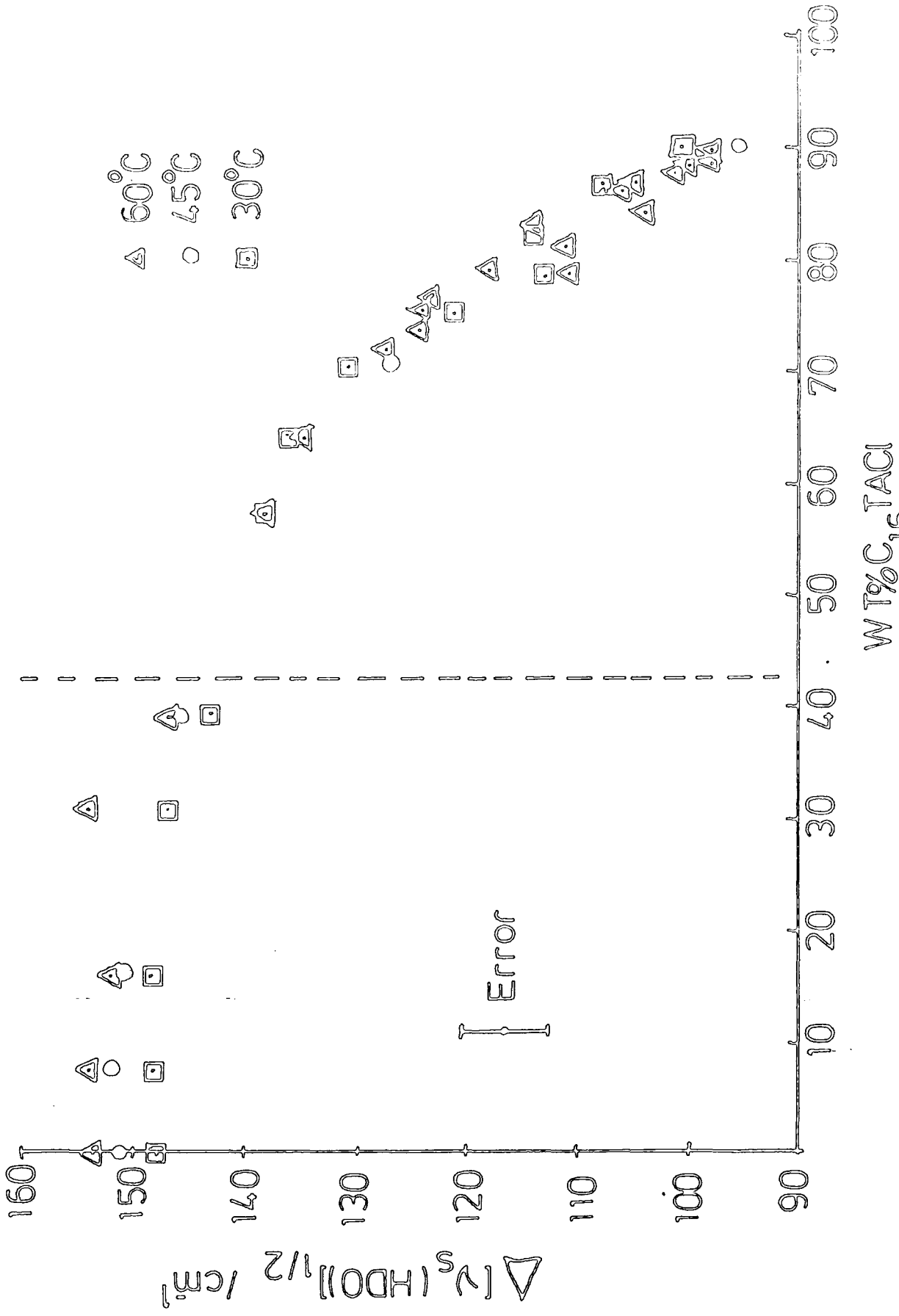

surfactant, the band widths remain independent of temperature, and show a gradual decrease. At low surfactant fractions, an increase in temperature has caused a larger bandwidth. The graph does not show phase boundaries since the data have been plotted at various temperatures and as established in Chapter Six, show no abrupt changes at phase boundaries. However, we have included the disorder-order boundary since it is independent of temperature and possibly has some relevance to our discussion. It seems as though the curve of Figure 7.11 begins to decrease more rapidly from this point. Unfortunately the disorder-order boundaries occur at approximately the same wt.% and mole ratio for C_{12}TACl and C_{16}TACl, so one cannot tell whether the effect is due to intermicellar interactions or simple micellar hydration. The temperature effect at low C_{16}TACl concentrations is probably due to the "normal bulk" water which decreases as the micelles come closer together thus reducing the difference in band widths (the bound water, which shows less H-bonding is not as sensitive to temperature). The decrease in width exhibited (at all temperatures) as the concentration is increased is consistent with the idea of a reduced number of H-bonded geometries, as discussed in Chapter Six. The results of Figure 7.11 have been plotted also as a function of water-surfactant mole ratio. Though this data is not shown here, the results are comparable over the whole concentration range. This is a very important result since it proves that the water-counter ion environment is independent of phase structure. Similarly there is no change on going from gel to lamellar phase which has been a subject of much interest in the past.[86] It therefore seems likely that individual intermicellar interactions are responsible

for the above results. In particular, the hydration force first proposed by Parsegian and others[119-121,130] shows similar behaviour when the bilayer thickness is decreased. Though we are not suggesting that our technique is measuring this hydration force, we believe that the narrowing which results from a reduced population of particular water species, is related.

The consistency in mesophase concentrations, *i.e.* lack of influence from atmospheric moisture, *etc.*, allowed the ν_{max} data for ν_s(O-D) to be plotted. Figure 7.12 shows that the shifts in ν_{max} are relatively small, though the major problem in interpreting this data is deciding whether the intensity maximum is influenced by a surfactant band. It seems unlikely for this to be the case considering the complex behaviour observed in Figure 7.12 and its similarity with the ν_{max} data of $\nu_A(H_2O)$ shown in Figure 7.15. For the time being we will therefore assume the shifts to be real. At low concentrations up to approximately 70% w/w C_{16}TACl, the frequency of ν_s(O-D) increases gradually and then unexpectedly starts to decrease. This behaviour is puzzling for two reasons:

(i) it does not follow the trend exhibited by the ν_s(O-D) band width (Figure 7.11), and

(ii) it does not show a change at the disorder-order boundary (as expected from our discussions in Chapter Six.

These results indicate that the mole ratio is the critical factor, resulting in a change in water structure when a value of 7.5 is reached. It suggests that, though some interaction between micelles does begin at the disorder-order

FIGURE 7·12 THE BEHAVIOUR OF THE ν_s(HDO) FREQUENCY MAXIMUM AS A FUNCTION OF CONCENTRATION.

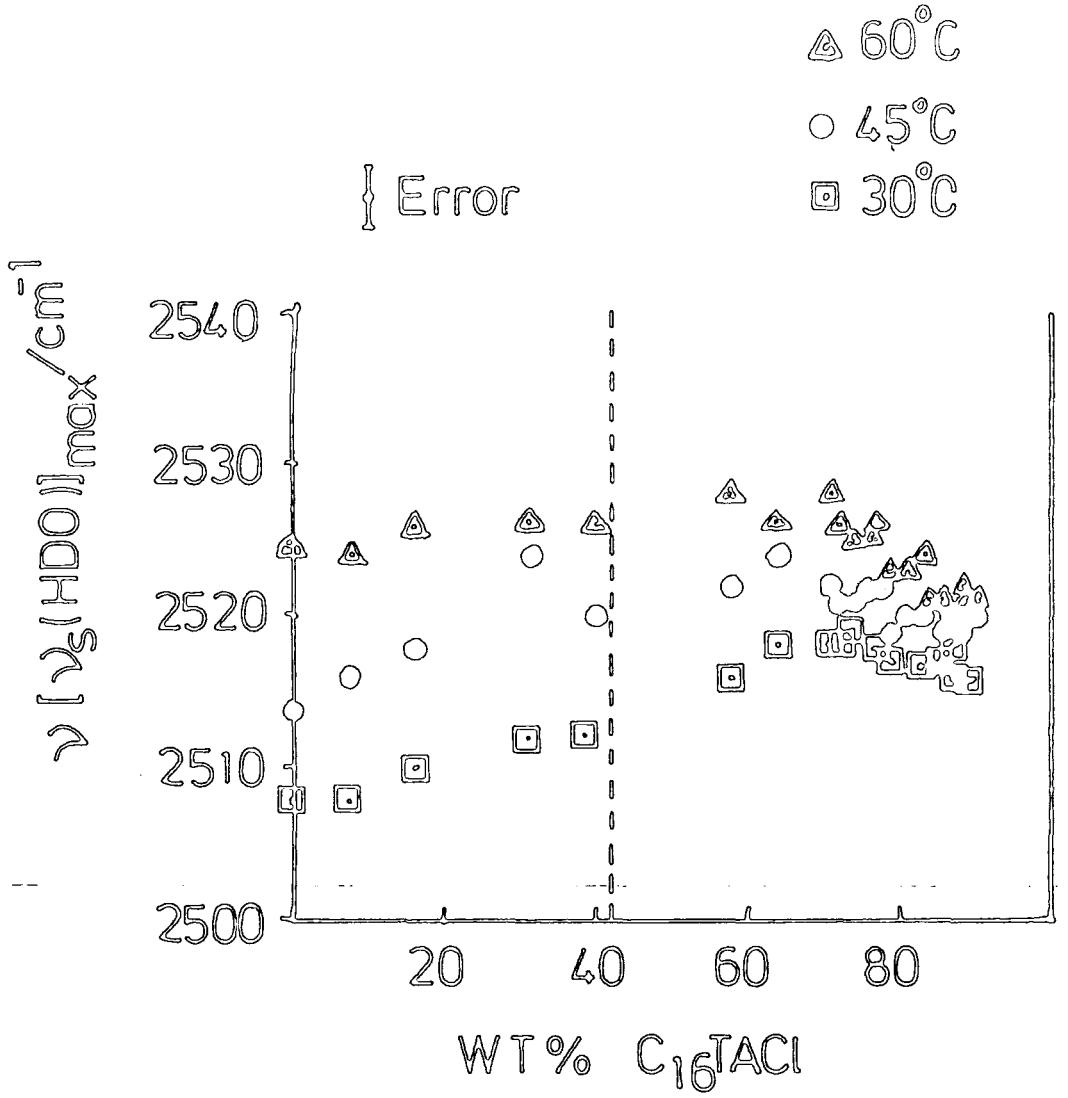

boundary (see $\Delta\nu_{1/2}$ data), a consistent alteration in water structure occurs for both C_{12}TACl and C_{16}TACl. At low C_{16}TACl concentrations, less than 70% w/w, the micelles and counter ions have an overall effect of increasing the ν_s(O-D) force constant. This may occur by simple disruption of inter-molecular H-bonding of water molecules. Above 70% w/w C_{16}TACl there is a decrease in the force constant and a corresponding decrease in frequency, possibly indicating an increase in H-bonding. One might imagine that the value of 7.5, for the water/surfactant mole ratio where the "discontinuity" occurs, corresponds to a minimum hydration number for both cation and anion. A possible interpretation therefore may be to postulate a simultaneous interaction of water molecules with both cation and anion resulting in an overall loss of electron density from the O-D bond. The situation envisaged is illustrated below.

Figure 7.13 Idealized diagram of possible structure of Mesophase at high C_{16}TACl Concentrations

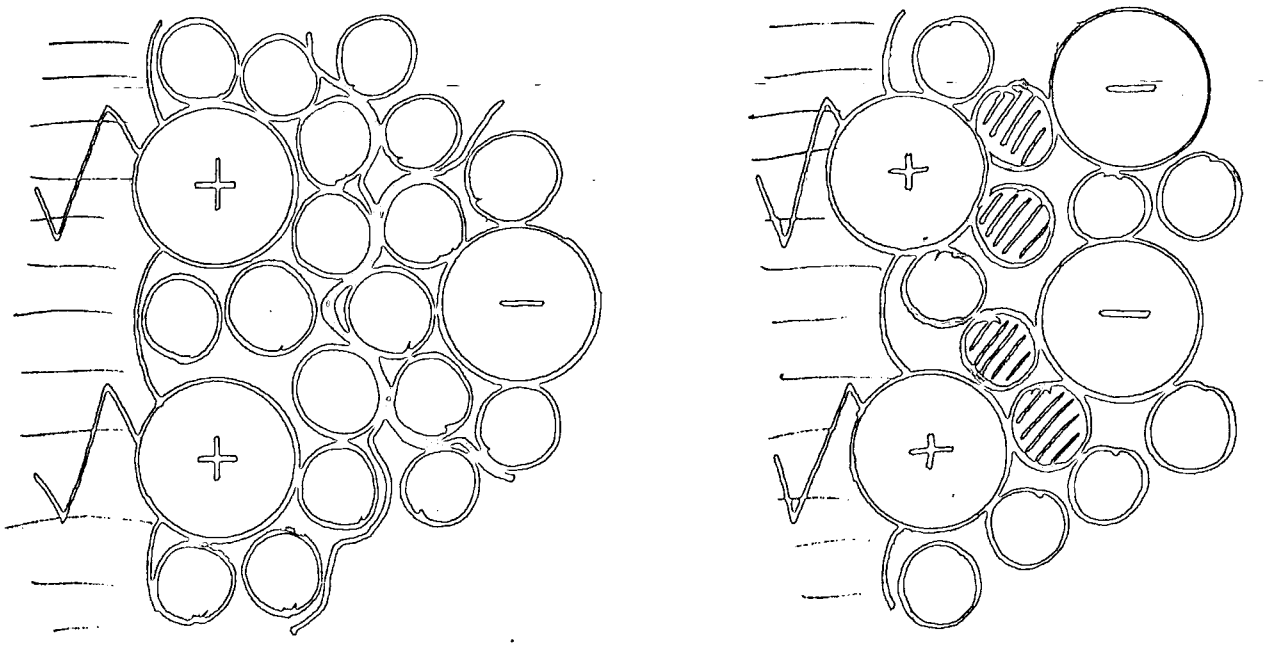

Mole Ratio >7.5

Mole Ratio <7.5

The heavily shaded water molecules of Figure 7.13 represent the simultaneous interaction of anion and cation which eventually correspond to an initial boundary water layer mentioned earlier. Other interpretations are possible, for example one may envisage a permanent initial boundary water layer which becomes further perturbed as the counter ions are drawn closer to their stoichiometric cations. It is difficult to say exactly what the situation might be, especially since it is not clear how many water species are observed in our spectra. The $\Delta\nu_{1/2}$ data are consistent with the above discussion since the number of H-bonded water species will decrease as the concentration of amphiphile increases.

The ν_{max} data of Figure 7.12 is not consistent with the behaviour of the far ir spectra of $C_{12}TACl$. If we assume that the systems are comparable, reasonable from the evidence so far observed, then the decrease in frequency of ν_s(O-D) at high concentrations (*i.e.* an increase in H-bonding) is contradictory to what is observed with ν_T in the far ir (this shifts to lower frequencies and suggests a decrease in H-bonding). There are several possibilities:

(i) That the shift of ν_s(O-D) at high amphiphile concentrations is independent of H-bonding strength, instead possibly due to electrostatic interactions with the surfactant environment.

(ii) That the band observed in the far ir is not a ν_T water band.

(iii) That the shift of ν_s(O-D) at high amphiphile concentrations is influenced by a surfactant band.

(iv) That the $\nu_A(H_2O)$ band has been mis-assigned.

Option (iii) seems unlikely since analogous behaviour has been observed with the $\nu_A(H_2O)$ data of Figure 7.15. The possibility of (ii) being correct is also highly improbable if one considers that the ν_T bands in the far ir also shift with concentration, something which would not occur if this were a surfactant band. Options (i) and (iv) appear more consistent with the evidence presented, particularly if one considers that hydrogen bonding is a complicated interaction. The assignment of $\nu_A(H_2O)$ by Williams[18] almost twenty years ago may be incorrect and further work will be required to establish its true origin.

Figure 7.14 shows the band width dependence of $\nu_A(H_2O)$ on $C_{16}TACl$ concentration at 30°, 45° and 60°C. The curves are very similar to those obtained for $\nu_s(O\text{-}D)_{HDO}$ of Figure 7.11, though in this case the band is initially much broader (its breadth being related to its origins as a combination mode). As with the $\nu_s(O\text{-}D)$ species the band initially resembles that of water. Beyond the disorder-order boundary a decrease in breadth is observed, which as before, has been assigned to a decrease in the distribution of different H-bonded water species. All the data show a small dependence on temperature, with $\nu_A(H_2O)$ broadening as this is increased. A comparison of this data with that of $C_{12}TACl$ of Figure 6.19 (mole ratio units) has again demonstrated that the behaviour in the two systems is very similar.

As with $\nu_s(O\text{-}D)$, the frequency maximum was measured for the $\nu_A(H_2O)$ band under the same conditions of temperature. The results are shown in Figure 7.15 and appear to mirror the

FIGURE 7·14 THE BEHAVIOUR OF THE $\nu_A(H_2O)$ BAND WIDTH AS A FUNCTION OF CONCENTRATION.

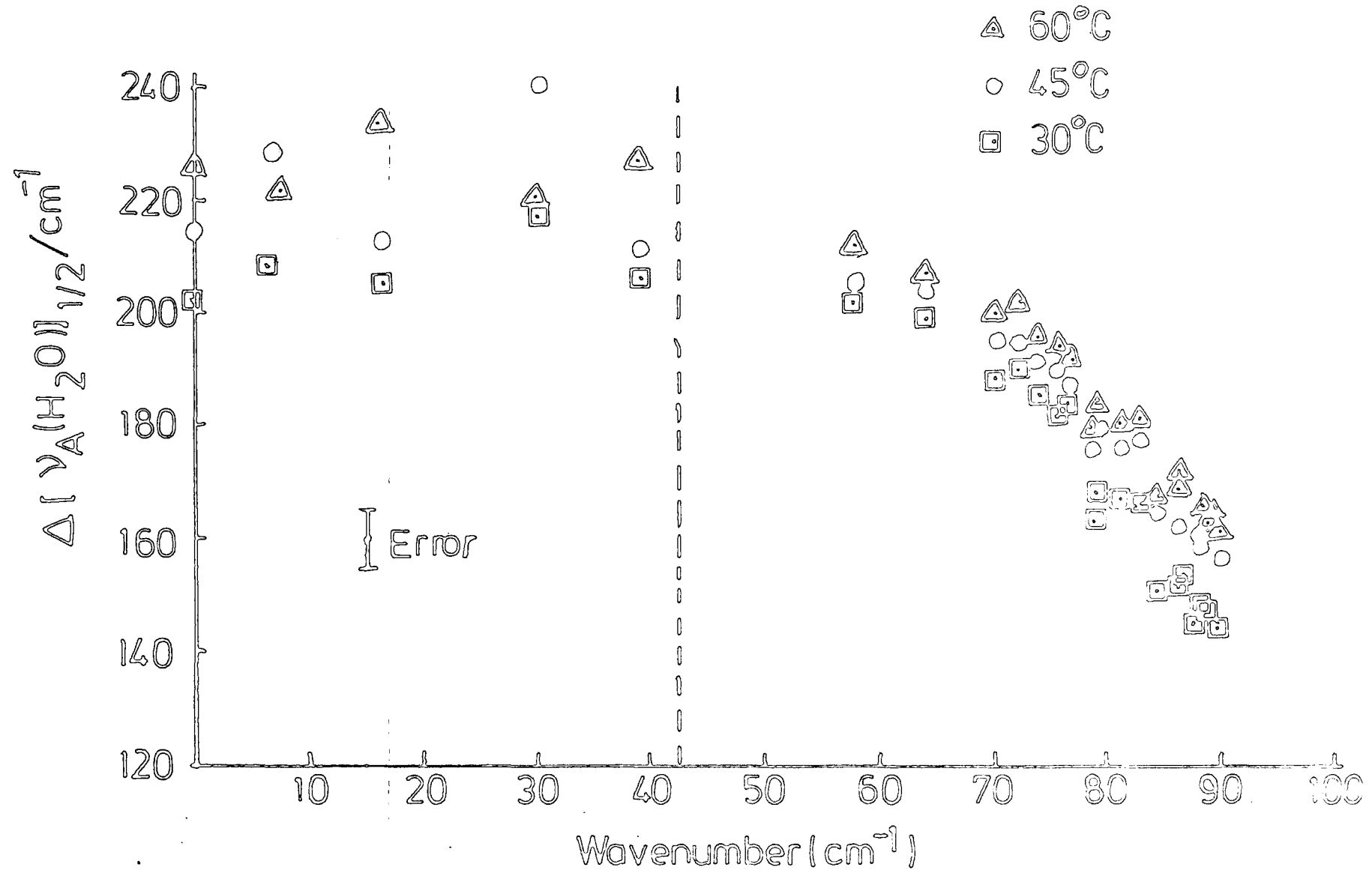

FIGURE 7·15. THE BEHAVIOUR OF THE $\nu_A(H_2O)$ FREQUENCY MAXIMUM AS A FUNCTION OF CONCENTRATION AT 30°, 45° AND 60 C°.

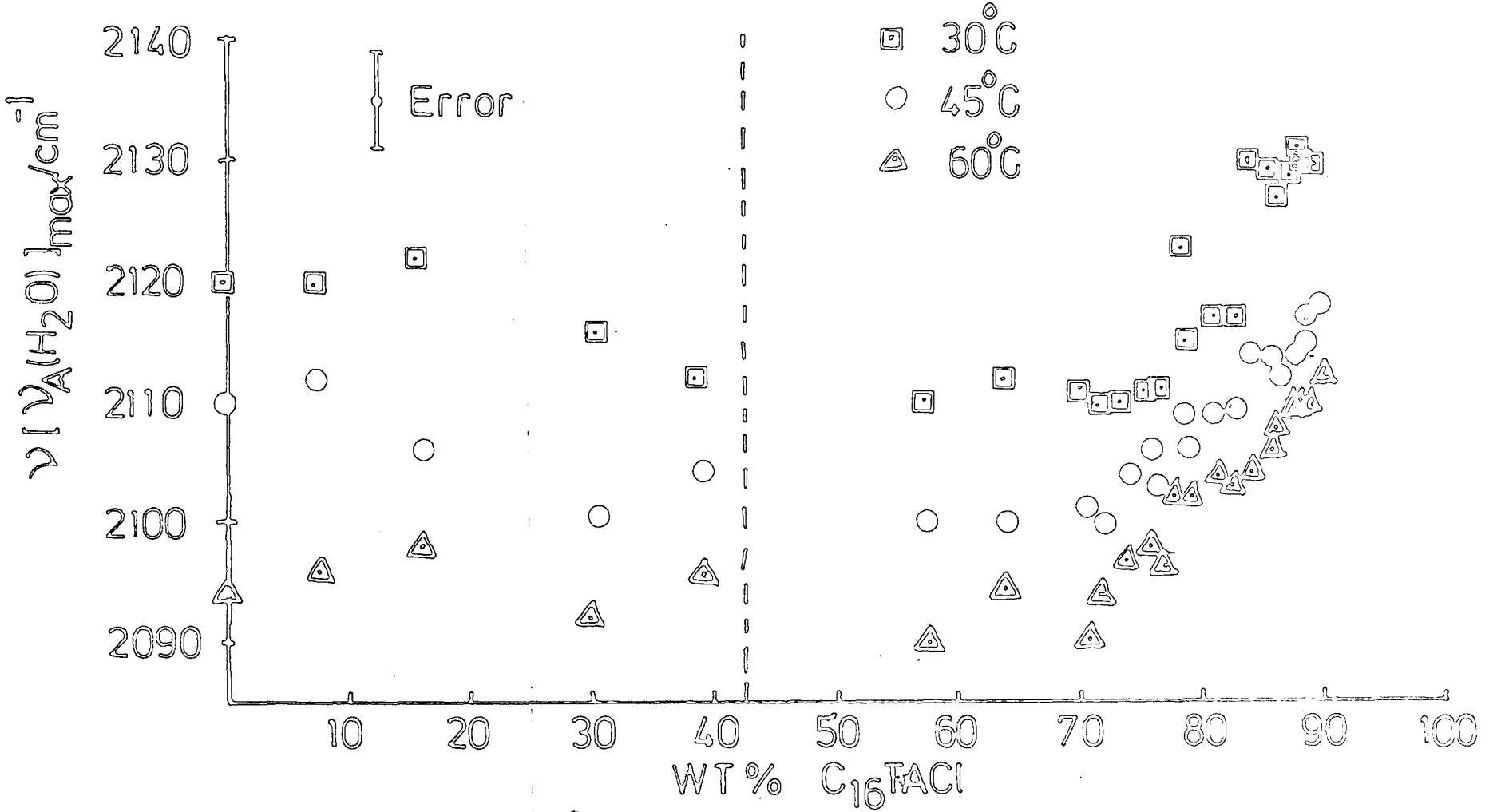

behaviour of the ν_s(O-D) frequency maxima in Figure 7.12. The temperature dependence of this data suggests that a decrease in frequency is paralleled with a decrease in H-bonding. Therefore, the results of Figure 7.15 indicate that at low C_{16}TACl fractions (below ≈70% w/w C_{16}TACl) an increase in concentration causes a decrease in H-bonding. However, though this data is entirely consistent with the ν_s(O-D) results of Figure 7.12, it leaves several questions unanswered. Previously, we assumed that any frequency shift displayed by $\nu_A(H_2O)$ is probably derived from a combination of ν_L and ν_T since ν_2 is thought to be independent of H-bonding. If this is correct, then the trends observed in the ν_{max} data of Figure 7.15 suggest that ν_L is more sensitive in these systems. Above 70% w/w C_{16}TACl the frequency maximum of $\nu_A(H_2O)$ increases implying that H-bonding is increasing. This latter statement is questionable since;

(a) one would expect a decrease in H-bonding in parallel with the $\Delta\nu_{1/2}$ data and

(b) that the far ir shift in ν_T of Chapter Six indicates that H-bonding is decreasing at high concentrations.

These points would indicate that both intermolecular components which constitute $\nu_A(H_2O)$ would cause a shift in the opposite direction. A possible answer to these queries is to assume the presence of a strong perturbing electrostatic interaction which starts to become evident at a mole ratio of 7.5 (at lower surfactant concentrations the expected trend is observed). This interaction, as mentioned earlier in this section when discussing the shift in ν_s(O-D), perturbs the O-H force constant and reduces electron density of this bond.

Though ν_2 is independent of H·bonding strength, it may very well be influenced by the strong 3-dimensional interaction displayed by the micellar surface and corresponding counter ions.

Figure 7.16 shows the $\nu_A(H_2O)/\nu_s(O\text{-}D)$ absorbance (determined by triangulation) ratio for both $C_{12}TACl$ and $C_{16}TACl$. The $C_{16}TACl$ data shows the familiar curved dependence as the mole ratio decreases. The data for $C_{12}TACl$ are seen to be translated slightly upwards from the $C_{16}TACl$ results. This behaviour is easily explained if we consider that two D_2O solutions were used. Though this would affect the $\Delta\nu_{1/2}$ and ν_{max} data it would cause a proportionate change in the two curves. Inspection of Figure 7.16 does, in fact, show a parallel change, with the 5% v/v D_2O solution ($C_{16}TACl$ data) lying below the 4% v/v D_2O solution of $C_{12}TACl$.

The curved behaviour of this ratio for $C_{16}TACl$ shows that the disappearance of the $\nu_s(O\text{-}D)$ band is also expected at low water/surfactant mole ratios. As mentioned in the discussions of Chapter Six this intensity change may be interpreted as arising from a depletion of outer layers of boundary water. The $\nu_A(H_2O)$ band remaining effectively proportional to H_2O concentration since its breadth and complicated origin may cause a superimposition of different water bands.

7.4 Far IR Spectroscopic Investigation of the $C_{16}TACl$-Water System

The $C_{12}TACl$ and $C_{16}TACl$ results obtained in the mid ir have been observed to be identical when plotted in mole ratio

FIGURE 7·16. A COMPARISON OF THE $\nu_{A(H_2O)}$/ $\nu_{S(HDO)}$ ABSORBANCE RATIO FOR C_{12}TACl AND C_{16}TACl.

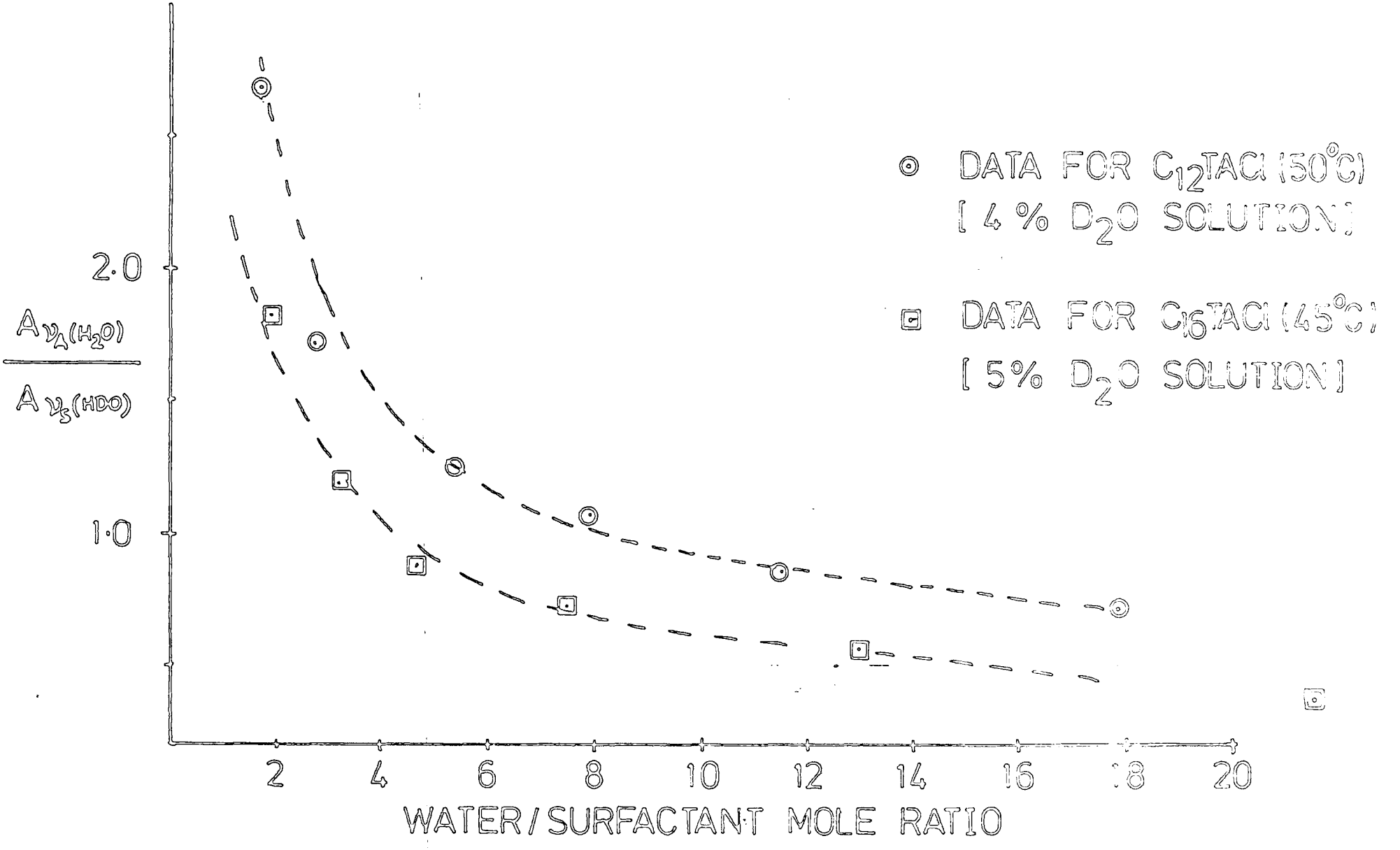

concentration units. We have interpreted this behaviour by postulating an independence of water microstructure on phase behaviour. To obtain further evidence we have recorded several far ir spectra of water in C_{16}TACl mesophases. In particular we have studied the H_1 + gel/Intermediate and gel/L_α phase boundaries of two samples containing 75.8 and 88.8% w/w C_{16}TACl, respectively. These boundaries were found to occur at 37^o and 40^o by optical microscopy.

Figure 7.17 shows the spectrum of a 75.8% w/w C_{16}TACl sample at 23^{o}C. It is almost identical to those observed for some C_{12}TACl mesophases (*e.g.* see Figures 6.26 and 6.29) of Chapter Six. Two bands are clearly visible, occurring at approximately 120 cm^{-1} and 55 cm^{-1}. They have been previously assigned to ν_T of an initial boundary water species and an intermolecular bending mode, respectively. This sample was then heated over the phase boundary to 45^{o}C with little apparent change (see Figure 7.18). Similarly, Figures 7.19 and 7.20 show the 23^o and 45^{o}C spectra of the 88.8% C_{16}TACl sample. Again, the spectra show no apparent change on crossing the gel/lamellar phase boundary. These results therefore support the idea that the microstructure of water in the above is phase independent.

7.5 Raman Spectroscopic Investigation of the C_{16}TACl-Water System

7.5.1 The C-C Skeletal Stretching Region

Figure 7.21 shows the Raman spectrum of crystalline C_{16}TACl at 45^{o}C between 650 and 1200 cm^{-1}. The assignment of bands illustrated in this figure are listed in Table 7.1.

FIGURE 7·17 FAR IR SPECTRUM OF A 75·8 % C_{16}TACl MESOPHASE.

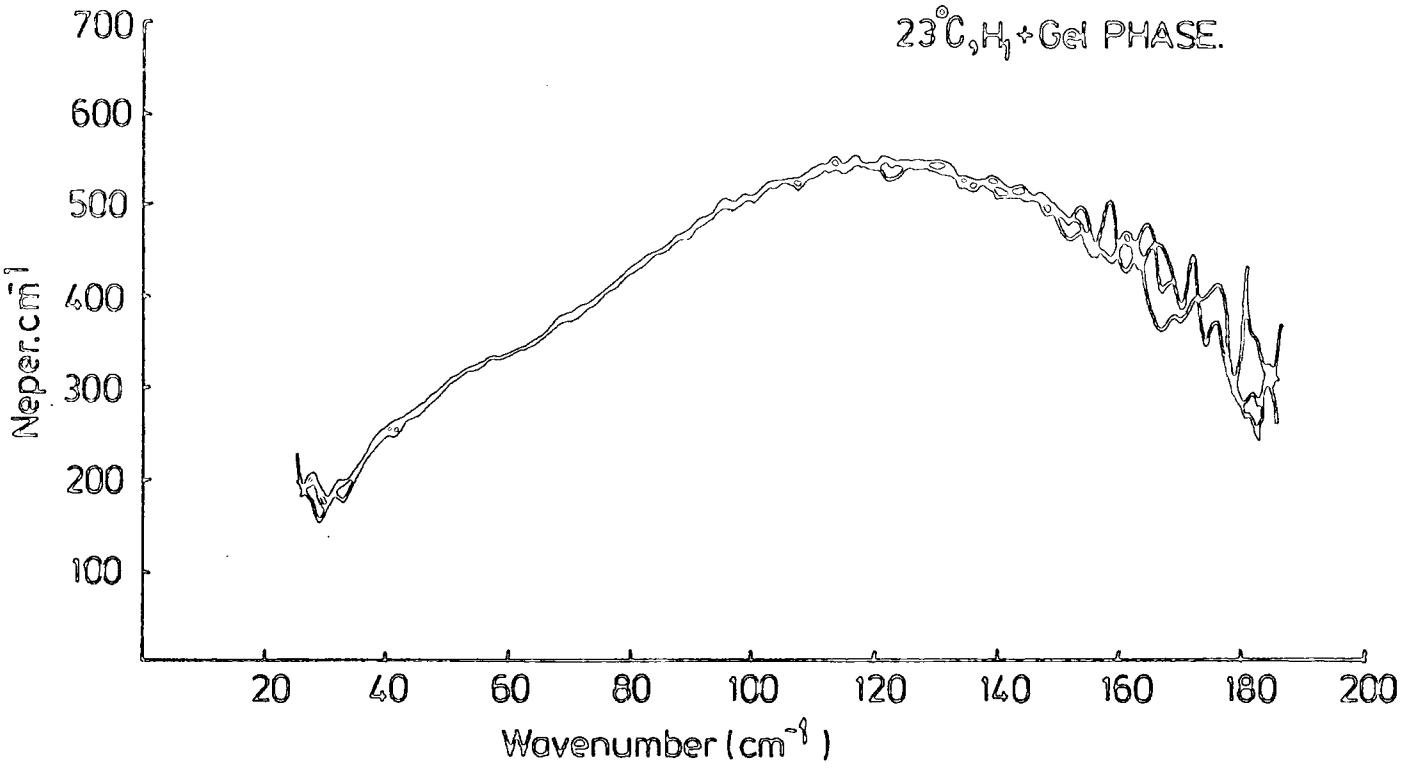

FIGURE 7·18. FAR IR SPECTRUM OF A 75·8% C_{16}TACl MESOPHASE.

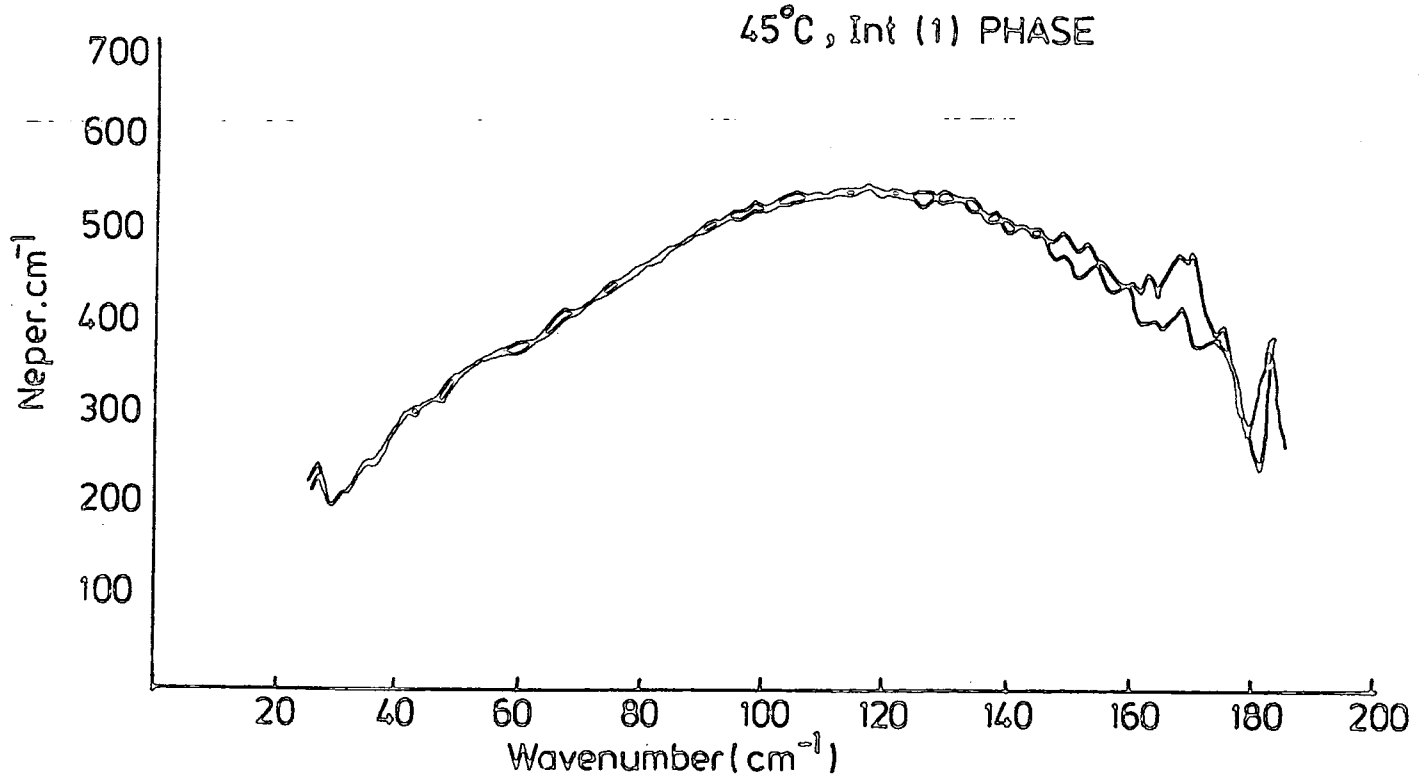

FIGURE 7·19. FAR IR SPECTRUM OF A 88·8% C_{16}TACl MESOPHASE.

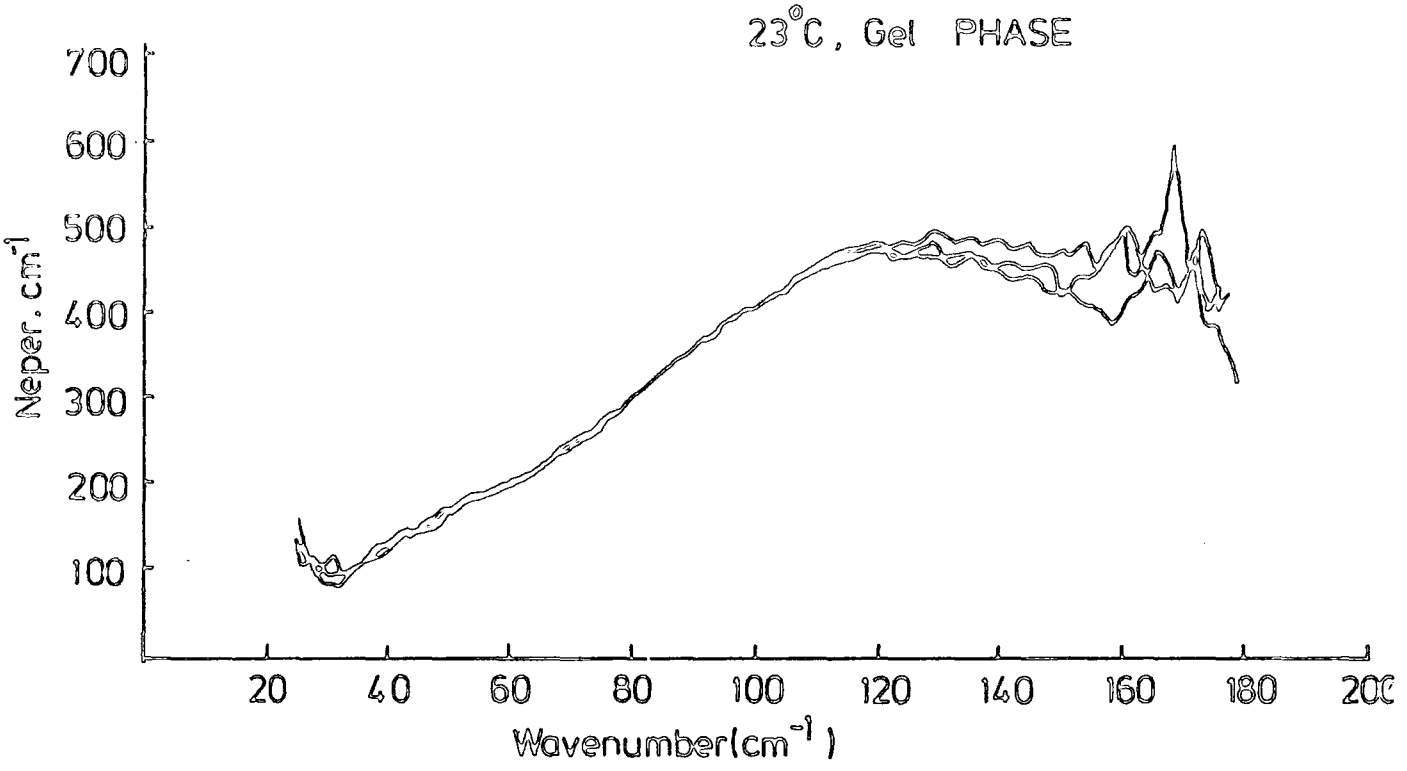

FIGURE 7·20. FAR IR SPECTRUM OF A 88·8% C_{16}TACl MESOPHASE

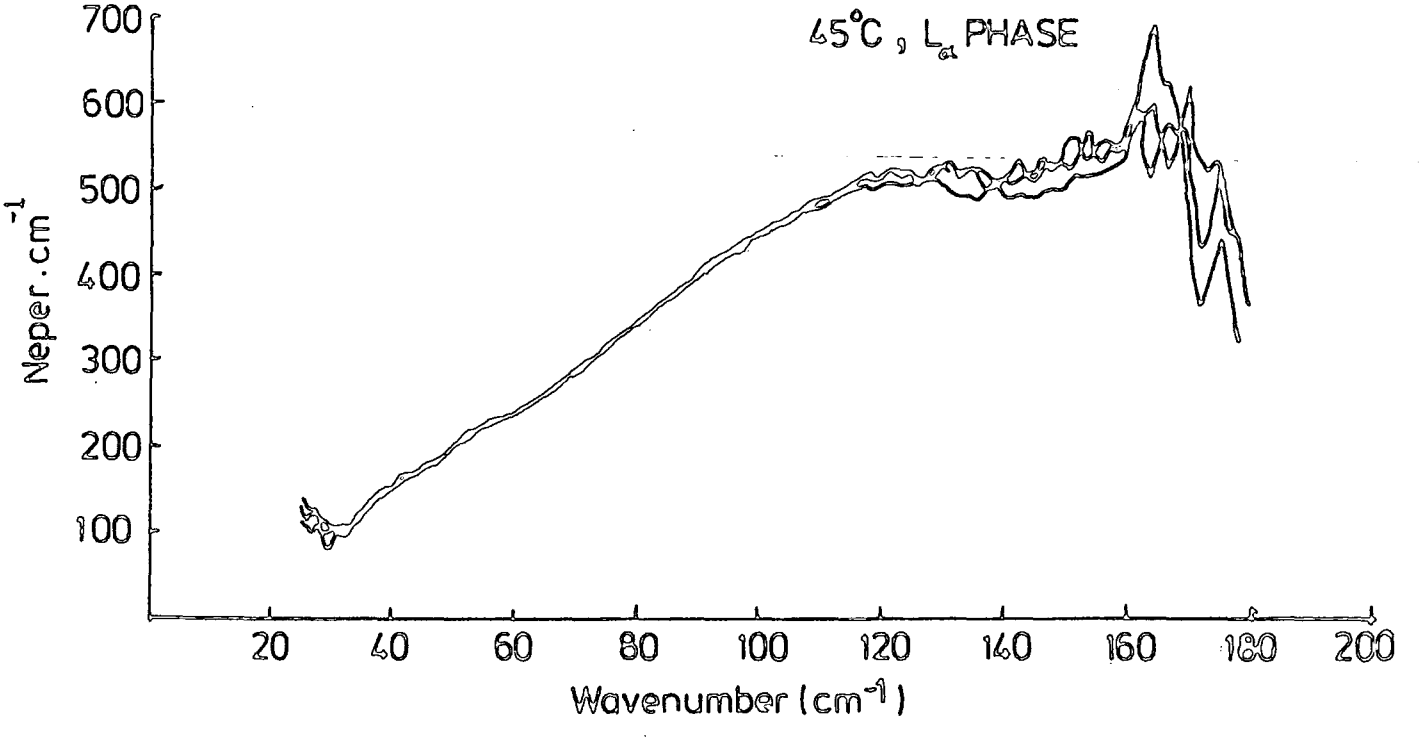

FIGURE 7·21 RAMAN SPECTRUM OF CRYSTALLINE $C_{16}TACl$ AT 45°C.

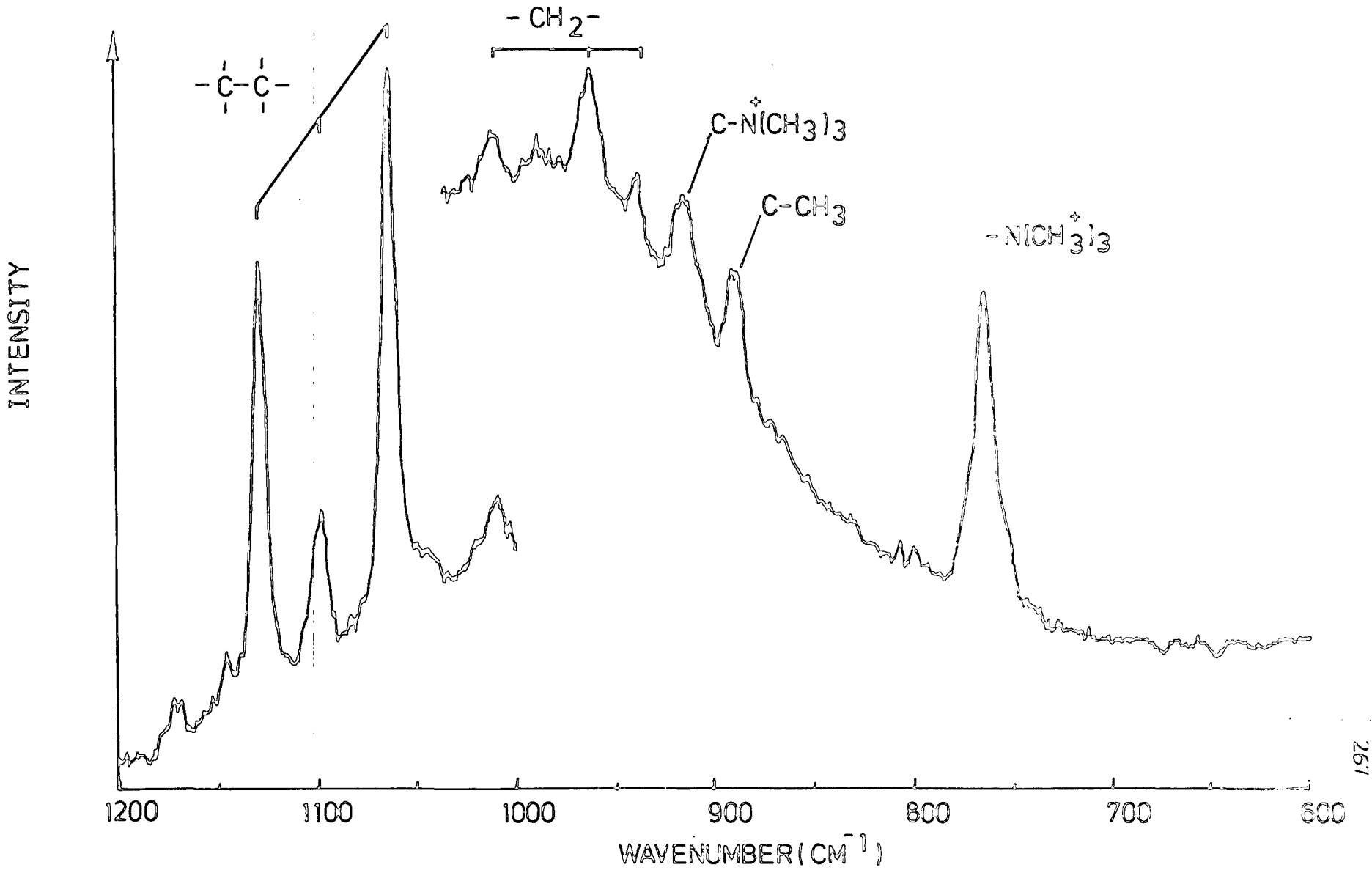

TABLE 7.1 Assignments of Solid $C_{16}TACl$ Raman Bands at 45°C

Wavenumber (cm^{-1})	Assignment*
763	CH_3 rock from $N^+(CH_3)_3$ group
889	CH_3 rock (terminal methyl)
915	C-N^+ stretch
939	CH_2 rock
962	
1011	
1064	C-C symm. stretch + CH_2 wag.
1098	C-C stretch, crystalline
1130	C-C asymm. stretch + CH_2 wag.

* Assignments reproduced from reference 41.

In general all the bands observed originate from the hydrocarbon chain with the exception of two head group vibrations at 915 and 762 cm^{-1}, corresponding to the C-N^+ stretch and CH_3 rocking of $N^+(CH_3)_3$, respectively.[41] These bands will be discussed later but the peaks of interest here occur between 1000 and 1200 cm^{-1} and are due to skeletal C-C stretching vibrations. As mentioned in Section 6.5 they may, to some extent, be used to gauge the trans/gauche ratio in these systems. However, this parameter is only semi quantitative since intramolecular coupling causes complex intensity changes in this region.[122] In this section our aims are to make a qualitative comparison of the C-C trans/gauche behaviour in the various mesophases.

The spectra of three samples are shown in Figures 7.22a, b and c. They correspond to a 43.4% hexagonal phase sample at 30°C, a 79.5% hexagonal and gel biphasic sample, and finally the same sample heated to 45°C to form the intermediate phase (see Figure 7.1). In the skeletal region four bands are observed, with the most important occurring at 1130, 1080 and 1060 cm^{-1} (all ±5 cm^{-1}). The 1130 and 1060 cm^{-1} bands have been assigned to the asymmetric and symmetric C-C stretches, respectively and their intensities have been interpreted as being due to trans bonds. The 1080 cm^{-1} band, which occurs in the mesophase spectra only, is known to be strongly influenced by intramolecular coupling and can, in some part, be interpreted as being due to gauche bonds.[131] Thus the relative intensities of these bands may be used as a qualitative measure of the trans/gauche ratio. The absence of the 1080 cm^{-1} band in the solid therefore indicates the lack of gauche bonds in crystalline C_{16}TACl. The mesophase spectra of Figure 7.22 are all similar and show an intense 1080 cm^{-1} band with a weak 1130 cm^{-1} species. This is evidence for the presence of gauche conformations with fluid hydrocarbon chains. The spectrum of Figure 7.22b however, is slightly different in that the relative intensity of the 1060 cm^{-1} peak is greater than in the other mesophases. This is due to the presence of gel phase (see below).

Figure 7.23, shows an 87.5% w/w C_{16}TACl sample at 30 and 45°C. At these temperatures the sample exists in the gel and lamellar phase, respectively.[86] The spectra are quite different from each other with the gel phase sample (Figure 7.23b) looking very much like the crystalline surfactant

FIGURE 7·22 RAMAN SPECTRA OF SOME C_{16}TAC1 MESOPHASES.

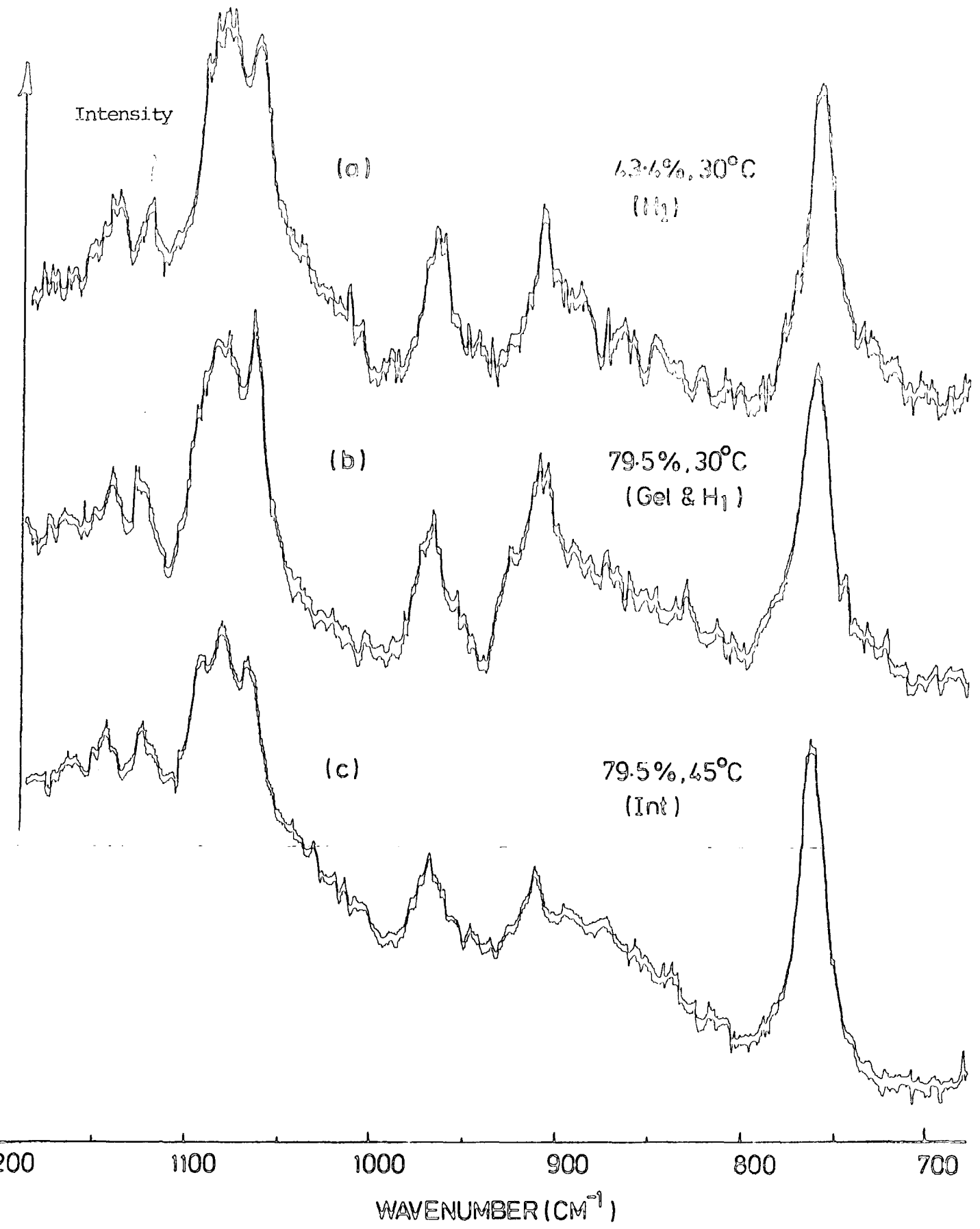

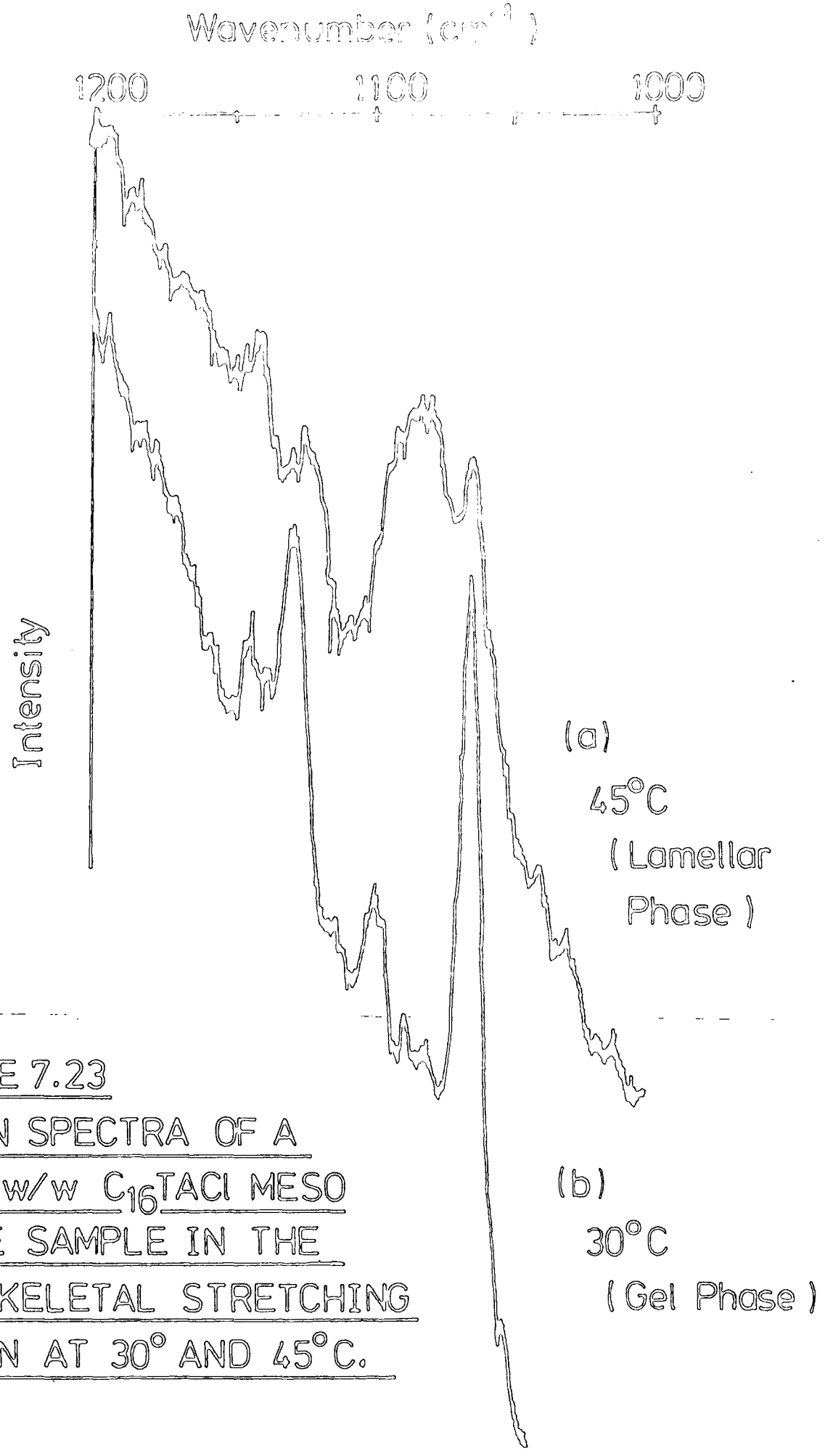

FIGURE 7.23
RAMAN SPECTRA OF A 87·5 %w/w C_{16}TACl MESO-PHASE SAMPLE IN THE C–C SKELETAL STRETCHING REGION AT 30° AND 45°C.

spectrum. This is to be expected since the gel phase is known to have hydrocarbon chains in a "solid like" configuration.[79,80] For the same reason the intensity of the 1080 cm^{-1} band is less intense in the H_1 + gel biphasic spectrum of Figure 7.22b. On heating, the 87.5% $C_{16}TACl$ melts to the lamellar phase with the result of a melting of the hydrocarbon chains. Consequently, the spectrum of Figure 7.23a shows an identical increase in the 1080 cm^{-1} species as found in the H_1 and intermediate phase spectra. A comparison of the I_{1130}/I_{1060} bands ratio has been made between the above gel phase spectrum and one of the solid at 30°C. The value for the solid (0.87) is larger than that of the gel (0.49) at the same temperature. Though some intramolecular coupling will be observed, these ratios suggest that there may be some residual gauche conformations in the gel phase. Unfortunately no spectra in this region were obtained for a mesophase in the V_1 cubic phase. From our results in Chapter Six we expect there to be no change from that observed in the H_1, intermediate and L_α phases.

7.5.2 The C-H Stretching Region

The results of Chapter Six, using the 2800-3100 cm^{-1} stretching region, showed novel behaviour at several isotropic/anisotropic phase boundaries. A measurement of the I_{2880}/I_{2850} intensity ratio across the concentration range revealed that this value was larger in anisotropic phases. Though an initial interpretation may have been to postulate changes in the trans/gauche ratios, we observed little change in the skeletal stretching region (with the exception of the gel phase).

We therefore decided that the intensity changes are likely to result from increased lateral interactions in the anisotropic phases. This interpretation based on careful consideration of Fermi resonance effects, is by no means completely unambiguous. It is puzzling to understand why there should be such abrupt changes at these phase boundaries since one would expect a gradual monotonic decrease in gauche conformers to facilitate changes in micelle surface curvature as the concentration is increased.

In this section we will examine the spectra crosss the whole concentration range with particular emphasis on the behaviour at phase boundaries. In this way we will be able to decide whether the effects previously observed are consistent with previous results and to categorize the effects shown by the intermediate phase. From the skeletal stretching region we have already established that no apparent changes occur in any of the phases (except the gel and crystalline surfactant samples) suggesting small effects, if any, on the gauche-trans equilibrium. The crystal and gel phase spectra are shown in Figures 7.25b and c. As expected these are different from the remaining mesophase samples since both exhibit varying degrees of hydrocarbon chain immobility (the gel phase showing slightly more gauche conformers). In this case the behaviour is well documented and we have assumed the spectral changes to be derived from changes in the trans/gauche equilibrium.[118] A selection of spectra obtained at various temperatures and phases are shown in Figures 7.24 and 7.25. The results of the I_{2880}/I_{2850} ratio at 30°C have also been plotted as a function of concentration in Figure 7.26. The figure, which has the approximate phase boundaries marked,

FIGURE 7.24 RAMAN SPECTRA OF SOME C_{16}TAC MESOPHASES IN THE C-H STRETCHING REGION.

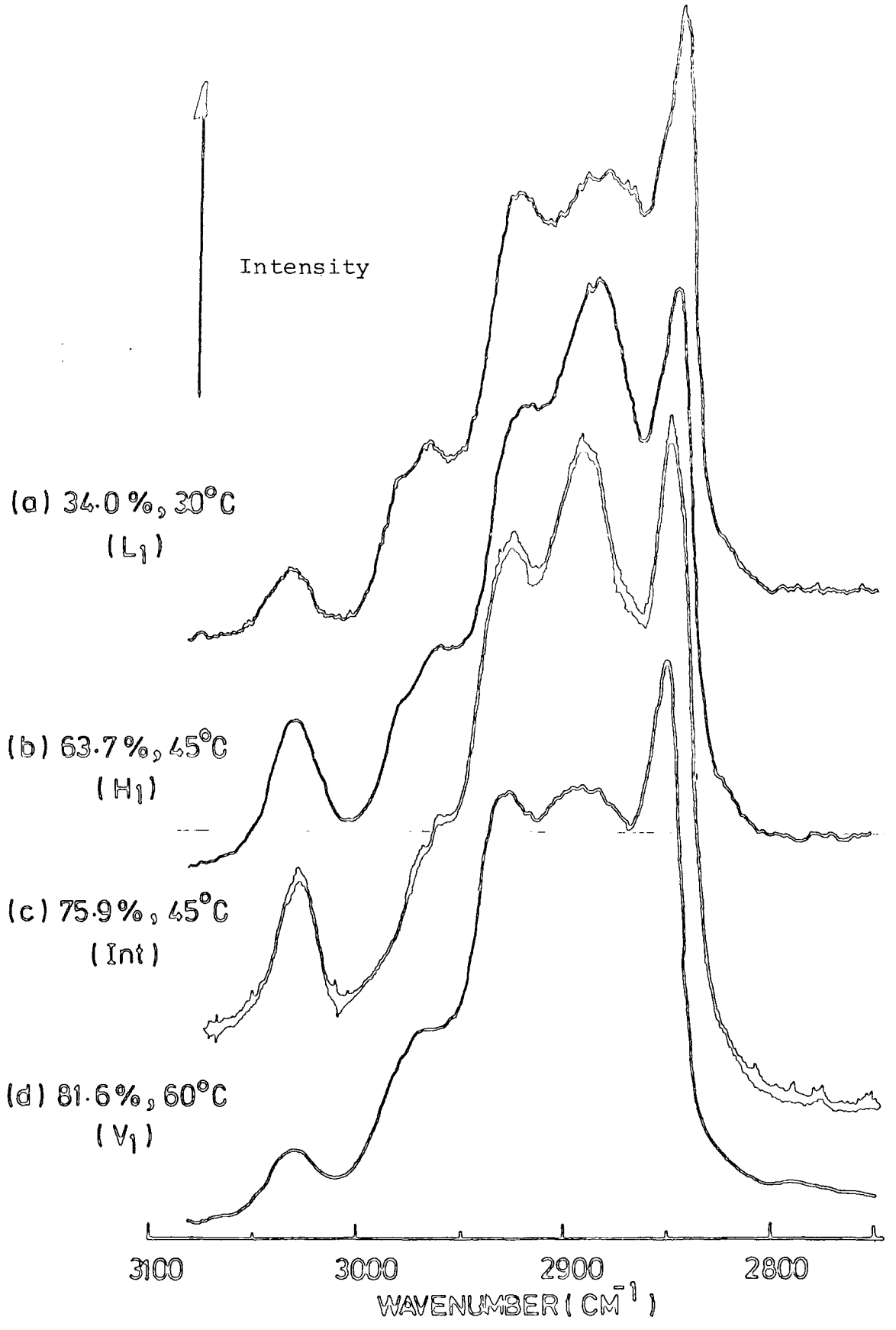

FIGURE 7·25 RAMAN SPECTRA OF SOME C_{16}TACl MESOPHASES IN THE C-H STRETCHING REGION.

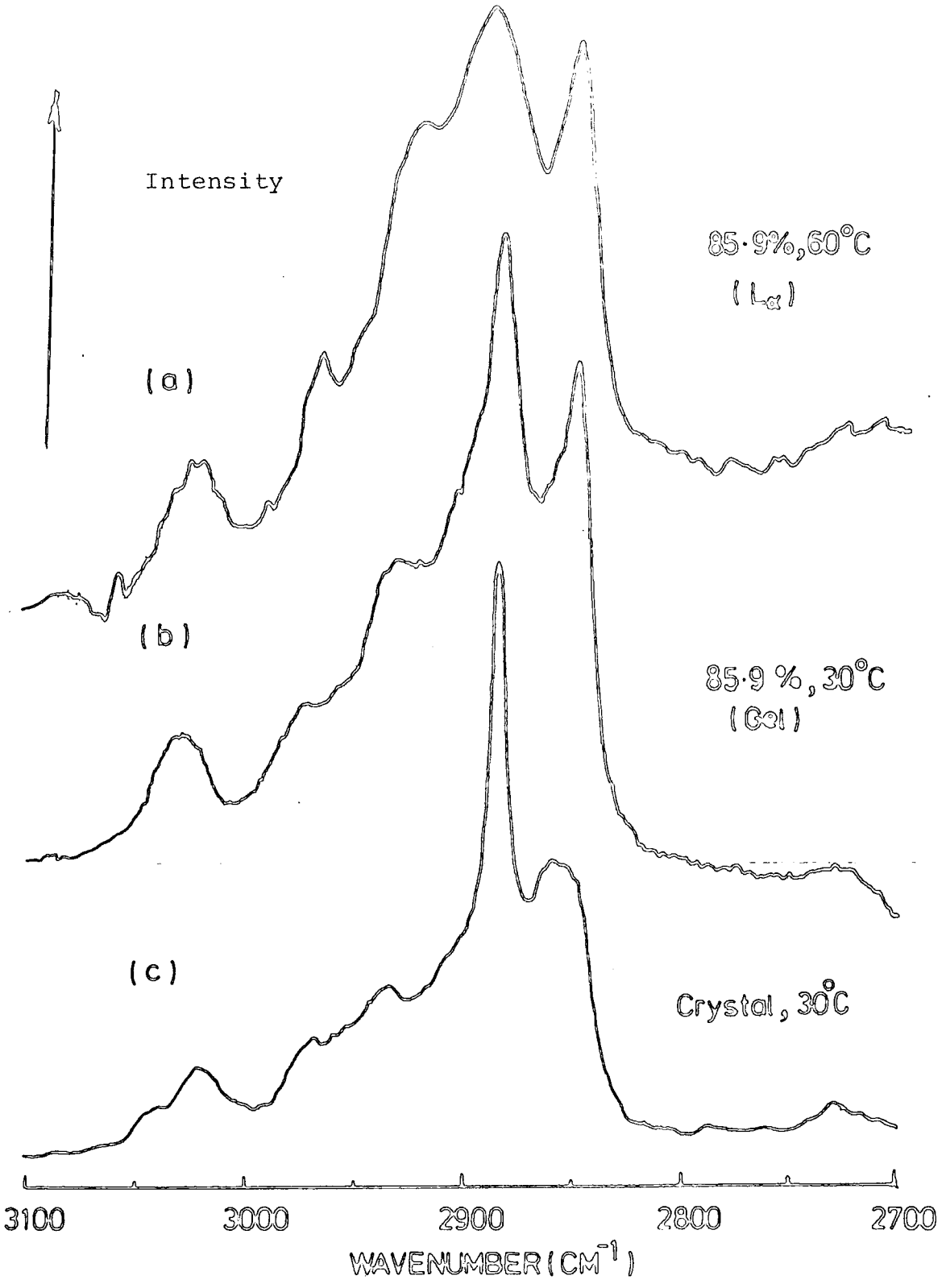

FIGURE 7·26 THE BEHAVIOUR OF THE I_{2880}/I_{2850} RATIO AS A FUNCTION OF CONCENTRATION AT 30°C.

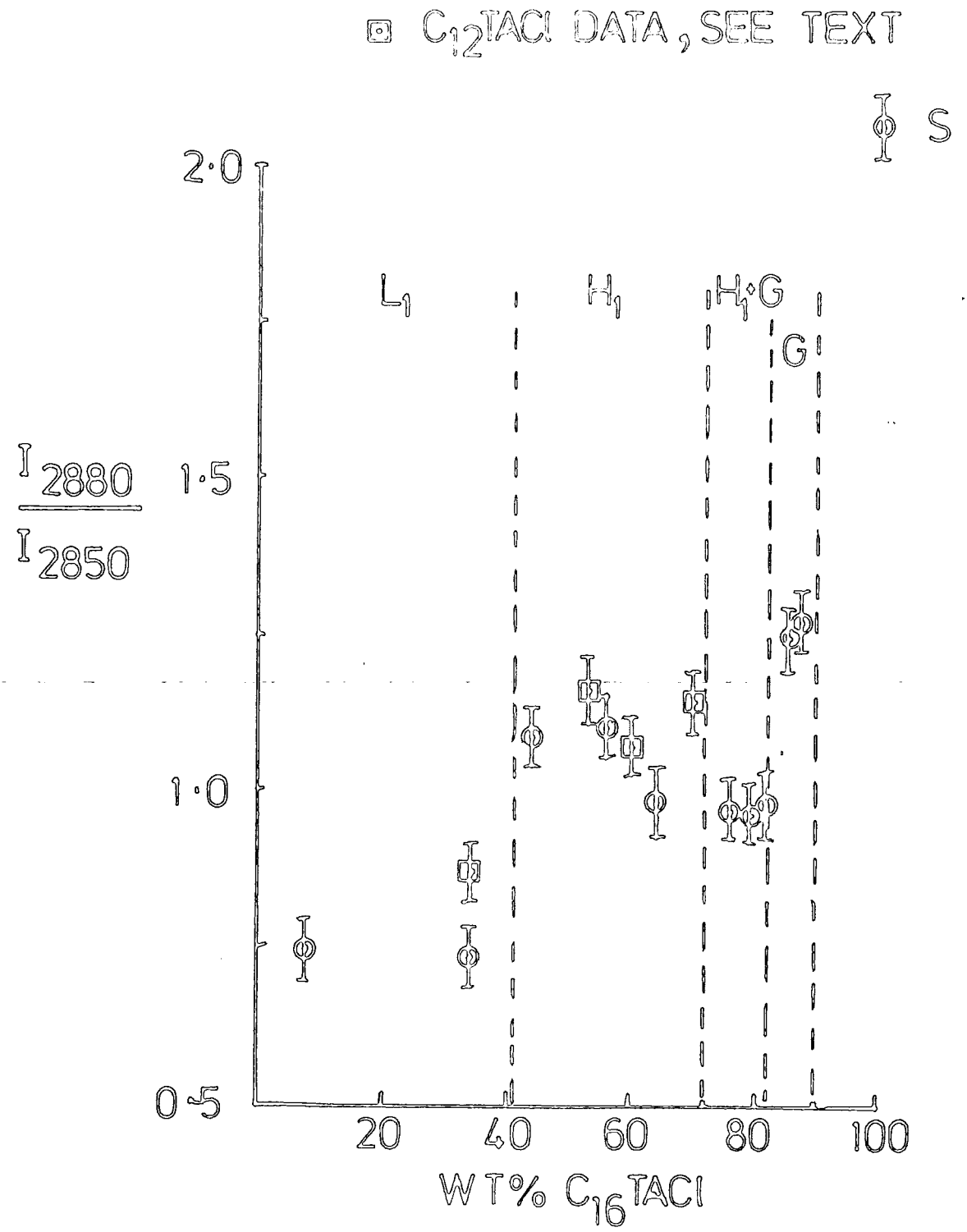

illustrates some interesting features. The first of these is displayed by the three samples found in the gel and hexagonal biphasic region of Figure 7.26. One would expect that as the concentration of C_{16}TACl increases, the proportion of gel phase in the sample would increase, with a concomitant influence on the I_{2880}/I_{2850} ratio. Without assuming some error in concentration, such that the proportion of gel phase is small in these samples, the interpretation is somewhat speculative. The subject will be discussed further, later in this section. Apart from the comments above, the results follow closely the trends observed for L_1, H_1 and crystalline surfactant in the C_{12}TACl system. Though the I_{2880}/I_{2850} ratio of the solid is larger in C_{16}TACl (2.06) than in C_{12}TACl (1.76) as expected from a longer all extended trans chain, the average values for this ratio (i) in the H_1 phase is about the same as in C_{12}TACl, but (ii) in the L_1 phase of C_{16}TACl is less than that found in the L_1 phase of C_{12}TACl (see Figure 7.26). These results might indicate that hydrocarbon orientation in the H_1 phase of both systems is the same, while the L_1 phase of C_{16}TACl is more isotropic than in C_{12}TACl. This anomaly may however be explained in terms of differences in Fermi resonance interactions found in the two L_1 phases.

The above measurements were repeated for a number of samples at 45°C. The results, plotted in Figure 7.27, show the familiar, slightly larger values of the I_{2880}/I_{2850} ratio obtained for the anisotropic phases. The data observed for the intermediate phase is not, however, consistent with the behaviour expected from an anisotropic material (this phase is thought to have a biaxial structure of long cylinders with

FIGURE 7.27 THE BEHAVIOUR OF THE I_{2880}/I_{2850} RATIO AS A FUNCTION OF CONCENTRATION AT 45°C

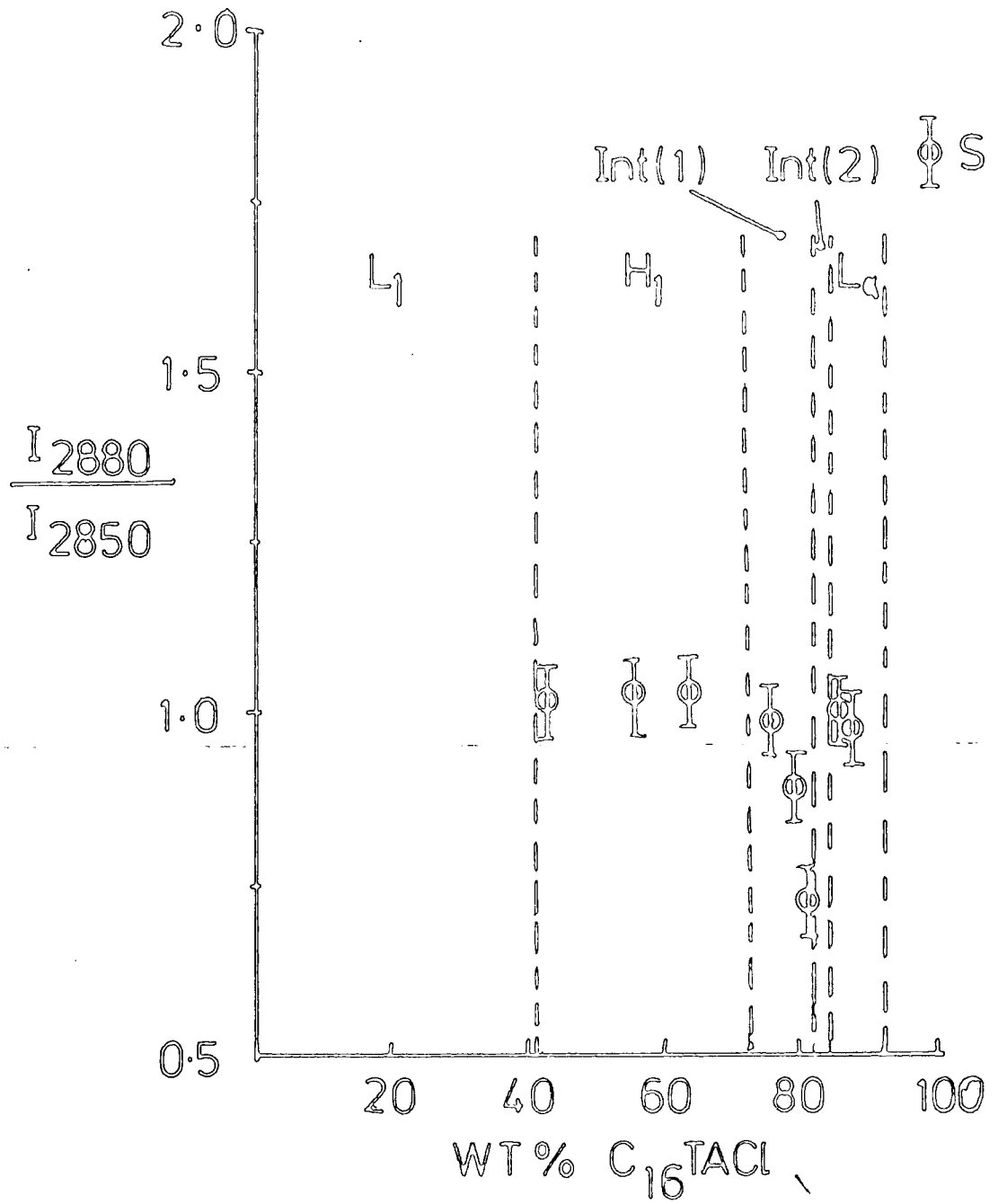

elliptical cross section[86]). The I_{2930}/I_{2850} ratio decreases in this phase, to a value observed in the isotropic L_1 phase of Figure 7.26. Indeed this decrease is also observed when the temperature is increased to 60°C. (Fig.7.28). In this case however, a V_1 phase exists at the lowest point, approximately 82% C_{16}TACl, and the result is consistent with an isotropic sample. There are several possibilities for the above behaviour:

(i) That, in terms of hydrocarbon chain organization, the intermediate and cubic phases are similar: the similarity increasing as the concentration is increased such that one might expect the two phases to be in some way continuous.

(ii) That the samples of compositions between 72% and ≈80% C_{16}TACl form the V_1 cubic phase during preparation (*i.e.* incubation at elevated temperatures), which supercool to lower temperatures. Indeed this may explain the unusually low values for these samples at 30°C (*i.e.* in the H_1 and gel biphasic region).

(iii) That the phase diagram is inaccurate, with the region between L_α and H_1 showing a V_1 phase coexisting with either L_α or the second intermediate phase.

Option (ii) seems unlikely since the Raman tubes were allowed to cool to room temperature and were left for a few hours which would cause the V_1 phase to disappear. Also, the analogous behaviour observed at 60°C is evidence enough to disprove this option. Results obtained by Tiddy[86] using NMR, have shown that the structure of the first intermediate phase is very similar to that of H_1. This makes option (i) unlikely and leaves (iii) as the most probable interpret-

FIGURE 7.28 THE BEHAVIOUR OF THE I_{2880}/I_{2850} RATIO AS A FUNCTION OF CONCENTRATION AT 60°C.

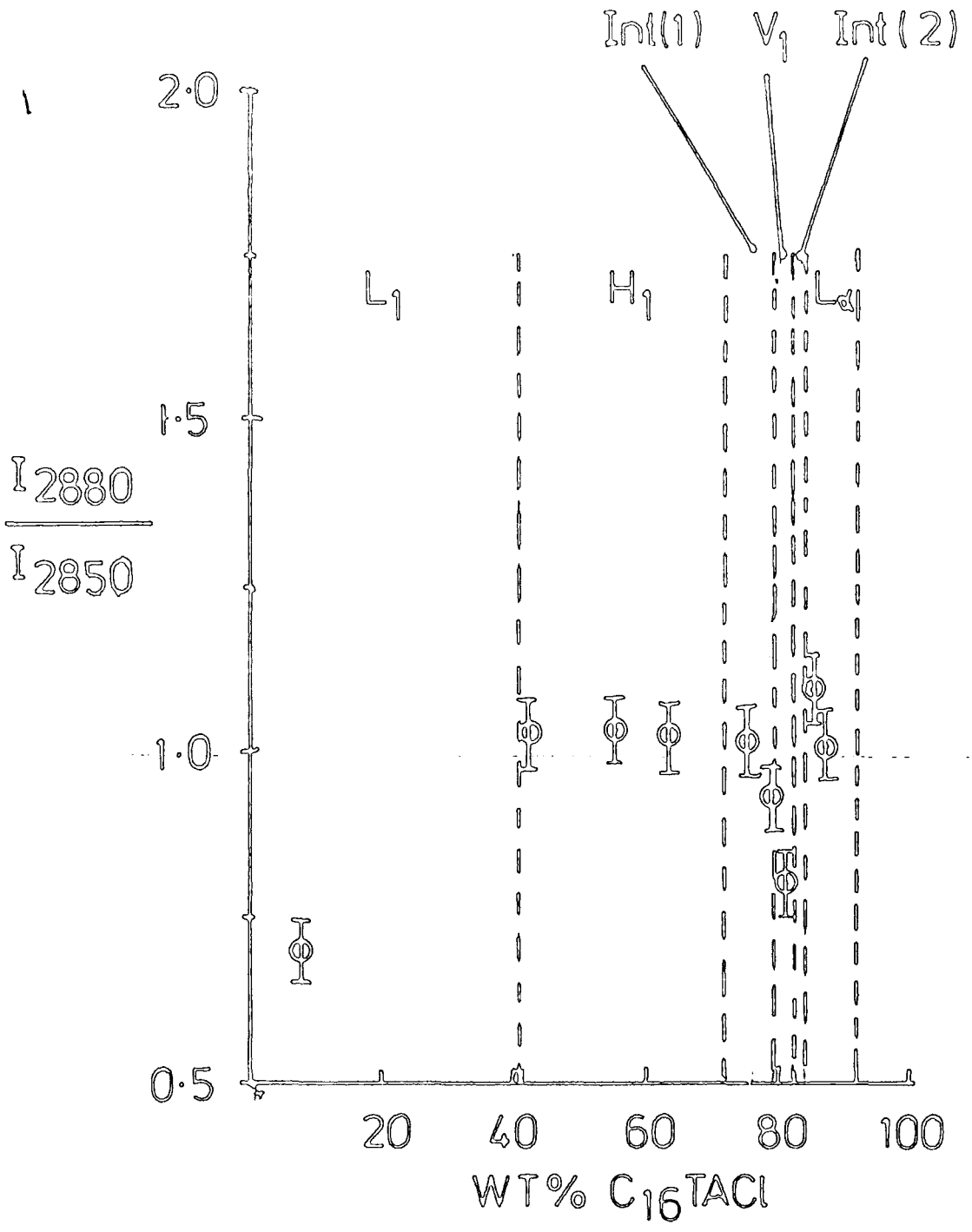

ation of the results, particularly in view of the poor knowledge of C_{16}TACl lyotropic phase behaviour.

7.5.3 The $R\text{-}N(CH_3)_3^+$ Head group Vibrations

The 650-1000 cm^{-1} region, as summarized in Table 7.1, shows various "rocking" modes and two head group vibrations.[41] These occur at 763 and 915 cm^{-1} in C_{16}TACl and have been assigned to the CH_3 rock of the $N^+(CH_3)_3$ group and $C\text{-}N^+$ stretch, respectively.[41] We have measured the band width and frequency maximum for the most intense of these bands, the $N^+(CH_3)_3$ "rocking" mode at 763 cm^{-1}. The band has shown no shift from this frequency and maintained a band width of $\Delta\nu_{1/2}$ = 18±2 cm^{-1} for all the mesophases (see Figure 7.22). This includes the gel and lamellar phases where one might expect an increased rotation about the long axis in the former. It contains fewer gauche bonds and "spinning" (with less hindrance) about this axis should broaden the band. The solid however, has a narrower band width of $\Delta\nu_{1/2}$ = 10±1 cm^{-1}, with a constant frequency maximum of 763 cm^{-1}. The narrowing is typical for that observed in solids.

The $C\text{-}N^+$ stretching mode, occurring at 915 cm^{-1}, is again narrower in the solid ($\Delta\nu_{1/2}$ = 11 cm^{-1}) but broadens in the mesophase samples. It has been difficult to measure these band widths due to the low frequency overlap with the terminal methyl rocking mode. This band shows considerable broadening in Figure 7.22, particularly in the intermediate phase. This may be due to an increased motion of the terminal portion of the hydrocarbon chain. As in the previous band there is no apparent shift in frequency of the $C\text{-}N^+$ stretching mode.

7.6 Optical Microscopy

The methods used in this section have been described in Section 7.2.2. We have tried in this case to obtain photomicrographs of the different phases as observed through crossed polars and to differentiate between their various textures. The first few photographs show the textures of various homogeneous phases and the remainder illustrate the technique of penetration microscopy[79,80,134] as applied to the C_{16}TACl system.

The first photomicrograph, of a 58% C_{16}TACl hexagonal phase at room temperature (23°C), is shown in Plate 7.1. The sample, birefringent, with a texture described as "simple (non-striated) non-geometric" by Rosevear,[81] is typical of the phase, particularly when its viscosity can also be investigated (medium viscosity). Plate 7.2, of an 83% C_{16}TACl sample at 30°C, shows a "speckled" texture probably due to the biphasic region of gel and hexagonal phase. When this sample is heated (40°C), the intermediate phase is formed (Plate 7.3) which has a texture very similar to that found in some hexagonal phases. This is in some ways expected since the structure of both phases is thought to be similar (see Section 7.1). A further increase in concentration causes a phase transition to the gel phase. Plate 7.4 shows this 88% C_{16}TACl sample at 30°C. Rosevear[81] again has described the phase as "viscous neat", and postulated that it is separate from the lamellar phase. The gel phase is very viscous and self orientates to a planar uniaxial texture.[81] When the same sample is heated, melting to the neat (lamellar) phase occurs with very much

lower viscosity. Plate 7.5 shows this phase illustrating the "oily streaks" texture when the coverslip is moved. Further heating or more mechanical disturbance causes the "mosaic" texture observed in lamellar phase samples. Plate 7.6 shows this texture, though slightly out of focus. It is less stable than the "oily streaks" but again is very common in mesophase systems.

As mentioned in Section 7.2.2 the relatively low solubility of $C_{16}TACl$ in water allowed penetration microscopy to be performed with relative ease. The first example of the system at about 30°C is shown in Plate 7.7. The phase diagram of Figure 7.1 reveals that three different phases are expected, the L_1 phase, the H_1 phase and the gel phase. From left to right, this is indeed observed in the photomicrograph with portions in between illustrating coexisting regions. The plate also shows some isotropic "bubbles" which are either due to air or the L_1 phase. Some solid is also observed in the bottom right hand corner of the photograph. Increasing the temperature to 40°C (Plate 7.8) increases the definition of the bands, with the formation of the intermediate phase. From left to right we see a hexagonal phase and then a darker layer which is probably due to the first intermediate phase. A light band follows which may well be due to the second intermediate phase and is followed by L_α and the solid. Plate 7.9, obtained at 50°C is very similar to the previous photomicrograph and confirms that the lighter band in Plate 7.8 was in fact due to lamellar phase.* This region of the interface shows that another phase, between Int(1) and L_α, exists which may again be due to the second intermediate phase. The gel

* This photomicrograph suggests that the Int(1) phase is not similar to the v_1 phase as discussed on page 279.

Plate 7.1 A Photomicrograph of a 58% w/w $C_{16}TACl$ H_1 phase sample at 23°C

Mag.^{n} x 100

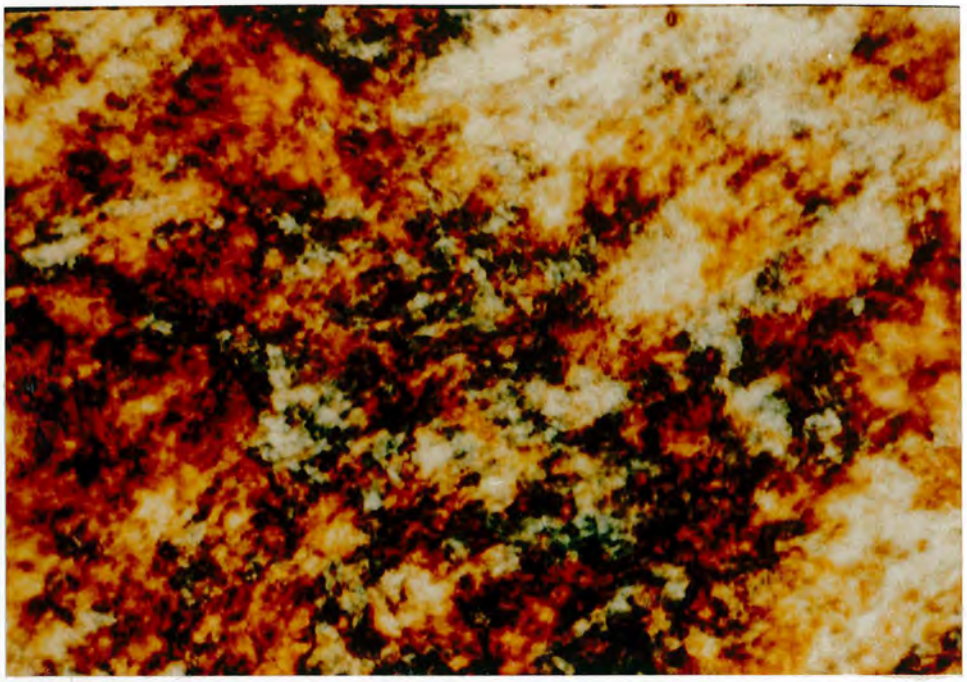

Plate 7.2 A Photomicrograph of an 83% w/w $C_{16}TACl$ sample at 30°C

Mag.^{n} x 100

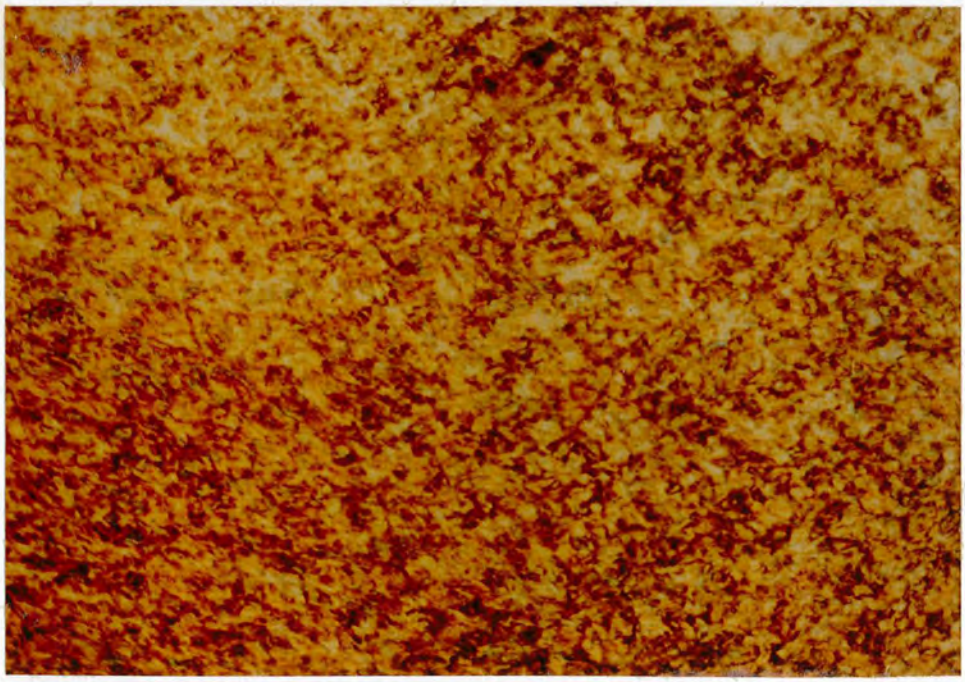

Plate 7.3 A Photomicrograph of an 83% w/w C_{16}TACl Int(1) Phase Sample at 40°C

Mag.^{n} x 100

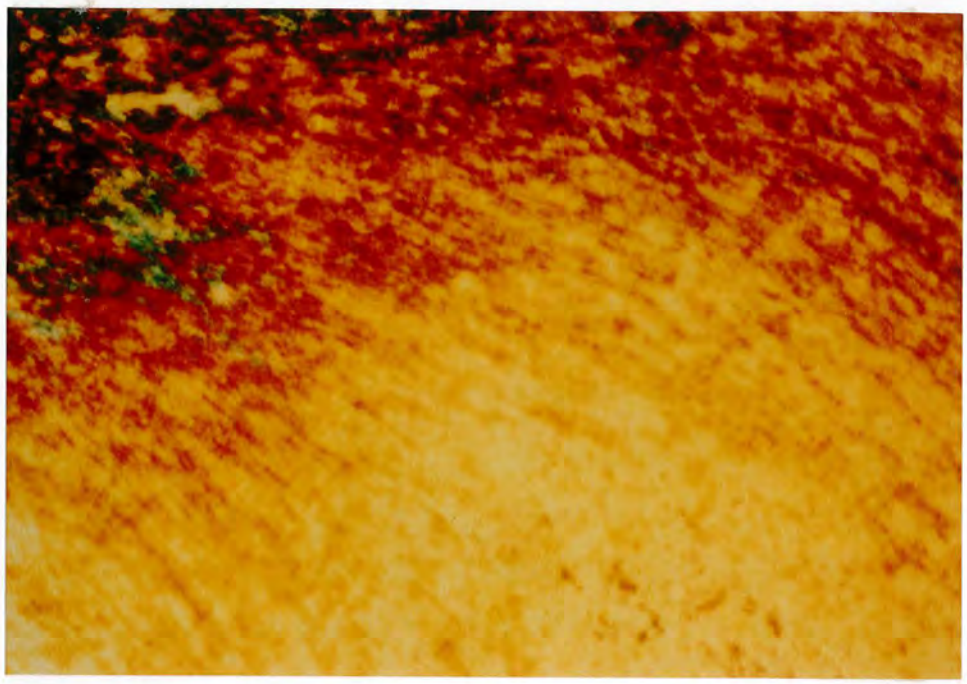

Plate 7.4 A Photomicrograph of an 88% w/w C_{16}TACl Gel Phase Sample at 30°C

Mag.^{n} x 100

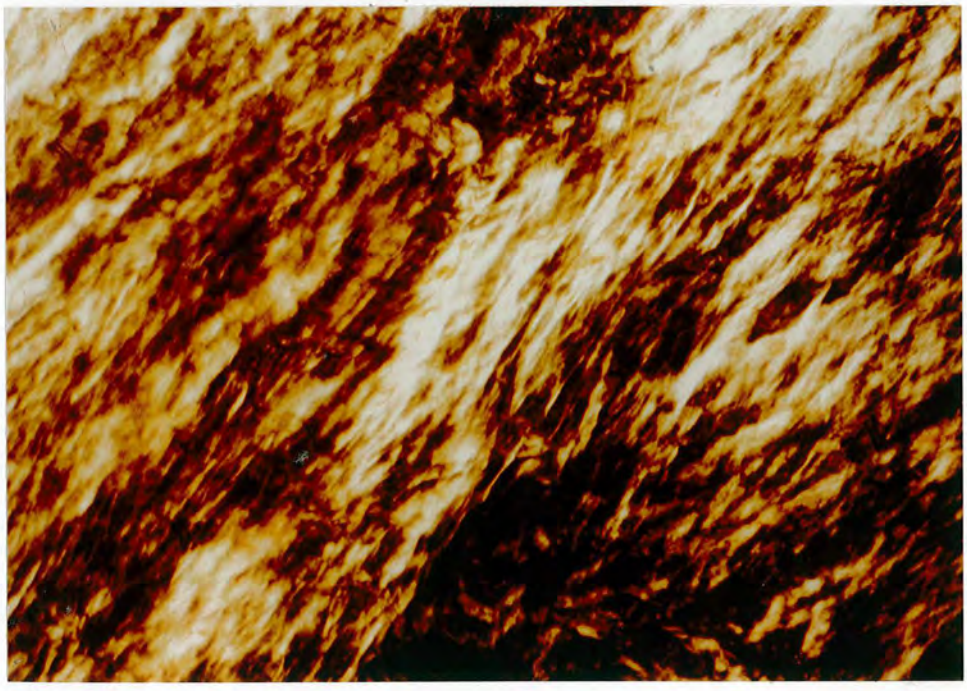

Plate 7.5 A Photomicrograph of an 88% w/w C_{16}TACl lamellar Phase Sample at 60°C. (oil streaks)

Mag.^{n}x 100

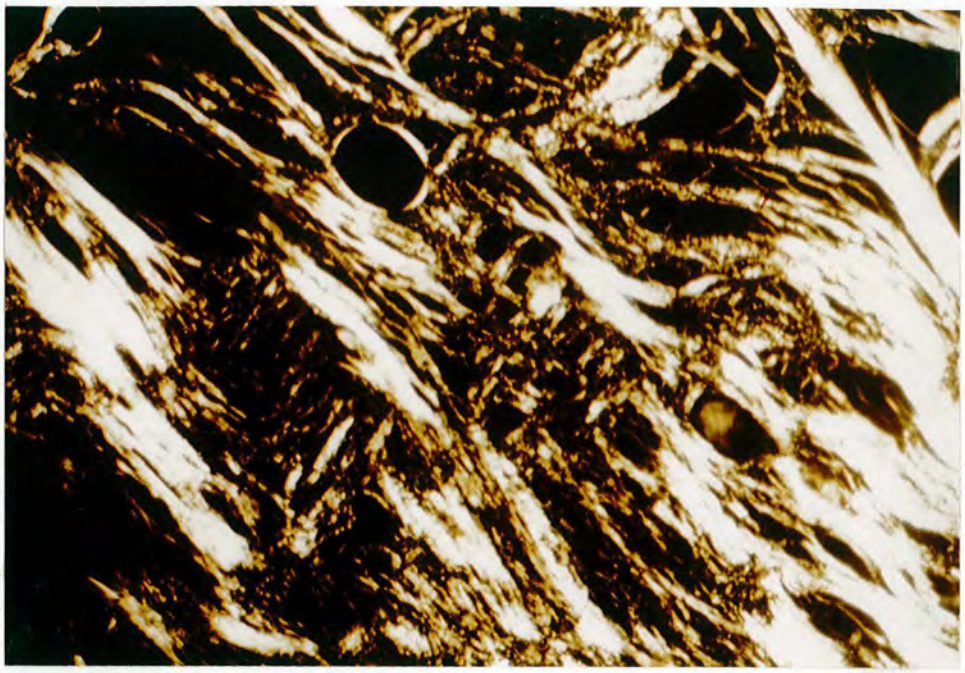

Plate 7.6 A Photomicrograph of an 88% w/w C_{16}TACl lamellar Phase Sample at 60°C. (mosaic texture)

Mag.^{n} x 100

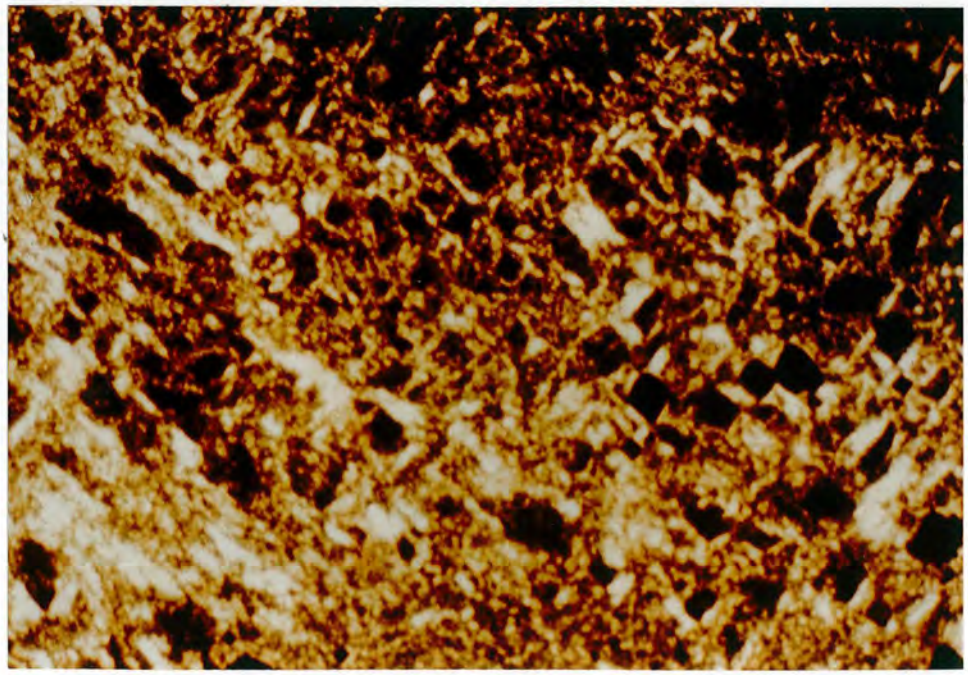

Plate 7.7 A Photomicrograph showing the C_{16}TACl-Water Interface at 30°C

Mag.^{n}x 100

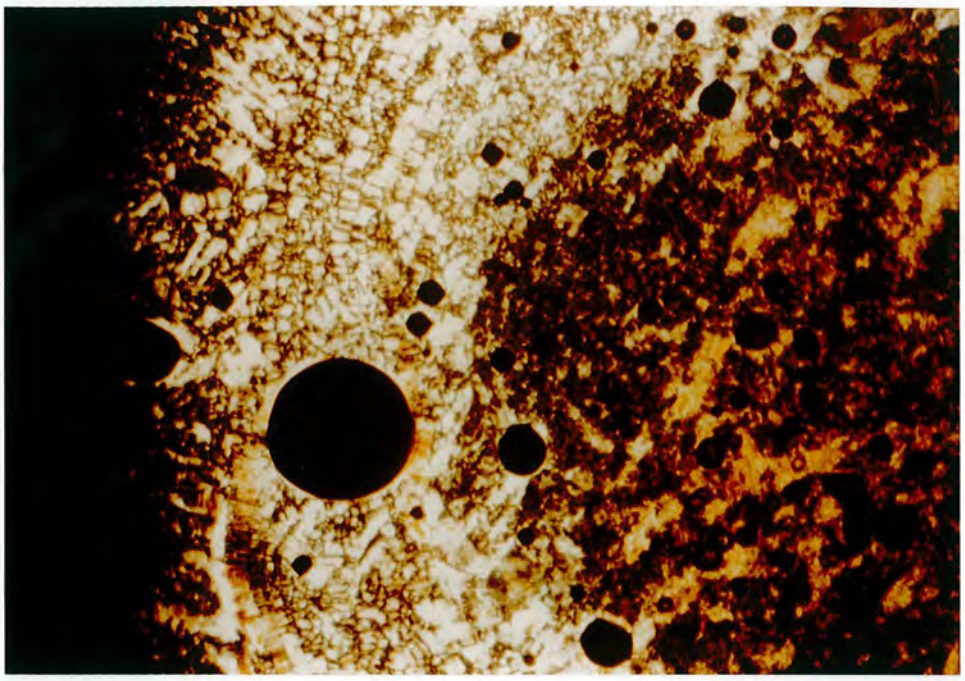

Plate 7.8 A Photomicrograph showing the C_{16}TACl-Water Interface region at 40°C

Mag.^{n} x 100

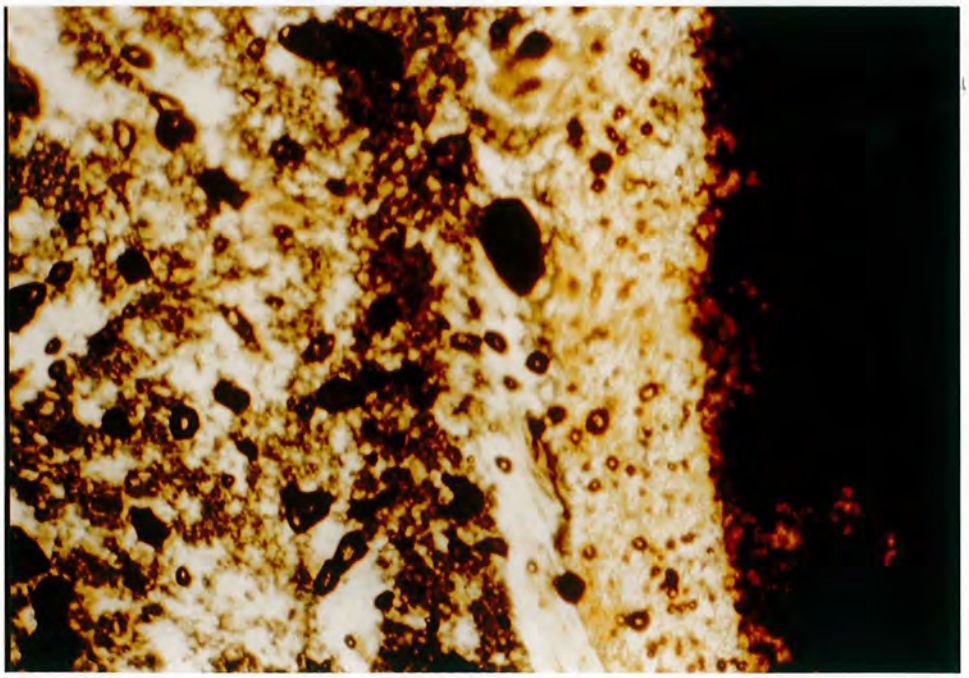

Plate 7.9 A Photomicrograph showing the C_{16}TACl-Water Interface region at 50°C

Mag.^{n} x 100

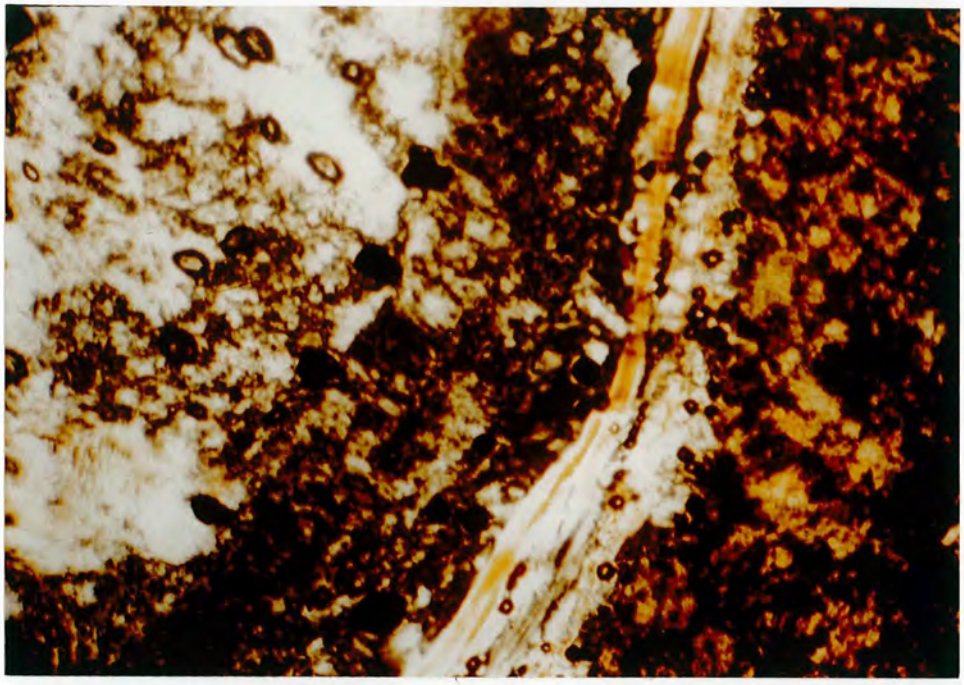

Plate 7.10 A Photomicrograph showing the C_{16}TACl-Water Interface region at 60°C

Mag.^{n} x 100

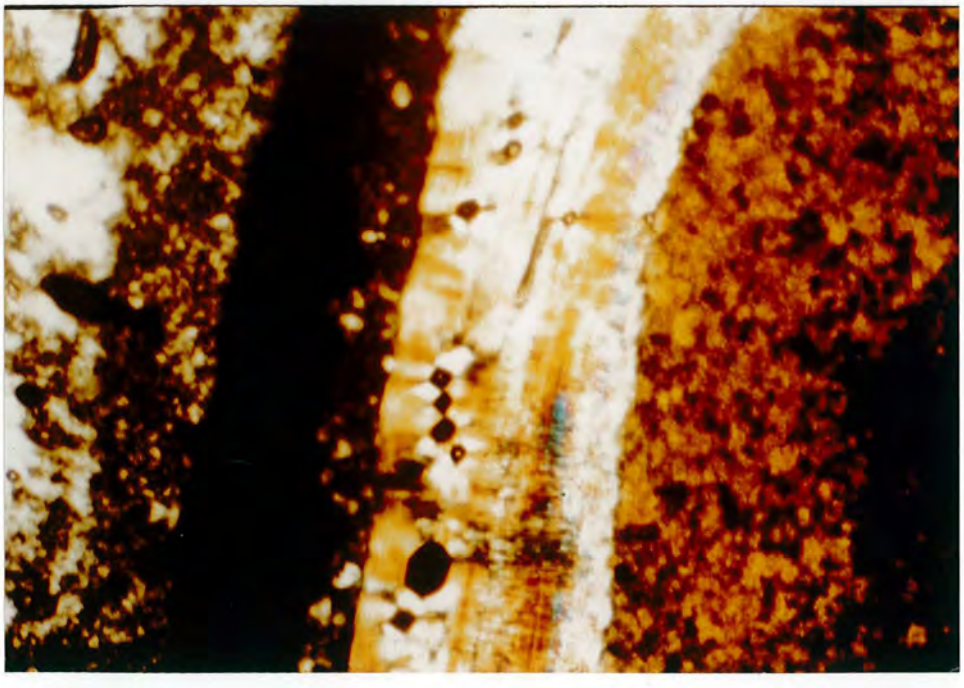

phase has now completely disappeared. Finally, Plate 7.10 shows almost all the phases found in the C_{16}TACl-water system, and is clearly in agreement with the phase diagram of Figure 7.1. This photomicrograph, obtained at 60°C shows both the hexagonal and intermediate phases and also the V_1 cubic (the black isotropic region) which has now also formed. The region between V_1 and L_α however shows at least one band which may well belong to the second intermediate phase.

7.7 Conclusions

One of the main questions remaining unanswered is the existence of one or more bands due to different water species. The spectra of the solid and gel show similarities in their spectra which suggest that some of the structure may well be due to the surfactant. However, this does not mean that other water bands do not exist. Indeed we have observed a species at 2675 cm^{-1} which may well be due to a highly perturbed water species as described by Wells[115] but further work will be needed to confirm this.

The data obtained for C_{16}TACl is directly comparable to that observed for C_{12}TACl. There are two implications of this:

(i) that the behaviour of water (and counter ions) is independent of phase structure, and

(ii) that there is no water reorientation when the gel phase melts to a neat phase.

The behaviour of $\nu_s(O\cdot\cdot D)$ and $\nu_A(H_2O)$ band widths have been monotonic at low concentrations and have shown more pronounced dependence above the disorder-order phase boundary. We have interpreted this in terms of intermicellar contact of boundary water layers which we believe to be related to the hydration force described by Parsegian and others[119-121,130] The ν_{max} data shows a maximum and minimum for $\nu_s(O\text{-}D)$ and $\nu_A(H_2O)$, respectively at a mole ratio of 7.5. We believe that this behaviour is due to strong electrostatic perturbations which influence the water molecules at mole ratios below 7.5.(approximately equal to the hydration number of head group and counter ion). The few far ir spectra that have been recorded have also been identical to that found in the C_{12}TACl system and have shown no changes across phase boundaries including the gel/lamellar boundary.

The Raman data of C_{16}TACl has reproduced the behaviour of the I_{2880}/I_{2850} ratio in both isotropic and anisotropic phases with no apparent changes in the skeletal region. We have again interpreted these results in terms of lateral interactions between hydrocarbon chains. The gel phase and solid spectra have shown the increases in the trans/gauche ratio (compared with other mesophases) as expected from the literature.[118] Finally in our studies of the C-H stretching region in the intermediate phase, we have observed a region where this phase coexists with the V_1 phase or has a structure which is similar.

7.8 Some Thoughts for the Future

Probably the most essential experiment which needs to be performed with these systems is to obtain spectroscopic evidence for the presence of further water species. The best way to do this is to study the same systems using a H_2O in D_2O solution, thus measuring the decoupled $\nu_s(O\text{-}H)_{HDO}$ and $\nu_A(D_2O)$ species in other regions of the spectrum (*i.e.* $\nu > 3000\ cm^{-1}$). Though this was initially tried earlier in our work we came up against the problem of hydrocarbon absorption which overlapped with the bands of interest. If further bands exist, band fitting procedures could be used to determine intensity ratios and eventually to define, at a microscopic level, the behaviour of interstitual water. This experiment would also allow us to compare the data obtained with H_2O across the concentration range and also to substantiate the presence of a highly perturbed water band at higher frequencies (than that of pure water).

The use of anionic surfactants would help in assigning any bands which were observed in the above experiment and would give further information concerning water and counter ion behaviour across the concentration range. The behaviour of sodium dodecyl sulphate and sodium dodecanoate would be of great interest in both the far and mid ir since it would determine whether the deformed hexagonal phase found in these systems was indeed due to an increased water interaction.[82,85] Other experiments to inform us of the behaviour of water in lyotropic systems would be the use of zwitterionic surfactants and also the addition of electrolyte.

The most important experiment as far as Raman spectroscopy is concerned would be the use of perdeuterated C_{12} and C_{16}TACl surfactants with a small dilution of the normal amphiphiles (or *vice versa*). This would remove one source of Fermi resonance, *i.e.* the intermolecular component and make interpretation less ambiguous.

APPENDIX

COLLOQUIA AND CONFERENCES

The Board of Studies in Chemistry requires that each postgraduate research thesis contains an appendix listing:

(A) all research colloquia, research seminars and lectures arranged by the Department of Chemistry during the period of the author's residence as a postgraduate student;

(B) all research conferences attended and papers presented by the author during the period when research for the thesis was carried out;

(C) details of the postgraduate induction course.

(A) RESEARCH COLLOQUIA, SEMINARS AND LECTURES

1. Durham University Chemistry Department Colloquia.

1981

14 October — Prof. E. Kluk (Katowice): "Chemoluminescence and photo-oxidation".

28 October — Dr. R.J.H. Clark (U.C.L.): "Resonance Raman Spectroscopy".

6 November — Dr. W. Moddeman (Monsanto): "High energy materials".

18 November — Prof. M.J. Perkins (London): "Spin-trapping and and nitroxide radicals".

25 November — Dr. M. Baird (Newcastle): "Intramolecular reactions of carbenes and carbenoids".

2 December — Dr. G. Beamson (Durham): "Photoelectron spectroscopy in a strong magnetic field".

1982

20 January — Dr. M.R. Bryce (University of Durham), "Organic metals".

27 January — Dr. D.L.H. Williams (University of Durham), "Nitrosation and nitrosoamines".

3 February — Dr. D. Parker (University of Durham), "Modern methods of determining enantiomeric purity".

10 February — Dr. D. Pethrick (University of Strathclyde), "Conformation of small and large molecules".

17 February — Prof. D.T. Clark (University of Durham), "Plasma Polymerization".

24 February — Prof. R.D. Chambers (University of Durham), "Recent reactions of fluorinated internal olefins".

2 March — Dr. L. Field (University of Oxford), "Applications of N.M.R. to biosynthetic studies on penicillin".

3 March — Dr. P. Bamfield (I.C.I. Organics Division), "Computer aided design in synthetic organic chemistry".

17 March — Prof. R.J. Haines (University of Natal), "Clustering around Ruthenium, Iron and Rhodium".

7 April — Dr. A. Pensak (DuPont, U.S.A.), "Computer aided synthesis".

5 May — Dr. G. Tennant (University of Edinburgh), "Exploitation of the aromatic nitro-group in the design of new heterocyclisation reactions".

7 May — Dr. C.D. Garner (University of Manchester), "The structure and function of Molybdenum centres in enzymes".

26 May — Dr. A. Welch, (University of Edinburgh), "Conformation patterns and distortion in carbometalloboranes".

14 June — Prof. C.M.J. Stirling (University College of Wales, Bangor), " How much does strain affect reactivity?".

28 June — Prof. D.J. Burton (University of Iowa, U.S.A.), "Some aspects of the chemistry of fluorinated phosphonium salts and their phosphonates".

2 July — Prof. H.F. Koch (Ithaca College, University of Cornell, U.S.A.), "Proton transfer to and elimination reactions from localized and declocalized carbanions".

13 September — Prof. R. Neidlein (University of Heidelberg, FRG), "New aspects and results of bridged annulene chemistry".

27 September — Dr. W.K. Ford (Xerox Research Center, Webster, N.Y.) "The dependence of the electron structure of polymers on their molecular architecture".

13 October — Dr. W.J. Feast (University of Durham), "Approaches to the synthesis of conjugated polymers".

14 October — Prof. H. Suhr (University of Tubingen, FRG), "Preparative Chemistry in Non-equilibrium plasmas".

27 October — Dr. C.E. Housecroft (Oxford High School/Notre Dame University", "Bonding capabilities of butterfly-shaped Fe_4 units implications for C-H bond activation in hydrocarbon complexes".

28 October — Prof. M.F. Lappert, F.R.S., (University of Sussex), "Approaches to asymmetric synthesis and catalyses using electron-rich olefins and some of their metal complexes".

15 November — Dr. G. Bertrand (University of Toulouse, France), "Crutius rearrangement in organometallic series. A route for hybridised species".

24 November — Prof. G.G. Roberts (Applied Physics, University of Durham), "Langmuir-Blodgett films: Solid state polymerisation of diacetylenes".

2 December — Dr. G.M. Brook (University of Durham), "The fate of the ortho-fluorine in 3,3-sigmatropic reactions involving polyfluoroaryl and -heteroaryl systems".

8 December — Dr. G. Wooley (Trent Polytechnic), "Bonds in transition metal-cluster compounds".

1983

12 January — Dr. D.C. Sherrington (University of Strathclyde), "Polymer-supported phase transfer catalysts".

9 February — Dr. P. Moore (University of Warwick), "Mechanistic studies in solution by stopped flow F.T.-N.M.R. and high pressure NMR line broadening".

21 February — Dr. R. Lynder-Bell (University of Cambridge", "Molecular motion in the cubic phase of NaCN".

2 March — Dr. D. Bloor (Queen Mary College, University of London), "The solid-state chemistry of diacetylene monomers and polymers".

8 March — Prof. D.C. Bradley, F.R.S. (Queen Mary College, University of London), "Recent developments in organo-imido-transition metal chemistry".

9 March — Dr. D.M.J. Lilley (University of Dundee), "DNA, Sequence, Symmetry, Structure and supercooling".

11 March — Prof. H.G. Viehe (University of Louvain, Belgium), "Oxidations on Sulphur", "Fluorine substitutions in radicals".
[The W.K.R. Musgrave Lecture].

16 March — Dr. I. Gosney (University of Edinburgh), "New extrustion reactions: Organic synthesis in a hot-tube

25 March — Prof. F.G. Baglin (University of Nevada, U.S.A.), "Interaction induced Raman spectroscopy in supra-critical ethane".

21 April — Prof. J. Passmore (University of New Brunswick,U.S.A "Novel selenium-iodine cations".

4 May — Prof. P.H. Plesh (University of Keele), "Binary ionisation equilibria between two ions and two molecules. What Ostwald never thought of".

10 May — Prof. K. Burger (Technical University of Munich,FRG) "New reaction pathways from trifluoromethyl-substituted heterodienes to partially fluorinated heterocyclic compounds".

11 May — Dr. N. Isaacs (University of Reading), The Application of high pressures to the theory and practice of organic chemistry".

13 May — Dr. R. de Koch (Caloin College, Grand Rapids, Michigan/Free University, Amsterdam) "Electronic structural calculations in organometallic cobalt cluster molecules. Implications for metal surfaces".

16 May — Prof. R.J. Lagow (University of Texas, U.S.A.), "The chemistry of polylithium organic compounds. An unusual class of matter".

18 May — Dr. D.M. Adams (University of Leicester), "Spectroscopy at very high pressures".

25 May — Dr. J.M. Vernon (University of York), "New heterocyclic chemistry involving lead tetraacetate".

15 June — Dr. A. Pietrzykowski (Technical University of Warsaw/University of Strathclude), "Synthesis, structure and properties of Aluminoxanes".

22 June — Dr. D.W.H. Rankin (University of Edinburgh), "Floppy molecules - the influence of phase on structure".

5 July — Prof. J. Miller (University of Camfinas, Brazil), "Reactivity in nucleophilic substitution reactions".

5 October — Prof. J.P. Maier (University of Basel, Switzerland), "Recent approaches to spectroscopic characterization of cations".

12 October — Dr. C.W. McLeland (University of Port Elizabeth, Australia), Cyclization of aryl alcohols through the intermediacy of alkoxy radicals and aryl radical cations".

19 October — Dr. N.W. Alcock (University of Warwick), "Aryl tellurium (IV) compounds, patterns of primary and secondary bonding".

26 October — Dr. R.H. Friend (Cavendish Laboratory, University of Cambridge), "Electronic properties of conjugated polymrs".

30 November — Prof. I. Cowie (University of Stirling), "Molecular interpretation of non-relaxation processes in polymer glasses".

14 December — Prof. R.J. Donovan (University of Edinburgh), "Chemical and physical processes involving the ion-pair states of the halogen molecules".

1984

10 January — Prof. R. Hester (University of York), "Nanosecond laser spectroscopy of reaction intermediates".

18 January — Prof. R.K. Harris (University of East Anglia), Multi-nuclear solid state magnetic resonance".

8 February — Dr. B.T. Heaton (University of Kent), "Multi-nuclear n.m.r. studies".

15 February — Dr. R.M. Paton (University of Edinburgh), "Heterocyclic syntheses using nitrile sulphides".

7 March — Dr. R.T. Walker (University of Birmingham), "Synthesis and biological properties of some 5-substituted uracil derivatives; yet another example of serendipity in antiviral chemotherapy".

21 March — Dr. P. Sherwood (University of Newcastle), "X-ray photoelectron spectroscopic studies of electrode and other surfaces".

23 March — (Informal colloquium) Dr. A. Ceulemans (Catholic University of Leuven), "The Development of Field-Type Models of the Bonding in Molecular Clusters".

2 April — Professor K. O'Driscoll (University of Waterloo), "Chain Ending Reactions in Free Radical Polymerisation

3 April — Professor C.H. Rochester (University of Dundee), "Infrared Studies of Adsorption at the Solid-Liquid Interface".

25 April — Dr. R.M. Acheson (Department of Biochemistry, University of Oxford), "Some Heterocyclic Detective Stories".

27 April — Dr. T. Albright (University of Houston), "Sigmatropic Rearrangements in Organometallic Chemistry".

14 May — Professor W.R. Dolbier, Jr., (University of Florida) "Cycloaddition Reactions of Fluorinated Allenes".

16 May — Dr. P.J. Garratt (University College, London), "Syntheses with Dilithiated Vicinal Diesters and Carboximides".

31 May — Dr. A. Haaland (University of Oslo), "Electron Diffraction Studies of some Organometallic Compounds".

11 June — Dr. G.B. Street (I.B.M. San José), "Conducting Polymers derived from Pyrroles".

2. DURHAM UNIVERSITY CHEMICAL SOCIETY LECTURES

1981

22 October — Dr. P.J. Corish (Dunlop): "What would life be like without rubber".

29 October — Miss J.M. Cronyn (Durham): "Chemistry in Archaeology".

12 November — Prof. A.I. Scott (Edinburgh): "An organic chemist's view of life through the n.m.r. tube".

19 November — Prof. B.L. Shaw (Leeds): "Big rings and metal-carbon bond formation".

3 December — Dr. W.O. Ord (Northumbria Water Authority): "The rôle of the scientist in a regional water authority"

1982

28 January — Prof. I. Fells (University of Newcastle upon Tyne), "Balancing the Energy Equations".

11 February — Dr. D.W. Turner (University of Oxford), "Photoelectrons in a Strong Magnetic Field".

18 February — Prof. R.K. Harris (University of East Anglia), "N.m.r. in the 1980s".

25 February — Prof. R.O.C. Norman, F.R.S. (University of York), "Turning Points and Challenges for the Organic Chemist".

4 March — Dr. R. Whyman (I.C.I. Ltd., Runcorn), "Making Metal Clusters Work".

14 October — Mr. F. Shenton (County Analyst, Durham), "There is death in the pot".

28 October — Prof. M.F. Lappert, F.R.S. (University of Sussex), "The Chemistry of Some Unusual Subvalent Compounds of the Main Group IV and V Elements".

4 November — Dr. D.H. Williams (University of Cambridge), Studies on the Structures and Modes of Action of Antibiotics".

11 November — Dr. J. Cramp (I.C.I. Ltd.), "Lasers in Industry".

25 November — Dr. D.H. Richards, P.E.R.M.E. (Ministry of Defence), "Terminally Functional Polymers, their Synthesis and Uses".

1983

27 January — Prof. D.W.A. Sharp (University of Glasgow), "Some Redox Reactions in Fluorine Chemistry".

3 February — Dr. R. Manning (Department of Zoology, University of Durham), "Molecular Mechanisms of Hormone Action"

10 February — Sir Geoffrey Allen, F.R.S. (Unilever Ltd.), "U.K. Research Ltd.".

17 February — [R.S.C. Centenary Lecture], Prof. A.G. MacDiarmid, (University of Pennsylvania), "Metallic Covalent Polymers: $(SN)_x$ and $(CH)_x$ and their derivatives".

3 March — Prof. A.C.T. North (University of Leeds), "The Use of a Computer Display System in Studying Molecular Structures and Interactions".

20 October — Prof. R.B. Cundall (University of Salford), "Explosives".

3 November — Dr. G. Richards (University of Oxford), "Quantum pharmacology".

10 November — Dr. J. Harrison (Sterling Organic), "Applied Chemistry and the Pharmaceutical Industry".

24 November — Prof. D.A. King (University of Liverpool), "Chemistry in two dimensions".

1 December — Dr. J.D. Coyle (The Open University), "The problem with sunshine".

1984

26 January — Prof. T.L. Blundell (Birkbeck College, London), "Biological recognition: Interactions of macromolecular surfaces".

2 February — Prof. N.B.H. Jonathan (University of Southampton), "Photoelectron spectroscopy - a radical approach".

16 February — Prof. D. Phillips (The Royal Institution), "Luminescence and photochemistry - a light entertainmentP.

23 February — Prof. F.G.A. Stone, F.R.S. (University of Bristol), "The use of carbene and carbyne groups to synthesise metal clusters".

[The Waddington Memorial Lecture].

1 March — Prof. A.J. Leadbetter (Rutherford Appleton Labs.), "Liquid Crystals".

8 March — Prof. D. Chapman (Royal Free Hospital School of Medicine, University of London), "Phospholipids and biomembranes: basic structure and future techniques'

28 March [R.S.C. Centenary Lecture]

Prof. H. Schmidbaur (Technical University of Munich, FRG), "Ylides in coordination sphere of metals: synthetic, structural and theoretical aspects".

(B) RESEARCH CONFERENCES ATTENDED

Graduate Symposium, Durham, April 1982.

Royal Society of Chemistry, Faraday Division, titled "Physical and Biological Aspects of Insoluble Monolayer and Multilayers", London, 14 December 1982.

Royal Society of Chemistry, Faraday Division, Symposium No. 17 titled "Hydrophobic Interactions", Reading, 15-16 December 1982.

Graduate Symposium, Durham, April 1983.

Royal Society of Chemistry, Residential School, titled "Surfactants", Bristol, 18-22 July 1983.

International Conference on "Fourier Transform Spectroscopy", Durham, 5-9 September 1983.

Meeting of the British Liquid Crystal Group, Abertystwyth, 20-23 September 1983.

A poster was presented by the author entitled" An IR and Raman Study of the Phase Behaviour of $C_{12}TACl$ in Water".

Graduate Symposium, Durham, April 1984.

A paper was presented by the author entitled "IR Studies of the Aggregation Properties of Polyoxyethylene Surfactants in Apolar Solvents".

Summer School titled "Infra red Spectroscopy in Material Anaylsis", Durham 10-13 July 1984.

(C) POSTGRADUATE INDUCTION COURSE

In each part of the course, the uses and limitations of the various services available were explained.

Departmental Organisation - Dr. E.J.F. Ross.

Electrical appliances and infrared spectroscopy - Mr. R.N. Brown.

Chromatography - Mr. J.A. Parkinson.

Microanalysis - Mr. T.F. Holmes and Mrs. M. Cocks.

Atomic absorption spectrometry and inorganic analysis- Mr. R. Coult.

Mass spectroscopy - Dr. M. Jones.

N.m.r. spectroscopy - Dr. R.S. Matthews.

Glassblowing techniques - Mr. R. Hart and Mr. G. Haswell.

Safety matters - Dr. M.R. Crampton.

REFERENCES

REFERENCES

1. B.P. Straughan, S. Walker, in "Spectroscopy", Vol.2, Chapman and Hall, London, 1976.

2. J. Yarwood, R. Ackroyd and G.N. Robertson, Chem.Phys., 32, 1978, 283-299.

3. M. Asselin, C. Sandorfy, J.Mol.Structure, 8, 1971, 145-158.

4. C.N. Banwell in "Fundamentals of Molecular Spectroscopy", McGraw Hill, 2nd Ed., London, 1972.

5. D. Eisenberg, W. Kauzmann in "The Structure and Properties of Water", Oxford Univ. Press, London, 1969.

6. J.L.Wood in "Spectroscopy and Structure of Molecular Complexes", Ed. J. Yarwood, Plenum Press, London, 1973.

7. G.E. Walrafen in "Water, A Comprehensive Treatise", Vol.1, Ed. F. Franks, Plenum Press, London, 1972, pg. 151.

8. G. Némethy in "Structure of Water and Aqueous Solutions", ed. W.A.P. Luck, Physik Verlag, Chap.2, p.74, (1974).

9. Perkin Elmer 580B Operators Manual, Beaconsfield, 1979.

10. R.J. Bell in "Introductory Fourier Transform Spectroscopy", Academic Press, New York, 1972.

11. P.R. Griffiths in "Chemical Infrared Fourier Transform Spectroscopy", John Wiley and Sons, 1975, Canada.

12. G.W. Chantry in "Submillimeter Spectroscopy", Academic Press, London, 1971.

13. J. Chamberlain in "The Principles of Interferometric Spectroscopy", Wiley Interscience, Chichester, 1979.

14. P.L. James, Ph.D. Thesis, Durham University, 1982.

15. T.R. Gilson, P,J. Hendra in "Laser Raman Spectroscopy", Wiley Interscience, 1967.

16. Varian Cary 82 Operating Manual.

17. R. Ackroyd, Ph.D. Thesis, Durham University, 1978.

18. D. Williams, Nature, 210, 1966, 194.

19. C. Tanford, in "The Hydrophobic Effect", J. Wiley & Sons, New York, 2nd Edn., 1980.

20. G.S. Hartley in "Paraffin Chain Salts", Herman et Cie, Paris, 1936.

21. M.J. Rosen in "Surfactants and Interfacial Phenomena", Wiley Interscience, 1978.

22. W.C. Preston, J. Phys.Colloid Chem. 52, 1948, 84.

23. D.J. Shaw in "Introduction to Colloid Chemistry", Butterworths, Third Ed., 1983, London.

24. Instruction Manual for the FT FS720 Spectrophotometer, Beckman RIIC, 1968, London.

25. J.N. Israelachvili, D.J. Mitchell and B.W. Ninham, J.Chem.Soc., Faraday Trans.2, 72, 1976, 1525.

26. D.J. Mitchell and B.W. Ninham, J.Chem.Soc., Faraday Trans. 2, 77, 1981, 601.

27. H. Wennerström, and B. Lindman, Physics Reports, 52(1), 1979, 1-86.

28. J.M. Corkill, J.F. Goodman, T. Walker and J. Wyer, Proc.Roy. Soc.A, 312, 1969, 243-255.

29. D.G. Hall, and B.A. Pethica, in "Nonionic Surfactants", ed. M.J. Schick, Marcel Dekkar, New York, 1967, Chapt.16.

30. R. Aveyard, B.J. Briscoe and J. Chapman, J.Chem.Soc., Faraday Trans.1, 69, 1973, 1772-1778.

31. I. Weil, J. Phys.Chem., 70, 1966, 133.

32. R.R. Balmbra, J.S. Clunie, J.M. Corkill and J.F. Goodman, Trans.Faraday Soc., 58, 1962, 1661.

33. E.J. Staples, G.J.T.Tiddy, J.Chem.Soc., Faraday 1, 74, 1978, 2530.

34. E.A.G. Aniansson, S.N.Wall, J.Phys.Chem., 78, 1974, 1024.

35. E.A.G. Aniansson, and S.N. Wall, J.Phys.Chem., 79, 1975, 857.

36. H.F. Eicke in "Micellization, Solubilization and Microemulsions", Vol.1, Ed. K.L. Mittal, Plenum Press, New York, 1977, 429.

37. A.S. Kertese in "Micellization, Solubilization and Microemulsions", Vol.1, Ed. K.L.Mittal, Plenum Press, New York, 1977, 445.

38. Z.A. Schelly in "Aggregation Processes in Solution", Ed. E. Wynn Jones and J. Gormally, Elsevier, Oxford, Vol.26,1983.

39. F.A. Smith, E.C. Creitz, J.Research NBS, 46(2), 1951, 145-164, RP2185.

40. W.A.P. Luck and O. Schrems, J.Mol.Struct., 60, 1980, 333-6.

41. K. Kalyanasundaram and J.K. Thomas, J.Phys.Chem., 80, 1976, 1462.

42. N.L.Fuller, R.P. Rand, and V.A. Parsegian, Biochemistry, 17(15), 1978, 3163.

43. A.S.N. Murphy and C.N.R. Rao, Appl.Spectr.Revs., 2(1), 1968, 69-191.

44. G. Brink, C. Campbell and L. Glasser, South African J.Sci., 73, 1977, 11-15.

45. G. Whetsel and L. Lady in "Spectrometry of Fuels", Chapt. 20, 1970, Plenum Press, New York.

46. R.A. Lebedev, V.P. Tikhonov, G.I. Fuks, Koll,Zhurn., 45(4), 1983, 689.

47. V.P. Tikhonov and G.I. Fuks, Koll.Zhurn., 38(5), 1976, 1025-9.

48. M.E. Ladhabhoy, Text.Dyer Printer, April 1981, 27-30.

49. K. Shinoda, H. Arai, J.Phys.Chem., 68, 1964, 3485.

50. C.R. Singleterry, J.Am.Oil Chemists Soc., 32, 1955, 446-52.

51. T. Miura, M. Nakamura, Bull.Chem.Soc.Jpn., 50(10), 1977, 2528.

52. L.E. Scriven, Nature, 263, 1976, 123-125.

53. J.C. Ravey, M. Buzier, and C. Picot, J.Colloid Interface Sci., 97(1), 1984, 9-25.

54. H. Kise, K. Iwanoto and M. Seno, Bull.Chem.Soc.Jpn., 55(12), 1982, 3856-60.

55. T. Kawai, J. Umemura, T. Takenaka, M. Kodama and S. Seki, J.Colloid and Interface Sci., 103(1), 1985, 56-61.

56. M. Zulauf and H.F. Eicke, J.Phys.Chem., 83, 1979, 480.

57. R.C. Little, C.R. Singleterry, J.Phys.Chem., 12, 1964, 3453.

58. W.J. Potts, Jnr., in "Chemical Infra red Spectroscopy", Vol.1, Wiley, 1966.

59. J. Pitha, and R.N. Jones, NRCC, Vol.12, Ottawa, 1968.

60. A.N. Fletcher and C.A. Heller, J.Phys.Chem., 71(12), 1967, 3742-59.

61. L.S. Prabhumirashi, and C.I. Jose, J.Chem.Soc., Faraday II, 71, 1975, 1545.

62. L.S. Prabhumirashi and C.I. Jose, J.Chem.Soc., Faraday II, 72, 1976, 1721.

63. L.S. Prabhumirashi and C.I. Jose, J.Chem.Soc., Faraday II, 74(2), 1978, 255.

64. L.S. Prabhumirashi and C.I. Jose, J.Chem.Soc., Faraday II, 74(9), 1978, 1567.

65. L.P. Kuhn and R.A. Wires, J.Amer.Chem.Soc., 86, 1964, 2161.

66. L.J. Bellamy in "Advances in Infrared Group Frequencies, Methuen & Co. Ltd., London, 1968, Chap. 4, pp.100-101.

67. G.J.T. Tiddy, P. Jones and E. Wynn Jones, Unpublished results.

68. R.M. Badger and S.H. Bauer, J.Chem.Phys., 5, 1937, 839.

69. J.R. Birch and M. Benouma, Infrared Physics, 21, 1981, 229-34.

70. J.N. Murrell and E.A. Boucher in "Properties of Liquids and Solutions", John Wiley and Sons, 1982, 27.

71. H. Christenson, S.E. Friberg and D.W. Larsen, J.Phys.Chem., 84, 1980, 3633-3638.

72. J.G. David, Spectrochimica Acta, 28A, 1971, 977-985.

73. K.K. Fox, Mol.Cryst.Liq.Cryst.Letters, 92(4), 1983, 135-140.

74. A. Tardieu and V. Luzzati, Biochem.Biophys.Acta, 219, 1970, 11.

75. M. Tamres and J. Yarwood in "Spectroscopy and Structure of Molecular Complexes", ed. J. Yarwood, Plenum Press, 1973, pp.277.

76. H. Christenson and S. Friberg, J.Colloid Interface Sci., 75, 1980, 276.

77. P. Ekwall in "Advances in Liquid Crystals", Ed.G.H.Brown. Academic Press, New York, 1975.

78. P.J. Flory, J.Polym.Sci., 49, 1961, 105.

79. G.J.T.Tiddy and M.F. Walsh in "Aggregation Processes in Solution", Ed. E.Wynn-Jones, J.Gormally, Studies in Physical and Theoretical Chemistry, Vol.26, Elsievier, Oxford, 1983, 151.

80. G.J.T.Tiddy, Physics Reports, 57(1), 1980, 1-46.

81. F.B. Rosevear, J.Amer.Chem.Soc., 31, 1954, 628-639.

82. I.D. Leigh, M.P. McDonald, R.M. Wood, G.J.T.Tiddy and M.A. Trevetnan, J.Chem.Soc., Faraday Trans.1, 77, 1981, 2867.

83. K. Fontell, Mol.Cryst.Liq.Cryst., 63, 1981, 59-82.

84. T.Bull and B. Lindman, Mol.Cryst.Liq.Cryst., 28, 1974, 155.

85. K. Rendall, G.J.T.Tiddy, and M.A. Trevethan, J.Chem.Soc., Faraday Trans.1, 78, 1982.

86. G.J.T.Tiddy, Unpublished Results.

87. D.J.Mitchell, G.J.T.Tiddy, L. Waring, T. Bostock and M.P. McDonald, J.Chem.Soc., Faraday Trans.1, 79, 1983, 975-1000.

88. H. Fabre, N. Kamenka, A.Khan, G. Lindblom, B. Lindman and G.J.T.Tiddy, J.Phys.Chem., 84, 1980, 3428-3433.

89. H. Wennerström, B. Lindman, G. Lindblom, and G.J.T.Tiddy, J.Chem.Soc., Faraday 1, 75, 1979, 663.

90. G. Gunnarsson, B. Jönsson and H. Wennerström, J.Phys.Chem., 84, 1980, 3114.

91. R.G. Laughlin in "Advances in Liquid Crystals", Ed.H.Brown, Vol.3, 50.

92. R.C. Little, J.Amer.Oil.Chem.Soc., 58(6), 1981, 734-7.

93. W.J. Moore in "Physical Chemistry", Longman, London, 1976, p.913.

94. S. Engström and H. Wennerström, J.Phys.Chem., 82, 1978, 2711.

95. B. Jönsson, H. Wennerström and B. Halle, J.Phys.Chem., 84, 1980, 2179.

96. P. Linse, G. Gunnarsson and B. Jönsson, J.Phys.Chem., 86, 1982, 413.

97. L. Guldbrand, B. Jönsson, H. Wennerström and P. Linse, J.Chem.Phys., 80, 1984, 2221.

98. H.F. Eicke in "Topics in Current Chemistry, Vol.87, Ed. M.J.S. Dewar *et al*, Springer-Verlag, Berlin, 1980.

99. V. Luzzati in "Biological Membranes", Ed. D. Chapman, Academic Press, London, 1968, Chap.3, p.71.

100. G.J.T.Tiddy, in "Nuclear Magnetic Resonance", Chem.Soc., S.P.R. Series, 1981, Vol.10, Chapt.12, p.267.

101. C. Chachaty and J.P. Quaegbeur, J.Phys.Chem., 87(22), 1983, 4341-43.

102. B. Halle, G. Carlström, J.Phys.Chem., 85(14), 1981,2142-47.

103. P.O. Eriksson, A. Khan, G. Lindblom, J.Phys.Chem., 86, 1982, 387.

104. E.D. Lawson, T.J. Flautt, J.Phys.Chem., 72, 1968, 2066.

105. N.O. Persson, B. Lindman, J.Phys.Chem., 79, 1975, 1410.

106. W. Niederberger, Y. Tricot, J. Magnetic Resonance, 28, 1977, 313-316.

107. N. Persson, and A. Johansson, Acta.Chem.Scandinavica, 25, 1971, 2118-2130.

108. E.I. Franses, and T.J. Hart, J.Colloid Interface Sci., 94(1), 1983, 1-13.

109. L. Hecker, L.W. Reeves and A.S. Tracey, Mol.Cryst.Liq. Cryst., 53, 1979, 77-87.

110. P.J. Françoise, Kolloid-Z.u.Z. Polymere, 251, 1973, 594-599.

111. M.P. McDonald and L.D.R. Wilford in "Liquid Crystals and Ordered Fluids", eds. J.F. Johnson and R.S. Porter, p.225, Plenum Press, New York, 1974.

112. D. Balasubramanian, J.Indian Chem.Soc., 58, 1981, 633-639.

113. J. Sunamoto, T. Hamada, T. Seto and S. Yamamoto, Bull. Chem.Soc.Jpn., 53, 1980, 583-389.

114. M. Lucas, A. de Trobriand and M. Ceccaldi, J.Phys.Chem., 79, 1975, 913.

115. M.A.Wells, Biochemistry, 13, 1974, 4937.

116. K. Colbow and B.P. Clayman, Biochimica et Biophysica Acta, 323, 1973, 1-6.

117. F. Mallmace, P. Migliardo, C. Vasi and F. Wanderlingh, Phys.Chem.Liq., 11(1), 1981, 47-57.

118. R. Faiman and D.A. Long, J.Raman Spec., 3, 1975, 371-377.

119. V.A. Parsegian, Advances in Colloid Interface Sci., 16, 1982, 49-56.

120. R.P. Rand, Ann.Rev.Biophys.Bioeng., 10, 1981, 277-314.

121. S. Marčelja and N. Radić, Chem.Phys.Lettrs., 42(1), 1976, 129-130.

122. R. Mendelsohn, R. Dluhy, T. Taraschi, D.G. Cameron and M.H. Mantsch, Biochemistry, 20, 1981, 6699-6701.

123. D.A. Pink, T.J. Green and D. Chapman, Biochemistry, 19(2), 1980, 349-56.

124. D.A. Pink, T.J. Green and D. Chapman, Biochemistry, 20, 1981, 6692-8.

125. R.G. Snyder, S.L. Hsu and S. Krimm, Spectrochemica Acta, 34A, 1978, 395.

126. R.G. Snyder, J.R. Scherer and B.P. Gaber, Biochem. et Biiphys.Acta, 601, 1980, 47.

127. B.P. Gaber and W.L. Peticolas, Biochem. et Biophys. Acta, 465, 1977, 260-274.

128. R.G. Snyder, J.Chem.Phys., 47, 1967, 1316-60.

129. P. Murkerjee, J.Colloid Interface Sci., 19, 1964, 722.

130. V.A. Parsegian, N. Fuller, and R.P. Rand, Proc.Natl.Acad. Sci., U.S.A., Biophys., 76(6), 1979, 2750-2754.

131. J.B. Rosenholm, P. Stenius and I. Danielsson, J.Colloid Interface Sci., 57(3), 1976, 551-563.

132. R.C. Weast (ed.). in "Handbook of Chemistry and Physics", 63rd Ed., CRC, 1982-3.

133. A.M. Amorim Da Costa, C.F.G.S. Geraldés and J.J.C. Texxeira-Dias, J.Colloid Interface Sci., 86(1), 1981, 254-9.

134. A.S.C. Lawrence, A. Bingham, C.B. Capper and K. Hume, J.Phys.Chem., 68, 1964, 3470.